# University of Alberta

## Solids Transport with Turbulent Flow of Non-Newtonian Fluid in the Horizontal Annuli

By

Majid Bizhani

A thesis submitted to the Faculty of Graduate Studies and Research
in partial fulfillment of the requirements for the degree of

Master of Science

in

Petroleum Engineering

Department of Civil and Environmental Engineering



Fall 2013

Edmonton, Alberta

## Abstract

An experimental investigation of turbulent non-Newtonian fluid flow and solids transport in horizontal concentric annulus is the main subject matter of this research. In the first part of this research, turbulent flow of water and non-Newtonian fluids in horizontal annuli were investigated by using the state of the art Particle Image Velocimetry technique. Different aspects of turbulent flow such as frictional pressure losses, velocity profiles, shear stress distributions and near wall turbulent intensities were analysed.

In the second part of the study, solid transport experiments were conducted using turbulent flow of water and polymer fluids. Various flow patterns of particle transport (i.e. dunes or separated sand clusters) were identified. Critical velocity and pressure loss required for initiating particle movement in different transport mode (i.e. rolling or saltation) were determined. Effects of fluid rheology (water vs. non-Newtonian fluid) and cuttings size (fine vs. coarse particles) on the critical conditions were investigated.

## Acknowledgement

I would like to express my sincere thanks to my supervisor, Dr. Ergun Kuru, for his support, advices and supervision throughout this study. His commitment to his students and research is exemplary and greatly appreciated.

I would also like to thank the committee members, Dr. Japan Trivedi and Dr. Sina Ghaemi, for serving in my MSc final exam committee. Their time and valuable feedbacks are appreciated.

Special thanks to Mr. Fabio Ernesto Rodriguez Corredor and Mr. Todd Kinnee for their helps and insightful suggestions during experiments.

DiCorp Co. (Ciba Specialty Chemicals) is also acknowledged for donation of the polymer (Alcomer 110 RD).

This research is financially supported through the funds available from Natural Sciences and Engineering Research Council of Canada (NSERC RGPAS 411966 KURU and NSERC RGPIN 238623 KURU).

## Table of Contents

## List of Tables

## List of Figures

## Nomenclature

| | |
|---|---|
| $U(t)$ | Axial Instantaneous Velocity (m/s) |
| $V(t)$ | Radial Instantaneous Velocity (m/s) |
| $\bar{u}$ | Axial Time Average Velocity (m/s) |
| $\bar{v}$ | Radial Time Average Velocity (m/s) |
| $u'$ | Axial Fluctuation Velocity (m/s) |
| $v'$ | Radial Fluctuation Velocity (m/s) |
| $u^*$ | Friction Velocity (m/s) |
| $u_{max}$ | Maximum Velocity (m/s) |
| $U_B$ | Bulk Velocity (m/s) |
| $U$ | Time Average Velocity (m/s) |
| $u_{RMS}$ | Root Mean Square of the Axial Fluctuation Velocity (m/s) |
| $v_{RMS}$ | Root Mean Square of the Radial Fluctuation Velocity (m/s) |
| $TI$ | Dimensionless Axial Turbulent Intensity (-) |
| $TI_{Radial}$ | Dimensionless Radial Turbulent Intensity (-) |
| $C$ | Concentration (%) |
| $y$ | Vertical Distance from the Wall (m) |
| $y^+$ | Dimensionless Distance from the Wall (-) |
| $u^+$ | Dimensionless Velocity (-) |
| $\delta_v$ | Viscous Sublayer Thickness (m) |
| $\tau$ | Total Shear Stress (Pa) |
| $\tau_{Re}$ | Reynolds Stress (Pa) |

| | |
|---|---|
| $\tau_v$ | Viscous Stress (Pa) |
| $\tau_w$ | Wall Shear Stress (Pa) |
| $\tau_o$ | Wall Shear Stress on the Outer Wall (Pa) |
| $\tau_i$ | Wall Shear Stress on the Inner Wall (Pa) |
| $\tau_A$ | Weighted Average Wall Shear Stress (Pa) |
| $\varphi^*$ | Jones Shape Factor (-) |
| $\alpha$ | Radius Ratio (-) |
| $D_H$ | Hydraulic Diameter (m) |
| $d_l$ | Characteristic Length (m) |
| $N_{Re}$ | Reynolds Number (-) |
| $N_{Re}{}^*$ | Modified Reynolds Number (-) |
| $\Delta p$ | Pressure Drop (Pa) |
| $f$ | Fanning Friction Factor (-) |
| $\varepsilon$ | Roughness (m) |
| $R_1$ | Outer Radius of Inner Pipe (m) |
| $R_2$ | Inner Radius of Outer Pipe (m) |
| $R_{max}$ | Radius of Maximum Velocity (mm) |
| $R_0$ | Radius of Zero Shear Stress (mm) |
| $\xi_{max}$ | Dimensionless Radial Location of Maximum Velocity (-) |
| $\xi_0$ | Dimensionless Radial Location of Zero Shear Stress (-) |
| $\rho$ | Fluid Density ($kg/m^3$) |
| $\nu$ | Kinematic Viscosity ($m/s^2$) |

| | |
|---|---|
| $\mu_w$ | Viscosity at the Wall (Pa. s) |
| $\mu_a$ | Apparent Viscosity (Pa. s) |
| $\mu$ | Fluid Viscosity (Pa. s) |
| $\gamma_w$ | Shear Rate at the Wall (1/s) |
| K | Fluid Consistency Index (Pa. $s^n$) |
| n | Flow Behaviour Index (-) |
| $R_{ep}$ | Particles Reynolds Number (-) |
| $d_p$ | Particles Diameter (m) |
| $\tau^*$ | Dimensionless Shear Stress or Shield's Parameters (-) |
| R | Cuttings Submerged Density (-) |
| g | Gravitational Acceleration ($m^2/s$) |
| $\rho_s$ | Cutting Density ($kg/m^3$) |
| $F_D$ | Drag Force (N) |
| $C_D$ | Drag Coefficient (-) |
| $\tau_{wc}$ | Critical Wall Shear Stress (-) |
| $U_{Dunes}$ | Dunes Velocity (m/s) |
| $\Phi$ | Sedimentological Scale (-) |
| $\delta$ | Standard Deviation (-) |
| $\delta_g$ | Geometric Deviation (-) |
| Pf | Cumulative Percentage (%) |

# Chapter 1:

# Introduction

An experimental investigation of turbulent non-Newtonian fluid flow and solids transport in horizontal concentric annulus is the main subject matter of this research. In this introductory chapter, we start with an overview of the current research status in this area and give the statement of the problem. Following the overview and the statement of the problem, objectives and methodology of the research are presented. Chapter 1 is concluded by presenting the summary of the main research contributions followed by the structure of the thesis at the end.

## 1.1 Overview

Fluid flow through annular conduits has many applications in industry. One of the common examples of such flow is encountered in drilling oil and gas wells where the drilling fluid is circulated through an annuli formed by drill string and borehole. The drilling fluid, which is usually a non-Newtonian fluid in nature have many different functions, amongst them, removing the cuttings generated by drill bit is one of the most important one. A significant portion of the drilling cost is associated with drilling fluids and its additives. Studying the flow behaviour and cuttings transport ability of drilling fluids in annular geometry is, therefore, essential and hence in order to develop effective drilling hydraulics program and hole cleaning strategies, which in turn would help to minimize operational cost associated with drilling fluids applications.

Horizontal and extended reach wells are widely used in off shore and on shore drillings and more recently for exploitation of unconventional resources (i.e. in-situ oil sands development projects, shale oil and gas reservoirs). An example of that would be in SAGD (Steam Assisted Gravity Drainage) operations, where two horizontal wells need to be drilled a few meters apart from each other. Use of horizontal drillings have dramatically increased over the past decades both in terms of number of horizontal wells drilled and length of the horizontal reach of the wells, which in some cases may be 10 km long.

One of the major problems in any drilling operations is the effective removal of cuttings generated by the bit. This problem seems to have been addressed adequately for the case of vertical well drilling, but for deviated wells cutting transport is still a major problem very often resulting costly non-productive time (NPT) situations.

In drilling highly inclined and horizontal wells, if the cuttings generated by the bit are not removed and carried out effectively by drilling fluid, a bed of cuttings may form on

the lower side of the annuli due to accumulation of these cuttings. This bed of cuttings, if not removed in a timely manner, may result in costly situations such as high torque and drag, wellbore instability and pipe sticking (Figure 1-1). Even if no problem arises during drilling, later, during the casing and cementing operations, presence of a bed of cuttings could cause problems. Cleaning up the well from cuttings and carrying them out of the well is therefore, a very important function of the drilling fluid.

The problem of cutting transport in horizontal and extended reach wells have received much of attention in the past. Large experimental facilities have been built and comprehensive experimental studies have been conducted in order to improve the cutting transport ability of drilling fluids ([1][27]). Effects of many drilling operational parameters have been investigated; inclination angle[1], rheology [2], drill pipe eccentricity[4], cutting size[6] and so on. Most of these studies aim at finding a velocity (called critical velocity) at which the fluid through annuli should be circulated in order to ensure removing all the cuttings. Some mechanistic models are also available in the literature ([7] to [10]), which may be used to estimate the critical velocity or wall shear stress for effectively removing the cuttings. So far great improvement can be observed in the area of cutting transport but there are still many problems remained to be resolved, one of which is effective removal of fine particles in the annuli which have not received that much of attention as larger cuttings had.

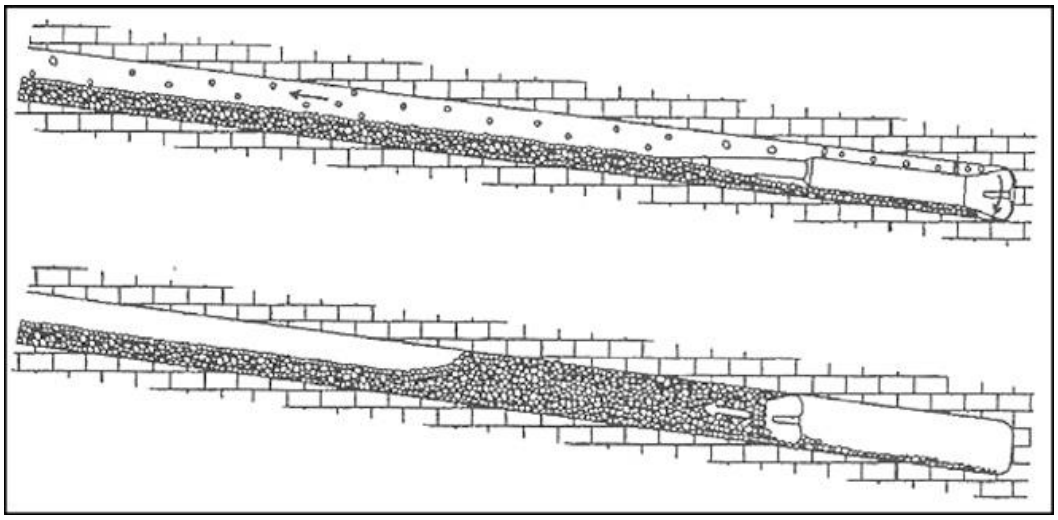

**Figure 1-1 Pipe Sticking during Tripping Due to Poor Well Cleaning[1]**

[1] Picture from Ramadan et.al [8]

A common practice in cuttings transport in horizontal and inclined wells is to pump the fluid in the annuli at as high rate as possible to ensure cuttings are removed effectively. This approach may be applicable in drilling wells of short horizontal or inclined sections, but when a long well is to be drilled, dynamic pressure losses would become excessively high and ultimately, either we reach to the limit of pump pressure capacity or dynamic bottom hole pressure could reach to the limit of rock fracture pressure. In any case, this would be the end point of drilling capability. In order to enhance the drilling of horizontal and extended reach wells in terms of both minimizing the cost and maximizing the length that can be drilled, cutting transport needs to be enhanced in terms of velocity and pressure loss.

A good understanding of the flow behaviour of drilling fluids through annuli is essential for effectively studying the problem of cutting transport. Investigation of fluid flow through annuli without consideration of cuttings has been the subject of many experimental studies in the past ([31] to[60]). The annular geometry causes unique problems which are difficult to study. Early studies focused on the flow of Newtonian fluids ([31]to[48]), but with the introduction of new techniques such as LDA (Laser Doppler Anemometry) and PIV (Particle Image Velocimetry) increased the number of studies have been conducted using non-Newtonian fluids ([49]to[60]).

Velocity profiles especially close to wall, where the drilled solids tend to settle in drilling operations, shear stresses which are important in removing the cuttings from a bed of particles, frictional pressure drops, and annuli configuration effect (radius ratio) all have been the subject of interest in many studies.

## 1.2 Statement of the Problem

Studying the behaviour of flow through annuli is associated with many difficulties which arise from the specific geometry of interest. Fluid flow through round tubes is symmetric and so behaviour would be similar in each half of the pipe[33] , [59]) while flow in annuli is not symmetric. Existence of turbulence or transitional flow regime exacerbate the difficulties as there is no theoretical solutions available for these flow regimes and only experimental and numerical simulation could be used to study the behaviour of the flow. Experimentation and simulation are associated with many obstacles themselves; simulation of the flow is limited to lower Reynolds numbers and is very time consuming, experiments needs accurate measurement tools and facilities and

the results most often is affected by the experimental set-up which are used. When a non-Newtonian fluid is to be examined, the problem becomes even worse as a higher level of difficulties is introduced by the complex rheological characteristics of these fluids. Finally, as sound measurement and flow visualization technology such as Particle Image Velocimetry are evolving rapidly, studying the behaviour of flow especially in the turbulent flow becomes easier and more accurate experiments could be carried out which may help in resolving problems, which have not been addressed properly in the past. In this section, we try to mark the problems associated with the flow in annuli, different results of the past studies are briefly cited to show the level of uncertainties in the measured parameters; this will automatically explain the problems, which may need further investigation.

Friction factor is one of the parameters, which almost in every single study of fluid flow in any geometry has been measured and discussed; this in fact facilitates the comparison of different flows in term of pressure losses. For Newtonian fluids, flow through pipes or channel of both smooth and rough walls, the correlations of friction factors are well-known and accepted among the investigators[31][32] [34]. For friction factor of flow in through annuli, on the other hand, there is no correlation which is wieldy accepted like pipe or channel flow. One of the reasons for the differences in friction factors for annular flow reported in the literature is the geometry of annuli in terms of radius ratio; while some investigators have found the friction factor to be a function of radius ratio[35] [36], some others found it independent of that[37]. Almost in all the studies with Newtonian fluid flow, friction factor has been reported to be higher than a pipe of equivalent diameter[35][36][38]. In studies with non-Newtonian fluids, the only common point in different studies is that they all have reported a reduction in friction factor of turbulent flow when polymeric liquids are used ([56] to [60]) but there is no unique correlation, which best represents the friction factor of all the results available. For polymeric liquids flow in pipes, there has been reported a correlation[51] for friction factor which is for the condition of maximum drag reduction. For conditions different than that there is no correlation and, therefore, friction factor has to be measured experimentally. Overall, although friction factor for flow of Newtonian fluids have been investigated and some correlations for flow in annuli have been reported[46] which are to some extent well accepted, but for the case of non-Newtonian fluids there is no unique correlation available. When a non-Newtonian fluid is examined, depending upon the

operational conditions, the friction factor may vary and only experimentally measured values can be reliable in such condition.

Another aspect of any wall bounded flow is the behaviour of the flow in the vicinity of the solid surfaces which is called the boundary layer. Velocity profiles in the boundary layer for flow of Newtonian fluids in through pipes, channels and plate flows have been studied and exact behaviour is known [31] [32]. Non-Newtonian fluid flow, on the other hand, has not been studied as much and similar to friction factor, the velocity profile is different in any experiments depending on operational conditions of that experiment. For flow in annuli many studies have confirmed the validity of the universal law of the wall in the immediate region next to the wall which is called the viscous sublayer [38][44][57][60]. For outer regions of the flow, however, the results differ for different authors even for Newtonian fluids. The difference sometimes is in the constants of logarithmic law [36][56][59], which governs the velocity profile and in some instances major deviation from the logarithmic law has been reported[36]. There are few studies, which have investigated the flow of non-Newtonian fluids in annuli and it has been found that velocity profiles are different in any experiments based on the fluid type and flow conditions[51]. Generally, from the data reported in the literature for flow of Newtonian fluids in annuli, it is expected that velocity profile to follow the universal law of the wall in the sublayer and a logarithmic law in the outer region (similar to that of governs the flow in pipes). For non-Newtonian fluids, it is known that universal law of the wall must be satisfied in the sublayer, but in the logarithmic zone major deviation from the Newtonian fluid law has been observed and reported [51][56][57][59] , which need further investigation.

When a flow in pipe is encountered, symmetry could be assumed, which assures that maximum velocity occurs at the center point of the pipe[33]. Flow in annuli is no longer symmetric as strong asymmetry in velocity profile has been observed and reported[35]-[44]. Radial location of velocity maximum has been of interest in many studies regarding annular geometry, but rather different and in some cases opposite results have been reported. The differences arise from variations in experimental setups (i.e., radius ratios). While some authors have found radius of maximum velocity to be similar for laminar flow and turbulent flow[35][40] , some others reported that this radius is less for turbulent flow[37] [39] . Some studies revealed that radius of maximum velocity depended upon radius ratio of the annuli[37] or the Reynolds number[40] of the flow while some others

suggesting it is independent of such parameters in fully developed laminar or turbulent flows[42]. Some authors have reported a change in the radial location of maximum velocity in the transitional flow regime while it is fixed in laminar and turbulent regime[40][42]. In general, the only point at which all the studies for fluid flow in annuli agree is that velocity profile is not symmetric and maximum velocity is biased toward one of the walls of the annuli which have been found to be the inner pipe wall. Radial location of maximum velocity needs further investigation especially for non-Newtonian fluids to see if this radius is a function of Reynolds number or if it is different for different fluids; these are some of the questions which are not answered in the literature.

Flow in annuli is no longer symmetric and unlike pipe flow where maximum velocity and zero shear stress occur at the mid-point of the pipe[33][59][60], in annuli they are biased towards the inner pipe wall. Now the question to be answered is that, is zero shear stress and maximum velocity coinciding in annular flow? For a symmetric flow like pipe these two radiuses are the same[59]. Although earlier investigation with Newtonian fluids flow in annuli have all assumed the coincidence of zero shear stress and maximum velocity [38] [40], it has been shown experimentally that these radiuses are not necessarily the same[36]. In addition, it has been reported that zero shear stress occurs closer to the inner wall of the annuli[36][44]. The issues associated with the radial location of zero shear stress are similar to those with radial location of maximum velocity; dependency of this radius on Reynolds number or radius ratio needs to be clarified. The additional problem here is that, is the radius of maximum velocity and zero shear stress different? The question seems to be answered for Newtonian fluids flow where it has been reported that the zero shear occurred closer to inner wall[36][44]. For non-Newtonian fluids there is no study available which have measured and reported the location of zero shear stress but with the aid of new techniques such as PIV or LDA measurement of this radius might be possible.

Due to difficulties in experimenting with turbulent flow especially in annuli, turbulent statistics have been the subject of interest only in few studies [45][56],[59]. Although arrival of LDA and PIV seems to have speeded up the investigation of turbulence, further investigations in this respect still need to be conducted. It has been reported that axial intensities is somehow higher around the outer pipe wall of the annuli[45][59]. Comparing to Newtonian fluids, whenever a drag reducing polymer is used a reduction in the radial intensities of the flow occur [45][56][59]. So far there are

very few studies on the subject of turbulent statistics in annular flow and further investigations are needed in studying the behaviour of flow in this type of geometry.

Generally, turbulent flow in annuli needs to be investigated more accurately specially for flow of non-Newtonian fluids. Friction factor for flow of non-Newtonian fluids has to be measured experimentally as there is no correlation available for these fluids. For Newtonian fluids there are correlations available, which may be used in order to validate the experimental results. Universal law of the wall can be used as the reference for the accuracy of measured velocity profiles. For flow in the outer region, there are no unique correlations available for velocity profile and further investigation is necessary. Radial locations of maximum velocity and zero shear stress are one of the issues associated with flow of non-Newtonian fluids, which have not been addressed properly and hence requires more study. At the end, the availability of accurate measurement techniques encourage investigators to examine other aspects of turbulence, which may not been of the subject of experiment in the past.

The use of directional and horizontal drilling technique has dramatically increased over the past decades but well cleaning still remained a challenge especially when an extended reach well with a long horizontal or inclined section is to be drilled. Although the problem seems to be addressed adequately for vertical drilling, in deviated wells, poor well cleaning often results in costly non-Productive time (NPT) situations. Pipe sticking have been found to contribute up to 70% of the unscheduled events[28] and it has been reported that one third of all pipe sticking cases resulted from poor well cleaning[29]. It was reported that [30], pipe sticking could cost somewhere between 100 to 500 million US dollars per year. Efficient well cleaning strategies and hydraulics have to be developed, which would help in reducing costs associated with well cleaning and also it would facilitate drilling longer directional wells.

There are many parameters, which affect the cutting transportation capacity, these parameters according to Bilgesu[11] could be categorized into three main groups : fluid parameters, cuttings related factors and operational variables. Numerous experimental and simulation works have been conducted to study the effect of each of these parameters[1] -[27]. Many theoretical and semi-theoretical models have been developed and proposed.

Since the focus of the presented research is on the effect of fluid rheology in transporting solids in horizontal concentric annuli, a brief review of the results of experiments on effect of rheology and also cutting size may help in understanding the problem. In fact citing the effects of other parameters are irrelevant since they have not change during the course of this study.

Effect of rheology has been extensively studied but there is no agreement on that. Some studies suggest that medium viscosity mud is superior to low and high viscosity muds in inclined wellbores[21]. Due to suppression of turbulence, high viscosity mud has been found to have a detrimental effect on cutting transport in high angle wells[2]. The same study has also reported although turbulence is favorable in horizontal annuli, the transport capacity mainly depends upon fluids density and not rheology[2]. Tomren[1] found the viscosity effect to be a function of flow regime; in laminar flow regime higher viscosity fluids always perform better and in turbulent flow both low and high viscous fluids are same with a small advantage of high viscosity fluid over low viscosity fluid. Kelessidis et.al [19] study have shown that rheology in fact has a minimal effect on cutting transport while another study suggested maintain correct rheology is of great importance[16]. Nguyen et.al[4] study has led to the conclusion that increasing the viscosity will enhance the cutting transport and in contrast ,Azar et.al[5] have reported increase in viscosity causes a decrease in hole cleaning ability. Results of a three layer bed model proposed by Cho et.al [23]have suggested that an increase in the flow behaviour index would result in a thicker bed deposits , which is stationary. In a recent study, Duan[6] stated that small cuttings are easier to transport with PAC solution over water, which means a positive effect of higher viscosity for transporting finer particles.

Parameters which affect the cutting transport ability and are related to cuttings are size, shape and density of the cuttings [11]. Most of these parameters are not controllable such as density which is most of the times around 2650 $kg/m^3$ [5]. Size and shape of the cuttings depends on the type of the bit and the formation. Most of the studies, which have considered the cuttings size effect have reported that small cuttings are more difficult to transport ([2], [6] and [21]). Duan et.al[6] have shown that when water is used smaller cuttings are more difficult to remove but when a solution of PAC is used small cuttings are easier to transport than large cuttings.

From the reported results in the literature, a rather ambiguous picture of the effect of rheology or cuttings size form in the readers mind. Apparently although some remedies for the problem of cuttings transport have been suggested, they are case sensitive and may vary in another situation. The problem is yet to be investigated properly and effect of each parameter still need to be clarified.

## 1.3 Objectives and Tasks

The ultimate goal of this study as the title of the thesis implies, has been investigation of solid transport in horizontal annuli using non-Newtonian fluids. A large scale flow loop has been used in order to simulate flow through horizontal annuli, which is analogous to horizontal drilling case. Overall, this research is an experimental study of cuttings transport with non-Newtonian fluid flow through horizontal concentric annuli which concerns turbulent flow in annuli. The goal is to find the critical condition for initiation of motion of cuttings. The effect of fluid rheology and cuttings size is to be investigated with turbulent flow.

The current work can be divided into two main parts: in the first part, turbulent flow in concentric annuli will be investigated and in the second part, using the knowledge acquired in the first part of the research, transportation of cuttings deposited on the low side of the annuli will be studied. The first phase of the experiments is essential in studying the mechanism of solid transport.

In the first phase of the research, turbulent fluid flow in annuli will be examined by using Particle Image Velocimetry technique. Main objectives of this phase of the research are to get more insight about turbulent flow of non-Newtonian fluids flow through annuli. The problems associated with regard to annular flow, which have been explained previously in the statement of the problem section, are all to be investigated.

One very first task in the first phase of the experiments is to implement the state of the art PIV technique for using with annuli, which have not been done in the past. There are several challenges associated with that; with the most difficult part being camera calibration.

Second task is to find and select a non-Newtonian fluid, which satisfies two important conditions. First it must be transparent for use with PIV and secondly the

properties of the fluid must be as close as possible to a real drilling fluid (i.e. shear thinning polymeric liquids).

Once the fluid is selected, next task is to consider the limitation of the experimental facility in term of pump capacity and according to that select the proper concentrations of the polymer which satisfies two conditions; first the flow must be turbulent and second the viscosity of the fluid must be as high as possible. In another word, the fluid should show a strong non-Newtonian behaviour in term of flow behaviour index and at the same time, turbulent flow must be achievable.

With the knowledge of turbulent fluid flow in annuli acquired from past studies, the following aspects of annular flow are the primary tasks of the first phase of the experiments with PIV.

- ✓ Measurement of frictional pressure drops for different fluids and comparing the results with available correlations
- ✓ Measuring near wall velocity distribution for different fluids and for both walls of the annuli
- ✓ Investigating radius of maximum velocity in the annuli and its dependency on Reynolds number for different fluids
- ✓ Measuring Reynolds stress profiles for Newtonian and non-Newtonian fluids and different Reynolds numbers
- ✓ Measuring viscous stress profiles for Newtonian and non-Newtonian fluids and different Reynolds numbers
- ✓ Investigating radius of zero shear stress and it is dependency on Reynolds number for different fluids
- ✓ Assessment of turbulent statistics such as turbulence intensities
- ✓ Comparison of the results with theoretical and experimental results to validate the measurements
- ✓ Comparison of non-Newtonian and Newtonian fluids turbulent flow

The mentioned objectives for PIV experiments are the primary targets of the experiments in this phase of the project. The results of PIV experiments may be analysed for further investigation of turbulent flow (other aspect of turbulence such as dissipation and production of turbulent energy may be obtained from PIV experiments).

Second phase of the experiments are those related to solid transport in annular configuration. There are few tasks, which need to be accomplished before starting the experiments of this phase of the project.

First task is to find and select proper particles. Two diameters are to be examined and they must be selected properly which satisfies a few conditions. Firstly, except the diameter, all other properties such as density must be the same. Secondly, one diameter should be representing fine particles (small cuttings) and the other particles diameter must be in the range of big cuttings (limitations of the flow loop must be taken into account in selecting particles diameter as well). Third condition is the uniformity of the particles which are to be used. Particles must be uniform in term of diameter, if not, through sieving particles size distribution must be narrowed down to obtain a uniform sample. Also it is desirable to conduct the experiments with natural particles which are not spherical and density is close to real drilling cuttings.

Second task in this phase of the experiments is to design a measurement technique for monitoring the statues of the bed of particles. The critical velocity at which particles start moving is to measured, and so accurate measurement technique must adopted.

For the solid transport experiments, the primary targets of the experiments may be summarized as follow:

- ✓ Investigation of critical condition require for initiating particle movement sitting on a bed by using different fluids
- ✓ Measurement of frictional pressure drop associated with cuttings transport using different fluids
- ✓ Investigation of effect of viscosity of non-Newtonian fluids on cutting transport and critical velocity
- ✓ Investigation of the effect of particle diameter on critical conditions (velocity, pressure drop) to be satisfied to initiate particle movement
- ✓ Developing models for critical conditions of particle movement and validating models with experimental results

In general, the key goal of the presented work has been the investigation of non-Newtonian fluids flow in through annuli and also their influence on solids transport in horizontal concentric annuli.

## 1.4 Methodology

Flow visualization techniques are the most powerful tools in experimenting in fluid mechanics. The advantage of these techniques over probe techniques such as Pitot tubes or hot wire anemometry (Figure 1-2) is that they are non-intrusive, which means they don't disturb the flow. These techniques are also superior to Ultra-Sonic Velocimetry techniques because they can be used to study the structures of the flow in 2 or 3 dimension. Particle Image Velocimetry technique is a relatively new measurement technique, which has found many applications in fluid mechanics in the past decade. PIV has been the main tool of measurements used in the present study.

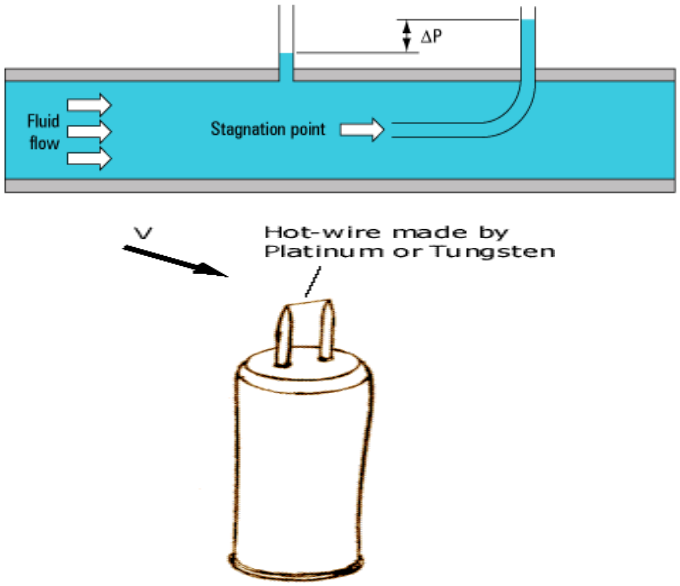


**Figure 1-2 Schematic of Working Principles of Pitot tube and Hot Wire Anemometry**[2]

The experimental work in the present thesis has been divided into two separate but not irrelevant phases. In phase one of the experiments, turbulent flow of Newtonian and non-Newtonian fluids has been studied carefully. The structures of turbulent flow have been investigated using one of the most powerful tools in flow visualization field which is referred as PIV or Particle Image Velocimetry technique. Different aspects of turbulent flow such as velocity profiles close to solid surfaces, distribution of shear stress, radiuses

[2] Pictures From http://www.efunda.com/designstandards/sensors/hot_wires/hot_wires_intro.cfm http://www.spiraxsarco.com/resources/steam-engineering-tutorials/flowmetering/principles-of-flowmetering.asp

of velocity maximum and zero shear stress and also turbulent intensities all have been examined for flow of different types of fluids. Since in most drilling operations polymeric liquids are used, in an attempt of simulating a real drilling fluid, a polymer additive which is commonly used in drilling fluid as an additive has been used as the non-Newtonian fluid.

Transportation of solids in horizontal annuli was investigated in the second phase of the project. Since PIV is no longer applicable for experiments in this phase, a different measurement technique has been developed and used. A high speed, high resolution camera and a light source have been used in order to track down particles movement in the annuli. This is helpful in finding the critical condition at which particles start to move along the bed.

The issues associated with cutting transport in highly deviated wells have been briefly addressed in previous sections. Since there are many different parameters involved, not all of these parameters could be investigated. The experiments have carried out in order to check the effect of different fluids in term of rheology on cutting transport. Also cuttings of two different sizes have been used which could be categorized into fine particles and coarse particles. Overall, the effect of rheology and to some extent effect of cutting size on critical condition for initiation of particles motion have been investigated in this part of the research and as a result a model has been developed which could be used in prediction of conditions required for an effective solid transport condition in horizontal annuli.

## 1.5 Contributions of the Research

The present study aimed in studying solid transport through concentric annuli using turbulent flow. Determining the effects of rheology and turbulence on cutting transport ability have been the goals of the research. It has been mentioned in the objectives of the research that the experimental work in this project has been divided in two phases. First phase investigates the turbulent flow in annuli by using PIV technique. Major contributions of this phase of the research could be summarized as follow:

- ✓ Examination of different aspects of turbulent flow such as frictional pressure losses, velocity profiles, shear stress distribution and turbulent intensities for flow of Newtonian and non-Newtonian fluids in through concentric annuli by implementation of PIV technique

The results from this part of the research are useful in interpreting and understanding the phenomenon which occurs in solid transport experiments. As it will be discussed, the results from these experiments will help in developing an experimental model for predicting critical condition for initiating cuttings movement. Additionally, the results of these experiments increase our knowledge of turbulent flow in annuli measured with PIV which have not been done in the past. Other possible uses and contributions of the results are in other industries (i.e. food processing) where fluids flow through annular geometries are encountered.

In the second phase of the research, transportation of solids in annuli has been examined. The main goal was to find the critical velocity at which particles start to move when different fluids and different particles are used. Major contribution of this part of the research may be summarized as follow:

- ✓ Investigation of the effects of fluid rheology and cuttings size on critical conditions (velocity and wall shear stress) for initiating different types of particles movement (i.e. rolling, saltation and suspension)

Although only two variables which affect cutting transport (rheology and cutting size) have been studied, but the results of these experiments are useful in enhancing our knowledge of solid transport in concentric horizontal annuli. The results may be used to validate simulation works. Other possible use of the results from solid transport experiments are mainly in drilling and slurry transport industries (such as mineral transportation).

## 1.6 Structures of the Thesis

The presented work is the results of an experimental study which concerns on the topic of cutting transport in horizontal annuli. In this section a brief introductory on each chapter of the thesis is given.

Literature review and background is the title of the second chapter which is dedicated to past studies relevant to the current work. Turbulence is briefly explained at the beginning of the chapter; very basic information about turbulence is cited which is useful in the results and discussion section with interpretation of data. Pertinent studies on flow through annuli for Newtonian fluids are discussed in section two of this chapter. Similar to section two, relevant studies for flow of non-Newtonian fluids is summarized in the

third section of the chapter 2. Literature review on the problem of cutting transport is included in the last section of chapter 2.

Chapter 3 discusses the experimental setup and procedures, which have been followed to obtain the results of the presented work. Detailed information on measurement instruments and techniques were provided.

Chapter 4 of the thesis contains the discussion on PIV (Particle Image Velocimetry) technique. In this chapter fundamentals and basics of imaging technique was explained. The proper installation and use of 2-D PIV was also discussed. Processing and post-processing of PIV images were explained step by step.

Since the focus of this study was on non-Newtonian fluids, chapter 5 has been dedicated to study the behaviour of the fluids which have been used in the experiments. Properties of the polymer additive along with proper instruction in preparing the fluid were reported in this chapter. Rheology measurements and rheology models were all reported in this chapter. Particle size distribution analysis on the sand particles used in solid transport experiments was included at the end of this chapter as well.

Results and discussion of PIV experiments comes in chapter 6. In this chapter results of experiments which concerns turbulent fluid flow in through annuli were reported. The results were reported for Newtonian fluids and non-Newtonian fluids separately and at the end of this chapter comparison between these fluids was given.

Cutting transport experiments, the results for these experiments were reported in chapter 7. Performance of different fluids in removing particles from a bed of particles formed on the low side of the annuli was compared. Effect rheology was investigated and also particles size effect was discussed to some extent.

The last chapter in this thesis includes the most important findings of the experiments reported in chapters 6 and 7 and also recommendations for future work. Structure of conclusion remarks was also similar to results and discussion chapters; first the results of PIV experiments were summarized and then the results of cutting transport experiments.

## 1.7 References


[1]. Tomren P. H., Iyoho A. W., Azar J. J., 1986, "Experimental Study of Cuttings Transport in Directional Wells", Presented at the 1983 SPE Annual Technical Conference and Exhibition held in San Francisco, SPE 12123

[2]. Okrajni S. S., Azar J. J., 1986, "The Effects of Mud Rheology on Annular Hole Cleaning in Directional Wells", Presented at the 1985 SPE Annual Technical Conference and Exhibition held in Las Vegas,, SPE 14178

[3]. Pilehvari A. A., Azar J. J., Shirazi S. A., 1999, "State-of-the –Art Cuttings Transport in Horizontal Wellbores" , SPE Drilling and Completion 14 (3), SPE 57716

[4]. Nguyen D., Rahman S. S., 1996, "A Three-Layer Hydraulic Program for Effective Cuttings Transport and Hole Cleaning in Highly Deviated and Horizontal Wells", Presented at IADC/SPE Asia Pacific Drilling Technology Conference, Kuala Lumpur, Malaysia

[5]. Azar J. J., Alfredo R., 1997, "Important Issues in Cuttings Transport for Drilling Directional Wells", Presented at the Fifth Latin American and Caribbean Petroleum Engineering Conference and Exhibition held in Rio de Janeiro, Brazil, August 1997, SPE 39020

[6]. Duan M., Miska S., Yu M., Takach N., Ahmed R., Zettner C., 2008, " Transport of Small Cuttings in Extended-Reach Drilling", SPE Drilling and Completion, SPE 104192

[7]. Gavignet A. A., Sobey I. J., 1989, "Models Aids Cuttings Transport Prediction", Journal of Petroleum Technology

[8]. Ramadan A., Skalle P., Johansen S. T., 2003, " A Mechanistic Model to Determine the Critical Flow Velocity Required to Initiate the Movement of Spherical Bed Particles in Inclined Channels", Chemical Engineering Science, Vol. 58, pp. 2153-2163

[9]. Clark R. K., Bickham K. L., 1994, " A Mechanistic Model for Cuttings Transport", Presented at SPE 69$^{th}$ Annual Technical Conference and Exhibition held in New Orleans, LA, U. S.A., September 1994 , SPE 28306

[10]. Wang Z. M., hao X. N., Guo X. L., Zhai Y. J., Sun L. L., 2011, " A Study on the Thickness of Cutting Bed Monitor and Control in an Extended Reach Well", Petroleum Science and Technology, Vol.29, No.13, pp. 1397-1406

[11]. Bilgesu H. I., Mishra N., Ameri S., 2007, "Understanding the Effects of Drilling Parameters on Hole Cleaning in Horizontal and Deviated Wellbores Using Computational Fluid Dynamics", Presented at the 2007 SPE Eastern Regional Meeting held in Lexington, Kentucky, U.S.A., October 2007, SPE 111208

[12]. Cleaver J. W., Yates B., 1972, "Mechanism of Detachment of Colloidal particles from a Flat Substrate in a Turbulent Flow", Journal of Colloid and Interface Science, Vol. 44, No. 3, pp. 464-474

[13]. Rabenjafimanantosa H. A., 2007, "Particle Transport and Dynamics in Turbulent Newtonian and Non-Newtonian Fluids", PHD Dissertation, University of Stavanger

[14]. Yu M., Melcher D., Takach N., Miska S. Z., Ahmed R., 2004, " A New Approach to Improve Cuttings Transport in Horizontal and Inclined Wells", Presented at the SPE Annual Technical Conference and Exhibition held in Houston, U.S.A, September 2004, SPE 90529

[15]. Lockett T. J., Richardson S. M., Worraker W. J., 1993, " The Importance of Rotation Effects for Efficient Cuttings Removal During Drilling", Presented at SPE/IADC Drilling Conference held in Amsterdam February 1993, SPE/ IADC 25768

[16]. Payne M. L., Cocking D. A., Hatch A. J., 1994, " Critical Technologies for Success in Extended Reach Drilling", Presented at SPE 69th Annual Technical Conference and Exhibition held in New Orleans, LA, U. S.A., September 1994, SPE 28293

[17]. Thomas R. P., Azar J. J., 1982, "Drillpipe Eccentricity Effect on Drilled Cuttings Behavior in Vertical Wellbores", Journal of Petroleu, Technology, Vol. 34, No. 9, pp. 1929-1937

[18]. Ford J. T., Peden J. M., Oyeneyin M. B., Gao E. Zarrough R., 1990, "Experimental Investigation of Drilled Cuttings Transport in Inclined Boreholes",

Presented at the 65th Annual Technical Conference and Exhibition of the Society of Petroleum Engineers held in New Orleans, LA, September 1990, SPE 20421

[19]. Martins A. L. et.al, 1992, " Evaluation of Cutting Transport in Horizontal and Near Horizontal Wells-A Dimensionless Approach", presented at the Second Latin Amencan Petroleum Engineering Conference, II LAPEC, of the Society of Petroleum Engineers held in Caracas, Venezuela, March 1992, SPE 23643

[20]. Kelessidis V. C., Bandelis G. E., 2004 " Flow Patterns and Minimum Suspension Velocity for Efficient Cuttings Transport in Horizontal and Deviated Wells in Coiled-Tubing Drilling", SPE Drilling and Completion, SPE 81746

[21]. Larsen T. I., Pilehavri A. A., Azar J. J., 1997, "Development of a New Cuttings-Transport Model for High-Angle Wellbores Including Horizontal Wells", SPE Drilling and Completion, SPE 25872

[22]. Phillips M., 1980, "A Force balance Model for Particle Entrainment into a Fluid Stream", Journal of Physics D: Applied Physics, Vol. 13, pp. 221-233

[23]. Cho H., Shah N., Osisanya S. O., 2000, " A Three-Layer Modeling for Cuttings Transport with Coiled Tubing Horizontal Drilling", Presented at the 2000 SPE Annual Technical Conference and Exhibition held in Dallas, Texas, October 2000 , SPE 63269

[24]. Walker S., Li J., 2000, "The Effects of Particle Size, Fluid Rheology, and Pipe Eccentricity on Cuttings Transport", SPE/ICoTA Coiled Tubing Roundtable, April 2000, Houston, Texas, SPE 60755

[25]. Peden J. M., Ford J. T., Oyeneyin M. B., 1990, "Comprehensive Experimental Investigation of Drilled Cuttings Transport in Inclined Wells Including the Effects of Rotation and Eccentricity", European Petroleum Conference , 21-24 October 1990, The Hague, Netherlands, SPE 20925

[26]. Li J., Walker S., 1999, "Sensitivity Analysis of Hole Cleaning Parameters in Directional Wells", SPE/ICoTA Coiled Tubing Roundtable, 25-26 May 1999, Houston, Texas, SPE 54498

[27]. Sifferman, T.R., Becker, T.E., 1992, “Hole Cleaning in Full-Scale Inclined Wellbores”, SPE Drilling Engineering, Vol. 7, No. 2, pp. 115-120

[28]. Massie G. W., Castle-Smith J., Lee J. W., Ramsey M.S., 1995, “Amoco's Training Initiative Reduces Wellsite Drilling Problems”, Petroleum Engineer International; Vol. 67, No. 3

[29]. Hopkins C. J., Leicksenring R. A., 1995, “Reducing the Risk of Stuck Pipe in the Netherlands”, SPE/IADC Drilling Conference, 28 February-2 March 1995, Amsterdam, Netherlands, SPE 29422

[30]. Bradley W. B., Jarman D., Plott R. S., Wood R. D., Schofield T. R., Auflick R. A., Cocking, D., 1991, “A Task Force Approach to Reducing Stuck Pipe Costs”, SPE/IADC Drilling Conference, 11-14 March 1991, Amsterdam, Netherlands, SPE 21999

[31]. Kundu P. K., Cohen I. M., 2010, “Fluid Mechanics”, 4th edition

[32]. Pope S. B., 2002, “Turbulent Flows”, Cambridge University Press

[33]. Pinho F. T., Whitelaw J. H., 1990, “Flow of Non-Newtonian Fluids in Pipe”, Journal of Non-Newtonian Fluid Mechanics, Vol. 34, pp. 129-144

[34]. Colebrook, C. R., 1939, "Turbulent flow in pipes with particular reference to the transition region between the smooth and rough pipe laws," J. Inst. Civ. Eng. (London), Vol. 11, pp. 133-156.

[35]. Rothfus R. R., Monard C. C., Senecal V. E., 1950, “Velocity Distribution and Fluid Friction in Smooth Concentric Annuli”, Industrial and Engineering Chemistry, Vol. 42, No.12, pp. 2511- 2520

[36]. Lawn C. J., Elliot C. J., 1972, “Fully Developed Turbulent Flow through Concentric Annuli”, Journal of Mechanical Engineering Science, Vol. 14, No.3, pp. 195-204

[37]. Quarmby A.,1967, “An Experimental Study of Turbulent Flow through Concentric Annuli”, Journal of Mechanical Science, Vol. 9, pp. 205-221

[38]. Brighton J. A., Jones J. B., 1964, "Fully Developed Turbulent Flow in Annuli", Journal of Basic Engineering, 86, 835-842

[39]. Rothfus R. R, Sartory W. K., Kermode R. I., 1966, "Flow in Concentric Annuli at High Reynolds Numbers", A.I.Ch.E. Journal, Vol. 2, No. 6, pp. 1086-1091

[40]. Walker J. E., Rothfus R. R., 1959, "Transitional Velocity Patterns in a Smooth Concentric Annulus", A.I.Ch.E Journal, Vol. 5, No. 1, 51-54

[41]. Clump C. W., Kwasnoski D., 1968, "Turbulent Flow in Concentric Annuli", A.I.Ch.E. Journal, Vol. 14, No. 1, pp. 164-168

[42]. Hanks R. W., Bonner W. F., 1971, "Transitional Flow Phenomena in Concentric Annuli", Industrial & Engineering Chemistry Fundamentals, Vol. 10, No.1, pp. 105-113

[43]. Lee Y., Park S. D., 1971, "Developing Turbulent Flow in Concentric Annuli: An Analytical and Experimental Study"

[44]. Rehme K., 1974, "Turbulent flow in smooth concentric annuli with small radius ratios", Journal of Fluid Mechanics", Vol. 64, part 2, pp. 263-287

[45]. Rehme K., 1975, "Turbulence measurements in smooth concentric annuli with small radius ratios", Journal of Fluid Mechanics, Vol. 72, part 1, pp. 198-206

[46]. Jones O. C., Leung J.C.M., 1981, "An Improvement in the Calculation of Turbulent Friction in Smooth Concentric Annuli1", Journal of Fluid Engineering, Vol. 103, pp. 615-623

[47]. Ahn S. W., Kim K. C., 1999, "Characteristics of Turbulent Flow in the Annuli with Smooth and Rough Surfaces", KSME International Journal, Vol. 13, No. 2, pp. 183-190

[48]. Dou H. S., Khoo B. C., Tsai H. M., 2010, "Determining the Critical Condition for Flow Transition in a Full-Developed Annulus Flow", Journal of petroleum Science and Engineering", Vol. 71

[49]. Fredrickson A. G., Bird R. B., 1958, "Non-Newtonian Flow in Annuli", Industrial and Engineering Chemistry, Vol. 50, No. 3, pp. 347-352

[50]. Dodge D. W., Metzner A. B., 1959, “Turbulent Flow of Non-Newtonian Systems”, A.I.Ch.E. Journal, Vol. 5, No. 2, pp. 189-204

[51]. Virk P. S., Mickley H. S., Smith K. A., 1970, “The Ultimate Asymptote and Mean Flow Structure in Toms' Phenomenon”, Journal of Applied Mechanics, 1970, pp. 488-493

[52]. Bird R. B., 1976 “Useful Non-Newtonian Models”, Annual Review. Fluid Mechanics, Vol. 8, pp. 13-34

[53]. Zakin J. L., Ni C. C., Hansen R. J., 1977, “Laser Doppler Velocimetry Stduies of Early Turbulence”, The Physics of Fluids, Vol. 20, No. 10, pp. 85-88

[54]. Hanks R. W., Larsen K. M., 1979, “The Flow of Power-Law Non-Newtonian Fluids in Concentric Annuli”, Industrial and Engineering Chemistry, Vol. 18, No. 1, pp. 33-35

[55]. Luo Y., Peden J. M., 1990, “Flow of Non-Newtonian Fluids through Eccentric Annuli”, SPE Production Engineering, Vol. 5, No.1, SPE 16692

[56]. Nouri J. M., Umur H., Whitelaw J. H., 1993, “Flow of Newtonian and Non-Newtonian Fluids in Concentric and Eccentric Annuli”, Journal of Fluid Mechanics, Vol. 253, pp. 617-641

[57]. Escudier M. P., Gouldson I. W., Jones D. M., 1995, “Flow of Shear-Thinning Fluids in Concentric Annulus”, Experiments in Fluids, Vol. 18, pp. 225-238

[58]. Escudier M. P., Oliveira P. J., Pinho F. T., Smith S., 2002, “Fully Developed Laminar Flow of Non-Newtonian Liquids through Annuli: Comparison of Numerical Calculations with Experiments”, Experiments in Fluids, Vol. 33, pp. 101-111

[59]. Japper-Jaafar A., Escudier M. P., Poole R. J., 2010, “Laminar, Transitional and Turbulent Annular Flow of Drag-Reducing Polymer Solutions”, Journal of Fluid Mechanics, Vol. 165, pp-1357-1372

[60]. Japper-Jaafar A., Escudier M. P., Poole R. J.,2009, “Turbulent pipe flow of a drag reducing, rigid “rod-like” polymer solution”, Journal of Non-Newtonian Fluid Mechanics, Vol.161,pp.86–93

# Chapter 2:

# Literature Review and Background

In this chapter a brief review of past works and studies on the subject related to turbulent flows through annuli and cutting transport is given. At the beginning of the chapter, Turbulence is discussed very shortly and basic definitions and fundamentals of turbulence are given. This is necessary throughout this work as many of these definitions will be used later.

Second part of this chapter is dedicated to works which have been done on the topic of Newtonian fluids flow through annuli. This is quite useful in many ways. First of all this is directly related to some of the results presented in this work which would facilitate comparison. Second of all it will give the readers a good idea of the problems associated with the geometry and experimental procedures for obtaining good quality data.

Non-Newtonian fluids are discussed in the third part of this chapter. Although most of the works for fluid flow though annuli has been done using Newtonian fluids or laminar flow of non-Newtonian fluids, but yet there are many studies which have been focused on non-Newtonian fluids not only in annuli's but in pipes as well which are cited in brief in this section.

Particle entrainment in turbulent flows and cutting transport in drilling operation is the title of the last part of this chapter. In this section different studies on particle entrainment are presented, mechanistic and experimental models are discussed and compared. In this section a mixture of works in drilling engineering area which are mostly concentrated on finding a critical velocity criterion and sedimentology's point of view which tries to define the threshold of entrainment by defining a critical wall shear stress is reported.

## 2.1 Turbulence

### 2.1.1 Definition of Turbulence

The term turbulence or turbulent flow is referred to a condition where chaotic motions and local events dominate the flow. Laminar flow, on the other hand, referred to a flow where flow structures are well organized and shear layers are moving parallel to each other[2]. Examples of turbulence are enormous even in everyday living; flow of water in a river, smoke form a factory, flow of water though pipes, flow of air in ventilation systems and so on are all examples of turbulence and chaos.

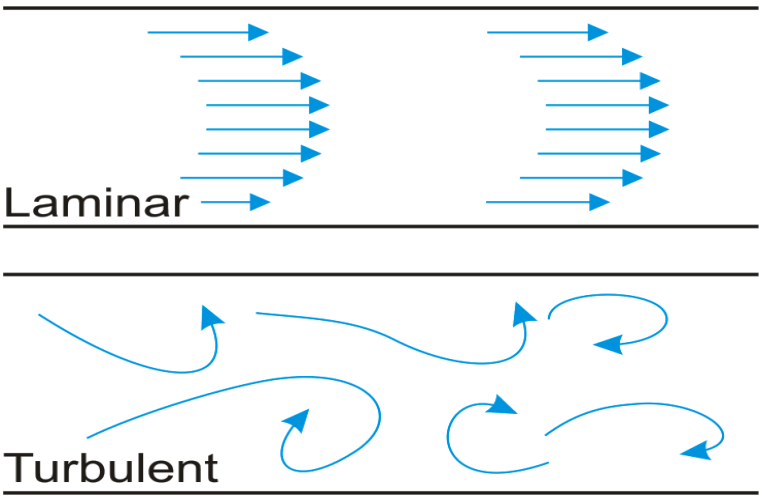


**Figure 2-1 A Sambolic Representation of Stream Lines in Turbulenrt and Laminar Flow[3]**

Momentum transfer in a laminar flow occurs through molecular diffusion while no mass is transferred between the shear layers. In a turbulent flow momentum transfer due to molecular diffusion is so small and convection and momentum transfer by eddies are the main source of momentum transfer. High rate of momentum transfer in turbulent flows comparing to laminar flow is the main reason of why mixing is enhances in presence of turbulence[1].

Turbulent flow is chaotic in nature and very irregular both in time and space; for example velocity in a turbulent flow is a function of space and time which makes the modeling and prediction of behaviour of a turbulent flow through theoretical analysis impossible. Statistical analysis has been used in order to model and explain turbulence. Beside irregularity, turbulence has some properties which are important and also absent in laminar flow. Energy dissipation is much higher in turbulent flow[1]; kinetic energy of turbulence dissipates through viscous action of viscosity and transform into heat or dissipates as pressure loss. Due to high rate of energy dissipation in turbulent flows, sustaining the flow requires a persistent source of energy[1].

[3]Picture from http://glossary.periodni.com/glossary.php?en=laminar+flow

**Figure 2-2: Laminar Flow versus Turbulent Flow[4]**

Another important feature of turbulence is rotation of flow which creates vortex structures, so it can be said that turbulent flow is rotational. Vorticity creates high level of fluctuations in a turbulent flow; flow visualization has revealed vortexes come in many different shapes (hairpin, horseshoe and so on) [3]. Nonlinearity is another feature of a turbulent flow. In fact nonlinearity causes three dimensional structures such as vortex activates in a turbulent flow[1].

### 2.1.2 Turbulence Characterization

Assume a point in a turbulent flow, the fluid velocity at this point would be a function of time. The velocity at this point will fluctuate around a mean value (Figure 2-3). This is in contrast with laminar flow where the velocity at a given point is constant at all times with no fluctuations. Applying the Reynolds decomposition procedure to instantaneous velocities is presented in Eq.( 2-1) and Eq.( 2-2).

$$U(t) = \bar{u} + u' \qquad \textbf{Eq.( 2-1)}$$

$$V(t) = \bar{v} + v' \qquad \textbf{Eq.( 2-2)}$$

[4] Photo from http://fineartamerica.com/featured/turbulence-james-marvin-phelps.html

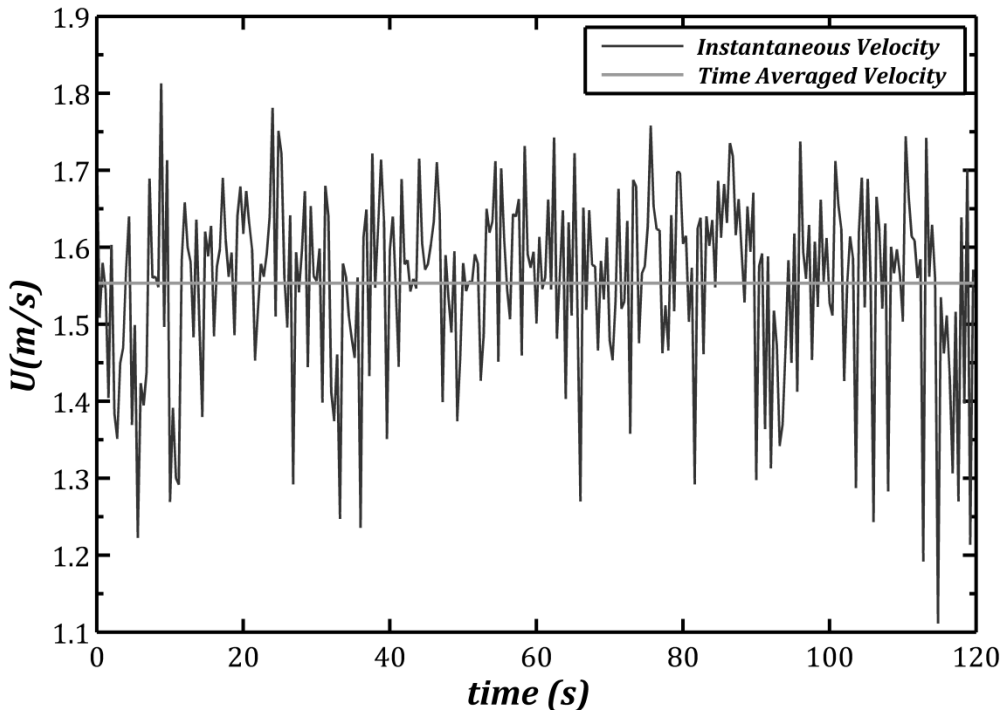


**Figure 2-3: A Typical Turbulent Instantenaeous Velocity Field and its Mean Value**

It has been explained that due to random nature of turbulence, statistical methods need to be used instead of theoretical analysis. For example in Eq.( 2-1) the time average velocity must be obtained using an integral which requires continuous measurements of the velocity Eq.( 2-3).

$$\bar{u} = \lim_{t\to\infty} \int_0^t U(t)dt \qquad \textbf{Eq.( 2-3)}$$

Equation 3 is the theoretical calculation of the time average velocity. In reality measurements of velocity in not continuous but rather as discrete points (similar to the measurement technique used in this work). In this case following equation is used for calculation of time average of velocity or any other variables which has a mean and fluctuating component.

$$\bar{u} = \frac{1}{N}\sum_{1}^{N} Ui \qquad \textbf{Eq.( 2-4)}$$

The fluctuation velocities are the difference between instantaneous velocity and time average velocity.

$$u' = U(t) - \bar{u} \qquad \textbf{Eq.( 2-5)}$$

### 2.1.3 Boundary Layer

#### 2.1.3.1 Friction Velocity

Friction velocity or shear velocity is the wall shear stress in unit of velocity. This definition of wall shear stress will facilitate deriving dimensionless groups in further analysis as it has dimension of velocity. Also it is known that turbulent fluctuations in the boundary layer scales with this velocity.

$$u^* = \sqrt{\frac{\tau_w}{\rho}} \qquad \textbf{Eq.( 2-6)}$$

Friction velocity characterizes the viscous sublayer thickness through Eq.( 2-7).

$$\delta_s = \frac{5\nu}{u^*} \qquad \textbf{Eq.( 2-7)}$$

#### 2.1.3.2 Law of the Wall

In the wall region next to a smooth surface from physics it's known that velocity is related to the fluid density, fluid kinematic viscosity, and distance from the smooth surface and shear stress which is the shear stress at the wall.

$$U = U(\rho, \tau_w, \nu, y) \qquad \textbf{Eq.( 2-8)}$$

By using the friction velocity and dimensional analysis Eq.( 2-8) becomes Eq.( 2-9).

$$U = U(u^*, \nu, y) \qquad \textbf{Eq.( 2-9)}$$

Further analysis according to pi theorem there must be two dimensionless groups which are related in some sort of universal relation[1].

$$\frac{U}{u^*} = f\left(\frac{yu^*}{\nu}\right) = f(y^+) \qquad \textbf{Eq.( 2-10)}$$

Very close to a solid surface the momentum transport is dominated by viscosity. In this region turbulence is suppressed by the action of viscosity and for many decades it was thought that flow in this layer is laminar, which turned out to be wrong due to existence of intermittent events which disturbs the viscous sublayer periodically [3]. In spite of strong fluctuations in the viscous sublayer, Reynolds stress are still negligible and therefore following equation can be taken as velocity gradient in this thin layer[1].

$$\tau_w = \mu \frac{\partial u}{\partial y} \qquad \textbf{Eq.( 2-11)}$$

$$\frac{U}{u^*} = \frac{yv}{u^*} \qquad \textbf{Eq.( 2-12)}$$

The dimensionless velocity is defined as Eq.( 2-13).

$$u^+ = \frac{U}{u^*} \qquad \textbf{Eq.( 2-13)}$$

And finally the universal law of the wall for a smooth surface is:

$$u^+ = y^+ \qquad \textbf{Eq.( 2-14)}$$

From experiments it is known that viscous sublayer extent until dimensionless distance of 5.

$$\delta_s = \frac{5u^*}{v} \qquad \textbf{Eq.( 2-15)}$$

#### 2.1.3.3 Outer Layer: Logarithmic law

Further away from the viscous sublayer the effect of viscosity diminishes while Reynolds stresses starts to dominate the shear stress. In this region the linear velocity profile (Eq.( 2-14)) is no longer valid. Dimensional analysis of the velocity and relevant parameters requires a logarithmic form of velocity in this zone [1] and[2].

$$U = \frac{u^*}{k} \ln(y) + Const \qquad \textbf{Eq.( 2-16)}$$

Equation 17 is the form of velocity distribution in the logarithmic layer which starts from a $y^+ = 30$. The upper limit of this velocity profile depends upon Reynolds numbers of the flow and as Reynolds number increases this limit becomes bigger.

#### 2.1.3.4 Buffer Layer

The buffer layer is a thin layer sandwiched between viscous sublayer and logarithmic region; buffer zone extends from $y^+ = 5$ all the way to $y^+ = 30$. In the buffer zone neither Reynolds stresses nor viscous stresses are negligible and both terms need to be considered in any analysis. Although buffer zone is a thin layer but from a dynamical point of view it is extremely important in turbulence; it is the origin of most vortical structures, turbulent production also takes its peak in this region[1].

While buffer zone is of utmost importance in turbulence generation near wall, there is no unique velocity profile equation such as universal law for the viscous sublayer or logarithmic law for velocity distribution in this zone. Many authors have tried to define a correlation for velocity in the buffer layer but so far none of them are complete and widely accepted by other researches.

One approach for approximating the velocity in the buffer layer is to use the point where the universal law of the wall intercepts the logarithmic law which occurs at $y^+ = 10.7$, for smaller $y^+$ the universal law of the wall maybe used and for bigger $y^+$ the logarithmic law could be used [1][2].

$$u^+ = \begin{cases} y^+, & y^+ < 10.7 \\ \frac{1}{k}\ln(y^+) + A, & y^+ \geq 10.7 \end{cases} \qquad \textbf{Eq.( 2-17)}$$

### 2.1.4 Turbulent Intensity (TI)

Turbulent intensity or strength of a turbulent flow is related to the level of fluctuations in the flow; the higher the fluctuations means stronger turbulence. Time average of fluctuation velocities is zero over a period of time and so root mean square (RMS) is used to time average the fluctuation velocities, for instance the RMS of axial fluctuation velocity is defined as:

$$u_{RMS} = \sqrt{\overline{(u'^2)}} \qquad \textbf{Eq.( 2-18)}$$

In fact turbulent intensity is scales with RMS of fluctuation velocities. In order to be able to compare the intensity of turbulence in different flows dimensionless intensity is preferred. Different authors use different criteria to nondimensionalize the RMS of fluctuation velocities. If the flow is in channel the free stream velocity could be used otherwise in a pipe flow or flow in a closed conduit the bulk velocity may be used to nondimensionalize the turbulent intensity. Some authors even used the time average of the velocity at the same location where the RMS velocity has been measured to nondimensionalize the turbulent intensity[2]. Friction velocity is known to scale up with the RMS of fluctuation velocity in the axial direction in the wall region for turbulent flows, so nondimensionalizing the turbulent intensity also could be done by using the friction velocity.

In order to keep consistency in presenting the results and also comparing the results for different type of fluids, friction velocity has been used in order to nondimensionalize the turbulent intensities in this research.

$$TI = \frac{u_{RMS}}{u^*} \qquad \textbf{Eq.( 2-19)}$$

$$TI_{Radial} = \frac{v_{RMS}}{u^*} \qquad \textbf{Eq.( 2-20)}$$

### 2.1.5 Momentum and Continuity Equations

In a turbulent flow Navier-Stocks equation is still valid and could be applied to the instantaneous velocity. Solving the equation, on the hand, to predict the flow behaviour is almost impossible. If one writes the Navier-Stocks equation for a turbulent flow with the assumptions that the flow is fully developed in the axial direction, and no gravitational change in the flow (horizontal flow) then the Navier-Stocks takes the following form[1].

$$\frac{\partial U}{\partial t} + V\frac{\partial U}{\partial y} = -\frac{1}{\rho}\frac{\partial P}{\partial x} + \nu\frac{\partial^2 U}{\partial y\,\partial y} \qquad \textbf{Eq.( 2-21)}$$

$$U = \bar{u} + u' \qquad \textbf{Eq.( 2-22)}$$

$$\frac{\partial \bar{u}}{\partial x} = 0 \qquad \textbf{Eq.( 2-23)}$$

$$\frac{\partial u'}{\partial x} = 0 \qquad \textbf{Eq.( 2-24)}$$

The momentum equation after introducing Eq.( 2-22) and simplifications takes the following form.

$$\frac{\partial \bar{u}}{\partial t} + \bar{v}\frac{\partial \bar{u}}{\partial y} + \frac{\partial(\overline{u'v'})}{\partial y} = -\frac{1}{\rho}\frac{\partial \bar{p}}{\partial x} + \nu\frac{\partial^2 \bar{u}}{\partial y\,\partial y} \qquad \textbf{Eq.( 2-25)}$$

Equation 38 is the simplified form of Navier-Stocks equation for the mean flow in the Cartesian coordinates. By rearranging this equation following form is obtained which is identical to Eq.( 2-21)[1].

$$\frac{D\bar{u}}{Dt} = -\frac{1}{\rho}\frac{\partial \bar{p}}{\partial x} + \frac{\partial}{\partial y}\left(\nu\frac{\partial \bar{u}}{\partial y} - \overline{u'v'}\right) \qquad \textbf{Eq.( 2-26)}$$

$$\frac{D\bar{u}}{Dt} = \frac{1}{\rho}\frac{\partial \overline{\tau_{xy}}}{\partial y} \qquad \textbf{Eq.( 2-27)}$$

$$\overline{\tau_{xy}} = \mu\left(\frac{\partial \bar{u}}{\partial y} + \frac{\partial \bar{v}}{\partial x}\right) - \rho\overline{u'v'} \qquad \textbf{Eq.( 2-28)}$$

Note that all the equations have been written in Cartesian coordinates with the assumption of main flow is in the x direction and gradients in the y direction.

### 2.1.6 Stresses in Turbulent Flow

#### 2.1.6.1 Normal Stresses

Stress tensor in Cartesian coordinates has 9 components; 3 diagonal or normal stresses and 6 off-diagonal or shear stresses.

$$\tau = \begin{bmatrix} \tau_{xx} & \tau_{xy} & \tau_{xz} \\ \tau_{yx} & \tau_{yy} & \tau_{yz} \\ \tau_{zx} & \tau_{zy} & \tau_{zz} \end{bmatrix} \qquad \textbf{Eq.( 2-29)}$$

A more general form of Eq.( 2-28) is given in Eq.( 2-30)[31].

$$\overline{\tau_{ij}} = -\bar{p}\delta_{ij} + \mu\left(\frac{\partial \bar{u}_i}{\partial x_j} + \frac{\partial \bar{u}_j}{\partial x_i}\right) - \rho\overline{u_i{}' u_j{}'} \qquad \textbf{Eq.( 2-30)}$$

According to Eq.( 2-30) and based on the stress tensor in Eq.( 2-29), following expression could be derived for normal stress in the axial direction.

$$\overline{\tau_{xx}} = -\bar{p} - \rho\overline{u'^2} \qquad \textbf{Eq.( 2-31)}$$

### 2.1.6.2 Shear Stresses

#### 2.1.6.2.1 Viscous Stresses

Recall Eq.( 2-28) in this equation shear stress in a turbulent flow is the summation of two components, the first component is the so called viscous or laminar stress.

$$\overline{\tau_{xy}} = \mu\left(\frac{\partial \bar{u}}{\partial y} + \frac{\partial \bar{v}}{\partial x}\right) - \rho\overline{u'v'} \qquad \textbf{Eq.( 2-32)}$$

The flow is in the x direction and there is no flow in the y direction, so $\bar{v} = 0$ and viscous stress reduces to:

$$\tau_v = \mu\left(\frac{\partial \bar{u}}{\partial y}\right) \qquad \textbf{Eq.( 2-33)}$$

The viscous stress is the shear stress produced due to viscosity which is the resistance of fluid to flow. It is expected that this stress gets high values where there is great velocity gradient or where the viscosity is important. These conditions (high velocity gradient and viscosity dominance) normally exist near a solid surface where the condition of no slip boundary needs to satisfy.

#### 2.1.6.2.2 Reynolds Stresses

Although from the continuity equation it's known that time average of fluctuation components of velocity is zero, the term $-\rho\overline{u'v'}$ is nonzero and is called Reynolds stress [31]. The stress tensor for Reynolds stresses becomes:

$$\tau_{Re} = -\begin{bmatrix} \rho\overline{u'^2} & \rho\overline{u'v'} & \rho\overline{u'w'} \\ \rho\overline{u'v'} & \rho\overline{v'^2} & \rho\overline{v'w'} \\ \rho\overline{u'w'} & \rho\overline{v'w'} & \rho\overline{w'^2} \end{bmatrix} \qquad \textbf{Eq.( 2-34)}$$

Reynolds stresses as the tensor of these types of stresses implies arises from the fluctuations in the velocity, so they are absent in a laminar flow where there are no fluctuations in velocity. For turbulent flows Reynolds stresses contribute to the total stress, both normal and shear stress and total stress is the summation of Reynolds stresses and viscous stresses.

$$\overline{\tau_{xy}} = \tau_v + \tau_{Re} \qquad \textbf{Eq.( 2-35)}$$

Reynolds stresses are important in turbulent flows. In the core flow of a turbulent flow Reynolds stresses are much higher (several order of magnitude bigger) than viscous stresses. In the regions close to solid surface, however, the Reynolds stresses tend to zero due to high viscosity effect.

## 2.2 Newtonian Fluids Flow through Annuli

In this section flow of Newtonian fluids through annuli configuration is discussed. Past studies and researches are summarized and the key findings and conclusion remarks of other investigators are cited.

Rothfus [4] has been one of the pioneers in studying flow through annular ducts. In 1950 Rothfus et.al conducted a series of experimental studies on flow of air through concentric annuli's of varying radius ratios. At the time they could measure velocity (point measurement) and pressure losses. In the laminar flow their data showed good agreement with theoretical prediction of viscous flow. In the transitional flow regime the authors claimed that it's believed that both laminar and turbulent flow exist simultaneously. Friction factor data were found to be a function of radius ratio. In comparison with friction factor for flow through a pipe with same equivalent diameter and Reynolds number, Rothfus et.al data have shown higher friction factor for annuli. Radius of maximum velocity was also investigated and found to be same for both laminar and turbulent flow. It is also been observed that velocity maximum starts moving toward the center of the annuli in transitional flow regime. Velocity data has been presented in law of the wall coordinates and satisfactory agreement was achieved with well accepted law of the wall and logarithmic law.

Walkers and Rothfus (1959)[5] have conducted a series of experiments in concentric annuli of radius ratio of 0.331 in order to study the transitional flow phenomena. The

working fluid was water, measurement technique was Pitot tube and Reynolds number varied such a way that all the flow regimes including laminar, transitional and lower turbulent flow were achieved. Fanning friction factor-Reynolds number correlation data have shown that transition region of flow depends on radius ratio (0.331). They have reported that major transitional change occurs at Reynolds numbers between 2200 and 3100. Walker and Rothfus have plotted their measured velocity data against distance for different Reynolds number; they further argued that the ratio of $\frac{u}{u_{max}}$ is only a function of Reynolds number for a given radius ratio. Radius of maximum velocity has been found to be similar in both laminar and turbulent flow. At a Reynolds number of about 650 they observed that $R_{max}$ starts to deviates from its laminar flow position. This radius progressively shifts toward the center of the annuli in the transitional flow regime until a critical Reynolds number of 2200 is reached. Pressure drop data also showed that at Reynolds number of 2200 friction factor reaches its minimum and sharply increases afterward. After passing Reynolds number of 2200, $R_{max}$ starts to reverse its path back toward its original laminar flow value. A Reynolds number of 3100 based on friction factor data marks the end of transitional flow regime. Transitional flow regime was found to be a function of radius ratio.

In 1964 Brighton and Jones[6] published the results of their experimental study for flow of air in a series of concentric annuli's of varying radius rations (α varied from 0.0625 to 0.562). The operational Reynolds numbers ranged from 46000 up to 327000 and their measurement tool was Pitot tube. They have reported an asymmetry in velocity profile by stating that radius of maximum velocity in a fully turbulent flow locates closer to inner wall of the annuli. Despite the fact that they have measured and reported Reynolds stress distribution, they could not locate the radius of zero shear stress and consequently they used the radius of maximum velocity in their calculations of wall shear stress. Measured friction factors by means of a water flow apparatus have shown some 1-10% higher values comparing to friction factors for flow at the same Reynolds number but in a pipe with the same diameter as hydraulic diameter of the annuli. Velocity data for the outer wall shows good agreement with the law of the wall and for all the radius ratios studied. Velocity data for the inner wall, in the other hand, only for the highest radius ratio follow the law of the wall and for the smaller radius ratios falls below the prediction of the law of the wall.

A method based on an eddy viscosity model for turbulent flow has been proposed in 1966 by Rothfus [7] for predicting velocity profiles in concentric annuli. According to the author comparison of the flow between pipe flow and flow through annuli is straightforward for a fully developed laminar flow which can be done based on radius of maximum velocity. For turbulent flows at high Reynolds numbers radius of maximum velocity occurs much closer to inner wall than in laminar flow and hence comparing annular flow with pipe flow would require a much more complicated approach. In turbulent flow dependency of $R_{max}$ on both radius ratio and Reynolds number has been reported. Generally $R_{max}$ decreases as Reynolds number increases in lower turbulent regime but for high Reynolds numbers this dependency becomes less. Two correlations for calculating radius of maximum velocity in a fully developed laminar and turbulent flow have been proposed by the author (Lambs and Walker work).

In a similar study to Brighton's work, Quarmby (1968)[9] investigated flow of air through 3 concentric annuli's. Experiments were done for turbulent flow at Reynolds numbers staring from 6000 up to 90000. Entrance effect or the length required after the inlet for flow development was found to be similar to round tubes of the same equivalent diameter (30-40 times the hydraulic diameter). Friction factor was found to be independent of radius ratio. Measured velocities in $y^+ u^+$ coordinate have shown strong dependency upon Reynolds number and radius ratio especially for Reynolds numbers less than 40000. Velocity profile didn't follow any universal form of velocity profiles available. One of the important findings in Quarmby work was that he found out that radius of maximum velocity is not the same in turbulent flow and laminar flow, the difference was also affected by change in radius ratio as well. Quarmby also reported that $R_{max}$ also changes with Reynolds numbers lower than 40000-50000; this radius decreases as Reynolds number increases, once this Reynolds number reached $R_{max}$ becomes constant with no further dependency on Reynolds number.

The transitional phenomenon from laminar flow was examined once again in 1971 by Hanks et.al.[11]. Through analytical analysis they have shown that flow around the inner body of an annuli configuration undergoes transition to turbulence earlier that the outer part. Their analysis also confirmed skewness of shear stress profiles while symmetry of stress tensor was remained. Experimental results also supported their earlier statement about a two stage transition process; first the inner wall and then the outer wall goes under transition. Deviation of friction factors from laminar values in the transitional

regime was also related to this two stage transition. According to Hanks et.al [42] radius of maximum velocity is constant in the laminar flow regime. At the onset of transition to turbulence around the inner wall this radius starts to move toward the center of the annuli. Radius of maximum velocity continuously increases until it gets its peak which occurs at a point where the flow around outer wall undergoes transition to turbulence. After this point $R_{max}$ starts to decrease rapidly with increasing Reynolds number until it reaches a value where no more change is observed; that is the radius of maximum velocity in turbulent flow. The authors also reported that $R_{max}$ for turbulent flow is less than that of laminar flow.

In 1972 Lawn and Elliot [12] have measured shear stress distribution and velocity profiles for flow of air in three concentric annuli's of radius ratios of 0.088, 0.176 and 0.396. Friction factors were found to be a function of radius ratio which is in contrast with earlier finding of Brighton and Jones[6]. Friction factor data for the smallest radius ratio showed the biggest difference than those of pipe flow; 8.5% higher values were recorded. For the other two radius ratios friction factor were found about 5% higher than those of pipe flow. Measured values of radius of maximum velocity by a double Pitot tube have shown different values than radius of zero shear stresses. In fact Lawn and Elliot have been the first to experimentally show that zero shear stress and maximum velocity don't coincide. In addition they have reported that zero shear stress in all of their experiments always occurred closer to the inner wall of the annuli comparing to maximum velocity. Ratio of radiuses of zero shear and maximum velocity to outer diameter of the annuli also increased as radius ratio was increased. Velocity data for the outer wall was well correlated by logarithmic law, although only 10% of the distance of nearest to the wall could be considered as constant stress zone (or viscous sublayer). Velocity data for the inner wall didn't correlate well logarithmic law and showed slight deviation from that.

In 1973, Rehme [14] has published the results of an experimental work on flow of air in concentric annuli's of small radius ratios. Three radius ratios of 0.02, 0.04 and 0.1 have been tested at operational Reynolds numbers ranging from 20,000 to 200,000. A development length $76D_H$ for achieving a fully developed flow after inlet has been assumed in Rehme's work. A dependency of pressure-drop-coefficient on radius ratio was found. As radius ratio increases pressure-drop-coefficient also slightly increases a conclusion which was found earlier by Quarmby[9]. For the highest radius ratio studied

(0.1) pressure-drop-coefficient have shown some 4% higher values than those of pipe flow. Similar to Lawn and Elliot[12] work, hot wire anemometry was employed in order to measure shear stress in the annuli by Rehme[14]. The accuracy of the technique according to the author was $\pm 0.55mm$. Results for the radiuses of maximum velocity and zero shear stress have shown that these radiuses are not same. In addition, it was found that in every case the radius of zero shear stress always occurs closer to the inner wall comparing to the radius of maximum velocity. For the outer zone (i.e. $y^+ > 30$) good agreement between the measured velocity and logarithmic law was found. For the inner wall ($y^+ < 5$), however, good agreement was found with the law of the wall only for the biggest radius ratio (0.1). For smaller radius ratios (0.02 and 0.04) major deviation of velocity data in the inner zone from the law of the wall was observed and reported.

Turbulent structures and statistics have been investigated by Rehme[15] in an experimental study. The conditions of the experiments were identical to his first publication. Turbulent intensities in three directions have been measured. Measured values showed that axial turbulent intensities in the outer part were higher in the case of flow in annuli comparing to round tubes. Furthermore it was confirmed that turbulent intensities were higher for smaller radius ratios. Axial turbulent intensities for inner part of the flow were found to be much lower than turbulent intensities in round tubes. For the highest radius ratio studied the dependency of turbulent intensities in the inner zone on distance was found to be similar to pipe flow. Reynolds number impact could not be identified. Turbulent intensities in radial and azimuthal directions have shown the same behaviour as axial intensities. Outer wall data were slightly higher than pipe data while inner values were significantly lower. One of the interesting findings was that turbulent intensities in all directions reached their minimum close to the radius where shear stress was zero. He further concluded that while for the outer flow zone the structures of turbulence are highly anisotropic, for the inner zone this is much less marked. Turbulent kinetic energy was found to be higher in the outer region of flow than those of tube flow while for the inner zone it was much lower. Additionally it was found that turbulent kinetic energy takes its minimum at exactly the location of zero shear stress. This was an important finding because the non-coincidence radiuses of zero shear stress and maximum velocity could be explained by using this fact reasonably.

In 1981 Jones and Leung[16] have analysed the pressure drop data reported in literature in an attempt to define a correlation for friction factor in smooth concentric

annuli for both laminar and turbulent flow regimes. They have shown that the reported data are showing a deviation of -25% up to 35% from the classic Colebrook[34] correlation. Jones and Leung suggested that hydraulic diameter is not sufficiently accurate in order to correlate the geometrical effects. Instead another characteristic length needs to be defined in order to replace the hydraulic diameter in Reynolds number calculation. Based on a previous work they have suggested the following correlation to be used as the geometric shape factor ($\alpha$ is the radius ratio).

$$\varphi^* = \frac{1}{(1-\alpha)^2}\left[1 + \alpha^2 - \frac{1-\alpha^2}{\ln\left(\frac{1}{\alpha}\right)}\right] \qquad \textbf{Eq.( 2-36)}$$

The proposed new characteristic length is then calculated based on the geometric shape factor.

$$d_l = D_H\, \varphi^* \qquad \textbf{Eq.( 2-37)}$$

While it is known that$f = f(N_{Re}, \frac{\varepsilon}{d})$, which for a smooth pipe would become $f = f(N_{Re})$ and Reynolds number defines as follow.

$$N_{Re}{}^* = \frac{\rho u d_l}{\mu} \qquad \textbf{Eq.( 2-38)}$$

The new proposed correlation for prediction of frictional pressure drop in smooth concentric annuli in the laminar flow regime is:

$$f = \frac{64}{N_{Re}{}^*} \qquad \textbf{Eq.( 2-39)}$$

The proposed correlation tends toward the theoretical value of friction factor in laminar flow in pipes as $\varphi^* \rightarrow 1$. The final equation of friction factor is similar to Colebrook equation with replacing Reynolds number definition.

$$\frac{1}{\sqrt{f}} = 2\log\left(N_{Re}{}^* \sqrt{f}\right) - 0.8 \qquad \textbf{Eq.( 2-40)}$$

In a recent paper Dou et.al (2010)[18] have discussed the transition of flow from laminar to turbulent in annuli's of varying radius ratios. They have proposed an energy gradient method in order to monitor the instability in a laminar flow for turbulent transition. In the energy gradient method according to the authors, "the whole flow field is treated as an energy field''. In fact any disturbance in the flow could either be amplified by energy gradient in the transvers direction or be dissipated and vanished by action of viscosity in the axial direction. The authors then proposed that the ratio of these two mechanisms would become important and could be used as an indicator of transitional flow regime. Based on their analytical analysis they have reported that critical Reynolds number for transition depends upon radius ratio and increases with increasing radius ratio. Radius ratios less than 0.12-0.18 have caused more instability while greater radius ratios enhanced the stability of the flow. They have claimed that critical Reynolds number of annuli with radius ratio bigger than 0.12-0.18 reached its value for flow through a pipe with the same equivalent diameter.

## 2.3 Non-Newtonian Fluids

In 1958 Fredrickson and Bird [19] have published the results of their analytical solution for shear stress distribution in annuli for Non-Newtonian fluids. Their analysis is for laminar flow and may be used to predict the friction factor for flow of a power law fluid. Hanks et.al (1979) [24]have presented an analytical solution to the integral proposed by Bird[19][25].

Dodge and Metzner[20] in 1959 have done an analytical analysis on non–Newtonian systems. The analysis was performed for pipe flow and a correlation relating mean flow rate and pressure drop was proposed. The authors also claimed that their analysis made it possible to predict turbulent velocity profile. The analysis has been done for power law type fluids and the general approach to the problem is similar to that of Newtonian fluids with an extra degree of freedom resulted by introducing the flow behaviour index of the fluid. The ultimate proposed correlations are a modified version of Reynolds number which incorporated the flow behaviour index and an equation for the velocity profile. Prediction of the proposed model has been compared with experimental data and according to the authors satisfactory agreement was achieved.

In 1970 Virk et.al[21] has studied the flow of polymeric liquids in pipes. They were interested in structures of the flow associated with the so called Tom's phenomenon or

the drag reduction. According to the authors the scattering of available data in literature for friction factor varied based on Reynolds number. Following correlation has been proposed by the authors for prediction of friction factor at the condition of maximum drag reduction.

$$f = 0.59{N_{Re}}^{-0.58} \qquad \textbf{Eq.( 2-41)}$$

The exponent 0.58 may vary from 0.55 up to 0.67. Equation 2-56 is the Prandtl type friction factor for condition of maximum drag reduction.

$$\frac{1}{\sqrt{f}} = (19 \pm 0.4)\log\left(N_{Re}\sqrt{f}\right) - (32.4 \pm 1.2) \qquad \textbf{Eq.( 2-42)}$$

For flows which have a moderate drag reduction the correlation should fall in a window between Newtonian fluids friction factor (Jones correlation[16]) and condition of maximum velocity.

Virk et.al[21] postulated that the constants in Prantle type friction factor are related to the constant of the velocity profile; if M and N are the constants in friction factor equation and A and B are the constants in velocity profile then:

$$\frac{1}{\sqrt{f}} = M\log\left(N_{Re}\sqrt{f}\right) + (N) \qquad \textbf{Eq.( 2-43)}$$

$$u^{+} = Aln(y^{+}) + B \qquad \textbf{Eq.( 2-44)}$$

These constants are related by the following system of equations.

$$\begin{bmatrix} M \\ N \end{bmatrix}\begin{bmatrix} 0.615 & 0 \\ 1.562 & 1.414 \end{bmatrix} = \begin{bmatrix} A \\ B \end{bmatrix} \qquad \textbf{Eq.( 2-45)}$$

This equation is valid if the constant A and B are independent of Reynolds number and also a region of the flow where logarithmic law doesn't apply (viscous sublayer) constitutes a small fraction of the total flow. A and B were found to be (11.7, -16.1) with a slight adjustment the following correlation have been proposed for the condition of maximum drag reduction.

$$u^+ = 11.7ln(y^+) - 17 \qquad \textbf{Eq.( 2-46)}$$

Four concentrations of CMC aqueous solutions have been tested by Pinho et.al[33] in pipe flow; velocity data, fluctuation velocities and normal stresses have been measured and reported. Reynolds number ranged from 240 up to 11000. According to the authors a delay in transition from laminar flow caused by shear thinning property of the solutions was observed. From fluctuation velocities a reduction in radial and tangential component for CMC solutions comparing with Newtonian fluids has been reported. It was also found that Virk asymptote of maximum drag reduction was appropriate for velocity data of CMC aqueous.

Flow of Newtonian and non-Newtonian fluids through concentric and eccentric annuli's was tested once again in 1992 by Nouri et al.[28]. They have tested flow of a Newtonian and a non-Newtonian fluid in one concentric and two eccentric annuli's. Reynolds numbers for flow of the Newtonian fluid ranged from 8900 to 26600 and flow data was measured by using LDA technique. The non-Newtonian fluid which according to the authors was a weak viscoelastic fluid was tested at Reynolds numbers of 1150, 6200 and 9200. Experimental data with Newtonian fluid flow showed that friction factor in concentric annuli is 8% higher than that of pipe flow. For the eccentric arrangement they have reported a reduction in friction factor comparing to concentric annuli. Law of the wall was found to be valid on both inner and outer wall of the concentric annuli. For the eccentric annuli's, however, it was found that velocity data in the smallest gap of the annuli don't follow the law of the wall. Transition from laminar to turbulent flow for the non-Newtonian fluid occurred at effective Reynolds numbers much higher than that of Newtonian fluid. A circumferential variation of radius of maximum velocity was detected and reported in eccentric annuli's for the Newtonian and 0.2 % CMC aqueous solution. Near wall velocity data for the outer region (logarithmic zone) for CMC solution was found to fall somewhere between the Newtonian fluid curve and Virk maximum drag reduction asymptote. Turbulent intensities in the axial direction was found to be suppressed in the case of non-Newtonian fluid compared to the Newtonian fluid flowing at the same effective Reynolds number. Radial component of the RMS of fluctuation velocities was also found to be much lower for the non-Newtonian fluid. Shear stress distribution was found for the Newtonian fluid and radius of zero shear stress could be distinguished from that of maximum velocity. For the non-Newtonian fluid radius of zero

shear stress and maximum velocity could not be distinguished from each other and ultimately the coincidence of these two radiuses was assumed.

In 1995 Escudier et.al[29] have employed LDA to study flow of Newtonian and non-Newtonian fluids; flow geometry was concentric annuli of radius ratio of 0.506. Three non-Newtonian fluids were tested; a solution of CMC (Sodium Carboxyl methyl Cellulose), an aqueous solution of Xanthan gum and the third fluid was a CMC/Laponite blend. Friction factor data for the Newtonian fluid was found to follow the theoretical predictions in the laminar flow regime. In turbulent flow good agreement was observed between experimental data and Jones and Leung correlation[16]. Friction factors for the CMC solution in the laminar flow regime showed good agreement with theoretical prediction of a power law type fluid. In turbulent flow regime friction factors were found to be much lower than that of Jones and Leung prediction which is clear indicator of drag reduction. Second non-Newtonian fluid was a Xanthan gum; two concentrations of this fluid were tested. Friction factors in the laminar flow felt below the theoretical prediction. This behaviour was related to the elasticity of Xanthan gum. Laminar friction factors of Laponite/CMC blend also showed an anomalous behaviour similar to Xanthan gum which according to the authors caused by thixotropic nature of this fluid. Turbulent flow friction factors for the latter two fluids were found similar to CMC, well below Newtonian fluids prediction which is caused by drag reduction properties of these types of fluids. Velocity data for the Newtonian fluid in law of the wall coordinate followed the law of the wall in the immediate vicinity of the walls and for the logarithmic law also good agreement with log law was observed and reported. For all the non-Newtonian fluids studied the validity of the law of the wall was reported for velocity data close to solid surfaces. Velocity data in the outer regions of the wall, i.e. logarithmic region, showed an upward shift comparing to Newtonian fluid case.

Recently Japper et.al[31] (2010) have published the results of an experimental study on flow of a Newtonian and two non-Newtonian fluids in concentric annuli of radius ratio equal to 0.506. First non-Newtonian fluid was a semi-rigid shear thinning polymer (A Xanthan gum) and the second fluid has been a solution of a polymer which exhibits yield stress (Carbpol). As the Newtonian fluid they used both water and a glycerin-water mixture with a density of 1070 $kg/m^3$ and viscosity of 38.6 cp. The first non-Newtonian fluid, a Xanthan gum, was found to be best represented by Carrau-Yasuda rheology model while for the second fluid they have used Herschel-Bulkley model.

Friction factor for the flow of Newtonian fluid was found to show good agreement with Shah and London[32] correlation in the laminar flow regime.

$$f = \frac{23.82}{N_{Re}} \qquad \textbf{Eq.( 2-47)}$$

For the higher Reynolds numbers Jones and Leung correlation[16] was sufficiently accurate in predicting the frictional pressure drops for the Newtonian fluids. Japper et al. in order to detect transition from laminar flow have adopted a method which was initially proposed by Zakin[23]. In this method turbulent intensities are measured at a fixed radial location in the annuli (usually close to the walls) at several Reynolds numbers. According to the authors, an abrupt increase in turbulent intensities is observed at the onset of transition from laminar flow to turbulent. The critical Reynolds numbers at which a sharp increase in level of turbulent intensities was observed was found to be the same for both walls in the case of Newtonian fluids. The upper limit of Reynolds number at which turbulent intensities reached its maximum (the end point of transitional flow regime) was found to be lower for the inner wall for Newtonian fluids. For the non-Newtonian fluids although the lower limit Reynolds numbers were found to be similar for both walls of the annuli, the upper limit was also the same for two of the tested fluids. The upper limit of Reynolds number which marks the end of transitional flow regime was found to be higher in the case of more shear thinning fluids which indicates that transitional flow regime last over a wider ranges of Reynolds numbers for the more shear thinning fluids.

Mean axial distribution of velocity for the Newtonian fluids have shown good agreement with theoretical predictions in the laminar flow regime for Reynolds numbers up to 2600, after this Reynolds number velocity profiles start to flatten which is expected in turbulent flow. The velocity profiles were much more flat for the non-Newtonian fluids. Velocity data for the Newtonian in law of the wall coordinate showed good agreement with the universal law of the wall in the immediate vicinity of the walls. Further away in the logarithmic region velocity data were best predicted by the logarithmic law with constants proposed by Clauser. Tested non-Newtonian fluids were all found to follow the universal law of the wall for $y^+ < 11$. For 0.0124% Xanthan gum velocity data in the core region showed an upward shift comparing to Newtonian velocity curve but remained parallel to that.

$$u^+ = 2.5\ln(y^+) + 4.5 \qquad \textbf{Eq.( 2-48)}$$

Although shear stress distribution has been measured and reported, distinction between radiuses of zero shear stress and maximum velocity couldn't be made and authors assumed equity of the two radius.

Suppression in axial turbulent intensities was observed for the 0.0124 solution of Xanthan gum for the outer wall of the annuli while for the inner wall a slight increase was reported. Radial turbulent intensities were found to be much lower for the Xanthan gum comparing to the Newtonian fluids.

## 2.4 Cutting Transport in Horizontal Annuli

The problem of sedimentation and erosion has been of interest for many decades. There are many aspects of the topic which have been investigated mostly for channel flow which resembles flow in rivers[33][46][50]. In drilling operation cuttings are being transported in an annular space formed between drill string and borehole. In drilling highly inclined and horizontal wells these cuttings will form a bed on the low side of the annuli over time; this bed continue to grow until the velocity over the bed reaches a critical value which would remove the bed. In this section a summary of past works on the subject of cutting transport is given briefly.

Tomren et.al[37] have studied effect of different parameters on cutting transport in a 40 feet long flow loop. The angle of inclination varied from 0 to 90 degrees and real drilling cuttings were used. A hole degree less than 10 was found to be practically similar to vertical case in cutting transport which doesn't impose any difficulties besides those of vertical case. As the angle of inclination was gradually increased to 20 and 30 degrees the author mentioned an increase in particles tendency in gong downward due to increase in radial component of the slip velocity. Angles of inclination between 30 to 60 s being considered as critical angles and a total of 96 tests were done on this range of inclination angles. Although in gradually increase the angle from 10 to 30 no dramatic and sudden change in the behaviour of the particles was observed, for angles above 30 and less than 60 dramatic change in the behaviour of the particles were reported. In this range of inclination more and more particles were forced down to deposit on the low side of the annuli. This range of angles is important not only because of dramatic change in behaviour of the cuttings but because the bed of cuttings was observed to slide backward

due to gravity. High angles of inclination (60 to 90) were found to be similar in a way that bed of particles formed instantaneously. This bed in contrast to critical angles was found to be stable and not roll back. Pipe rotation was found to help in lifting some of the cuttings from the bed into the main stream flow. Effect of eccentricity was also investigated and it was found although eccentricity may change the behaviour in subsections of the annular space in vertical wells, but overall performance of concentric and eccentric annuli's were the same from cutting transport point of view. For the inclined wells the eccentricity was found to have a negative effect on cutting transport and bed build up especially positive eccentricity. The best case scenario was the concentric annuli with respect to the rate of bed buildup. Effect of viscosity was found to be related to the flow regime. In laminar flow higher viscous fluids were found to be performing better in preventing formation of the bed. In turbulent flow although the higher viscosity caused a smaller bed but both cases (low and high viscosities) were same in respect to how fast the bed formed.

Effect of rheology on cutting transport was investigated by Okrajni and Azar[36] using the University of TUSLA flow loop facility. Their results showed that in absent of drill pipe rotation (or rotation at low speeds) using high viscosity muds in high angle wells could be detrimental because high viscosity muds in fact suppress the turbulence while low viscosity muds promotes turbulence. Further analysis of rheology data has shown that performance of cutting transport best correlates with low shear rate viscosity.

Larsen et.al[44] by using university of TULSA flow loop facility have investigated the critical velocity required for transporting the cuttings in high angle wellbores including horizontal wells. In their definition, critical velocity is a velocity at which no bed would form on the low side of the annuli; this is called the critical velocity while velocities lower than this is called subcritical velocity. Their results suggest that medium rheology mud is superior to low and high rheology muds in inclined wellbores. While drill pipe rotation enhanced the velocity required to carry the cuttings from 3 to 4 feet per second down to 1 to 2 feet per second, pipe eccentricity, in the other hand was found to have negative effects on cutting transport capacity. In fact eccentricity caused the mud to move away from the lower side where cuttings tend to go and form the bed. The smaller cuttings size (0.1 in) was found to be more difficult to remove than the medium and large ones. Sliding of the bed of particles backward was observed for angles of inclination

between 35-55 degrees while for angles between 55 to 90 degrees no significant change in bed thickness was reported.

In 1999 Pilehavri et.al[45] have published a summary on the advancements and results of other researches in the area of cutting transport. According to the author early works has been started by building the wellbore simulator at the University of TULSA; this flow loop was designed in such a way that was able to change the angle of inclination, pump flow rate, drilling rate and drill pipe rotation and eccentricity. Many studies has been carried out using this flow loop and all of these studies confirmed that cutting transport in inclined wellbores (angles of inclination bigger than 10) are completely different than that of vertical case.

Gavignet et.al [39] developed a model which may be used in cutting transport predictions; they have developed their models based on Willson et.al[38] two layer bed model. The two layers bed model assumes the bed constitutes of two layers: a stationary lower layer which is in contact with the wall and a dynamic layer on top which is interacting with the fluid flowing over the bed. Instead of assuming saltation as the main mechanism of particles movement, the authors have used the momentum balance equation between the upper layer of the bed and the fluid. The final form of the proposed model is in term of bed thickness and may be used to predict the bed thickness.

An experimental study was carried out by Ford et.al (1990)[40] in search of the effects of different drilling parameters on cutting transport in inclined wells. They have reported two different mechanism of cutting transport. First mechanism is rolling at which particles roll and slide along the bed while keeping in contact with the bed. Suspension is the second mechanism of transporting the cuttings which occurred at higher flow rates. Although both types of transporting mechanisms would clean up the well but their respond to changes in mud properties have been observed to be completely different. Critical velocity required for initiating either one of the two mechanisms described was found to be a function of wellbore inclination. Flow regime of the circulating fluid (i.e. Laminar or Turbulent) and also fluid rheology were found to have some effects on the critical velocity. Inner pipe rotation was found to reduce the critical velocity when using viscous fluids while no change was observed when using water as the carrier fluid. Sensitivity to cutting size was also reported. During the experiments for finding the minimum velocity of transportation of cuttings, Ford et.al.[40] have observed

distinct bed types formed at different velocities. Ford et al. have reported the following bed morphologies which were observed during the experiments.

- Stationary Bed: at velocities lower than critical velocity of rolling
- Continuous moving bed
- Separated moving bed (Dunes)
- Sand Clusters
- Suspension/ Saltation
- Heterogeneous Suspension
- Homogenous Suspension

Cleaver and Yates[34] have studies the literature on boundary layer and coherent structures in order to define detachment criteria for a particle sitting on a substrate based on the forces related to burst events. They have described the burst events like tornados which may create a force big enough to lift a particle. From these analysis they have proposed a criterion which relates the bed shear stress and particle diameter and according to them as soon as $\tau_w {d_p}^{3/4} > const$ the particle would be removed. In further analysis of the data available in the literature on the frequency of coherent structures they have proposed a correlation which may be used to predict the rate of removal based on the condition of the flow and fluid.

A mechanistic model for entrainment condition based on force balance has been proposed by Phillips[35] in 1979. The nature of forcers is divided into two categories: first group are the holding forces which include gravity and adhesion force, second group of the forces are called lifting forces. Adhesion force between the particles and solid surface and also particle- particle interaction is dominating for fine particles (this force is caused by Van der Waals effect) while gravitational force which is caused due to particle wright dominates the holding forces for larger particles. In the lifting forces a few forces are recognizable; a force caused by coherent structures which has been described earlier by Cleaver and Yates[34] and is called updraft under a burst, hydrodynamic drag force which is the drag force caused by fluid flow and finally all other possible lifting forces are considered under one single category. Depending upon particle diameter four possible flow regimes is identified; in each flow regime two of the mentioned forces are dominating and other forces are negligible. For instance for particles finer than 30 micron net weight force and drag are negligible while the other two forces are important.

Correlations for particle entrainment in each regime is developed and furthermore transformed into their dimensionless form for comparison with other investigator's results.

A new approach to the problem of cutting transport in horizontal and deviated wells was introduced by Yu et.al (2004)[51]. While traditional view is to increase the drag force on the cuttings, the author suggesting a new technology to reduce the gravitational force and at the same time increasing the drag on the cuttings. The proposed technology is to attach air bubbles to drilled cuttings by using chemicals and surfactants; the gas bubbles would pull the particles upward due to gravity differences. Experimental work was arranged and performed in support of this proposal. In the experimental work effect of many different parameters including particle size and PH of the testing fluids were carefully examined; performance of different chemicals which helps in attaching air bubbles to cuttings were also investigated. During the experiment it was found that air bubbles were able to lift particles smaller than 1.4 mm while bigger particles remained stationary on the bottom of the test beaker. The optimum PH for the chemicals to perform was found to be in the range of 9 to 11.

Rabenjafimanantsoa[48] have conducted a series of experimental and numerical simulation on particle transport and dynamics in pipe flow. PIV and UVP (ultrasonic Velocity Profile) techniques have been employed to study the incipient motion of particles in dune-beds in pipe flow. The author challenges the traditional concept of multi-layer bed and claim this concept is not sufficient in understanding and modeling cutting transport. Pressure drop data have been used in order to identify the flow regime of the bed of the particles. Four distinct flow regimes have been reported by to occur during slurry flow.

1. Stationary beds
2. Moving Bed
3. Heterogeneous flow
4. Homogeneous flow

A plot of frictional pressure drop against flow rates should show all these four flow regimes; the presence of bed of particles acts like pipe roughness inducing instabilities near the bed , these instabilities and fluctuations will ultimately cause the particles to move to regions of low speed fluids forming dunes structures. At lower flow rates the

pressure drop is mainly due to roughness and a two layer bed is expected to form, a bottom stationary and a thin moving layer on top. In transition regime dunes form; the dominating mechanism of particle movement and detachment is Saltation (Drag force). One remarkable feature of this regime is existence of a locally minimum pressure. At higher flow rates the dune starts to flatten, and lower fluctuations in pressure drop will occur (The last two regimes are expected). According to the author, in transporting slurry flow in pipes transitional flow regime is more favorable than laminar flow because of its ability for keeping particles in suspension; also energy consumption would be less. In the boundary layer, forces acting on the bed scale with the shear stress which makes the shear stress a good indicator of entrainment criteria. Local events like burst and sweep give rise to local Reynolds stress much higher than its mean value which in return will cause the particles detachment (Burst) or deposition (Sweep). Large Eddy Simulation also supports the former statement, the particle detachment from the bed occurs where the shear stress is highest.

Niño et al. (2003)[46]have conducted an experimental study on threshold of entrainment for different particle diameters in channel flow of both smooth and rough walls. Measurement technique has been a high speed video system and five particle diameters ranging from 38 micron up to 532 micron was tested. Although the authors confirms the earlier statement made by Grass about threshold of entrainment which is similar to Williams[38] point of view (there is no threshold below which no particles move), but they are convinced that defining a threshold of entrainment has practical uses and is a convenient way for correlating experimental data which may be used in field readily. In transitionally rough beds by increasing bed shear stress, the particles movement is dominated by saltation which is lifting of the particles from the bed and moving it in suspension. The authors related this phenomenon to turbulent structures called coherent structures as described by Robinson (1991) [3]. Although Niño et.al[46] only considered threshold of suspension and not rolling but they have concluded that particles with diameter less than viscous sublayer thickness could be entrained into suspension if wall shear stress was high enough, a conclusion which is contrast with previous works. Additionally, it is been found that as particle diameter progressively decreases, higher bed shear stress are required to entrain these particles.

## 2.5 References


[1]. Pijush K. Kundu, Ira M. Cohen, 2010, “Fluid Mechanics”, 4th edition

[2]. Stephen B. Pope, 2002, “Turbulent Flows”, Cambridge University Press

[3]. Robinson S. K., 1991, "Coherent Motions in the Turbulent Boundary Layer," Annual Review of Fluid Mechanics, 23(1), pp. 601-639

[4]. Rothfus R. R., Monard C. C., Senecal V. E., 1950, “Velocity Distribution and Fluid Friction in Smooth Concentric Annuli”, Industrial and Engineering Chemistry, Vol. 42, No.12, pp. 2511- 2520

[5]. Walker J. E., Rothfus R. R., 1959, “Transitional Velocity Patterns in a Smooth Concentric Annulus”, A.I.Ch.E Journal, Vol. 5, No. 1, 51-54

[6]. Brighton J. A., Jones J. B., 1964, “Fully Developed Turbulent Flow in Annuli”, Journal of Basic Engineering, 86, 835-842

[7]. Rothfus R. R, Sartory W. K., Kermode R. I., 1966, “Flow in Concentric Annuli at High Reynolds Numbers”, A.I.Ch.E. Journal, Vol. 2, No. 6, pp. 1086-1091

[8]. Roberts A., 1966, “A Comment on the Turbulent Flow Velocity profile in a Concentric Annulus”, J. Hear MOSS Transfer, Vol. 10, pp. 709-712

[9]. Quarmby A.,1967, “An Experimental Study of Turbulent Flow through Concentric Annuli”, Journal of Mechanical Science, Vol. 9, pp. 205-221

[10]. Clump C. W., Kwasnoski D., 1968, “Turbulent Flow in Concentric Annuli”, A.I.Ch.E. Journal, Vol. 14, No. 1, pp. 164-168

[11]. Hanks R. W., Bonner W. F., 1971, “Transitional Flow Phenomena in Concentric Annuli”, Industrial & Engineering Chemistry Fundamentals, Vol. 10, No.1, pp. 105-113

[12]. Colebrook, C. R., 1939, "Turbulent flow in pipes with particular reference to the transition region between the smooth and rough pipe laws," J. Inst. Civ. Eng. (London), Vol. 11, pp. 133-156.

[13]. Lawn C. J., Elliot C. J., 1972, “Fully Developed Turbulent Flow through Concentric Annuli”, Journal of Mechanical Engineering Science, Vol. 14, No.3, pp. 195-204

[14]. Rehme K., 1974, “Turbulent flow in smooth concentric annuli with small radius ratios”, Journal of Fluid Mechanics”, Vol. 64, part 2, pp. 263-287

[15]. Rehme K., 1975, “Turbulence measurements in smooth concentric annuli with small radius ratios”, Journal of Fluid Mechanics, Vol. 72, part 1, pp. 198-206

[16]. Jones O. C., Leung J.C.M., 1981, “An Improvement in the Calculation of Turbulent Friction in Smooth Concentric Annuli1”, Journal of Fluid Engineering, Vol. 103, pp. 615-623

[17]. Ahn S. W., Kim K. C., 1999, “Characteristics of Turbulent Flow in the Annuli with Smooth and Rough Surfaces”, KSME International Journal, Vol. 13, No. 2, pp. 183-190

[18]. Dou H. S., Khoo B. C., Tsai H. M., 2010, “Determining the Critical Condition for Flow Transition in a Full-Developed Annulus Flow”, Journal of petroleum Science and Engineering”, Vol. 71

[19]. Fredrickson A. G., Bird R. B., 1958, “Non-Newtonian Flow in Annuli”, Industrial and Engineering Chemistry, Vol. 50, No. 3, pp. 347-352

[20]. Dodge D. W., Metzner A. B., 1959, “Turbulent Flow of Non-Newtonian Systems”, A.I.Ch.E. Journal, Vol. 5, No. 2, pp. 189-204

[21]. Virk P. S., Mickley H. S., Smith K. A., 1970, “The Ultimate Asymptote and Mean Flow Structure in Toms' Phenomenon”, Journal of Applied Mechanics, 1970, pp. 488-493

[22]. Bird R. B., 1976 “Useful Non-Newtonian Models”, Annual Review. Fluid Mechanics, Vol. 8, pp. 13-34

[23]. Zakin J. L., Ni C. C., Hansen R. J., 1977, “Laser Doppler Velocimetry Stduies of Early Turbulence”, The Physics of Fluids, Vol. 20, No. 10, pp. 85-88

[24]. Hanks R. W., Larsen K. M., 1979, “The Flow of Power-Law Non-Newtonian Fluids in Concentric Annuli”, Industrial and Engineering Chemistry, Vol. 18, No. 1, pp. 33-35

[25]. Bird R. B., Armstrong R. C., Hassager O., 1987, “Dynamics of polymeric liquids”, Wiley-Interscience, New York, Vol. 1

[26]. Pinho F. T., Whitelaw J. H., 1990, “Flow of Non-Newtonian Fluids in Pipe”, Journal of Non-Newtonian Fluid Mechanics, Vol. 34, pp. 129-144

[27]. Luo Y., Peden J. M., 1990, “Flow of Non-Newtonian Fluids through Eccentric Annuli”, SPE Production Engineering, Vol. 5, No.1, SPE 16692

[28]. Nouri J. M., Umur H., Whitelaw J. H., 1993, “Flow of Newtonian and Non-Newtonian Fluids in Concentric and Eccentric Annuli”, Journal of Fluid Mechanics, Vol. 253, pp. 617-641

[29]. Escudier M. P., Gouldson I. W., Jones D. M., 1995, “Flow of Shear-Thinning Fluids in Concentric Annulus”, Experiments in Fluids, Vol. 18, pp. 225-238

[30]. Escudier M. P., Oliveira P. J., Pinho F. T., Smith S., 2002, “Fully Developed Laminar Flow of Non-Newtonian Liquids through Annuli: Comparison of Numerical Calculations with Experiments”, Experiments in Fluids, Vol. 33, pp. 101-111

[31]. Japper-Jaafar A., Escudier M. P., Poole R. J., 2010, “Laminar, Transitional and Turbulent Annular Flow of Drag-Reducing Polymer Solutions”, Journal of Fluid Mechanics, Vol. 165, pp-1357-1372

[32]. Shah R.K., London A.I., 1978, “Laminar flow first convection in ducts,” Academic Press, New York.

[33]. Bagnold R. A., 1966, "An Approach to the Sediment Transport Problem from General Physics", Geology Survey Professional Paper

[34]. Cleaver J. W., Yates B., 1972, "Mechanism of Detachment of Colloidal particles from a Flat Substrate in a Turbulent Flow", Journal of Colloid and Interface Science, Vol. 44, No. 3, pp. 464-474

[35]. Phillips M., 1980, "A Force balance Model for Particle Entrainment into a Fluid Stream", Journal of Physics D: Applied Physics, Vol. 13, pp. 221-233

[36]. Okrajni S. S., Azar J. J., 1986, "The Effects of Mud Rheology on Annular Hole Cleaning in Directional Wells", Presented at the 1985 SPE Annual Technical Conference and Exhibition held in Las Vegas,, SPE 14178

[37]. Tomren P. H., Iyoho A. W., Azar J. J., 1986, "Experimental Study of Cuttings Transport in Directional Wells", Presented at the 1983 SPE Annual Technical Conference and Exhibition held in San Francisco, SPE 12123

[38]. William J. L., Mofjeld H. O., 1987, "Do Critical Stresses for Incipient Motion and Erosion Really Exist?" , Journal of Hydraulic Engineering, Vol. 113, pp. 370-385

[39]. Gavignet A. A., Sobey I. J., 1989, "Models Aids Cuttings Transport Prediction", Journal of Petroleum Technology

[40]. Ford J. T., Peden J. M., Oyeneyin M. B., Gao E. Zarrough R., 1990, "Experimental Investigation of Drilled Cuttings Transport in Inclined Boreholes", Presented at the 65th Annual Technical Conference and Exhibition of the Society of Petroleum Engineers held in New Orleans, LA, September 1990, SPE 20421

[41]. Graham D. I., Jones T. E. R., 1994, "Settling and transport of Spherical Particles in Power-Law Fluids at Finite Reynolds Number", Journal of Non-Newtonian Fluid Mechanic, Vol. 54, pp. 465-488

[42]. Clark R. K., Bickham K. L., 1994, " A Mechanistic Model for Cuttings Transport", Presented at SPE 69$^{th}$ Annual Technical Conference and Exhibition held in New Orleans, LA, U. S.A., September 1994 , SPE 28306

[43]. Kelessidis V. C., Bandelis G. E., 2004 " Flow Patterns and Minimum Suspension Velocity for Efficient Cuttings Transport in Horizontal and Deviated Wells in Coiled-Tubing Drilling", SPE Drilling and Completion, SPE 81746

[44]. Larsen T. I., Pilehavri A. A., Azar J. J., 1997, "Development of a New Cuttings-Transport Model for High-Angle Wellbores Including Horizontal Wells", SPE Drilling and Completion, SPE 25872

[45]. Pilehvari A. A., Azar J. J., Shirazi S. A., 1999, "State-of-the –Art Cuttings Transport in Horizontal Wellbores" , SPE Drilling and Completion 14 (3), SPE 57716

[46]. Nino Y., Lopez F., Garcia M., 2003, "Threshold for Particle Entrainment into Suspension", Sedimentology, VOl. 50, 247-263

[47]. Nguyen D., Rahman S. S., 1996, "A Three-Layer Hydraulic Program for Effective Cuttings Transport and Hole Cleaning in Highly Deviated and Horizontal Wells", Presented at IADC/SPE Asia Pacific Drilling Technology Conference, Kuala Lumpur, Malaysia

[48]. Rabenjafimanantosa H. A., 2007, "Particle Transport and Dynamics in Turbulent Newtonian and Non-Newtonian Fluids", PHD Dissertation

[49]. Azar J. J., Alfredo R., 1997, "Important Issues in Cuttings Transport for Drilling Directional Wells", Presented at the Fifth Latin American and Caribbean Petroleum Engineering Conference and Exhibition held in Rio de Janeiro, Brazil, August 1997, SPE 39020

[50]. H. Garcia, 2008, "Sedimentation Engineering: Processes, Measurements, Modeling and Practice", American Society of Civil Engineers

[51]. Yu M., Melcher D., Takach N., Miska S. Z., Ahmed R., 2004, " A New Approach to Improve Cuttings Transport in Horizontal and Inclined Wells", Presented at the SPE Annual Technical Conference and Exhibition held in Houston, U.S.A, September 2004, SPE 90529

[52]. Lockett T. J., Richardson S. M., Worraker W. J., 1993, " The Importance of Rotation Effects for Efficient Cuttings Removal During Drilling", Presented at

SPE/IADC Drilling Conference held in Amsterdam February 1993, SPE/ IADC 25768

[53]. Payne M. L., Cocking D. A., Hatch A. J., 1994, " Critical Technologies for Success in Extended Reach Drilling", Presented at SPE 69th Annual Technical Conference and Exhibition held in New Orleans, LA, U. S.A., September 1994, SPE 28293

[54]. Thomas R. P., Azar J. J., 1982, "Drillpipe Eccentricity Effect on Drilled Cuttings Behavior in Vertical Wellbores", Journal of Petroleu, Technology, Vol. 34, No. 9, pp. 1929-1937

# Chapter 2:

# Experimental Setup and Instrumentation

In this chapter experimental facility and instruments used for measurements are described in two subsections. In the first part, the horizontal flow loop and different parts of the main system are presented in detail. Specification and accuracy of all monitoring devices mounted on the flow loop are given. Data acquisition procedure using LABVIEW software and also calibration of pressure transducers are also explained. PIV technique, which has been used in measurements with turbulent flow, is explained thoroughly in a separate chapter following this one. The second section of this chapter is dedicated to experiments with cuttings. Detailed procedures of experiments, measurement techniques and analysis of the data are all explained.

## 3.1 Horizontal Flow Loop

Figure 3-1 is a schematic of the flow loop and its elements. The horizontal flow loop mainly consists of the following parts: Tank, Mixer, Centrifugal Pump, Pipe Lines, Glass Tubes & Annular Section, Pressure Transducers, Flow Meter, Control & Safety Valves, and temperature monitoring devices.

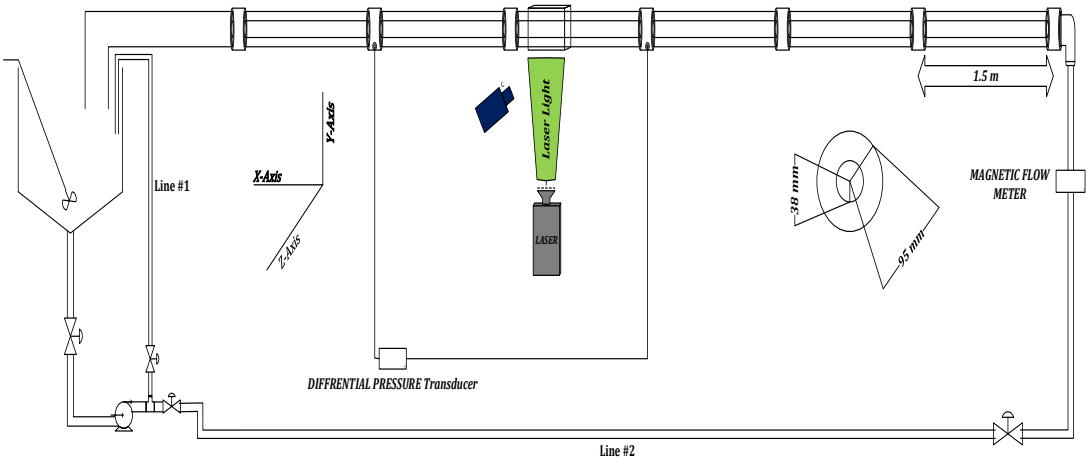


**Figure 3-1: Schematic of the Flow Loop**

The tank has a capacity of about 600 liter and is made out of stainless steel; it can be used for storing the fluid or as mixing pit for preparing solutions (Figure 3-2). The mixer is an air operating mixer with adjustable RPM. The tank is equipped with cooling jackets

as well as weight measurement sensors. Temperature sensors are mounted at the bottom of the tank and are used to monitor the temperature variations, if necessary by using cooling jackets, temperature of the fluid in the tank could be reduced to room temperature for isothermal experiments. A slurry centrifugal pump equipped with VFD (Variable Frequency Drive) is used for circulating the fluid through the pipelines (Fig.3.2). VFD feature of the pump allows setting the flow rate at desired value which is critical in repeating experiments at the same condition.


Figure 3-2 Pictures of the Flow Loop Component; The Tank, Pump, Mixer and Safety Valves and also Bypass line Could be Observed in the Picture

The pump exit is connected to two lines, one is going back to the tank (Figure 3-1; Line #1) which is a bypass and the other one is going to the flow meter and the annular section of the flow loop (Figure 3-1, Line#2). Line # 1 is always closed for PIV (Particle Image Velocimetry) experiments but as will be explained later it will be used in cutting transport experiments. For line #2 there is two pipes available to use (1 and 2 inches in diameter); for PIV experiments either line can be used as they do not have any effect on experimental conditions in the annular section. However, it is important to use the line

with smaller diameter in particle transport experiments to make sure that no particle settles down in this part of the system as we would like to have all solids to be transported to the test section and settle there. Small diameter of these lines allows us to achieve very high velocity and hence, fully developed turbulent flow conditions, which in turn guarantees that the solid particles do not settle as they are transported through these lines.

The flow rate is measured by means of a magnetic flow meter installed at the inlet of the annular section of the system (Figure 3-3). The flow meter is a Ω OMEGA IS 2.140 type and has a display monitor at the location where the flow meter is installed.

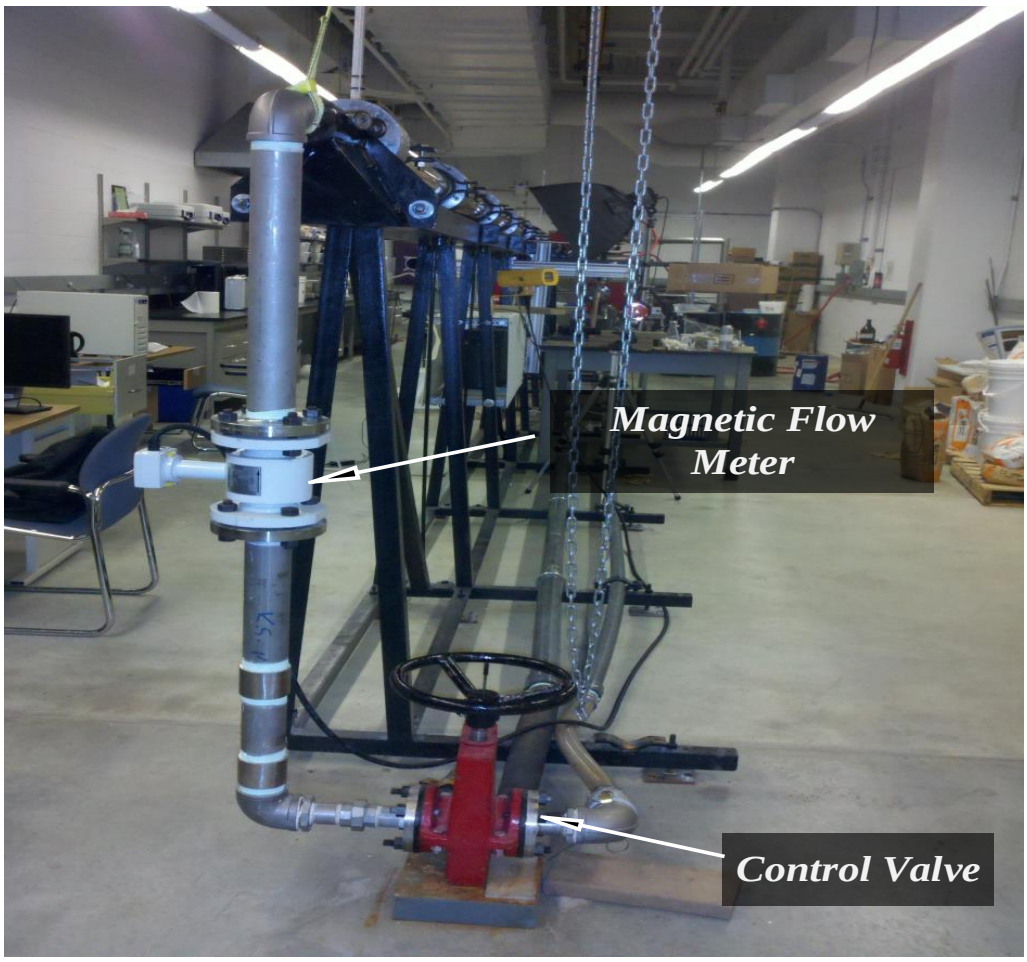


**Figure 3-3 Picture of the Vertical Section of the Flow Loop including the Magnetic Flow Meter**

Pressure drop is measured using a differential pressure transducer of type PX769. The accuracy of this transducer is 1 Pa. The distance between the two tap lines is 3.08 meter.

The first differential pressure tap line is located approximately $\sim 80D_H$ downstream of the flow to ensure a fully developed flow. Calibration of the pressure transducer needs to be done regularly. A digital pressure calibrator is used for calibration of pressure transducers.

The horizontal annular section of the flow loop is 9 meter long compromised of six 1.5 meter long glass tubes (Figure 3-4).

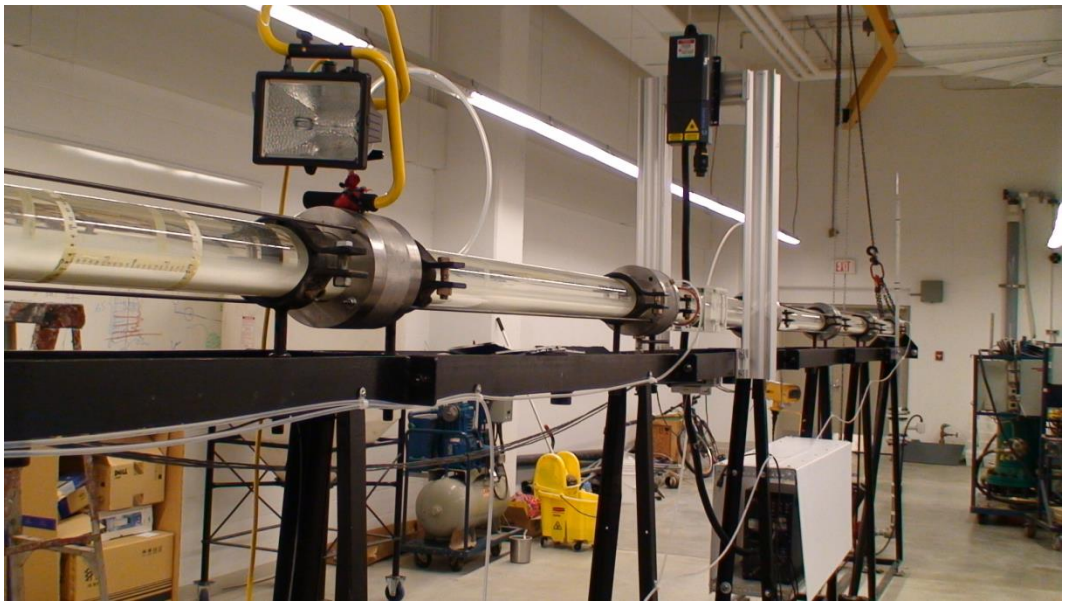

**Figure 3-4 Picture of the Glass Pipes and Connections**

The glass tubes are made of high quality optical glass with 100% transparency required for imaging technique. Glass pipes are Borosilicate glass with a refraction index of 1.47. The glass tubes are connected by means of specially designed stainless steel joints. The joints are having an inner diameter identical to the pipes ensuring a smooth path for the flow with minimal disturbance due to connecting the pipes. The inner pipe of the annuli is also made of high quality optical glass as well. Thickness of the inner pipes has been chosen properly in order to reduce sagging and vibration of the inner body during experiments. Inner pipes are 3 meter long each and are kept in the center of the annuli by means of 3 spikes at each end.

The outer pipe of the annuli has an inner diameter of 95 mm and wall thickness of 0.5 mm. The inner pipe has an outer diameter equal to 38 mm. with the given dimensions the hydraulic diameter and radius ratio of the annuli would be $D_H = 57$ mm , $\alpha = 0.4$.

There are in total 5 safety and control valves included in the experimental setup. The valves could be used to change the passage of the fluid or isolating a section of the system from the rest of the flow loop. Usage of the valves is in cutting transport experiments and it will be discussed later.

All devices mounted on the flow loop including pump, flow meter, temperature monitoring devices and pressure transduces are all connected to data acquisition system which is controlled by LABVIEW software by National Instrument (Figure 3-5). The software is programmed in such a way that allows the user to input the pump RPM which is controlled through VFD system. Data acquisition has been done by using LABVIEW with a frequency of recording of 20 HZ.

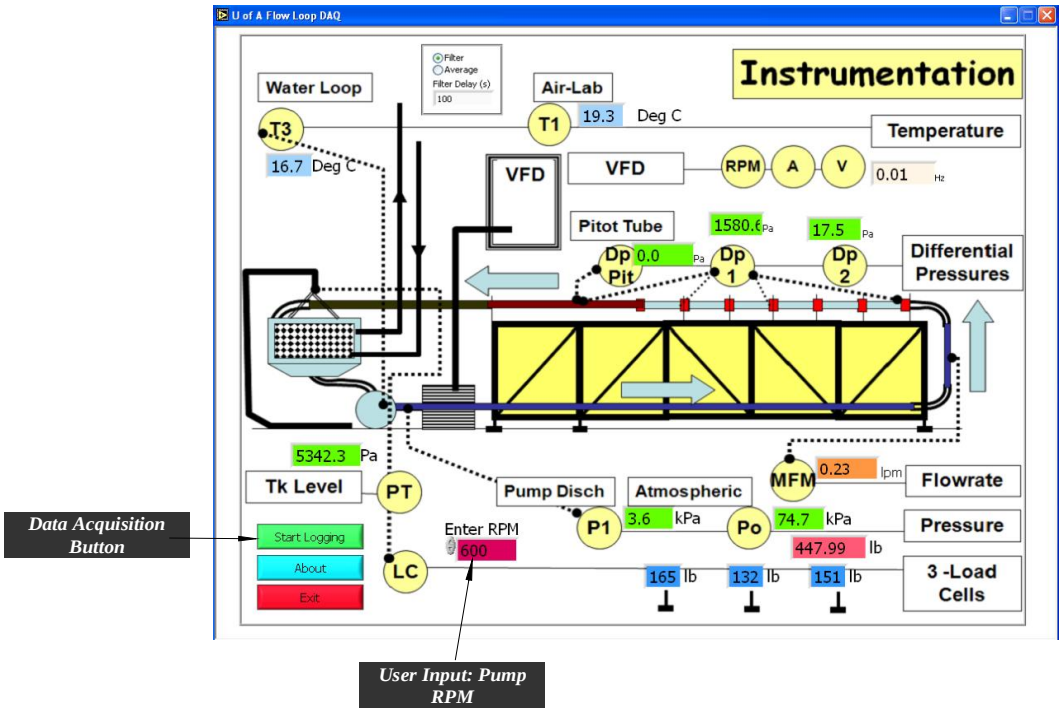


**Figure 3-5 Picture of the LABVIEW Software user Interface**

## 3.2 Cutting Transport in Horizontal Annuli

The primary focus of these experiments is to find the critical velocity required for entrainment of particles from the surface of a bed of particle deposits formed in the annuli. This is similar to hole cleaning process in oil and gas wells, where a bed of cuttings starts to form over time in the lower side of the annular space.

In this section, the procedure of how to establish a bed of particles from a given concentration of the cuttings in the flow is explained. Measurement tools and techniques are explained thereafter and at the end, methodology for data processing and also output data obtained from these experiments are discussed.

### 3.2.1 Establishing Bed of Particles

Objective is to add sand particles to the flow in order to form a bed in the annular section of the flow loop. Referring to Figure 3-6, all the steps are explained in the exact same order as needs to be done.

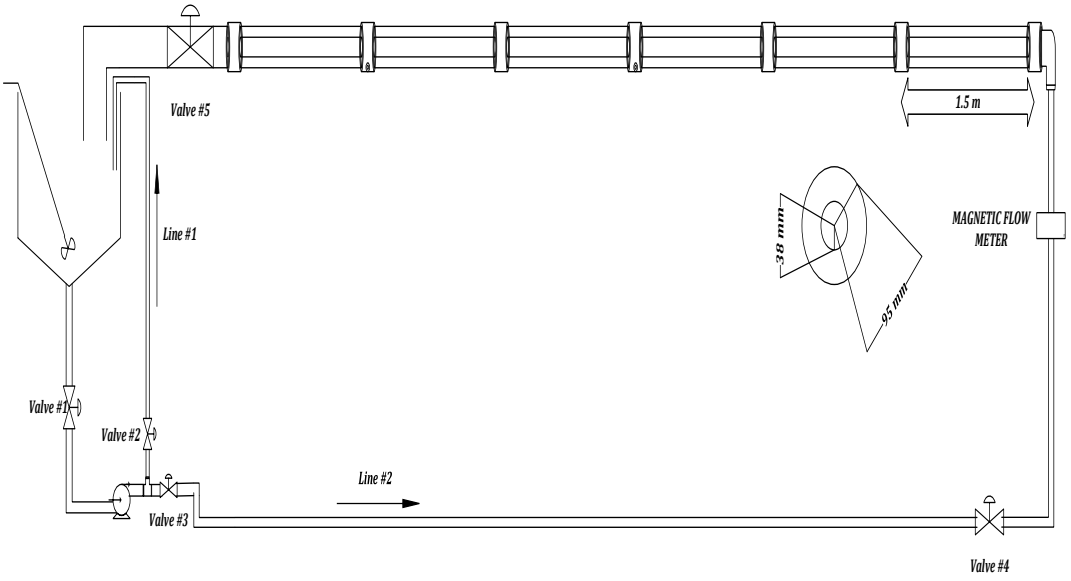


**Figure 3-6 Schematic of the Flow Loop**

I. Fill out the tank with water, 450 liter, and start circulating the water at the highest flow rate possible (In this step only valve # 2 is closed)

II. Based on the desired concentration of particles, start adding the weighed particles to the water in the tank gradually while stirring with the mixer.

III. After adding the particles to the flow, keep circulating the slurry mixture at highest flow rate possible until a homogenous mixture of particles and water forms in the annuli.

IV. Stop the pump quickly and isolate the horizontal section of the annuli by closing valves # 4 and 5.

V. The pump, tank and transport line (Line # 2) needs to be washed carefully after isolating the annular section of the flow loop.

VI. The fluid in the annuli need to be allowed to rest for 24 hours in order to let all the particles in suspension to settle down in the bed..

One consideration in establishing a bed is to make sure circulation velocity is high enough in transport lines to avoid particle deposition in this part of the system. One solution for this problem is to use smaller transport lines in order to make sure that the velocity is high enough to carry the particles out of this pipes. There are two diameter sizes available for transport line # 2 in Figure 3-6, however, for these experiments the smaller line needs to be used always while for PIV experiments doesn't matter which line is used.

In real drilling operation it's desirable to keep the cuttings concentrations below 5% in order to avoid pipe stuck or any other problems which may occur due to high cutting concentration. A concentration of 3% (volumetric) has been used throughout the experiments in this study. The cuttings used in these experiments were natural sands with density of 2650 $kg/m^3$. Each experiment would require about 20 kg sand. Detailed analysis on particles size distribution is explained in the chapter.

### 3.2.2 Measurement Tools and Techniques

The primary goal of particle entrainment experiments is to find the critical velocity at which particles starts to move in different form of motions (i.e., rolling, saltation and suspension). Flow visualization is a powerful, tool which can be used in order to track the changes in flow or monitor the bed movement. A high resolution recording camera and a light projector was used to record particle motion in a bed (Figure 3-7).

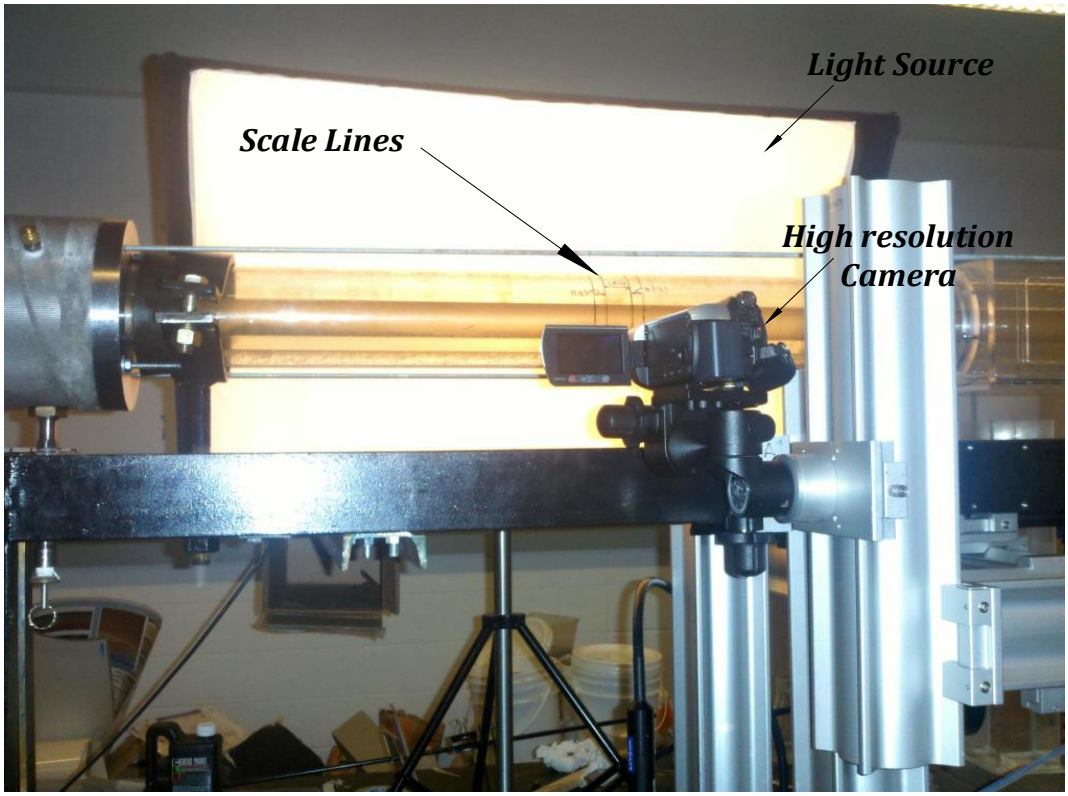


**Figure 3-7 Experimental Setup in Cutting Transport Experiments**

Experiments are tried to be conducted as similar as possible to real drilling case. One condition for that is to prevent the particles from going back to the flow after they are removed from the bed. In real drilling operation, sands and cuttings are separated from drilling fluids at the surface using solid control equipment such as shale shaker before the drilling fluid is pumped back into the well. The flow loop is a closed system meaning that the fluid under circulation is always the same fluid during the experiments. In order to collect the particles which are removed from the bed, two special filters with opening sizes smaller than sand particles are attached at the end of the pipeline returning to the tank (i.e., at the exit of the annular section of the flow loop ). The filters catch the particles and at the same time let the fluid go back to the tank. Although the loop is a closed system, by using filters it acts like an open flow loops.

The camera and light source are located at approximately $\sim 100 D_H$ in order to make sure that the flow is fully developed at the point of observation. After adjusting the camera and light source, attaching the filters to the exit of the flow line and preparing the fluid, the experiment can be started.

The experiments always starts with the lowest possible flow rate to ensure that the velocity in the annulus is lower than the critical velocity of particle movement (usually at around 0.15 m/s), then the velocity is gradually increased by changing the pump RPM until the critical velocity is reached, which is determined based on particles movement captured by the camera. The increment of velocity on each step can be as low as 0.02 m/s but after changing the velocity sufficient time must be given to the flow and bed to stabilize before concluding anything about the flow condition in hand.

At each fluid velocity, pressure drop is recorded as well. This is useful in wall shear stress calculation and comparison of performance of different fluids.

In summary, the experiment start with the lowest velocity, after allowing the flow and bed to stabilize, pressure drop and a video film of the bed along with velocity data are recorded before increasing the velocity to the next level.

In an attempt to measure dunes velocity 4 lines have been drawn on the outer surface of the outer pipe of the annuli (Figure 3-7). The distance between the lines are known and while recording the motion of particles in the bed, these lines are in the view plan of the camera. Once dunes formed, they will move at certain velocity along the horizontal axis (parallel to the flow direction). This whole process of particle/dune movement is recorded by camera. After the experiment, the video film is post processed to obtain time required for dunes to move between two marker lines. By using the time it takes for the head or tail of a dune to pass two of the marked lines, the velocity is then calculated as the distance between the marker lines is known.

### 3.2.3 Data Processing and Output results

Critical velocity of particle movement in different form and wall shear stress required for that motion for different type of fluids and particle diameter are the main output results of these experiments. Different type bed motion (i.e. dunes, rolling, saltation, and suspension) at different velocities could also be added to the output list as well. In later processing of the results, dunes velocities also can be achieved through the instruction explained earlier.

# Chapter 4:

# Particle Image Velocimetry

In these chapter fundamentals concepts of Particle Imaging Velocimetry (PIV) technique are discussed. Proper setup configuration along with adjustment of the devices are shown and explained. Processing and post-processing of PIV images and type of output results are discussed in detail.

## 4.1 PIV Technique: Concepts and Fundamental

PIV technique allows measurement of the velocity field by imaging the track of particles in the flow. The concept is as easy as obtaining the displacement of a tracer particle in a short but known period of time and then calculating the velocity. In order to obtain a particle displacement, one needs to know the location of the particle at time $t_0$ and $t_1$ which is done by taking two pictures at these two times. In the first picture at time $t_0$, the exact location of the tracer particle can be calculated in a 2-D plane with respect to a predefined origin of the axis. $\Delta t$ second later in the second picture, location of the same tracer particle can be found through statistical analysis and by subtracting the recorded displacement .

Although the concept of the imaging technique seems relatively easy, implementation of such concept in micron size is not a trivial task. As PIV basically works with images, one of the first conditions for using PIV technique is the transparency of the measurement environment. In order to obtain best results with PIV, measurement environment has to be 100 % transparent to light and visible to camera. Because PIV can be utilized in a 2-D or 3-D configuration, from now on the discussion will be on 2-D PIV as this is the set-up used in this research.

A 2-D PIV setup requires a light source and a camera or recording device. The light source has been a double Pulsed Laser with a special diffuser at the end in order to emit the light in plan shape. A CCD camera featured as double frame was the mean of recording and taking the pictures of the flow, the double framing and double pulsing features are the most important properties of the devices in PIV and will be discussed later.

The proper orientation of the camera and laser light sheet is that the camera view is perpendicular to laser light, Figure 4-1. Once the camera and laser light are properly aligned, measurements can be started if a seeded flow is already in place as well.

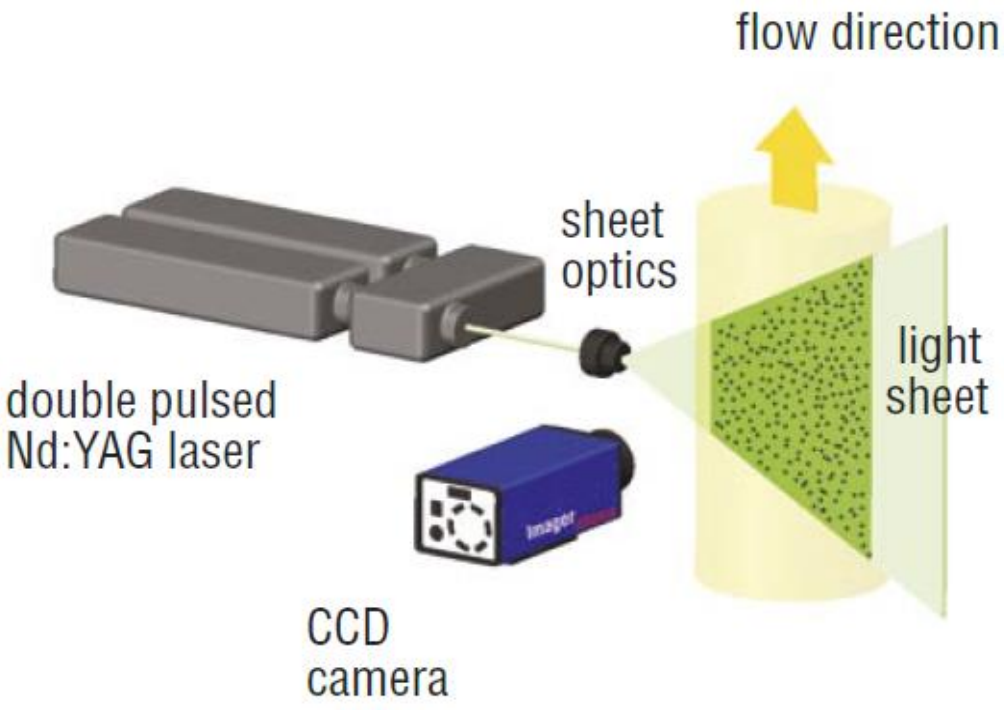


**Figure 4-1 Typical 2-D PIV Setup**[5]

Following discussion assumes that a 2-D PIV setup as described in Fig. 4-1 and a flow with tracer particles are used. A beam light will be emitted from the laser; the light sheet will illuminates the flow and tracer particles. As soon as the flow is illuminated, a picture of the flow could be acquired by the camera. In this picture tracer particles appear like bright points on a black background (Figure 4-2). Until now, only one picture of the flow is acquired. $\Delta t$ second later another pulse from the laser is emitted and the second picture of the flow is then obtained. A pair of pictures has been obtained with $\Delta t$ difference, location of each tracer particle can be calculated through some statistical method and once the displacement is known, the instantaneous velocity field can be obtained. In the following section details of statistical procedures followed by PIV in order to obtain the location of tracer particles and also post processing procedures along with output results are discussed.

[5] Picture from http://www.uwyo.edu/mechanical/facilities/aerodynamics/piv/index.html

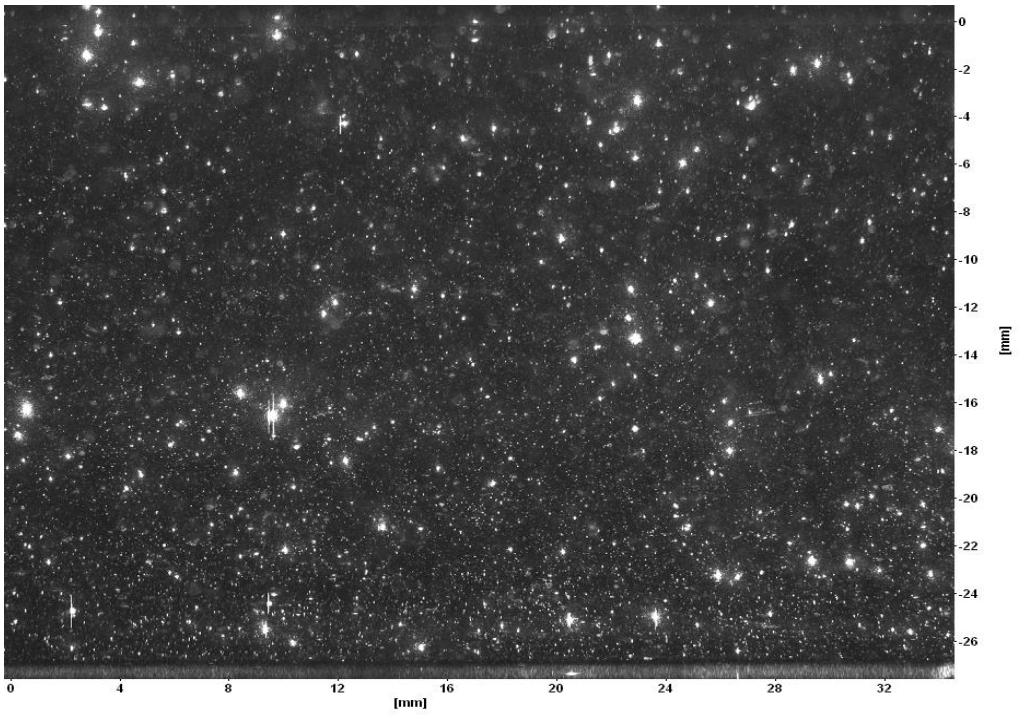


**Figure 4-2 A Typical PIV Picture, Note That the Bright Points are Tracer Particles in the Flow**

## 4.2 FFT-Based Cross-Correlation and Output Results of PIV

In this section the method and procedure underlying how instantaneous velocity vector can be obtained through statistical analysis of a pair of pictures is discussed. The main software for processing PIV images is DAVIS 7.2, which will be discussed here briefly. Output results obtained by processing n pairs of pictures will also be explained.

Assume a pair of pictures is obtained by using the instructions given before and now we want to get the instantaneous velocity field out of this pair. In the first step, an interrogation window with the size of N×N pixels will be chosen in the first picture and following that a search region in the second picture will be examined for similarities. Direct Cross-Correlation Method (DCM) will be applied for finding the local similarities. After searching, bright points showing the highest correlation will be chosen as the most likely destination of the bright points in the first frame [3].

Displacement of a particle can be calculated after finding its destination. In order to obtain the displacement in real world scales the camera has to be calibrated or the images

need to be scaled. This will be explained in camera calibration section. The displacement, $\Delta s$ , of a tracer particle is known. Time difference, $\Delta t$ ,between two pictures is also known. $\Delta s$ is broken down into its component and instantaneous velocity field is then obtained through Eq.( 4-1).

$$\begin{cases} U = \dfrac{\Delta x}{\Delta t} \\ V = \dfrac{\Delta y}{\Delta t} \end{cases} \qquad \textbf{Eq.( 4-1)}$$

One more step is required before finalizing the velocity field, which is exactly similar to the previous steps with the only difference being in the size of interrogation windows. In this step, an interrogation window of size of $\frac{N}{2} \times \frac{N}{2}$ is chosen and again through applying DCM or FFT-based (Fourier transformation) Cross Correlation, local similarities are searched. The other difference in this step and previous step is that vector field obtained in previous step is taken as an offset value in the second attempt of finding the velocity field. Instantaneous velocity field is then obtained and can be processed for more information about the flow. Figure 4-3 is a graphical representation of PIV processing procedures [6]**[**1].

The procedure explained previously applies for a pair of pictures. Processing say n pairs of pictures involve some extra steps, which will be explained here. First of all, in each experiment 300 pairs of pictures were taken and analysed in order to make sure that local events which may appear in one or more pairs of pictures do not affect the average and final results. In fact, considering the shutter speed of the camera (5 pairs/sec), obtaining 300 pairs of pictures takes about 60 second, which seems sufficient for monitoring a turbulent flow. In reality, the frequency depends upon the computer which is used to control the camera and in most of the experiments this frequency was recorded to be 2.5 pairs per second.

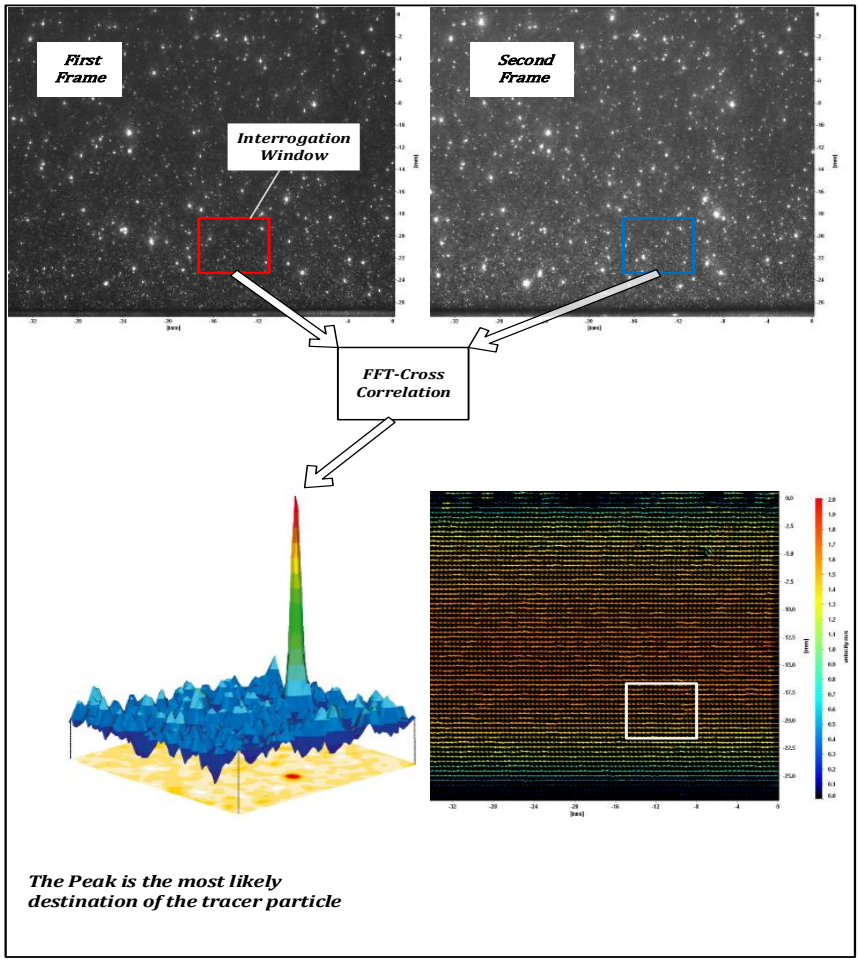


**Figure 4-3 PIV Post-Processing Procedure in Obtaining Instantaneous Velocity Field**

Averaging all pairs of pictures is always the first step. Normally due to light scattering or light dispersion or even noises in the environment, PIV pictures contain some distortion especially close to solid surfaces. Pictures averaging are an effective way to reduce the noises in the pictures. The concept is that the ransom fluctuations which are below or higher than the actual picture data will be accumulated in one average picture. The more the number of the averaged picture, the more accurate would be operation. In the second step one should subtract all the raw images from the average picture acquired in the previous step. This will help in reducing the distortions in each individual frame.

The third step is to apply FFT-based Cross-Correlation to n pairs which are obtained from previous step. Although this step has been explained earlier, there are some

parameters, which need to be picked up correctly in order to get accurate results. First parameter is the size of interrogation window. Very small or very large interrogation window sizes are not favourable. It is recommended by LAVISION in their manual for PIV that interrogation windows of size of 64×64 pixels followed by 32×32 pixels to be used for processing the images and obtaining the instantaneous velocity field. The size of interrogation windows for this study are chosen as the same as the ones recommended by LAVISION. Another parameter which needs to be set before applying DCM is the overlapping percentage of interrogation windows. LAVISION recommends 50 % and that is used throughout this research [6]. A typical vector field after applying DCM is shown in Figure 4-4.

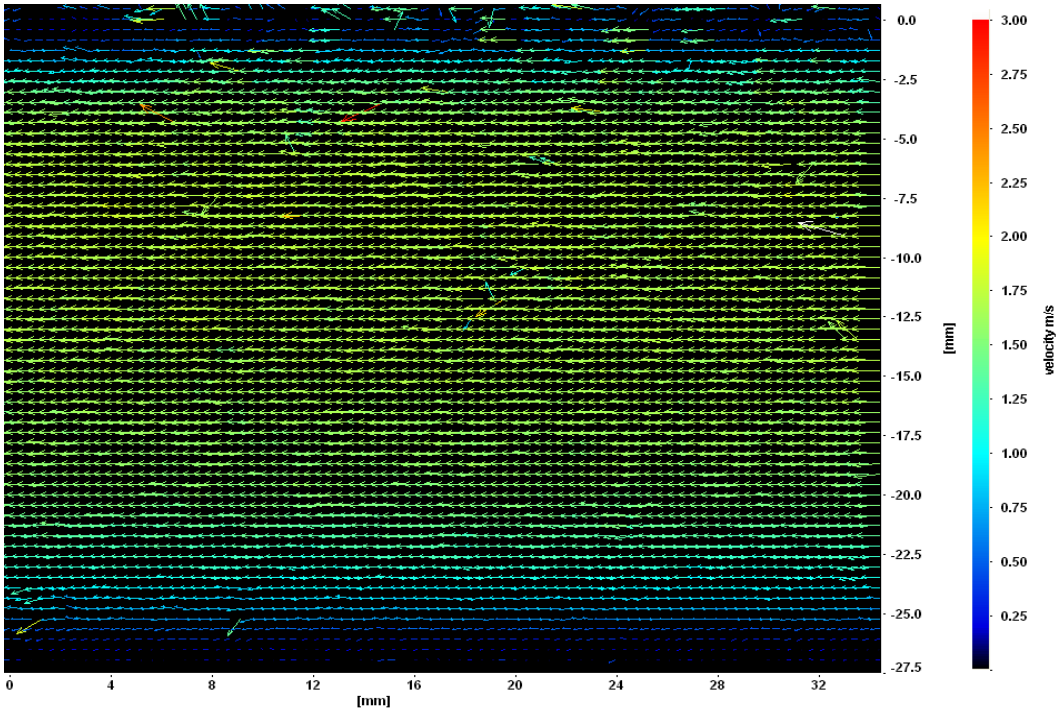


**Figure 4-4 Instantaneous Velocity Field Obtained after Applying FFT-based Cross-Correlation to PIV Pictures**

Before finalizing the instantaneous velocity field, one more step needs to be performed and that is called vector post-processing. Vector post-processing basically check each individual velocity field for anomalous vectors which may have resulted because of error in cross correlation of the images. If any vector appears completely off the trend of its neighbour vectors, it is eliminated. Vector post-processing helps in smoothing the vector field and removing the bad vectors which are for sure not correct.

For example, sometimes it is observed in a vector field that one vector showing velocity in a different direction than the all other surrounding velocity vectors, which means it is for sure not correct. After finishing this step the instantaneous velocity field is obtained for n pairs, which give n vector fields. Figure 4-5 is the final vector field after post processing operation.

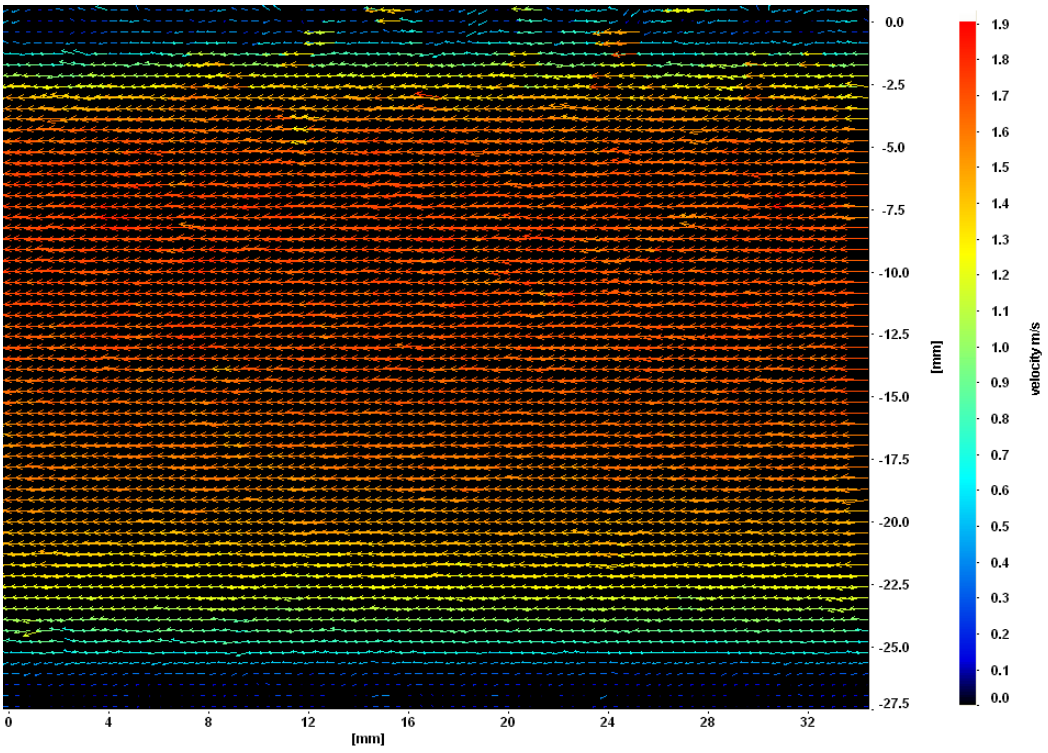


**Figure 4-5 Instantaneous Velocity Field after Applying Vector-Postprocessing**

Based on what is needed, users can perform many different operations on vector fields obtained previously. Since mean axial velocity is of great interest in this research, the next step is dedicated for calculation of the time average of the velocity. Time averaging of instantaneous velocity fields is also done using DAVIS, which in return gives the time average velocity of the flow $(\bar{u}, \bar{v})$. Also at the same time, along with the calculations of $\bar{u}$ and $\bar{v}$ other properties of the flow such as RMS of fluctuation velocities, Reynolds stresses, Turbulent Kinetic Energy can also be calculated by just selecting the proper options.

As a summary for the discussion on PIV, after taking pictures of a seeded flow, each pair of these pictures are analysed by applying DCM in order to find the instantaneous velocity field. Vector post-processing is then applied to remove the bad vectors. Time

average of velocity, RMS of fluctuation velocities, Reynolds stresses velocity gradients, turbulent kinetic energy, mean kinetic energy, swirling and vorticity all are the parameters, which can be calculated from instantaneous velocity fields and DAVIS software.

## 4.3 PIV Components: Descriptions and Details

### 4.3.1 Double Pulsed Laser

A double pulsed ND.YAG laser (Figure 4-6) from NEW WAVE INC. capable of emitting two pulses of light in a short and adjustable period of time was used as the light source in all PIV measurements. The wavelength of the light is 532 nm with a frequency of 50 HZ. The laser is connected to a special diffuser at the end, which emits the light in plan shape [7].

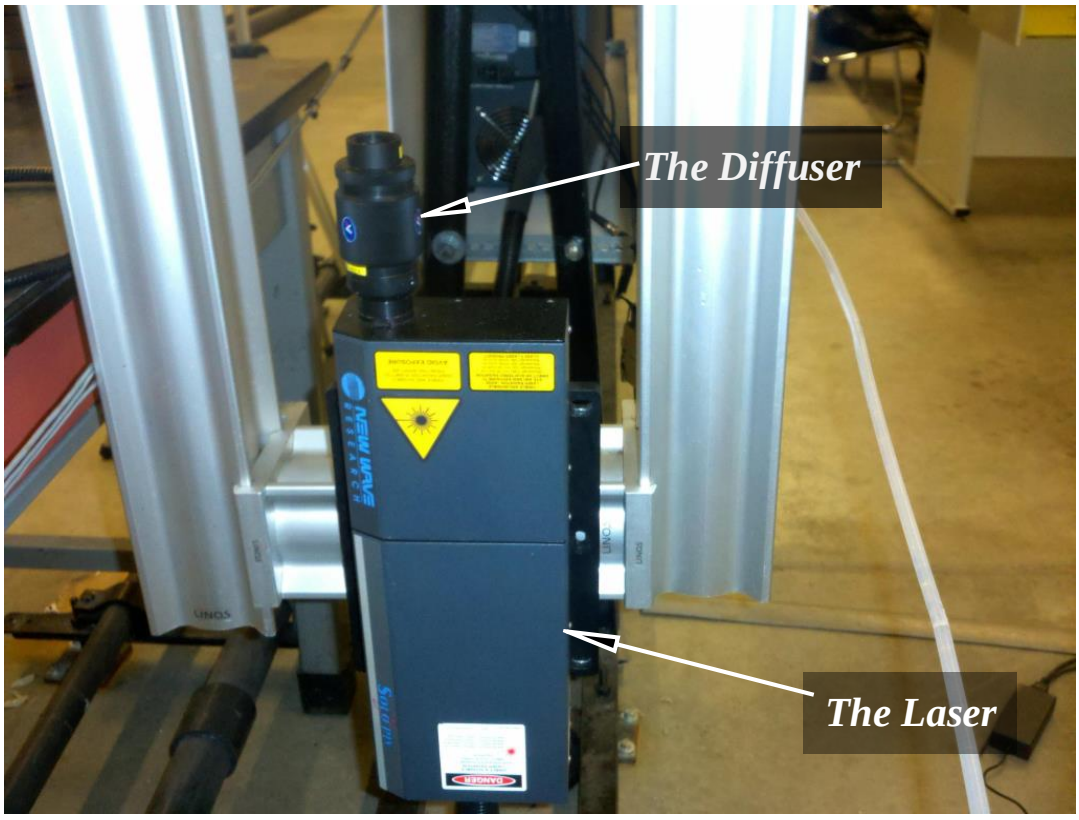


**Figure 4-6 Picture of the Double Pulsed Laser and Special Light Diffuser**

Thickness of laser light beams varies from 0.5 mm up to 3.5 mm, however, in this study it was kept at 0.5 mm for all the experiments. Thick laser light is not favourable and may cause errors in measurements, this is especially important when there is a big gradient of one of the parameters in the direction of the camera view or normal to laser light sheet. For example, if there is a big change in axial (along x axes) velocity say at $z_1$ which is the closer side of the laser light to camera and $z_2$ which is the far side of the light sheet, then there will be a big error in velocity measurements. In this study, the flow is unidirectional (only axial, no radial or tangential flow) which means there is no significant change in flow parameters along z axis where laser light thickness may affect the readings. Therefore, it can be concluded that laser light thickness has no considerable effect on measured properties of the flow in this study [2].

### 4.3.2 CCD Camera and Lenses

A double frame high resolution (1376×1040 pixels) CCD camera has been used for capturing the pictures of the flow in this research (Figure 4-7). The framing rate of the camera varies and can be as high as 5 frames per second (each frame is a pair of pictures). The most important feature of the camera is its double framing capability which allows taking pictures in a very short period of time. The time interval between two pictures of a pair is adjustable and can be as low as 500 ns. This time interval depends upon fluid velocity and field of view of the camera (field of view itself depends upon zooming and the type of lens used) and has to be adjusted prior to taking any data. Normally, the time interval should be selected properly that allows an individual tracer particle to move about 5 to 8 pixels from the first picture of a pair to the second picture [8].

Depending upon what type of results one is interested to obtain, different types of lenses may have to be used. For example, for catching the behaviour of the flow in a very small region (i.e., close to the solid surfaces) lenses with high zooming capabilities need to be utilized, while for monitoring the behaviour in larger areas smaller lenses are needed. A 60 mm Nikon AF Micro Nikkor plus an extension tube of size of 30 mm has been the primary lens of taking data in wall region where deep zooming is required. For the purpose of taking data in the whole annular gap, which is needed for quantifying the radial locations of maximum velocity and zero shear stress, a 50 mm Nikon AF Nikkor with a 12 mm long extension tube was used.

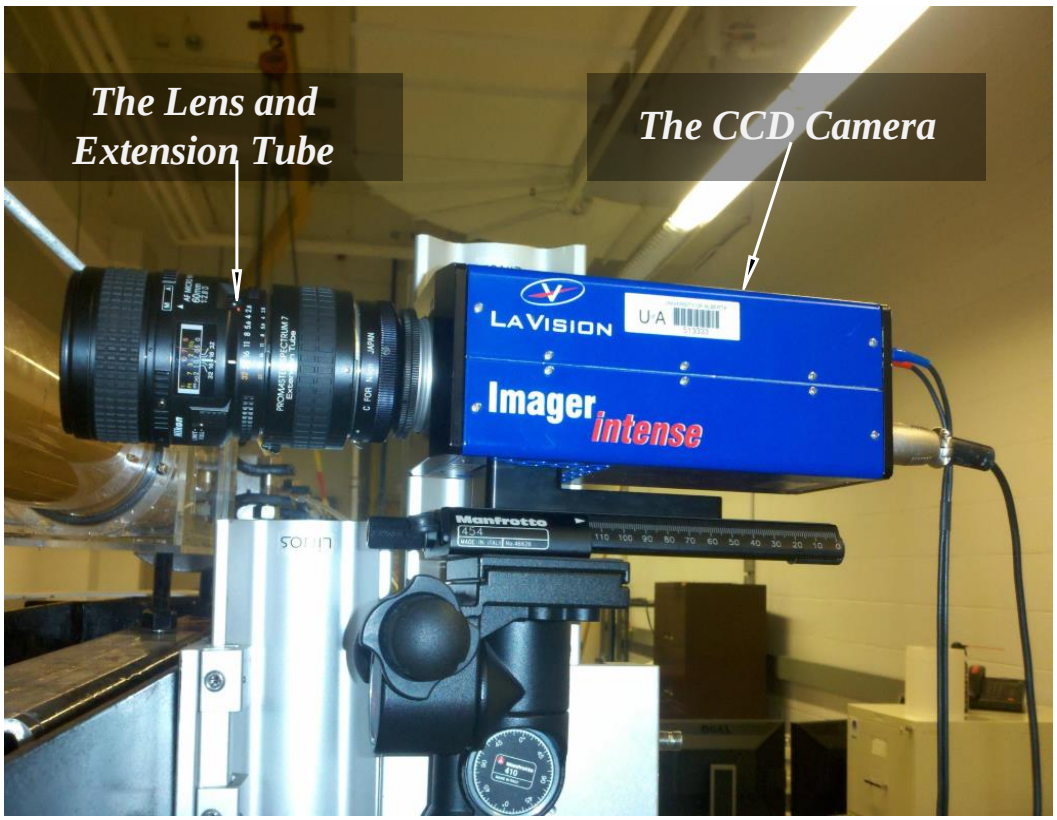


**Figure 4-7 Picture of the CCD Camera and the Lens with Extension Tube**

## 4.4 Camera Calibration

It has been stated that the proper timing between two images of a pair of pictures should allow one particle to move about 5 to 8 pixels in that time. In order to convert pixels to real world coordinates, one must calibrate the camera with respect to the plan at which laser is illuminating the tracer particles. Calibration of the camera means specifying the distance between two points in an image taken by the camera and then scaling up the whole picture with respect to this distance; of course during the calibration and after that, during data acquisition, the position of the camera should not change at all [1], [2].

For 2-D PIV, calibration of the camera can be done in different ways. One way is to put a scale visible to camera at the exact location of laser light sheet and then taking a picture of the scale. Once the picture is acquired calibration could be done by using DAVIS software under calibration tab. This is the easiest way but it is not recommended.

A second approach is to design a calibration target. This approach is adopted in all the experiments conducted for this research. Calibration target could be circles of known diameter. The distance between centers of the circles has to be constant and also known. It could also be crosses instead of circles. The target needs to have a black background with circles or crosses being white. The advantage of using calibration targets instead of scale or ruler is that they also reduce the image distortion because calibration is done with respect to both axes. Figure 4-8 shows an example of the target with circles.

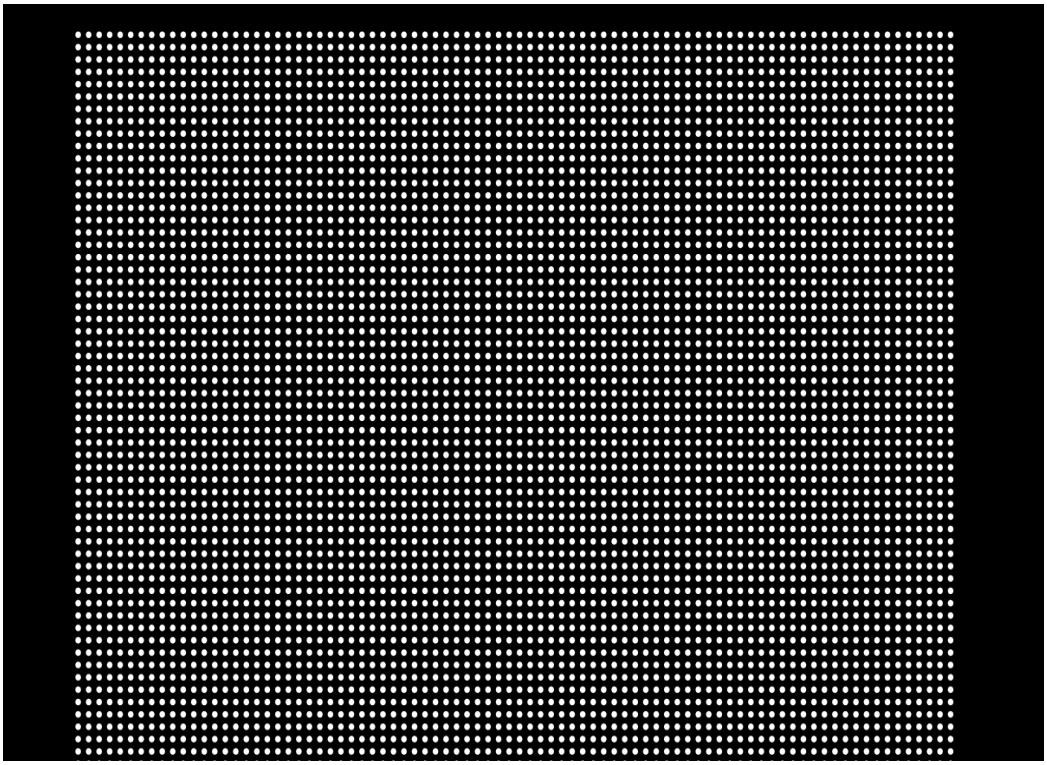

**Figure 4-8 Calibration Target used for Calibrating the CCD Camera**

For calibration of the camera, in each experiment a calibration target similar to Figure 4-8 was placed in the camera view plan and exactly in a sheet illuminated by the laser light. After taking a picture of the target in DAVIS software, under calibration tab one must select the proper calibration target type (for example circles here) and also specifies the distance between centers of two adjacent circles and their diameter. In the next step three circles have to be identified and marked by the user. The proper order is first choose any circle (must pick the center), next circle has to be the one closest to the first one and on the right side of it and finally, the third one is the circle right on top of the first selected circle. In the next step, the LAVISION software will search for other circles and

all other circles will be marked (Fig. 4-9). In this step, the software needs to find at least 25 circles in a 5 by 5 grid block that is the minimum number of grids required for a reliable calibration. The last step is automatically done by the software which is scaling up the picture and axis with respect to dimensions acquired previously [6].

Although the calibration of the camera is done at this point, it is always useful and sometimes necessary to define an origin point for the axis. This becomes important in analysing the data, where one needs to know the exact distance from the solid surfaces. The origin point is always taken on one of the walls in order to simplify later analyses, where y distance would be exactly the distance from the wall.

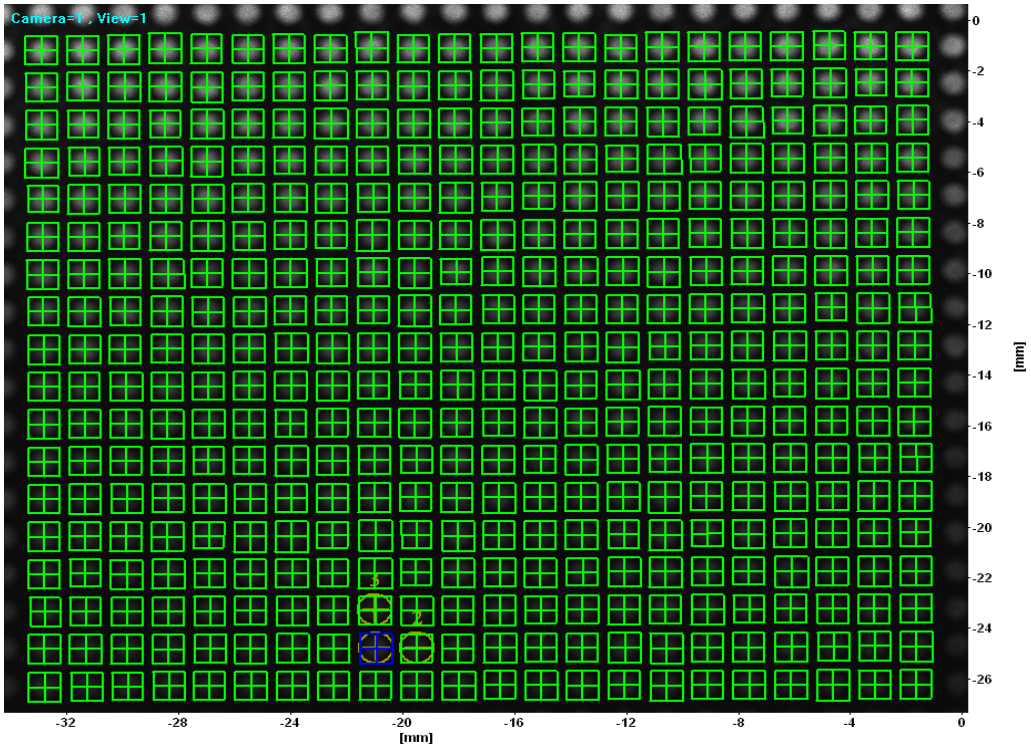


**Figure 4-9 Picture of the Calibration Target after the Step at which Davis Software have Searched for the Circles ; Note that Blue Circle is the First Choosen Circle by the User**

## 4.5 Data Acquisition

A special computer is dedicated for data acquisition and processing of the PIV data. The computer is equipped with two special boards, which controls the camera triggering

and laser light pulses, which indeed synchronises these two and also adjust camera exposure time during each laser shot.

The primary and main tool of image processing has been DAVIS 7.2 provided by LAVISION. All the processing has been done using this software and as output file the data can be transferred as text file for further analysis in MATLAB or Microsoft Excel.

## 4.6 The Observation Window

One of the problems associated with PIV technique is the light scattering and refraction of the light. This problem is especially important in round tubes and may affect the results for near the wall data.

Light scattering happens because of the cylindrical shape of the glass pipe. One solution for this problem is to use pipes with rectangular outer appearance and round inner shape. Designing and ordering such pipe can be expensive and may take a very long time. One alternative solution to this problem is to design a rectangular box which can surround the glass pipes. This box is rectangular and is made out of Plexiglas with 100% transparency. The rectangular shape of the box will prevent and reduce light scattering due to cylindrical shape of the glass tubes. This box is called the "Observation Window" and is located approximately $\sim 100 D_H$ downstream of the inlet, where all the PIV measurement are taken while ensuring the flow is fully developed at this point (Fig.4-10).

Refraction of the light happens when light passes through one medium (air) to another (glass) with different refraction indexes. To reduce light refraction due to difference in refraction indexes, the rectangular box which is explained earlier was filled up with Glycerol. Glycerol has a refraction index of 1.47 which is very close to the refraction index of the borosilicate glass pipes used in our flow loop.

Overall, the Observation Window is a rectangular box filled up with Glycerol surrounding the glass tubes at a location where PIV measurements are taken. The purpose of installing this box is to reduce the light scattering and refraction of the light in the measurement section of the flow loop.

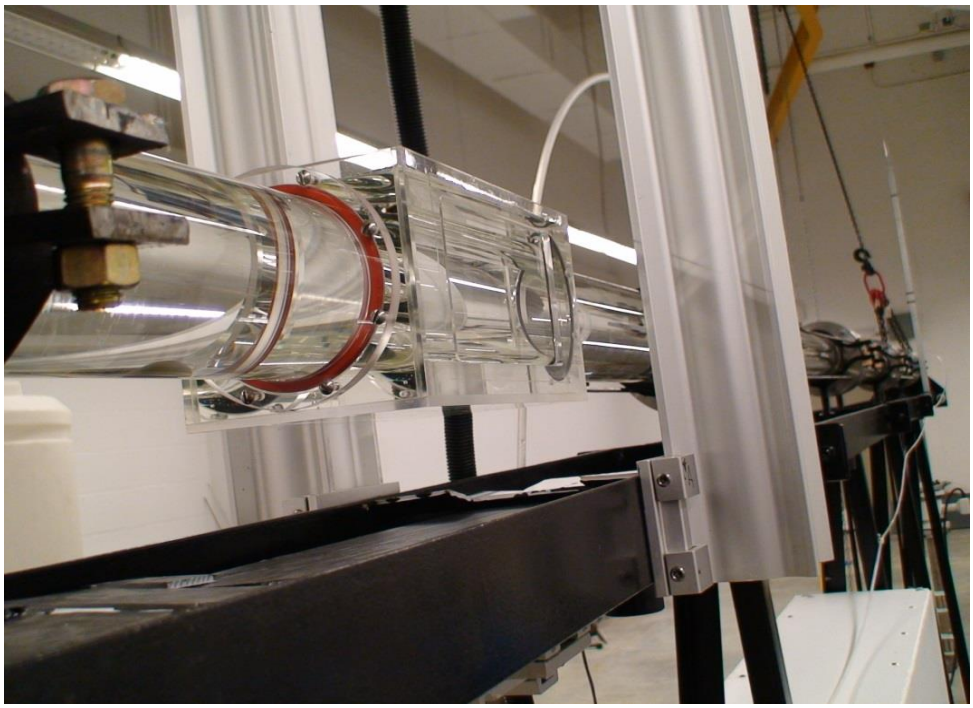

**Figure 4-10 Picture of the Observation Window; the Rectangular Box Filled with Glycerol**

## 4.7 Seeding the Flow and Tracer Particle Properties

PIV technique works by capturing the pictures of impurities (small particles) in the flow. These particles upon incident of laser light change the direction of the light towards camera, which makes them visible to camera. Usually there are not enough particles in fluids for PIV imaging and hence, tracer particles are needed to be added into flow artificially. Tracer particles have to be very small in order to be able to follow the flow instantaneously and also have a different refraction index from the fluid to reflect laser light toward the camera upon incident of the light. One more important feature of the seeding particles is that they should be neutrally buoyant in order to stay in suspension, avoiding deposition or flotation. Based on what have been said every fluid demands its own seeding particles based on the properties of the fluid and flow conditions.

Hollow glass particles with a mean diameter of 10 μm and a density equal to $1.1 \pm 0.05\,\mathrm{g/cc}$ were added to the fluid in order to enhance resolution of PIV pictures; consequently increasing the number of vectors and accuracy of the measurements. The concentration of the tracer particles should not be too high; in that situation many points would show high correlation in the FFT-based cross-correlation, which would result in

erroneous results for velocity field. A concentration of maybe 20 up to 100 PPM should be enough for tracer particles.

One consideration in choosing proper tracer particles is that they should follow the flow instantaneously. This is critical in obtaining accurate results of the behaviour of the flow especially in very chaotic and turbulent flows. Stocks number is an indicator of how fast a particle responding to the flow and normally if this number is smaller than 1 it can be said that the particle follows the flow instantaneously. Stocks number is defined through following equations [47].

$$St = \frac{\tau_p}{\tau_f} \qquad \textbf{Eq.( 4-2)}$$

$$\tau_p = \frac{\rho_p {d_p}^2}{18\mu} \qquad \textbf{Eq.( 4-3)}$$

$$\tau_f \sim \frac{\nu}{{u^*}^2} \qquad \textbf{Eq.( 4-4)}$$

$\tau_p$ is the particle relaxation time. The effect of seed particle size and density, pronounce itself through this parameter. The smaller the diameter or density, the faster the respond of the particle to the flow. $\tau_f$ can be called the macroscopic relaxation time and depend solely upon flow conditions and not particle properties. Generally Stock's number smaller than 1 is favourable but for precaution the upper limit of 0.1 has been taken for this study. Table 4-1 is a summary of calculated Stock's number for experiments with water at 6 different flow rates. As the numbers in Table 4-1 show, the highest Stock's number is actually smaller than 0.05 which means the selected tracer particles are following the flow instantaneously. Figure 4-11 also show a plot of Stock's number versus flow rate for water.

**Table 4-1: Calculated Stock's Number of Tracer Particles for Water**

| $Q(\frac{lit}{min})$ | $\tau_p$ | $\tau_f$ | $St$ |
|---|---|---|---|
| 110 | 5.55556E-06 | 0.002505 | 0.002218 |
| 175 | 5.55556E-06 | 0.001129 | 0.004921 |
| 238 | 5.55556E-06 | 0.000674 | 0.008248 |
| 303 | 5.55556E-06 | 0.000471 | 0.011788 |
| 365 | 5.55556E-06 | 0.000334 | 0.016629 |
| 429 | 5.55556E-06 | 0.000262 | 0.021216 |

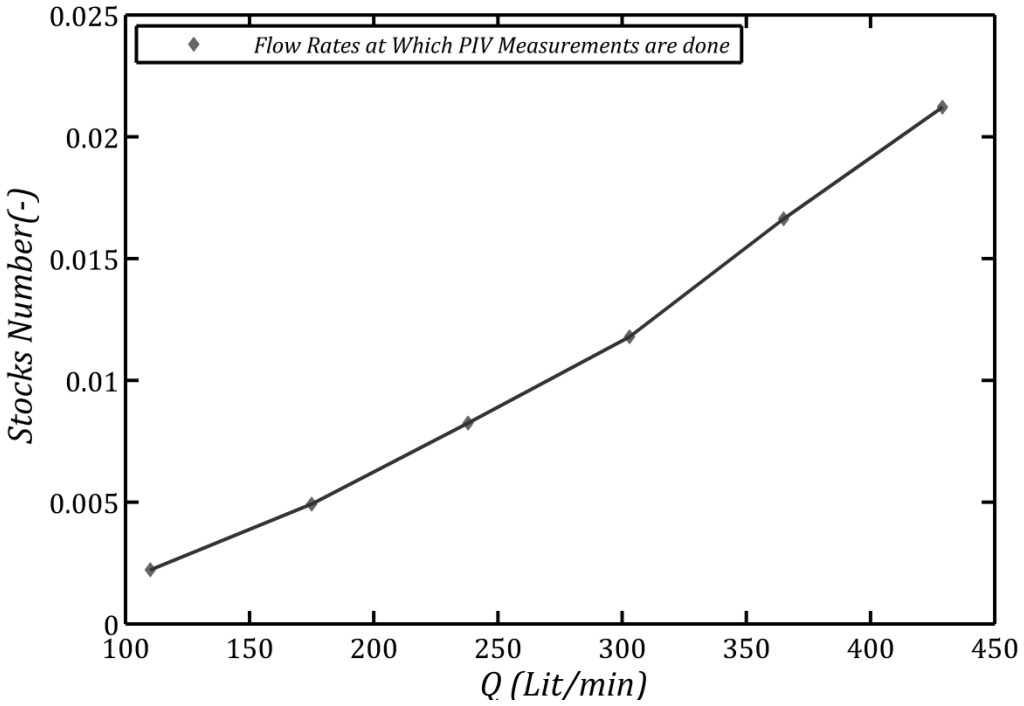


**Figure 4-11 Stocks Number versus Flow Rate for Tracer Particles Used in PIV Experiments**

## 4.8 References


[1]. Adrian R. J., 2005, " Twenty Years of Particle Image Velocimetry", Experiments in Fluids, Vol. 39, pp. 159-169

[2]. Wieneke B., 2005, "Stereo-PIV Using Self-calibration on Particle Images", Experiments in Fluids, Vol. 39, pp. 267-280

[3]. Nezu I., Sanjou M., 2011, " PIV and PTV Measurements in Hydro-Sciences with Focus on Turbulent Open-Channel Flow'', Journal of Hydro-environment Research, Vol. 5, pp. 215-230

[4]. Zeinali H., 2012, "Effect of Near-Wall Turbulence on Selective Removal of Particles from Sand Beds Deposited in Pipelines" , PHD dissertation

[5]. Rabenjafimanantosa H. A., 2007, "Particle Transport and Dynamics in Turbulent Newtonian and Non-Newtonian Fluids", PHD Dissertation

[6]. LAVision, Flow Master, Product Catalogue, 2006

[7]. Solo PIV. Nd:YAG Laser System. Operator's Manual, 2003.

[8]. LaVision. Imager intense, Product catalogue, 2006

[9]. LaVision. Flow Master Getting Started. Product manual (2006).

# Chapter 5:

# Fluid Preparation, Rheology Data and Particle Size Distribution

In this chapter physical and chemical properties of the polymer additive which has been used are reported as well as detail instructions of mixing procedure for preparing the fluid according to suppliers recommendation are discussed.

Rheological behaviour of polymeric fluids at different concentrations have been studied intensely and analysed. Correlations for rheology and viscosity of the fluid have been investigated which are used in next chapters. These correlations along with experimental data are reported altogether.

At the end of this chapter detailed analysis of sand particles size distribution which have been used in the cutting transport experiments are reported. Particle size distribution and statistical analysis on these distributions are discussed in some detail.

## 5.1 Physical and Chemical Properties of the Polymer Additive

Studying the behaviour of turbulent flow of non-Newtonian fluid in annuli which is the most common case in drilling operations has been the primary focus of this research. Although there are different types of additives in drilling industry but due to the nature of the experiments transparency of the fluid has been the biggest constraint in choosing the additive for the experiments. Xanthan gum, CMC (Carboxymethyl cellulose) and also solution of Laponite RDS have been tried; Xanthan gum was found to be not transparent for PIV application. CMC although has been used in studies involving Laser Doppler anemometry but was not found the best candidate for this research. For the Laponite grade RDS in addition to transparency issues there was the problem with viscosity build up as well; the viscosity barley increased even at very high concentrations. All these reasons and constraints imposed by transparency issue have led to choosing a polymer which is commonly used in drilling operations mostly as a viscosifier.

The polymer which has been used in this study is an anionic, water soluble, acrylamide based copolymer which comes under commercial name of ALCOMER 110RD. ALCOMER 110RD is used for many purposes in clear water or low solid concentration drilling namely, providing viscosity, shale stabilization, flocculation, and lubrication, but the main use of this polymer in drilling is building up viscosity.

According to literature this polymer has been specially processed to achieve excellent dispersability in water. Although Alcomer is from PHPA type drilling fluid additives but it does have the dispersability advantage over conventional PHPA’s. Alcomer 110RD

chemically is an anionic copolymer of sodium acrylate and acrylamide. Table 5-1is a summary of the physical and chemical properties of Alcomer 110RD [8].

**Table 5-1 Physical and Chemical Properties of the Polymer Additive**

| Physical | | Chemical | |
|---|---|---|---|
| Appearance: | White powder, no odor | **Type:** | Anionic, acrylamide co-polymer |
| Specific Gravity: | 0.65 | **Solubility:** | Soluble |
| Bulk Density: | 640 | **pH:** | 5.5 – 6.5 (1% solution) |
| Flash Point: | N / A | **Microtx:** | Controlled above 3.0 kg/m3 |

## 5.2 Mixing Procedure of Polymer Solutions

Preparation of polymer solution is important both in getting a homogenous fluid and also repeatability of the experiments. According to supplier Company recommendation the polymer powder needs to be adding to the water very slowly in order to avoid humping of the polymer. While adding polymer to water, the solution must be stirred at very low RPMs, usually less than 50 RPM; this will help in dispersion of polymer molecules while ensuring degradation of polymer solution is not taking place due to high shear rates. Also it is recommended to prepare high concentrated batches of polymer solution in advance and then by adding clear water diluting the batch to the desired concentration [8].

Depending upon the required concentration for each experiment a batch of polymer aqueous was prepared and then diluted to the desired concentration, this was done by isolating the tank from the rest of the flow loop using control valves in the system. The polymer solution is then allowed to stay stagnant for 50 minutes; this will help is dispersion of polymer powders. After 50 minutes the solution was pumped and recirculated in the flow loop at the highest flow rate for another 45 minutes before start taking any data; the last two steps is to make sure that the fluid is completely homogenous.

In both PIV experiments and cutting transport experiments after start of recording data every 10 minutes a sample of the fluid was taken for rheological analysis to check if any changes have happen in the behaviour of the fluid or not. A 6 reading Fanning viscometer has been available and used to check for real time measurements of viscosity; however this was just for checking the fluid statues and the results from this viscometer

have not been used in any analysis. In order or prevent fluid degradation due to circulating the solution for too long time, the duration of each experiment (data acquisition time) was kept as short as possible. Based on the needs and goals of each experiment different concentration of polymer has been used which is reported in the results section of this chapter.

## 5.3 Rheology Measurement Instruments

The rheology of the fluids has been tested by a BOHLIN C-VOR 150 modular rheometer. This rheometer is equipped with spectrometry system which has a triple mode motor control. The rheometer allows measurements both in control stress and control shear rate mode; based on recommendations in measuring viscosity of polymeric liquid the control stress mode has been used in this study [7].

A Fanning viscometer with 6 readings was also used during the experiments but not as a tool of measuring viscosity but rather to monitor the fluid changes over time.

## 5.4 Results and Rheology Models

Non-Newtonian fluids are different from Newtonian fluids by dependency of their viscosity upon the shear rate while Newtonian fluid's viscosity is constant at any shear rate. The behaviour of non-Newtonian fluids may change over different ranges of shear rates; for instance a fluid may follow the power law correlation for medium range shear rate but for very low or very high shear rates this may not be valid. Apparently finding a correlation which describes a fluid rheological behaviour for a wide range of shear rates may not be easy or even accurate, but this behaviour can be well represented by accurate correlations in different zones of shear rate. Based on real shear rates which a fluid is subjected to in any experiments the rheology model needs to be specific for that range of shear rate with importance given to the higher shear rates and not lower limit (this was the case in this study). For flow in the annuli configuration the highest shear rate occurs at the walls of the annuli and that is the most important point in further analysis of the data so efforts must be toward obtaining a rheology model which predicts the fluid behaviour in around this range of shear rates.

It is well known that polymeric liquids are mostly shear thinning fluids and almost all of these fluids could be well represented by a simple two constant power law correlation ([1], [24][56]), Eq. ( 5-1)

$$\tau = k\gamma^n \qquad \textbf{Eq. ( 5-1)}$$

With k being flow consistency index and n is called flow behaviour index.

Equation 4-1 could be used for a wide range of fluids, shear thinning (n <1), shear thickening (n>1) or even Newtonian fluids where n is 1. In order to find the constants in Eq. ( 5-1) some experimental points where shear rates have been measured at some shear stresses are needed (BOHLIN C-VOR 150 measures the shear rate at controlled shear stress points meaning the fluid is sheared under a known value shear stress and then shear rate is measured), once this data are obtained one should plot them in a log-log scaled graph. If the plot of shear stress versus shear rate is linear in a log-log plot the fluid is said to be following a power law model and the slope of this line would be n and the interception (at shear rate of 1) would be k.

All the polymer solutions in this research were found to follow a power law model for the range of shear rates which have been studied. In the following sections rheology results are reported for PIV experiments as well as the solutions which have been used in cutting transport experiments.

## 5.5 PIV Experiments

For PIV experiments two concentrations of the polymer have been tested. The selection of the concentrations has been based on the focus of the research which was investigation of the effect of viscosity of non-Newtonian fluids on cutting transport in horizontal annuli while the flow is turbulent, so the concentrations have been selected to give a high viscosity while having a turbulent flow. Two concentrations of 0.175% and 0.2 % have been tested and it has been found that the fluid is a power law fluid with strong shear thinning behaviour.

### 5.5.1 0.175% Solution

Figure 5-1 is the actual measured shear stress-shear rates for the polymer solution with 0.175 % concentration in log-log scale. It is apparent that the relationship is linear and power law model should be well fitting this data.

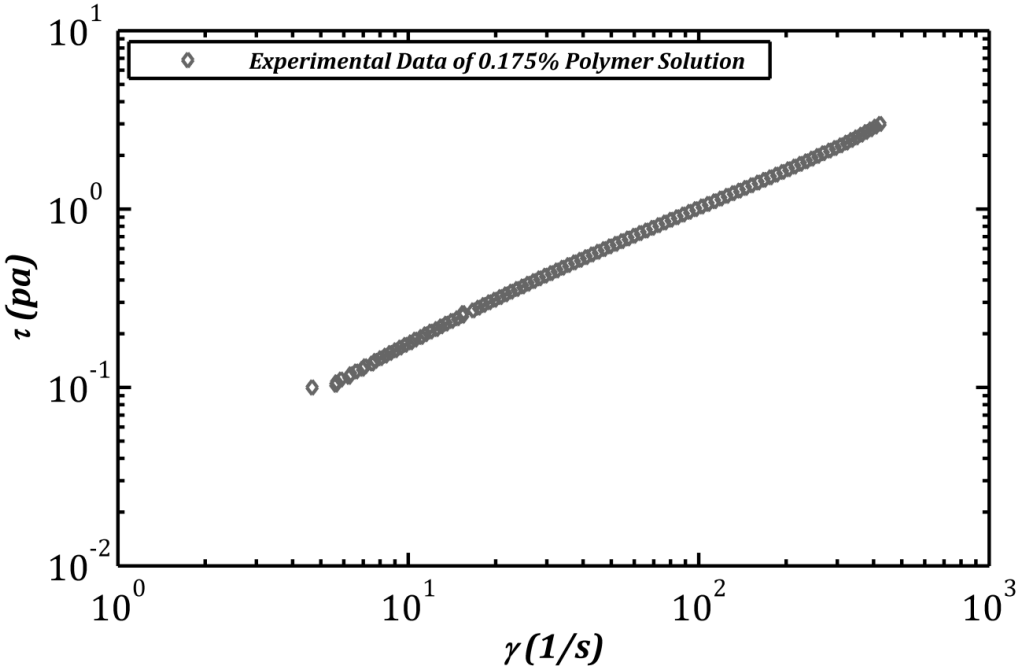


**Figure 5-1: Experimentaly Measured Shear Stress-Shear Rate Relationship of the Polymer Solution at C=0.175%**

Shear stress shear rate relationship for this concentration of polymer is best represented by Eq. ( 5-2).

$$\tau = 0.0315\gamma^{0.7527} \qquad \textbf{Eq. ( 5-2)}$$

Figure 5-2 is a graphical representation of the proposed model predictions and actual experimental data points. The match between the model and the experimental data are exceptionally good in the range of shear rates studied.

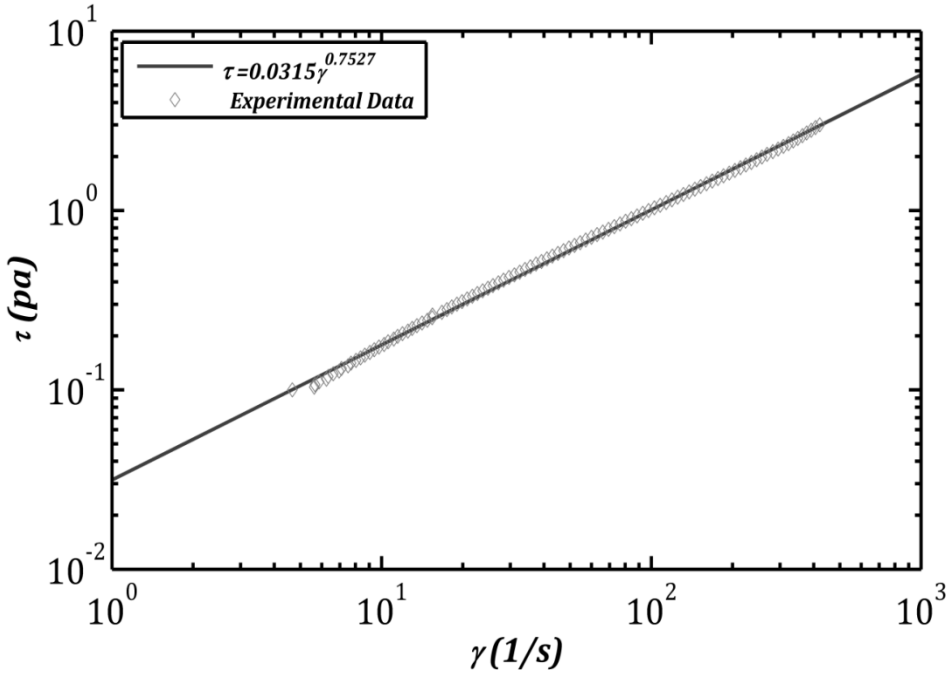


**Figure 5-2: Experimental and Prediction of the Rheology Model for C=0.175% Solution**

Viscosity for a non-Newtonian fluid is not constant and is a function of shear rate. In order to define a viscosity like viscosity of Newtonian fluids an apparent viscosity is defined at each shear rate which is the ratio of shear stress to shear rate at that point.

$$\mu_a = \frac{\tau}{\gamma} \qquad \textbf{Eq. ( 5-3)}$$

.

Substituting Eq. ( 5-1) in Eq. ( 5-3) would give the apparent viscosity for a power law type of fluids.

$$\mu_a = k\gamma^{n-1} \qquad \textbf{Eq. ( 5-4)}$$

For 0.175% solution the apparent viscosity based on the rheology model in Eq. ( 5-2) is Eq. ( 5-5) with actual viscosity data and this model prediction plotted in Figure 5-3.

$$\mu_a = 0.0315\gamma^{-0.2473} \qquad \textbf{Eq. ( 5-5)}$$

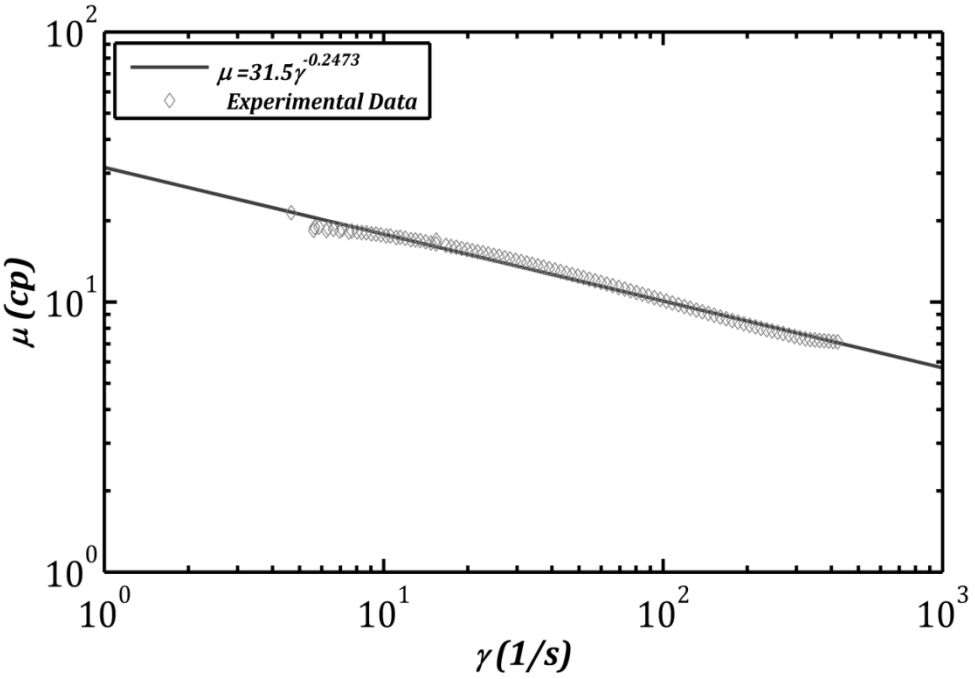


**Figure 5-3: Experimentally Measured Viscosity versus Rheology Model Prediction for C=0.175% Solution**

### 5.5.2 0.2% Solution

Another polymer solution which has been tested is 0.2%; this concentration is also showing the same behaviour as previous one with different power law constants. Equations 4-6 and 4-7 are the rheology models for this concentration, Figure 5-4 and Figure 5-5are the experimental results of rheology measurements along with rheological models prediction.

$$\tau = 0.047\gamma^{0.7003} \qquad \textbf{Eq. ( 5-6)}$$

$$\mu_a = 0.047\gamma^{-0.2997} \qquad \textbf{Eq. ( 5-7)}$$

Summary: two concentrations of polymer solution (0.175% & 0.2%) have been tested in PIV experiments. Studying the behaviour of non-Newtonian fluids especially the effect of high viscosity in turbulent flow have been the major reasons of choosing these concentrations; while these two solutions increase the viscosity significantly and assure a turbulent flow in the annuli due to pump capacity for higher concentrations turbulent flow

was not achievable. Rheology behaviour of the two solutions have been found to be following a simple power law model in the range of shear rates studied with relevant constants reported.

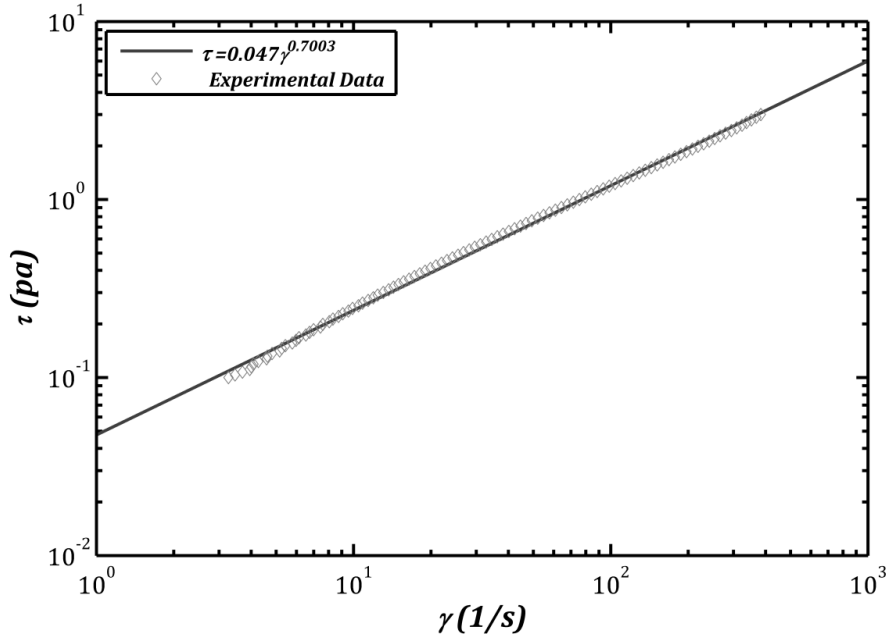


**Figure 5-4 Experimental and Prediction of the Rheology Model for C=0.2% Solution**

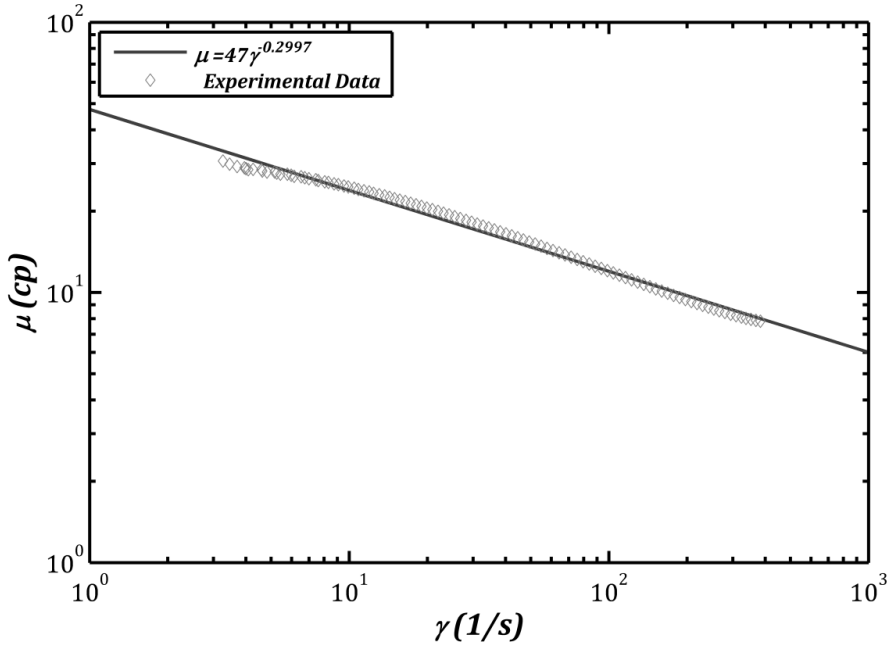


**Figure 5-5 Experimentally Measured Viscosity vursus Rheology Model Prediction for C=0.2% Solution**

## 5.6 Solids Transport Experiments

### 5.6.1 Fluid Preparation Procedures and Concentrations

For experiments with sand particles the procedure for preparing the fluid and start-up of the experiments are different than PIV and is explained here. After establishing a bed in the horizontal section of the annuli this section will be isolated from the rest of the loop for 24 hours and no fluid can be recirculate in this portion of the system.

In order to prepare a polymer solution to be used in this type of experiments first the tank is isolated from the rest of the system by closing Valve #1 (Figure 5-6) (Attention: Valves #4 and 5 are already closed because the bed has to be established a day in advance) and then the batch solution can be prepared following the proper instruction given in previous section. The batch is then diluted to the desired concentration by adding water to the tank. The solution is allowed to rest for 45 minutes after this the solution has to be circulated for sometimes before pumping it to the pipelines and bringing it up to annular section where the bed is. For this purpose the bypass line will be used, valves # 1 and 2 will be open while the other valves are closed; the fluid will be circulated in this part of the flow loop until a homogeneous fluid is achieved which can be used for the experiments.

Another instruction on these experiments is that for establishing the bed of particles always water have been used in order to make sure the initial conditions for all the fluids are the same (Bed thickness should be more or less similar for all the experiments), while isolating the horizontal section the water cannot be drained in this part and that will be always a part of the experiments. For experiments with water this is no problem as the fluid in the tank and pipes are all the same but for experiments with polymer solutions the fluid in the annuli must be replaced with polymer aqueous without disturbing the bed structures. The steps which need to be followed in order to displace the water in the annuli with polymer solution which is in the tank are:

I. Close valve 2 and open valve 3; this will allow the fluid in the tank and pump to fill transport line 2
II. Open valve 4; due to hydrostatic head of the fluid in the tank and transport line 2 the water wont flow back down the vertical part of the flow loop
III. Open valve 5

IV. Start circulating at lowest flow rate possible; this flow rate is below the critical velocity of particle movement for water which ensures that while water is flowing over the bed, particles are not moving

V. After a few minutes all the water has been replaced with polymer and experiment can be start

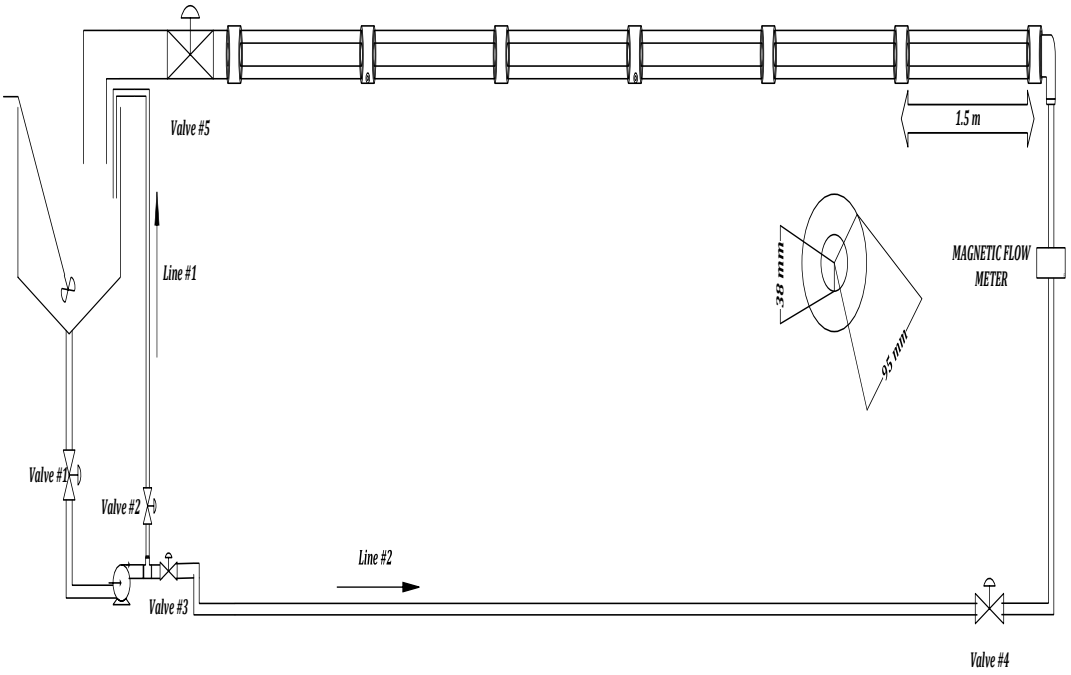


**Figure 5-6: Schematic of the Flow Loop and Valves**

Three concentrations of polymer have been tested in cutting transport experiments; 0.175%, 0.1% and 0.05%. The concentrations have been selected in order to build different fluids with different viscosities and also different non-Newtonian behaviours. 0.2 % which has been tested in PIV experiments has been found not suitable for these types of experiments because this fluid was not able to remove any particles from the bed due to its high viscosity.

Note that due to differences in instructions for preparing the fluids in PIV experiments and cutting transport experiments the fluids with the same concentration may show different constants (the difference is not big and is caused because of the circulation before starting data acquisition), however real time measurement for each experiments are reported here and for each experiment a rheology model have been used which best

represents the fluid in that single experiment which ensures that always best rheology model is used.

### 5.6.2 Rheology Measurements and Models

For a solution of 0.175% concentration following model has been found to be valid over the range of shear rates studies [24][1].

$$C = 0.175\% \begin{cases} \tau = 0.031\gamma^{0.6977} \\ \mu_a = 31\gamma^{-0.3023} \end{cases} \quad \textbf{Eq. ( 5-8)}$$

For 0.1% solutions following correlation have been found.

$$C = 0.1\% \quad \begin{cases} \tau = 0.015\gamma^{0.804} \\ \mu_a = 0.015\gamma^{-0.196} \end{cases} \quad \textbf{Eq. ( 5-9)}$$

And finally for the lowest concentration (0.05%) Eq. ( 5-10) has been found accurate enough for rheology modeling.

$$C = 0.05\% \begin{cases} \tau = 0.0059\gamma^{0.948} \\ \mu_a = 0.0059\gamma^{-0.052} \end{cases} \quad \textbf{Eq. ( 5-10)}$$

Figure 5-7 to Figure 5-9are the experimentally measured rheology data and also proposed rheology models prediction for the three concentrations studied.

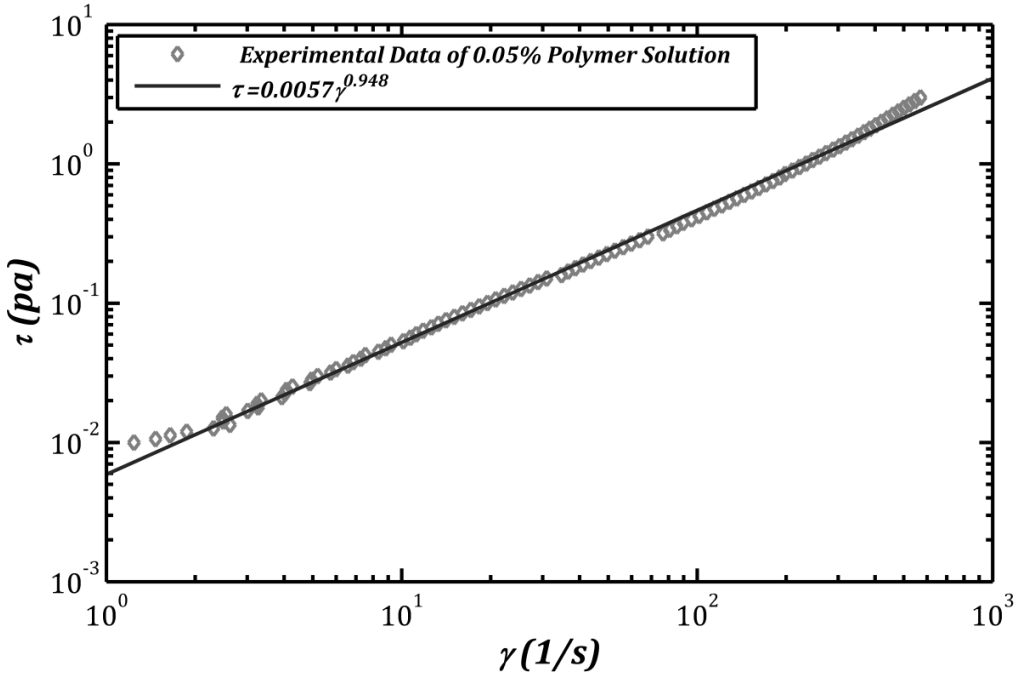


**Figure 5-7 Shear Stress-Shear Rate data for 0.05% Polymer Solution**

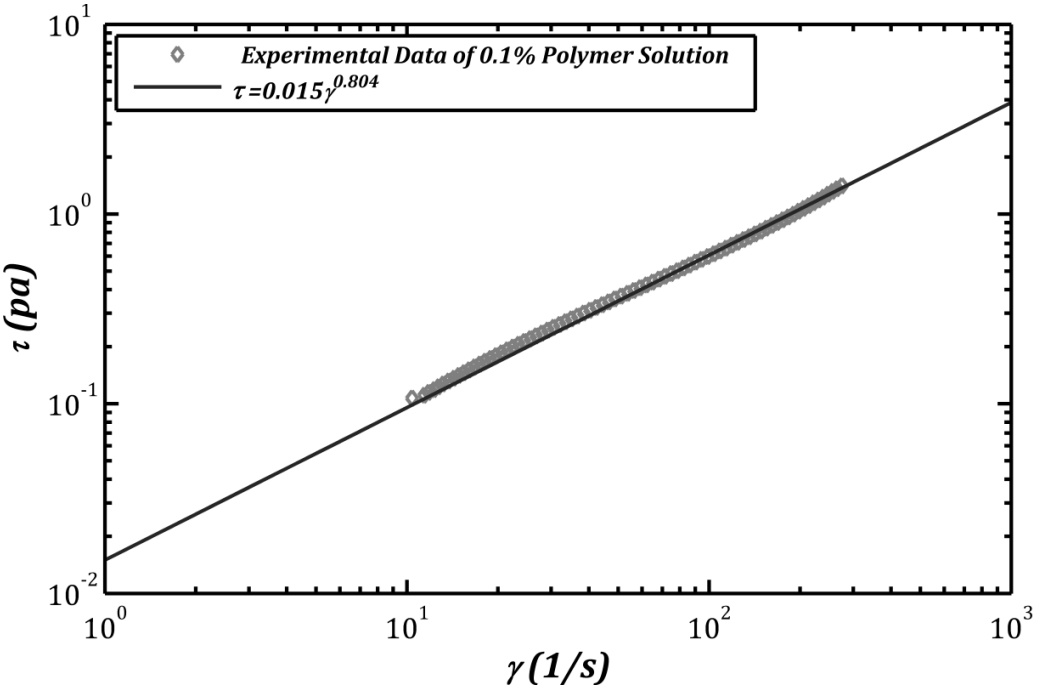


**Figure 5-8 Shear Stress-Shear Rate data for 0.1 % Polymer Solution**

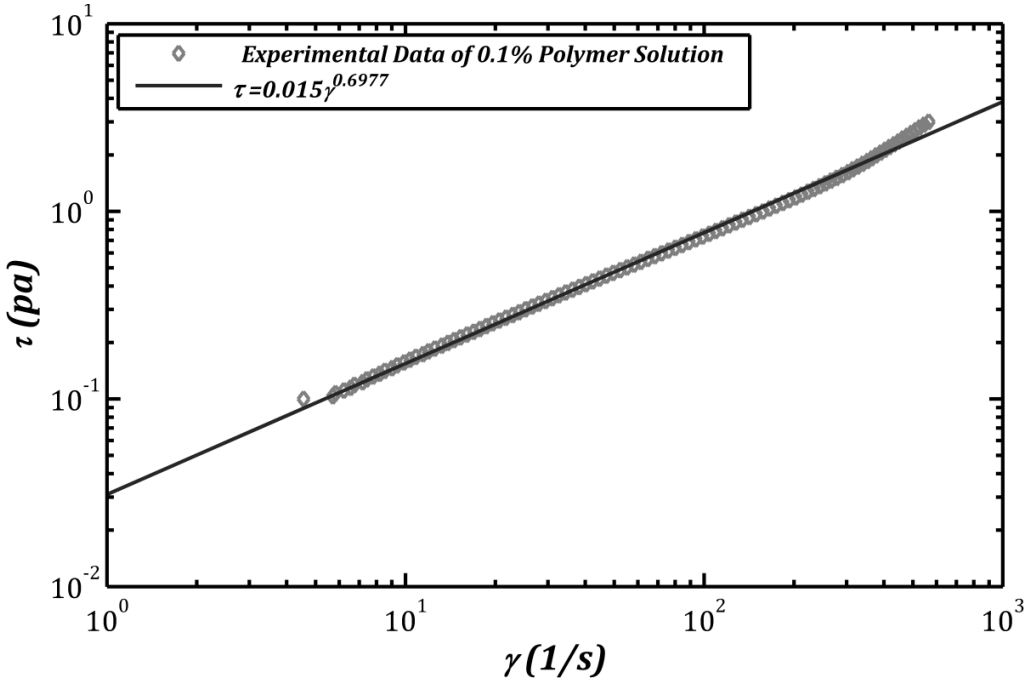


**Figure 5-9 Shear Stress-Shear Rate data for 0.175% Polymer Solution**

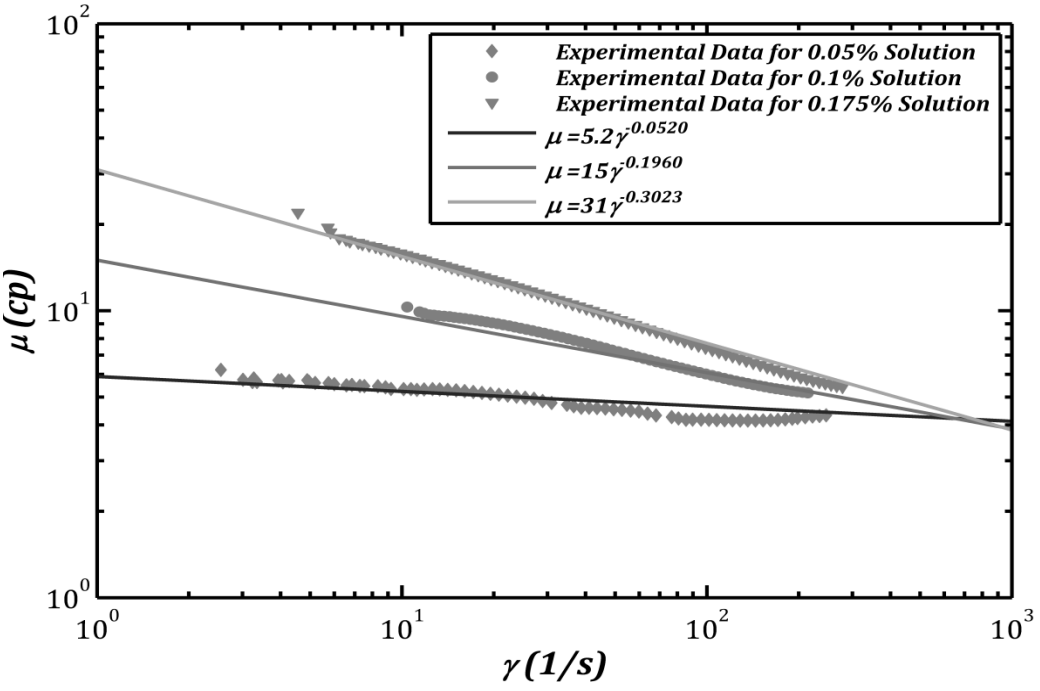


**Figure 5-10 Viscosity Data for the Three Polymer Solutions Used in Cutting Transport Experiments**

## 5.7 Particles Size Distribution Analysis

In this section analysis of particles size distribution is discussed, detailed measurement of particle sizes which have been used in cutting transport experiments are reported.

Generally two different types of particles which could be categorized as fine particles and coarse particles with respect to their diameter have been used in these experiments. Although the diameters are different but other properties like densities are the same which is important in final analysis of the results.

### 5.7.1 Particles Physical Properties

Table 5-2 and Table 5-3 are the reported properties of the sand particles. Note that the most important property in these experiments is the density which has to be same for both sand particles.

**Table 5-2: Physical Properties of Fine Sand Particles[6]**

| Property | Test Method | Unit | Typical Values |
|---|---|---|---|
| Mineral | Petrographic | -- | Quartz |
| Shape | Krumbein | -- | Sub-Angular |
| Hardness | Moh | 6.5 | |
| Specific Gravity | ASTM C-128 | -- | 2.65 |
| Bulk Density, aerated | ASTM C-29 | Lbs/Ft3 | 92-95 |
| compacted | ASTM C-29 | Lbs/Ft3 | 98-100 |

**Table 5-3: Physical Properties of Coarse Sand Particles**

| Property | Test Method | Unit | Typical Values |
|---|---|---|---|
| Mineral | Petrographic | -- | Quartz |
| Shape & Hardness | Visual | Moh | Sub-Angular/6.5 |
| pH | AFS | -- | 7.2-7.4 (Neutral) |
| Specific Gravity | ASTM C-128 | -- | 2.65 |
| Bulk Density, aerated | ASTM C-29 | Lbs/Ft3 | 92-95 |
| compacted | ASTM C-29 | Lbs/Ft3 | 98-100 |

[6] Data of the Table 5-2 and Table 5-3 have been taken from Sil Inc. Website

### 5.7.2 Fine Sand Particles

As the term fine implies the sand particles in this category have a diameter in micron size. Particle size distribution can be presented in different ways; one way is to plot the percent of the weight of a sample which is finer than a $d_p$ versus particles diameter. When working with sand particles finer than 1mm it is better to use the sedimentological $\Phi$ scale instead of actual particles diameter [50].

$$d_p = 2^{-\Phi} \qquad \textbf{Eq. ( 5-11)}$$

$$\Phi = -\log_2(d_p) = -\frac{\ln(d_p)}{\ln(2)} \qquad \textbf{Eq. ( 5-12)}$$

Using $\Phi$ instead of $d_p$ for particles less than 1 mm has the advantage of being bigger for finer particles. As explained earlier, particle size distribution comes in term of percent of the weight which is finer than a given diameter (Pf% of particles is smaller than $d_p$). Usually either Pf is plotted against $\Phi$ in a linear scale or versus $d_p$ in semi-log scale for reporting size distribution of a sample.

Table 5-4 is the results of sieve analysis of a sample of the fine particles.

**Table 5-4: Sieve Analysis on Fine Sand Sample**

| Mesh number | Corresponding Mesh size diameter (μm) | Weight Retained on the mesh (gram) | Normalized Weight |
|---|---|---|---|
| 35 | 500 | 0 | 0 |
| 40 | 425 | 8.863 | 9.1043 |
| 45 | 355 | 43.515 | 44.7 |
| 50 | 300 | 31.14 | 31.988 |
| 60 | 250 | 8.168 | 8.3904 |
| 80 | 180 | 5.078 | 5.2163 |
| 100 | 150 | 0.275 | 0.2825 |
| 120 | 125 | 0.3 | 0.3184 |
| | | 97.345 | 100 |

Resulted size distribution analysis are plotted in Figure 5-11 and Figure 5-12 where both plots are Pf versus Φ in Figure 5-11and versus $d_p$ in Figure 5-12.

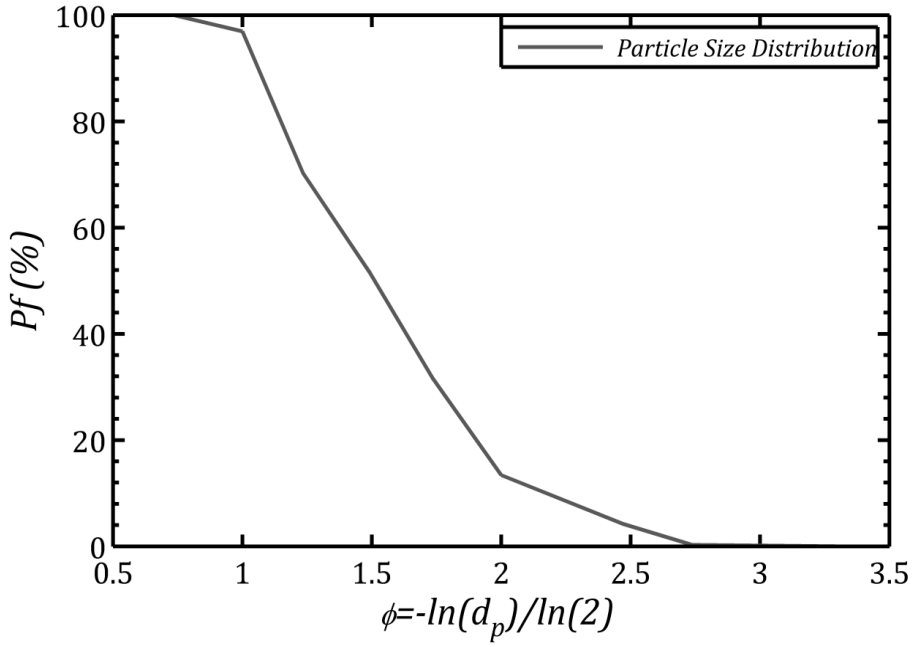


**Figure 5-11: Size Distribution of Fine Particle in Term of Sedimentological Φ Scale**

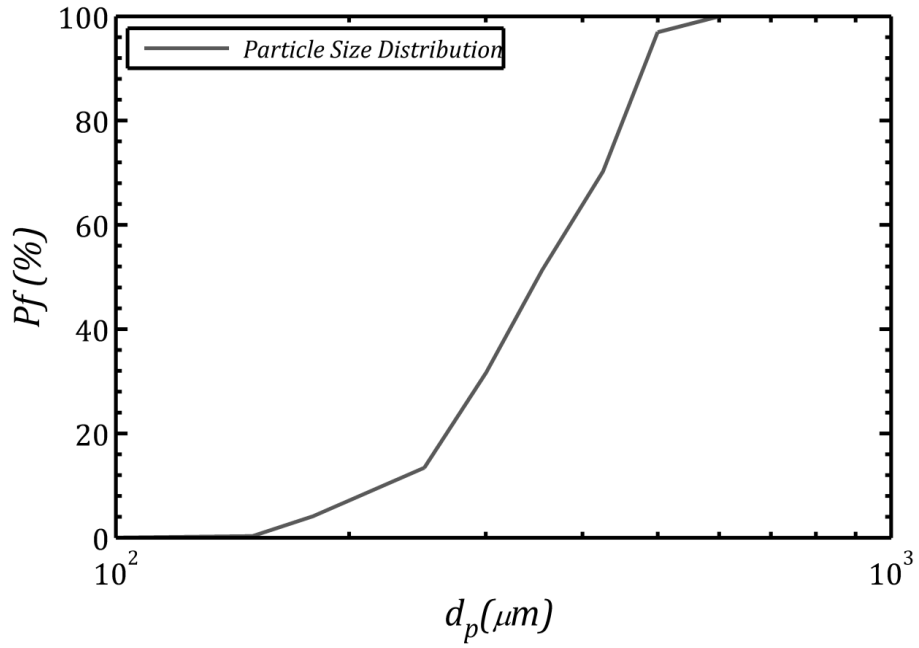


**Figure 5-12: Size Distribution of Fine Particles in Term of Particles Diameter**

Pf% is the fraction of the particles finer than a corresponding diameter for the given Pf.

Some useful statistical data are the standard deviation and geometric deviation of particles diameter which show how uniform is the sample. Normally for a perfectly uniform distribution the standard deviation is 0 with a geometric deviation of 1. If geometric deviation is less than 1.3 the sample can be treated as uniform samples while if it is bigger than 1.6 the sample is poorly sorted. Definition of these function are given below;

$$\Phi_m = \int \Phi \, P(\Phi) d\Phi \qquad \textbf{Eq. ( 5-13)}$$

$$\delta^2 = \int (\Phi - \Phi_m)^2 \, P(\Phi) \, d\Phi \qquad \textbf{Eq. ( 5-14)}$$

$$\delta_g = 2^{\delta} \qquad \textbf{Eq. ( 5-15)}$$

Equation 4-14 is the standard deviation and Eq. ( 5-15) is the geometric deviation. Following statistical data has been obtained for the fine sand particles.

| | |
|---|---|
| $\delta = 0.2759$ | Standard Deviation |
| $\delta_g = 1.2107$ | Geometric Deviation |
| $D_m = 349\ \mu m$ | Mean Diameter |

The geometric deviation of the sand particles is about 1.2 and as explained earlier for a sample having geometric deviation less than 1.3, uniformity could be assumed and further analysis of the sample can be done using the mean diameter of the sample. Also it is worth mentioning in uniform sample the mean diameter and $d_{50}$ are equal.

### 5.7.3 Coarse Sand Particles

Table 5-5 is the sieve analysis results for coarse particles used in this study.

**Table 5-5 Sieve Analysis on Coarse Sand Sample**

| Mesh number | Corresponding Mesh size diameter (μm) | Weight Retained on the mesh (gram) | Normalized Weight |
|---|---|---|---|
| 10 | 2000 | 0 | 0 |
| 12 | 1700 | 0 | 0 |
| 16 | 1180 | 58.8 | 59.2324 |
| 20 | 850 | 36.47 | 36.73819 |
| 25 | 710 | 2.6 | 2.61912 |
| 30 | 600 | 1.4 | 1.410295 |
| | | 99.27 | 100 |

For coarse sand particles Φ scale is not good as for particles larger than 1mm this would return negative numbers and because there are some particles finer than 1mm Sedimentological Ψ scaling which is the negative of Φ scale is not applicable as well. The size distribution in terms of Pf% versus particle diameter is shown in Figure 5-13.

Also statistical analysis has yielded following numbers for standard deviation, geometric deviation and mean diameter.

$$\delta = 0.2824 \qquad \text{Standard Deviation}$$

$$\delta_g = 1.2163 \qquad \text{Geometric Deviation}$$

$$D_m = 1.2142 \text{ mm} \qquad \text{Mean Diameter}$$

The geometric deviation has been found to be 1.2163 which means this sample of sands is uniform and mean diameter which is 1.2142 mm could be assumed as the representative diameter of these sands.

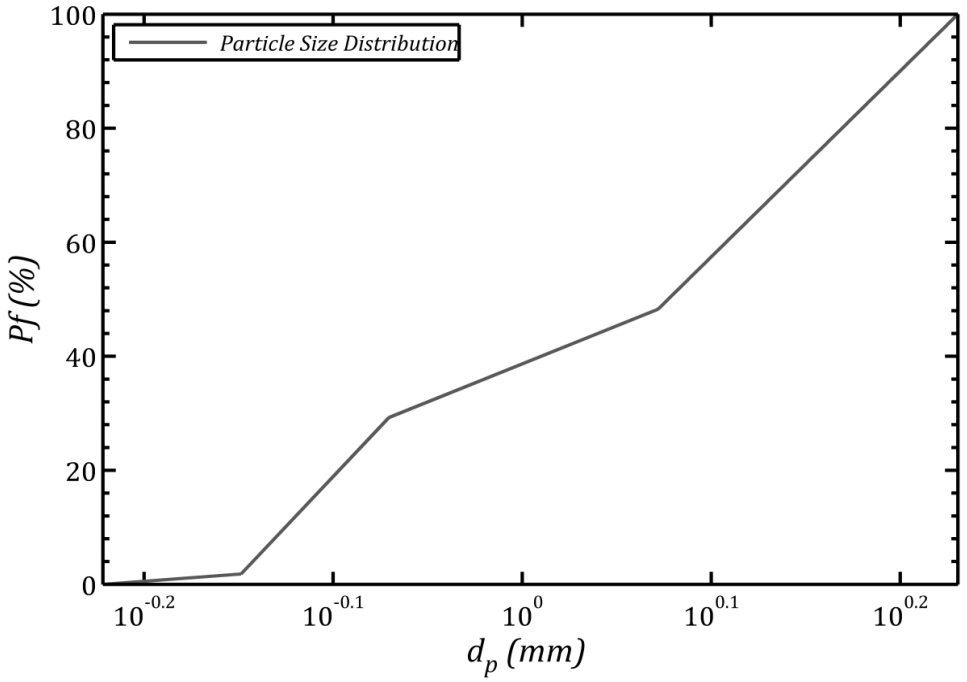


**Figure 5-13 Size Distribution of Coarse Particles in Term of Particles Diameter**

## 5.8 References


[1]. Bird R. B., 1976 "Useful Non-Newtonian Models", Annual Review. Fluid Mechanics, Vol. 8, pp. 13-34

[2]. Bird R. B., Armstrong R. C., Hassager O., 1987, "Dynamics of polymeric liquids", Wiley-Interscience, New York, Vol. 1

[3]. Nouri J. M., Umur H., Whitelaw J. H., 1993, "Flow of Newtonian and Non-Newtonian Fluids in Concentric and Eccentric Annuli", Journal of Fluid Mechanics, Vol. 253, pp. 617-641

[4]. Escudier M. P., Gouldson I. W., Jones D. M., 1995, "Flow of Shear-Thinning Fluids in Concentric Annulus", Experiments in Fluids, Vol. 18, pp. 225-238

[5]. Japper-Jaafar A., Escudier M. P., Poole R. J., 2010, "Laminar, Transitional and Turbulent Annular Flow of Drag-Reducing Polymer Solutions", Journal of Fluid Mechanics, Vol. 165, pp-1357-1372

[6]. Garcia H., 2008, "Sedimentation Engineering: Processes, Measurements, Modeling and Practice", American Society of Civil Engineers

[7]. Malvern Instruments Limited, 2005, "Bohlin C-VOR", Product Catalogue

[8]. DiCorp Co., "ALCOMER 110RD Guide", Product Bulletin.

# Chapter 6:

# Results and Discussion on PIV Experiments

This chapter includes the results for all the experiments related to PIV including Newtonian and Non-Newtonian fluids flow. Chapter 6 is divided in 3 main subsections, Newtonian fluid flow, and Non-Newtonian fluids and at the end a comparison between these two types of fluid is given and similarities and differences are highlighted.

ATTENTION: The results for flow of water (Newtonian fluid) presented in this thesis has been obtained and used by two graduate students[7]

## 6.1 Introduction

Annular flow of Newtonian and Non-Newtonian fluids is of great interest in many engineering and industrial applications. Oil and gas well drilling operations, where a non-Newtonian drilling fluid is circulated through the annular space between the drill string and borehole constitute a good example of flow in annular geometry.

Flow through annuli is associated with many difficulties due to the specific geometry studied. Determining the radial locations of the maximum velocity and zero shear stress is one of these problems yet to be addressed adequately. In fully laminar and turbulent pipe flow of Newtonian and non-Newtonian fluids, the flow is symmetric and so the two positions coincide[3]. However, this assumption does not apply for annular flow, as strong asymmetry has been observed and reported ([5] to[10]). Coincidence of the positions of maximum velocity and zero shear stress has been assumed in some of the earlier studies such as, Rothfus et.al[5] Brighton & Jones[6] ,and Walker & Rothfus[7]. However, this assumption was proved not to be valid in later studies. Lawn & Elliot[8] have shown that zero shear stress occurs closer to inner wall. Later, Rehme[9] came to the same conclusion as Lawn & Elliot by using hot wire anemometry for flow of air in three concentric annuli of varying radius ratio (0.02, 0.04 & 0.1).

Nouri et.al[10] conducted an experimental study to examine the flow of water at bulk Reynolds number of 8900 and 26600 and then flow of non-Newtonian shear thinning polymer fluid with effective Reynolds numbers ranging from 1150 to 9600. They found that the transition from laminar flow for the non-Newtonian fluid happens at effective Reynolds number much higher than those of the Newtonian fluid. Within their experimental precision, they were not able to measure and quantify the location of zero shear stress so they preferred to use the location of maximum velocity in wall shear stress

[7] Results for flow of water are also reported by Fabio Ernesto Rodriguez-Corredor

calculations instead of the zero shear stress position. A similar investigation of flow of non-Newtonian fluids in concentric annuli (Radius ratio 0.506) was performed by Escudier et.al[11] by using LDA. Three non-Newtonian shear thinning fluids were studied and mean axial velocity data along with pressure drop and friction factor were reported by the authors. The friction factor-Reynolds number ($f - Re$) data for aqueous CMC solution has shown good agreement with the theoretical values predicted for a power law fluid in laminar regime. In turbulent flow regime, $f - Re$ correlation was found well below the correlation for Newtonian fluids indicating the effect of drag reduction. Second and third non-Newtonian fluids (aqueous solutions of Xanthan gum and a LAPONITE CMC blend) have shown lower values of friction factor comparing to the theoretical prediction for a power law fluid in laminar regime. Authors argued that elasticity of Xanthan gum and thixotropic nature of LAPONITE/CMC blend was the reasons for this anomalous behavior. Mean axial velocity data were found to obey the universal law of the wall ($u^+ = y^+$) in the immediate vicinity of the walls (i.e., $y^+ < 10$) with an upward shift further away in the logarithmic region.

Recently Jaafer et.al[30] has conducted an experimental study for flow of three non-Newtonian and one Newtonian fluid in concentric annuli of radius ratio of 0.506 by using LDA. They measured the pressure drops and RMS of fluctuation velocities near the walls in order to identify the transition from laminar to turbulent flow. They reported that transitional flow regime lasted over a wider range of Reynolds numbers for the fluids showing more shear thinning characteristics. Velocity data in all fluids studied tends to follow the universal law of the wall close to solid surfaces. Positions of maximum velocity and zero shear stress could not be distinguished and the authors ultimately used the location of the maximum velocity in their calculations of wall stresses.

## 6.2 Experimental Facility

The horizontal flow loop described in chapter 3 has been used in obtaining the results presented in this chapter of thesis.

PIV technique as the measurement tool for the experiments in this chapter has been discussed in detail in chapter 4.

## 6.3 Rheology Analysis

Rheological analysis of the fluids used in the current study is reported in detail in chapter 5 of the thesis.

## 6.4 Newtonian Fluid Flow through Annuli[8]

### 6.4.1 Friction Factor & Pressure Drop Data

A conventional and standard way of presenting pressure drop data in any geometry including annuli is to convert these data into friction factor coefficient. Friction factor is a dimensionless number which facilitate comparison of different sets of data.

There are three main sources which contribute to pressure drop: change in elevation, change is velocity and friction Eq. ( 6-1)

$$\frac{\Delta p}{\Delta l} = \left(\frac{\Delta p}{\Delta l}\right)_e + \left(\frac{\Delta p}{\Delta l}\right)_v + \left(\frac{\Delta p}{\Delta l}\right)_f \qquad \text{Eq. ( 6-1)}$$

In a horizontal system like the setup in this study there is no change in height so the first component in Eq. (1) has no contribution in pressure drop. Change in velocity occurs due to change in cross section available for passage of the flow; hence the cross section of the annuli is fixed so this component of the pressure drop is also zero. Equation 1 reduces to only frictional pressure drop which implies that the only source of energy loss is friction which depends upon roughness of pipe walls.

Generally Fanning friction factor is related to wall shear stress and is defined as Eq. ( 6-2):

$$f = \frac{2\tau_w}{\rho U^2} \qquad \text{Eq. ( 6-2)}$$

Reynolds number which is the ratio of inertial forces to viscous forces is the key dimensionless number in relating different flows Eq. ( 6-3).

[8] A version of this chapter has been presented
Rodriguez-Corredor F. E., Bizhani M., Ashrafuzzaman M., Kuru E.,2012, "An Experimental Investigation of Turbulent Flow in Concentric Annulus Using Particle Image Velocimetry Technique," ASME 2012 International Mechanical Engineering Congress & Exposition (IMECE), Technical paper. Houston, Texas, US

$$N_{Re} = \frac{\rho U d}{\mu} \qquad \text{Eq. ( 6-3)}$$

Flow through round pipes especially for Newtonian fluids has been intensely studies and it is known for laminar flow of Newtonian fluids friction factors follows Eq. (6-4) regardless of pipe wall roughness.

$$f = \frac{16}{N_{Re}} \qquad \text{Eq. ( 6-4)}$$

For turbulent flow however the more complex and implicit correlation of Colebrook[31] is being widely used.

$$\frac{1}{\sqrt{f}} = -4\log_{10}\left(\frac{\frac{\varepsilon}{d}}{3.7} + \frac{1.256}{N_{Re}\sqrt{f}}\right) \qquad \text{Eq. ( 6-5)}$$

For flow in round conduit one may take $N_{Re} = 2100$ as the critical Reynolds number at which flow starts to depart from laminar flow to turbulent.

All the equations presented previously are applicable for pipe flow while annular flow is different in many ways from pipe flow; new correlations or consideration of geometrical changes have to be applied before using these equations. Characteristic length scale for calculation of Reynolds number in annular flow would be hydraulic diameter instead of pipe diameter.

$$D_H = D_{out} - D_{in} \qquad \text{Eq. ( 6-6)}$$

$$N_{Re} = \frac{\rho U D_H}{\mu} \qquad \text{Eq. ( 6-7)}$$

Equations 6-6 & 6-7 are definitions of hydraulic diameter and Reynolds number for flow through annuli. In order to calculate friction factor one would need wall shear stress and it is well known for Newtonian fluids wall shear stresses are not equal on both walls of annuli and accurate knowledge of position of zero shear stress is required for calculating these stresses accurately while for pipe flow due to symmetry zero shear stress occurs at the middle. Equations 6-8 & 6-9 are definition of shear stress on inner and outer walls of annuli respectively[10].

$$\tau_i = -\left(\frac{dp}{dl}\right)\left(\frac{{R_0}^2 - {R_1}^2}{2R_1}\right) \qquad \text{Eq. ( 6-8)}$$

$$\tau_o = -\left(\frac{dp}{dl}\right)\left(\frac{{R_2}^2 - {R_0}^2}{2R_2}\right) \qquad \text{Eq. ( 6-9)}$$

Where i stand for inner wall, o for outer wall and $R_0$ is the radius of zero shear stress which will be discussed later. As mentioned earlier for pipe flow $R_0$ happens at the center of the pipe and hence wall stress for pipe flow reduces to Eq. ( 6-10)[11].

$$\tau_w = -\frac{D}{4}\frac{dp}{dl} \qquad \text{Eq. ( 6-10)}$$

One approach which has been used by some authors and could be used in absent of any reliable information about $R_0$ is to use Eq. ( 6-10) with hydraulic diameter in order to obtain wall shear stress in annuli. In this method it is assumed that wall stress is equal on both walls of annuli and the resulted wall shear stress is then called weighed average wall shear stress.

For Newtonian fluid flow through annuli Jones & Leung is the most in use correlation. Laminar flow regime is best represented by Eq. ( 6-11)[19].

$$f = \frac{64}{{N_{Re}}^*} \qquad \text{Eq. ( 6-11)}$$

Equation 6-12 is Jones & Leung [46] correlation for turbulent flow through annuli of radius ratio equal to 0.4.

$$\frac{1}{\sqrt{f}} = 4\log\left(1.386 N_{RE} f^{\frac{1}{2}}\right) - 1.6 \qquad \text{Eq. ( 6-12)}$$

Before presenting and discussing the results its worth mentioning the operating conditions at which measurements have been taken. As it has been discussed in chapter 3 the pump is equipped with VFD which allows for different RPMs and that is the only parameter that users can control and change, so every reading is in term of pump RPM which in return gives a flow rate and bulk velocity. Table 6-1 is a summary of relation between pump RPMs, flow rates (Q) and bulk velocity ($U_B$).

Note: all experiments for water have been done at the 6 pump RPMs reported in Table 6-1 (Flow rates have been rounded).

**Table 6-1: Operational Flow Rates and Bulk Velocities for Expeiments with Water**

| Pump RPM | Flow Rate (Lit/min) | Bulk Velocity (m/s) |
|---|---|---|
| 400 | 110 | 0.308067 |
| 600 | 172 | 0.481705 |
| 800 | 232 | 0.649741 |
| 100 | 295 | 0.82618 |
| 1200 | 356 | 0.997017 |
| 1400 | 414 | 1.159452 |

Figure 6-1is the resulted friction factor obtained for flow of water. Wall shear stresses have been calculated using Eq. ( 6-8) and Eq. ( 6-9) with values for zero shear stress radiuses obtained from PIV experiments which will be discussed later. Due to operational limitations of the pump no laminar flow could be achieved. Friction factors for none of the tested velocities fall in the laminar region of the $f - N_{Re}$ plot. It is observed that friction factor is slightly higher for the inner wall which caused by the strong asymmetry in velocity profile and bias of zero shear stress radius toward the inner wall.

A good agreement in the trend of experimental data and Jones & Leung correlation has been achieved although the experimental data are showing higher values. The reason for having higher friction factor than what Jones correlation predicts is because this correlation is for perfect annuli with no restriction in path of flow. In the experimental flow loop used for this research in order to keep the inner pipes at the middle of the annuli 3 spikes at each end of annuli has been used; these spikes causes more pressure drop and therefore higher values of friction factor, this issue also has been considered and reported by Rheme [44].

Wall shear stresses based on weighted average method also have been calculated and resulted friction factors are shown in Figure 6-2. These approach is not necessary here as zero shear stress radiuses are known but as it will be shown later for the case of Non-Newtonian fluid this approach has to be adopted due to lack of information about $R_0$; this is just to confirm that this method also yields accurate and acceptable results for later use in other experiments.

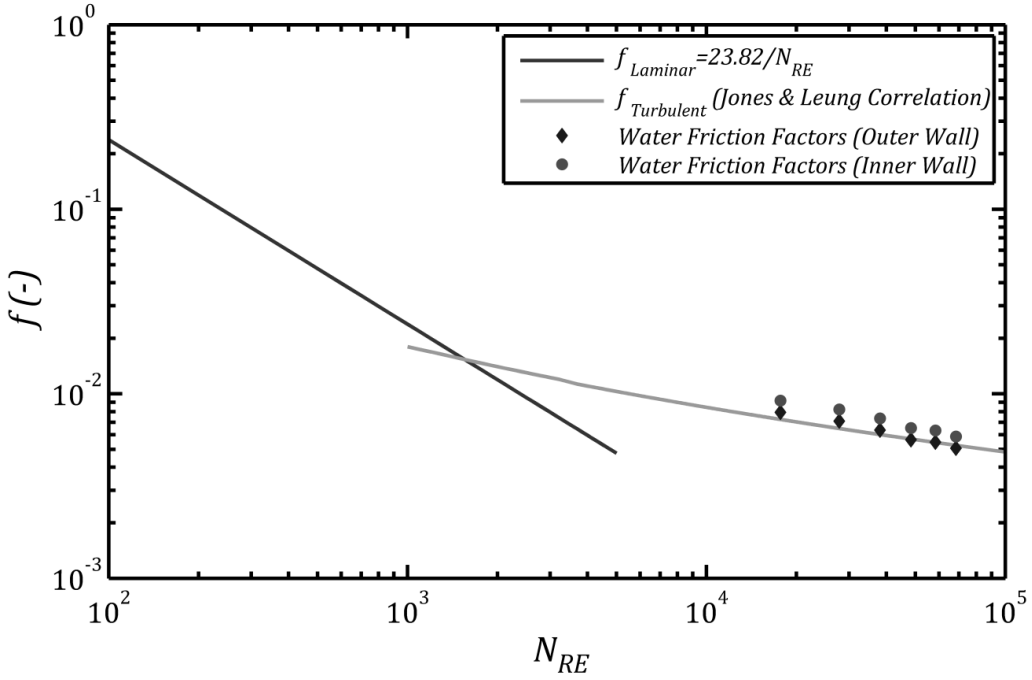


**Figure 6-1: Friction Factor Data for Flow of Water, Note that Data are Separated for Both Walls of the Annuli**

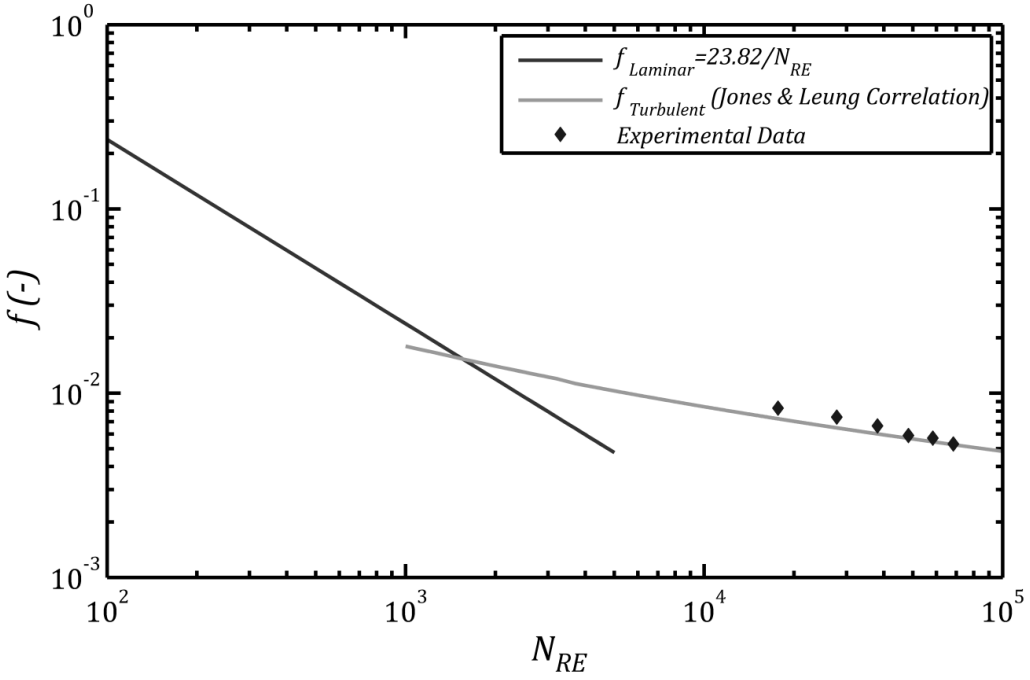


**Figure 6-2: Friction Factor for Flow of Water Calculated Based on Weighted Average Wall Shear Stress**

### 6.4.2 Flow Regime Assessment

Although one can identify the flow regime by using $f - N_{Re}$ plot, it is more convenient to define a critical Reynolds number at which the flow starts to depart from laminar flow. Reynolds number which is a dimensionless number is the ratio of inertial forces to viscous forces; the smaller this numbers the bigger viscous force which means less turbulence. For annuli configuration using hydraulic diameter Eq. ( 6-13) would be the Reynolds number for flow of Newtonian fluids.

$$N_{Re} = \frac{\rho U D_H}{\mu} \qquad \text{Eq. ( 6-13)}$$

In the literature usually investigators take 2100 as the critical Reynolds number in pipe and annuli flow, keeping this number in mind Figure 6-3 is the graphical representation of operational Reynolds numbers encounter during water experiments. Table 6-2 is the Reynolds numbers for each specific flow rate examined in each experiment.

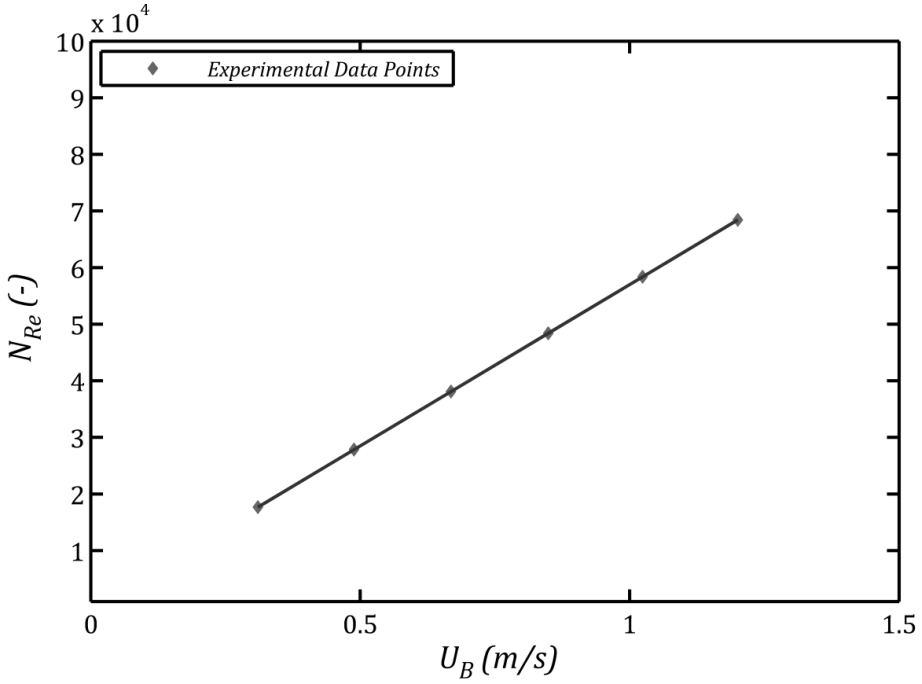


**Figure 6-3: Operational Reynolds Numbers for Experiments with Water**

**Table 6-2: Operational Reynolds Numbers for Experiments with Water**

| Q (Lit/min) | $N_{Re}$ |
|---|---|
| 110 | 17700 |
| 172 | 26800 |
| 232 | 38000 |
| 295 | 46000 |
| 356 | 54000 |
| 414 | 68000 |

The lowest Reynolds number for the range of flow rates studies from Table 6-2 is 17700 for a flow rate of 110 Lit/min, recalling that critical Reynolds number is expected to be about 2100, one can conclude that the flow is turbulent with no doubt. Indeed analysis of flow regime and flow regime assessment would become essential in later case which is a Non-Newtonian fluid but in order to keep the results comparative for both fluids the same analysis has been done for water as well so readers would be able to compare the two fluids performance.

### 6.4.3 Wall Region: Velocity Profiles

Behaviour of flow around solid surface which is called wall bounded shear flow or boundary layer has been of great interests since long time ago. Since boundary layer is playing a critical role in many applications, knowing the behaviour in this thin layer of fluid would become more critical. Many researchers have employed different tools in order to study the boundary layer; early investigators were taking the flow regime in viscous sublayer as laminar regardless of ongoing flow regime in the core flow. Later studies have shown the behaviour of viscous sublayer is anything but laminar.

One of aspects of a turbulent boundary layer is the velocity distribution in this wall bounded region. A turbulent boundary layer is divided into three zones: Viscous sublayer, buffer zone and logarithmic zone. Viscous sublayer is the immediate layer next to the solid surface and extends until $y^+ = 5$, viscous sublayer is dominated by viscous forces but the flow is not laminar in this layer as strong and intermittent events (Coherent Structures) disturb the flow in this layer. Velocity profile in the viscous sublayer has to

follow Eq. ( 6-14) regardless of geometry or the fluid type; this is called the universal law of the wall.

$$u^+ = y^+ \qquad \text{Eq. ( 6-14)}$$

Logarithmic zones start from $y^+ = 30$ and a logarithmic equation of type Eq. ( 6-15) governs the velocity distribution for Newtonian fluids flow through pipes and channels.

$$u^+ = 2.5 \ln(y^+) + 5.5 \qquad \text{Eq. ( 6-15)}$$

Buffer layer which is sandwiched between viscous sublayer and logarithmic layer is extending from $y^+ = 5$ all the way to $y^+ = 30$. Buffer layer is the zone where most vortical activates and turbulence production and dissipation takes place and hence is of great importance. Although some researchers have tried to present equations or correlations of form Eq. ( 6-15) for buffer layer but this zone is still not well known and an accurate formula for the velocity distribution doesn't exist for buffer layer. Due to lack of any equation for velocity profile in buffer layer researcher extrapolate the equations for viscous sublayer and logarithmic layer and take the intersection of these two layers as the transition from one to another one and completely ignore the buffer layer. If one does the extrapolation following equation would be obtained for velocity profile in turbulent boundary layer of a Newtonian fluid.

$$u^+ = \begin{cases} y^+ & , \quad y^+ < 10 \\ 2.5 \ln(y^+) + 5.5 & , \quad y^+ \geq 10 \end{cases} \qquad \text{Eq. ( 6-16)}$$

From PIV time averaged axial velocity or u plus distance from the wall or y are obtained, but in order to check the validity of Eq. ( 6-16) or validating the results one would have to transform these parameters into their dimensionless form Eq. ( 6-17) ad Eq. ( 6-18).

$$y^+ = \frac{y \rho u^*}{\mu} \qquad \text{Eq. ( 6-17)}$$

$$u^+ = \frac{u}{u^*} \qquad \text{Eq. ( 6-18)}$$

$$u^* = \sqrt{\frac{\tau_w}{\rho}} \qquad \text{Eq. ( 6-19)}$$

Calculation of friction velocity through Eq. ( 6-19) requires knowledge of wall shear stress; calculation of wall shear stress and required parameters has been explained thoroughly in previous sections and is skipped in this section. After calculating the friction velocity one should be able to transform PIV results into dimensionless groups and plot them.

Figure 6-4 to Figure 6-9 are the velocity profiles obtained for flow of water in the annuli of radius ratio of 0.4. Each plot includes the velocity profile for one Reynolds number and both walls of the annuli.

The main conclusions of the near wall velocity profiles is that velocity data tend toward the universal law of the wall in the immediate vicinity of the solid surface and that is valid for both inner and outer wall of the annuli at any Reynolds number. Indeed the results are in good agreement with previous researches for viscous sublayer which shows regardless of geometry velocity profile have to follow the universal law of the wall in any wall bounded shear flow. In the logarithmic zone the results are in good agreement with the prediction of the Eq. ( 6-15) for both inner and outer wall.

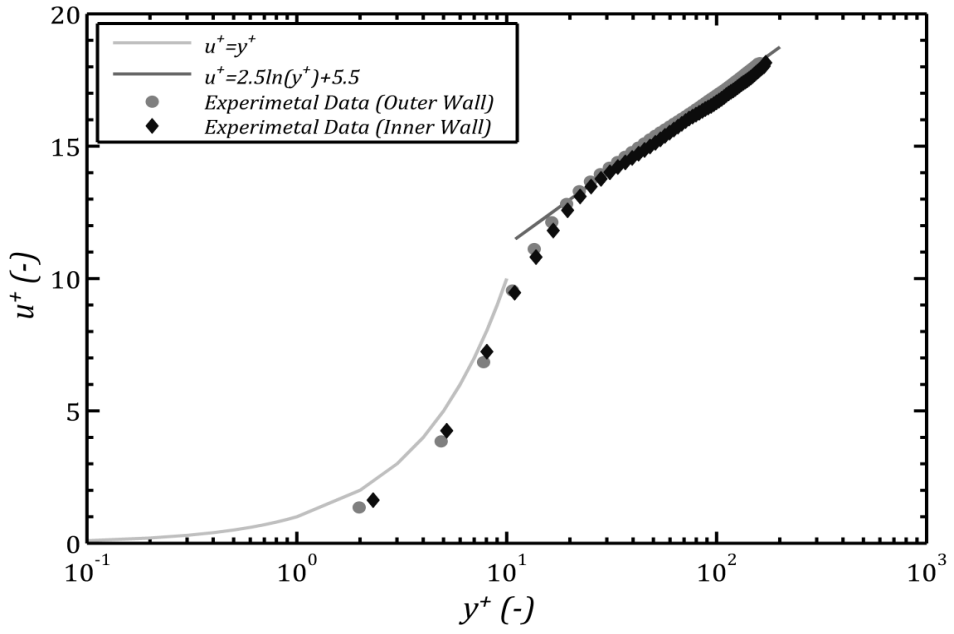


**Figure 6-4: Near Wall Velocity Profiles for Flow of Water at $N_{Re} = 17700$**

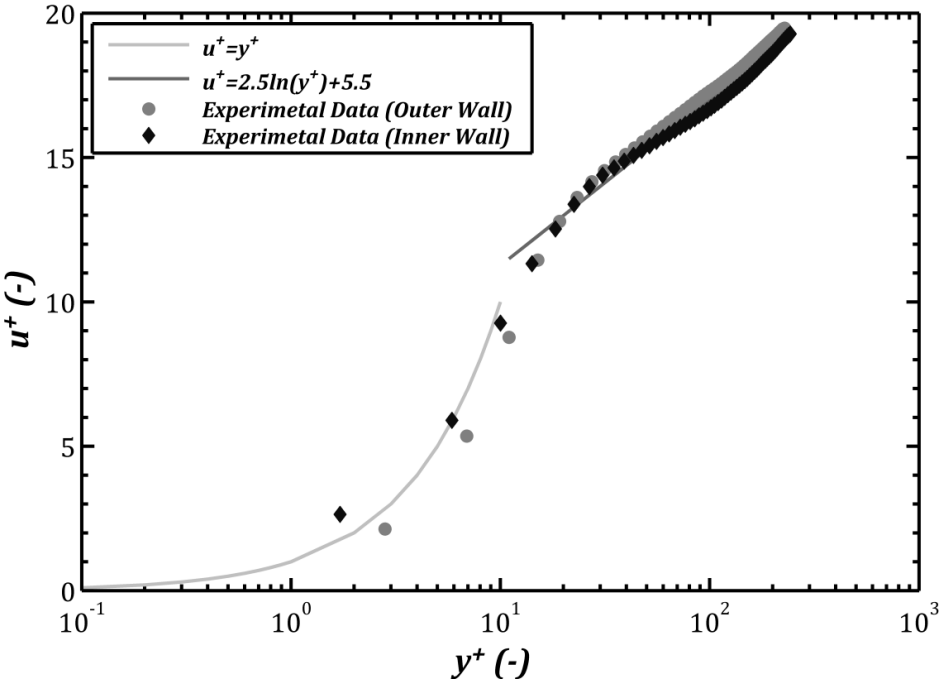


**Figure 6-5 Near Wall Velocity Profiles for Flow of Water at $N_{Re} = 26800$**

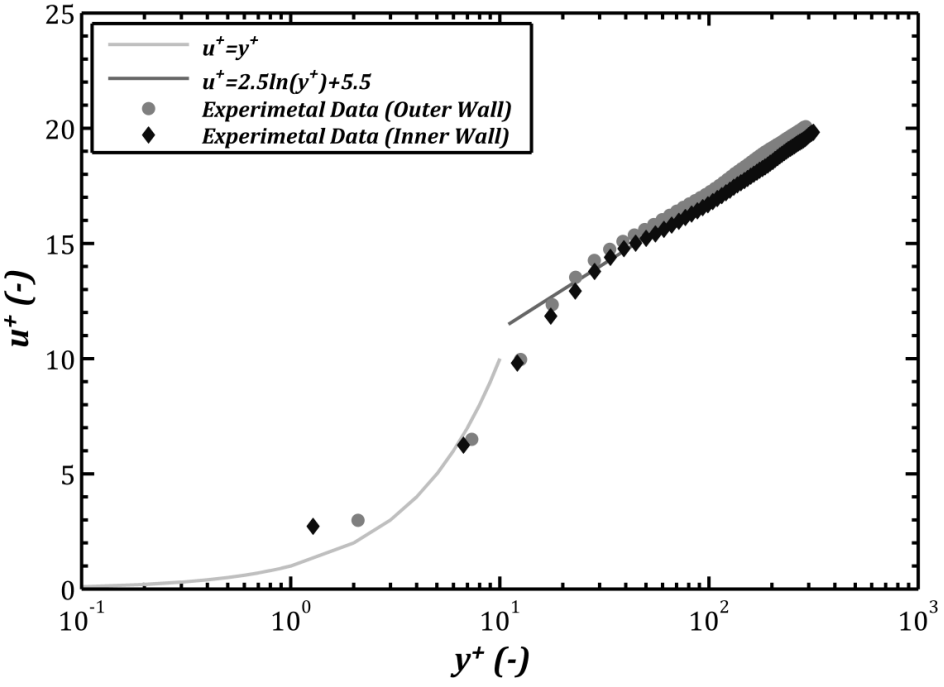


**Figure 6-6 Near Wall Velocity Profiles for Flow of Water at $N_{Re} = 38000$**

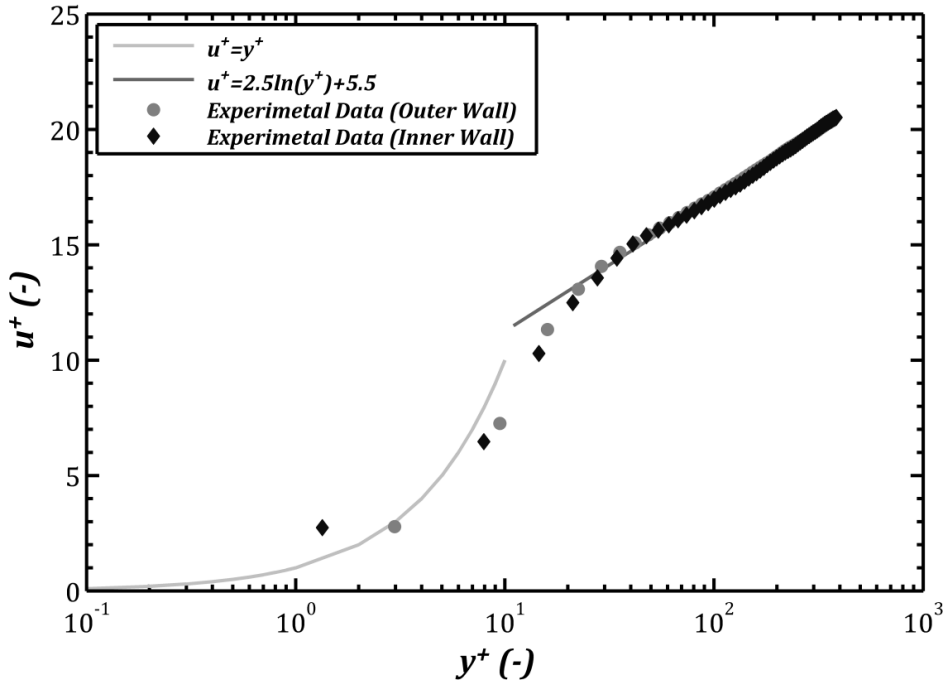


**Figure 6-7 Near Wall Velocity Profiles for Flow of Water at $N_{Re} = 46000$**

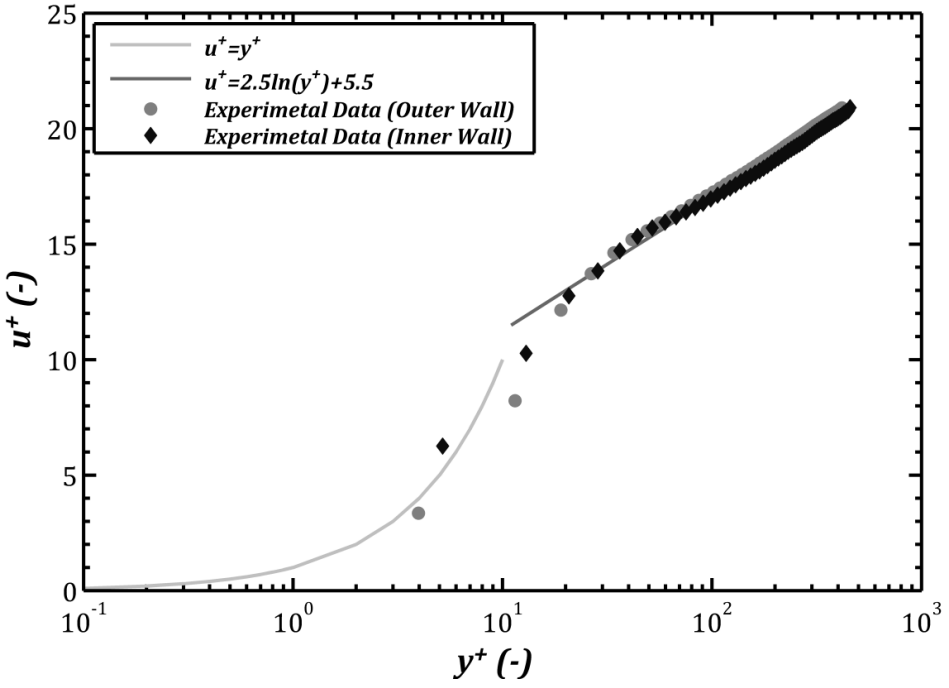


**Figure 6-8 Near Wall Velocity Profiles for Flow of Water at $N_{Re} = 54000$**

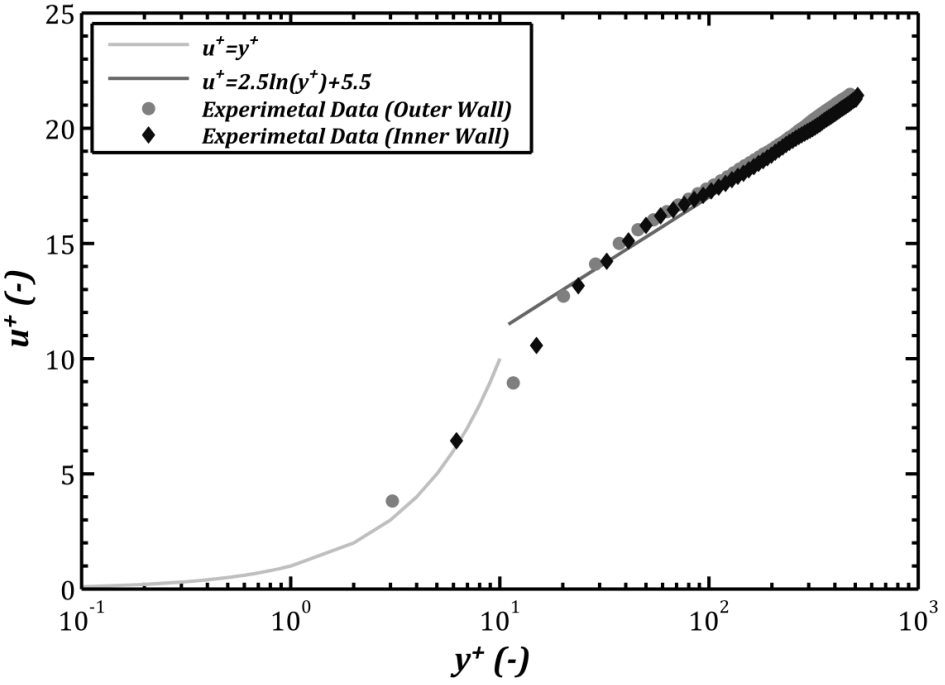


**Figure 6-9 Near Wall Velocity Profiles for Flow of Water at $N_{Re} = 68000$**

Summary: velocity profiles have been found to be in agreement with universal law of the wall for $y^+ < 10$ for both inner wall and outer wall of the annuli and at all six Reynolds numbers studied. Further away from the wall for $y^+ > 10$ logarithmic law consistent for flow of Newtonian fluids in channels and pipes were found to be valid for annular flow as well.

### 6.4.4 Velocity Profiles in Whole Annular Gap and Radius of Maximum Velocity

One of the unsolved debates for annular flow is the location of maximum velocity. Is maximum velocity occurs at the midpoint of annuli? Is this radius is the same as the radius of zero shear stress? Asymmetry in the velocity profile has been observed and reported by early investigators which imply that velocity maximum is biased toward one of the walls.

Figure 6-10 to Figure 6-12 are the resulted velocity profiles presented against dimensionless radial location in the annuli. In order to show the differences, each plot contains the data for flow of water at three Reynolds numbers, the last plot though is a plot of all six Reynolds numbers tested. Although close to the walls of the annuli all the six flow rates are showing more or less same velocity data, in the core region big

differences is observed in for maximum velocity magnitude which is of course normal because of difference in flow rates. The general trend of all the velocity profiles are similar and no significant change occurs from changing Reynolds number from 17000 to 68000.

Summary: velocity profiles in the whole annular gap which are useful in determination of radius of maximum velocity have been reported with no significant change in the shape of the profiles for the range of Reynolds numbers studied.

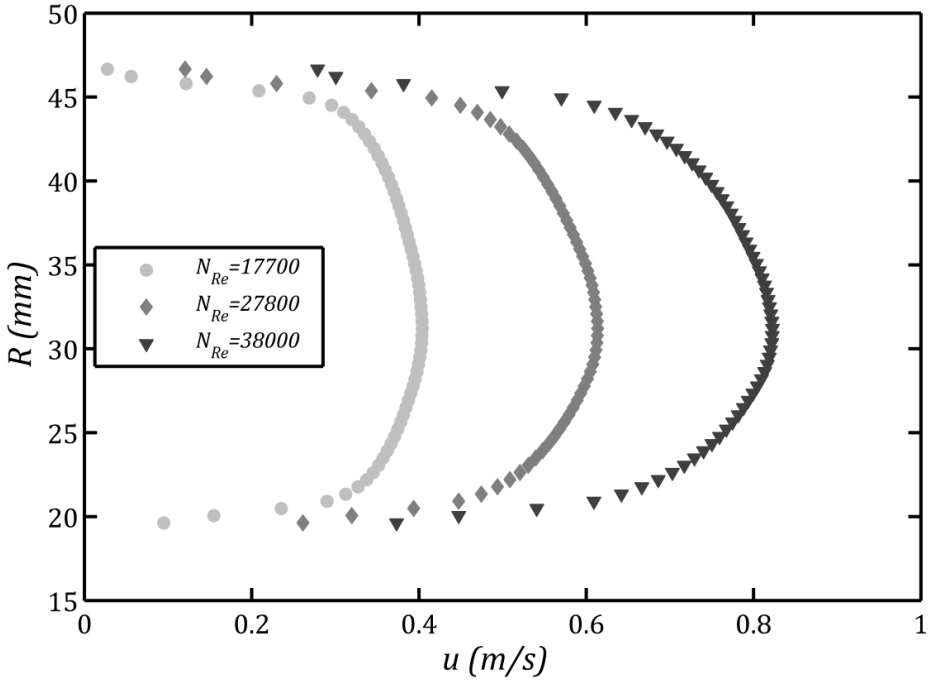


**Figure 6-10: Velocity Profiles in Whole Annular Gap for Flow of Water at Three Reynolds Numbers of 17700, 28600 and 3800**

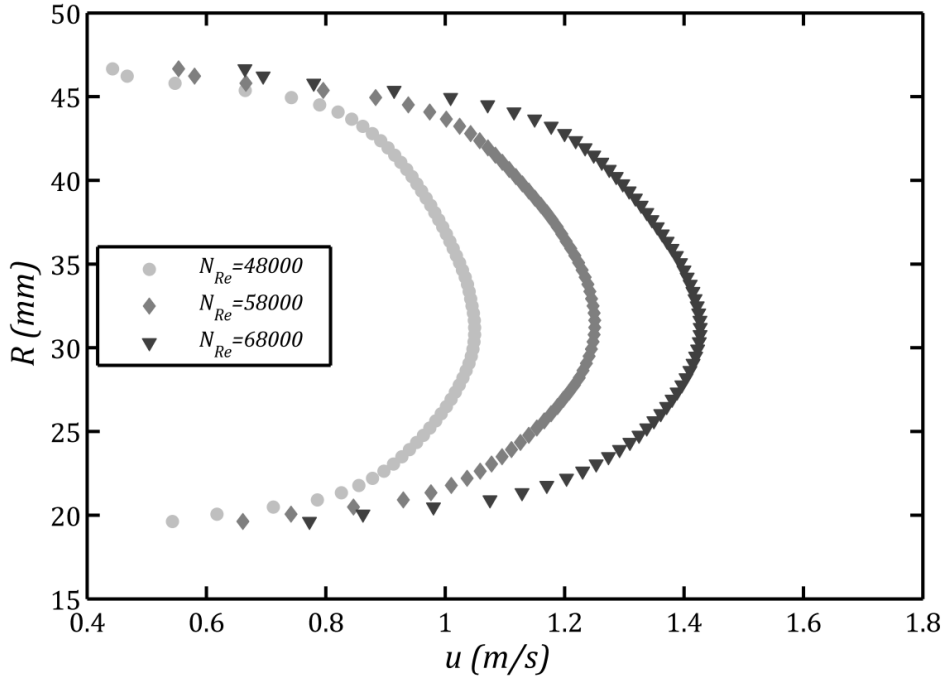


**Figure 6-11 Velocity Profiles in Whole Annular Gap for Flow of Water at Three Reynolds Numbers of 46000, 54000, 68000**

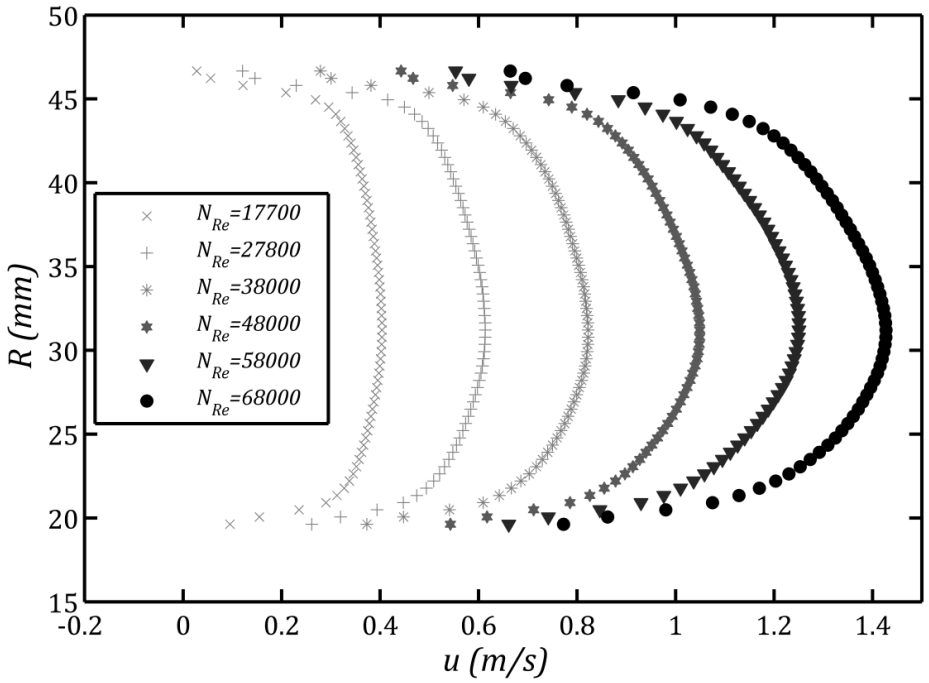


**Figure 6-12: Velocity Profiles in Whole Annular Gap for Flow of Water**

Radius of maximum velocity has been obtained by analysing the velocity distribution in the whole annular gap presented previously. Because velocity profiles in the core of a turbulent flow is flat finding the maximum of velocity can be challenging and an accurate way needs to be adopted. In order to get the exact radius of maximum velocity MATLAB has been utilized with the cure fitting tools. Table 6-3 is a summary of the founded radiuses of maximum velocity, dimensionless radial location in the annuli is also reported which would be used later for comparison purposes.

**Table 6-3: Radiuses of Maximum Velocity for Flow of Water in the Annuli**

| $N_{Re}$ | $R_{max}(mm)$ | $\xi_{max}(-)$ |
|---|---|---|
| 17700 | 31.213 | 0.428526 |
| 26800 | 31.213 | 0.428526 |
| 38000 | 31.213 | 0.428526 |
| 46000 | 31.213 | 0.428526 |
| 54000 | 31.642 | 0.443579 |
| 68000 | 31.213 | 0.428526 |

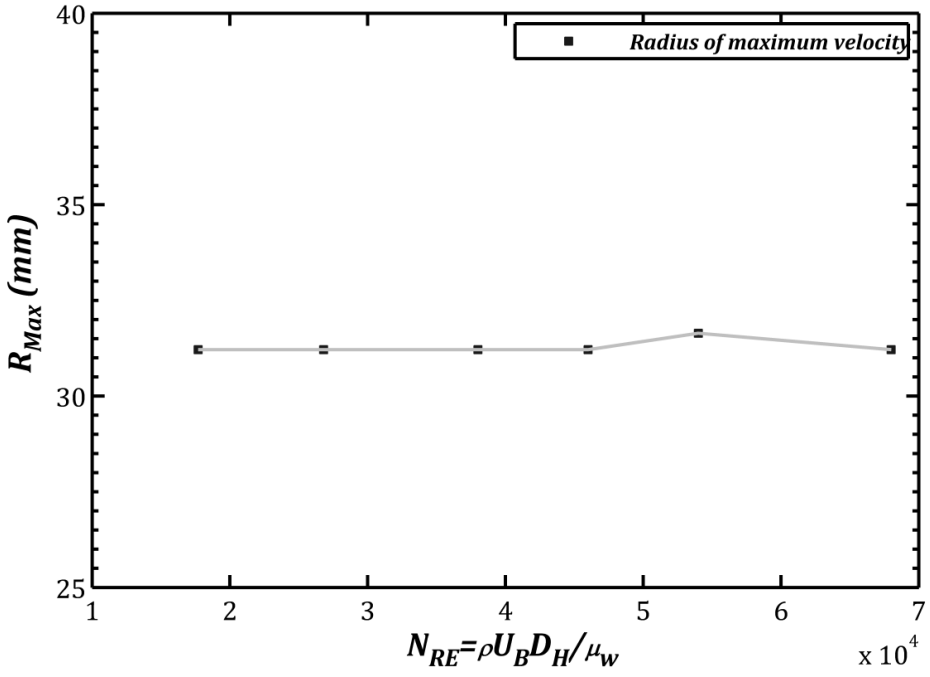


**Figure 6-13 Radiuses of Maximum Velocity vs Reynolds Number for Flow of Water in the Annuli**

Radius of maximum velocity (Table 6-3) has been founded independent of Reynolds number for flow of water at the range of Reynolds number studied; it is also shown

graphically (Figure 6-13) that this radius is independent of Reynolds number. Another conclusion from maximum velocity radius is that velocity maximum always occurs closer to the inner wall of the annuli. Indeed by just glimpsing the velocity profiles in whole annuli it is obvious that velocity profiles are biased toward the inner wall which indicates the strong asymmetry in these velocity profiles behaviour absent in pipe flow where a perfect parabolic velocity profile happens with maximum velocity at the center.

Summary: radius of maximum velocity for flow if water in turbulent flow regime has been found independent of Reynolds number. This radius also was found to be closer to inner wall of the annuli.

### 6.4.5 Shear Stresses

#### 6.4.5.1 Reynolds Stresses

Reynolds stress or turbulent induced stress causes by fluctuations in velocity which is a result of turbulence itself. This component of shear stress is absent in the case of laminar flow as there is no fluctuation velocity. Reynolds stress is defined as time average of product of axial and tangential (Radial) fluctuation velocity times the fluid density Eq. ( 6-20).

$$\tau_{Re} = -\rho\overline{u'v'} \qquad \text{Eq. ( 6-20)}$$

As mentioned earlier in chapter 3 PIV measures the instantaneous velocity field which through post processing one can calculate the time average velocity and get the fluctuation velocity components. Reynolds stress is then obtained by using the same software (Davis) which is calculated from the measured velocity field. Figure 6-14 to Figure 6-16 are the Reynolds stress profiles for flow of water in the annuli.

Note that the stresses are presented in dimensional form in order to separate the results for different Reynolds numbers.

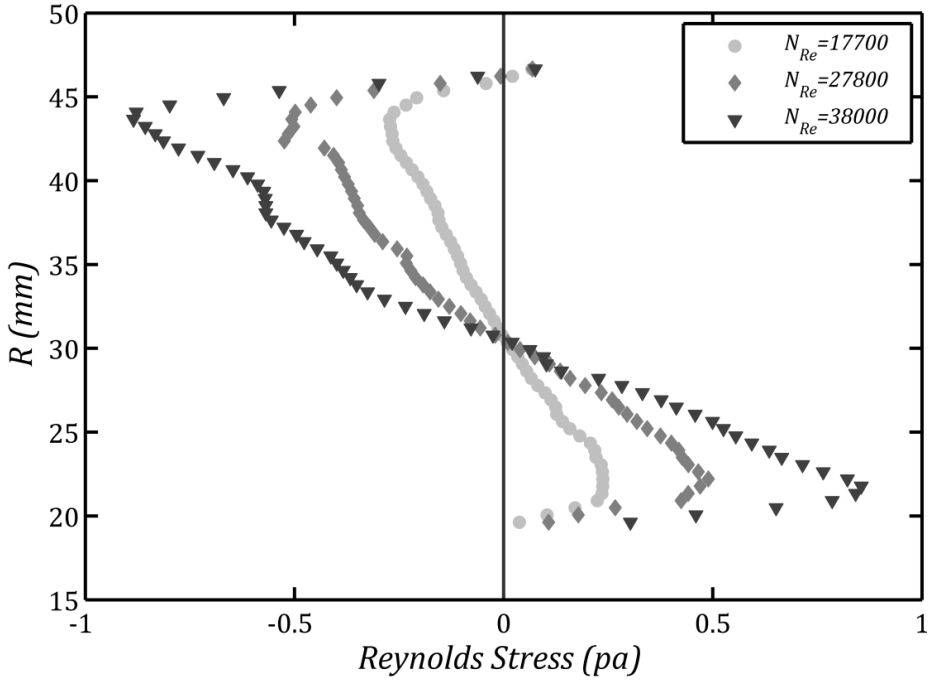


**Figure 6-14: Reynolds Stress Profiles in Whole Annular Gap for Flow of Water at Three Reynolds Numbers of 17700, 26800, 38000**

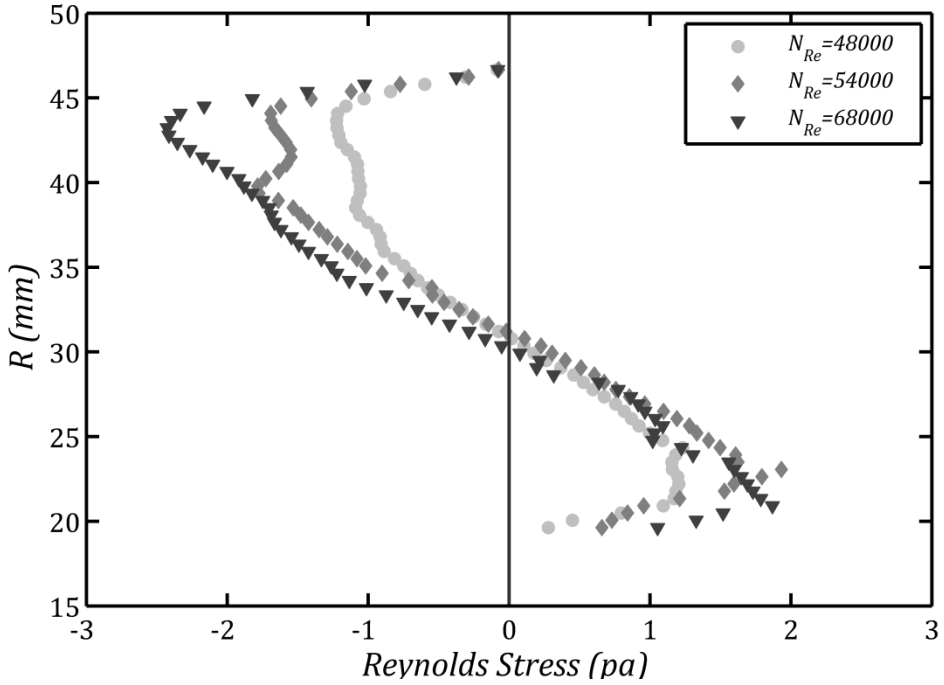


**Figure 6-15 Reynolds Stress Profiles in Whole Annular Gap for Flow of Water at Three Reynolds Numbers of 46000, 54000, 68000**

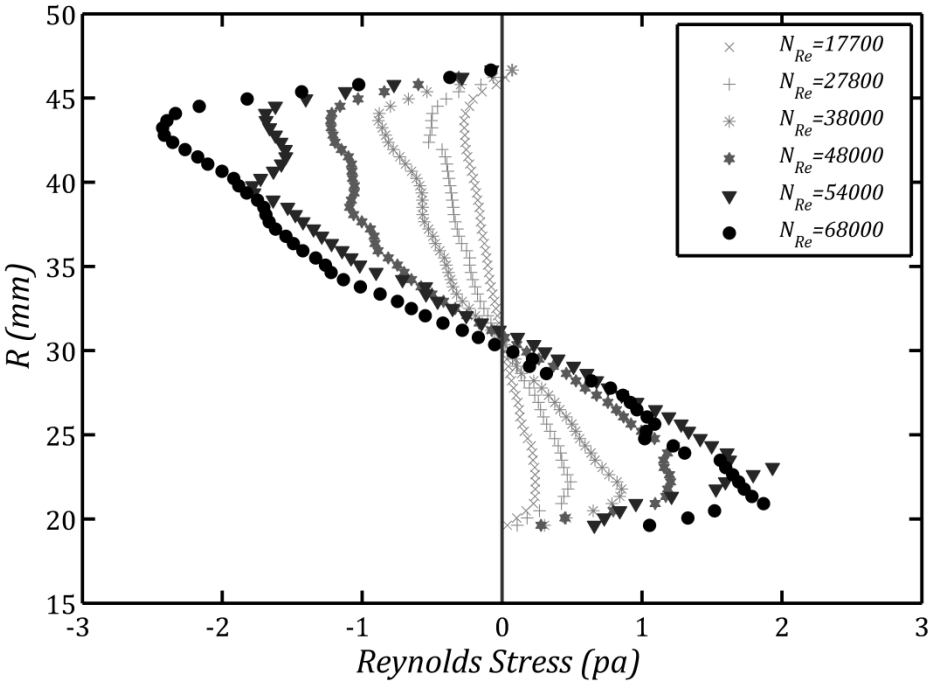


**Figure 6-16 Reynolds Stress Profiles in Whole Annular Gap for Flow of Water**

Measured Reynolds stresses as shown in Figure 6-14 to Figure 6-16 are showing exact behaviour as expected. Starting from one of the walls ($\xi = 0\ or\ 1$) Reynolds stresses are zero, this is the viscous sublayer where the viscous forces are dominating and although the flow is not laminar in this region but Reynolds stresses are negligible as strong viscous modification of turbulence structures is taking place. Moving away from viscous sublayer Reynolds stresses increases continuously until it gets to a peak. After passing the maximum point Reynolds stress starts to decrease moving toward passing a zero point that is the radius of zero shear stress and will be discussed later.

Summary: Reynolds stress profiles were found to have a maximum close to the walls but they rapidly decrease to zero as the walls are approached. In the core regions of the flow these stresses pass through a zero which is not in the middle of the annuli.

#### 6.4.5.2 Viscous Stresses

In contrast with Reynolds stresses which are results of fluctuations in velocity, viscous stresses are result of viscosity action and this component of shear stress exists in both laminar flow and turbulent flow. Indeed for a Newtonian fluid in general total shear

stress is the summation of viscous stresses and Reynolds stresses, the last term is zero for laminar flow. Viscous stress is defined as Eq. ( 6-21).

$$\tau_v = \mu \frac{\partial u}{\partial y} \qquad \text{Eq. ( 6-21)}$$

From Eq. (21) it can be concluded that viscous stress is high where the velocity gradient is high. Going back to Figure 6-10 to Figure 6-12 it is obvious for turbulent flow in the core flow (away from wall region) the velocity profile is pretty much flat with a very small gradient in velocity which means small or negligible viscous stress in these regions of the flow. In fact because the viscosity is so low for water one may even assumes inviscid flow (inviscid flow: a flow with no viscous resistance) in the core region of turbulent flow. Generally from velocity profiles it is expected to obtain a very small or zero viscous stress in the core region of the flow.

Close to the walls the story is different as sharp changes in velocity could be observed which implies high velocity gradient and high vicious stress. Indeed this is expected to happen, by looking at Reynolds stress profiles it seems that close to the walls Reynolds stresses are zero but from pressure drop data one expect to get the highest shear stress at the wall; wall shear stress. In order to restore the shear stress close to the walls and obtain a value equal to wall shear stress required by pressure drops viscous stress term comes to play the important role in this region.

Generally the core flow can be assumed inviscid flow with negligible viscous stress because of flatness of velocity profile in this region and very low viscosity of water. Very close to walls sharp increase in viscous stress is to be seen because Reynolds stresses are zero in this zone and also sharp change in velocity is observed as well. Viscous stresses are presented in Figure 6-17 to Figure 6-19.

Viscous stress profiles are showing values very close to zero in the core flow, consistent with earlier discussion and conclusion on inviscid flow idea in the core flow due to flatness of the velocity profiles. In total, viscous stresses could be assumed zero in the case of flow of water at the range of Reynolds number studied in the core region of the flow comparing to Reynolds stresses.

Close to the walls sharp increase in viscous stress is observed that is the result of sharp increase in velocity gradient. Viscous stress must get a value equal to wall shear

stress required by pressure drop at the walls, from Figure 6-17 to Figure 6-19 this is not the case and viscous stress at wall is almost an order of magnitude smaller than wall shear stress; this behaviour need extra explanation. One explanation would be because there is not enough velocity data points presented in the viscous sublayer to give rise to velocity gradient as much as it should do. Another explanation is that because of dispersion of light and also taking pictures of the flow form longer range (bigger field of view in pictures means less points close to the walls) less accuracy is obtained in the viscous sublayer where the viscous stress is higher.

Overall, viscous stress in the core flow is negligible comparing to Reynolds stresses or even viscous stresses close to the walls and the assumption of inviscid flow does apply for flow of water at operational Reynolds numbers in this study. Close to the walls viscous stresses is much higher than core region and that is because of strong effect of viscosity and large velocity gradient in this zone.

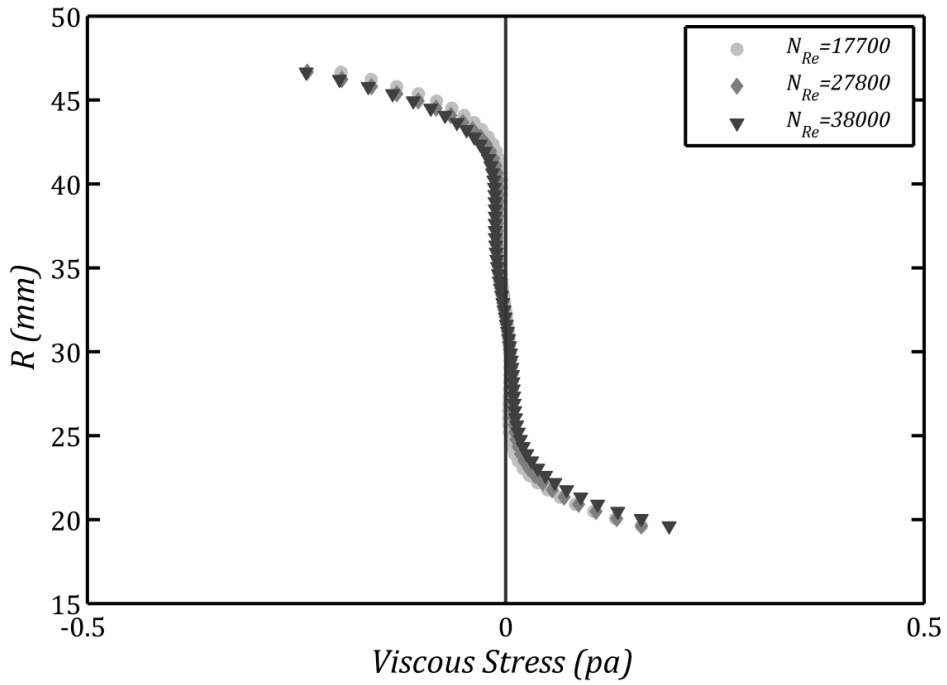


**Figure 6-17 Viscous Stress Profiles in Whole Annular Gap for Flow of Water at Three Reynolds Numbers of 17700, 26800, 38000**

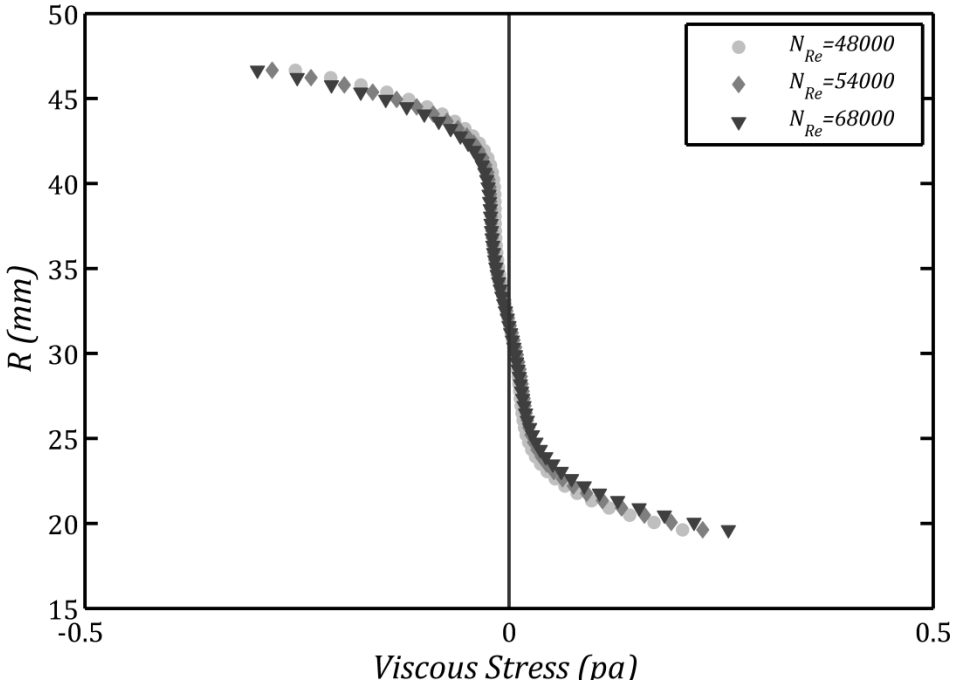


**Figure 6-18 Viscous Stress Profiles in Whole Annular Gap for Flow of Water at Three Reynolds Numbers of 46000, 54000, 68000**

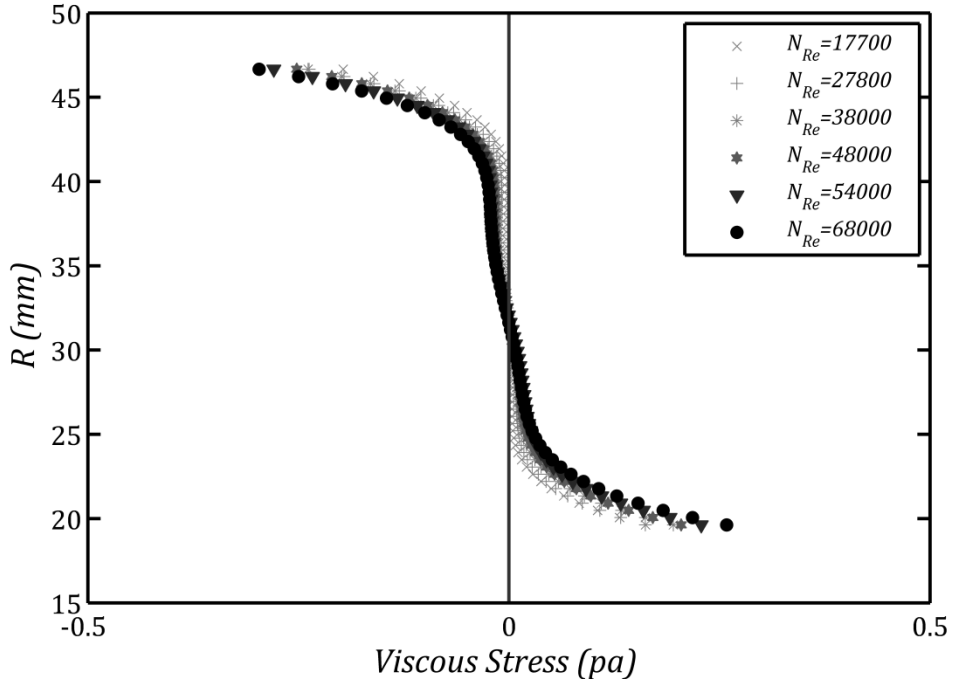


**Figure 6-19 Viscous Stress Profiles in Whole Annular Gap for Flow of Water**

Summary: Viscous stresses were found to be negligible in the core region of the flow. Sharp increase in viscous stress has been observed in the vicinity of the walls and viscous sublayer.

### 6.4.6 Zero Shear Stress Radius

Total stress is the summation of viscous stress and Reynolds stress, Eq. ( 6-22).

$$\tau = \tau_{Re} + \tau_{v} \qquad \text{Eq. ( 6-22)}$$

Equation 22 has been applied to the PIV results for flow of water. The results of this equation are very close to Reynolds stresses at least in the core regions of the flow. Note that because of the reasons given for why viscous stresses doesn't converge to wall shear stress, total stress is also not converging for the same reasons. In the core flow however total stresses are reliable because the flow is inviscid and viscous stress has no or very small contribution to total stress. Total stress profiles are very close to Reynolds stresses and are not presented in order to avoid repetition of the same graphs.

Radiuses of zero shear stress for the 6 Reynolds numbers studied have been obtained from total stress profiles and are summarized in Table 6-4.

Radius of zero shear stress is independent of Reynolds number based on the data in Table 4-1-4; this was also the case for the maximum velocity radius. So one conclusion from experiments with water at the range of Reynolds number studied is that radiuses of maximum velocity and zero shear stress are independent of Reynolds number.

**Table 6-4: Radius of Zero Shear Stress for Flow of Water in Annuli**

| $N_{Re}$ | $R_0(mm)$ | $\xi_0(-)$ |
|---|---|---|
| 17700 | 30.7 | 0.410526 |
| 26800 | 30.7 | 0.410526 |
| 38000 | 30.5 | 0.403509 |
| 46000 | 30.8 | 0.414035 |
| 54000 | 31.1 | 0.424561 |
| 68000 | 30.2 | 0.392982 |

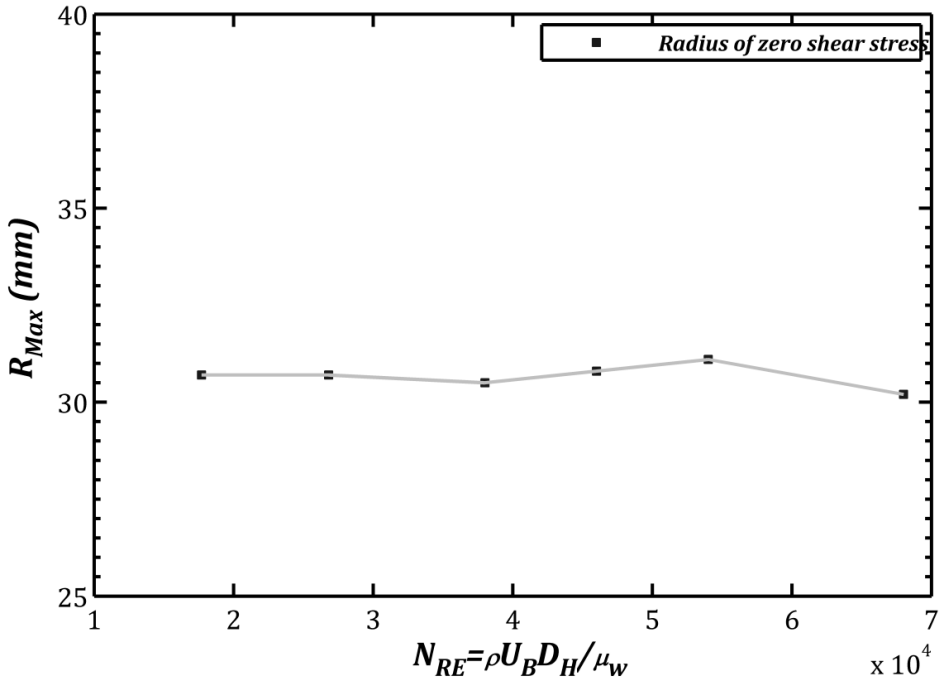


**Figure 6-20 Radius of Zero Shear Stress vs Reynolds Number for Flow of Water in Annuli**

Radius of zero shear stress is also closer to inner wall of the annuli than the outer wall; a behaviour similar to maximum velocity. Actually the asymmetry in the velocity profile can also be observed in Reynolds stresses which implies to the asymmetry in the radius of zero shear stress.

Summary: radius of zero shear stress for flow of water in turbulent flow regime has been found independent of Reynolds number. This radius is closer to inner wall of the annuli.

### 6.4.7 Radius of Zero Shear Stress versus Radius of Maximum Velocity

Comparison of radiuses of maximum velocity and zero shear stress shows that zero shear stress do occur closer to the inner wall rather than the maximum velocity. Table 6-5 is a comparison of these two radiuses. Based on this data, radius of zero shear stress is some number 1.6 to 3.25% closer to the inner wall of the annuli.

**Table 6-5: Radius of Maximum valocity vs Radius of Zero Shear Stress for Flow of Water**

| $N_{Re}$ | $R_{max}(mm)$ | $R_0(mm)$ | Difference (%) |
|---|---|---|---|
| 17700 | 31.213 | 30.7 | 1.643546 |
| 26800 | 31.213 | 30.7 | 1.643546 |
| 38000 | 31.213 | 30.5 | 2.284305 |
| 46000 | 31.213 | 30.8 | 1.323167 |
| 54000 | 31.642 | 31.1 | 1.712913 |
| 68000 | 31.213 | 30.2 | 3.245443 |

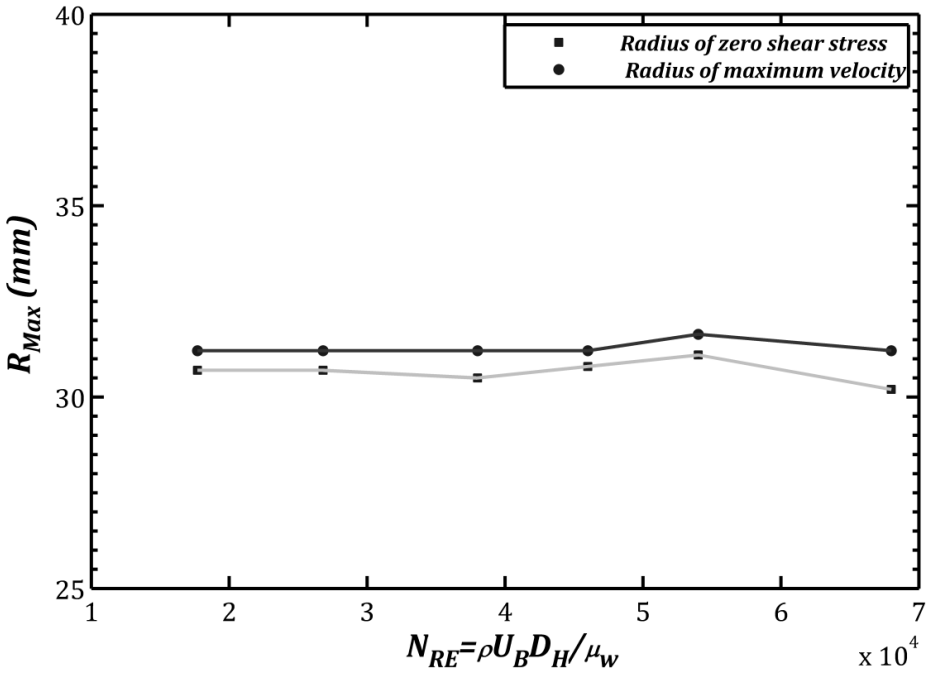


**Figure 6-21Comparison of Radiuses of Maximum Velocity and Zero Shear Stress for Flow of Water**

Figure 6-21 is the graphical representation of the data in Table 6-5 but in term of dimensionless radial location. From this figure it is obvious that both maximum velocity and zero shear stress radiuses are independent of Reynolds number and also the fact that zero shear stress occurs closer to inner wall could be concluded from the same figure.

### 6.4.8 Turbulent Intensities (TI)

Turbulent intensity as the name implies is an indicator of the level of turbulence in the flow; the higher the intensity the higher would be turbulent activities. The RMS of fluctuation velocity in the main flow direction ($U_{RMS}$) is taken as the TI; while some authors normalized TI by the velocity at the same location where $U_{RMS}$ has been measured, others have used the free stream velocity and some others presents this in wall coordinates by using the friction velocity. The advantage of using wall coordinates is in studying the near wall behaviour which is critical in comparing the results for flow of different fluids; this approach has been adopted in presenting the results of this works.

$$TI = \frac{U_{RMS}}{u^*} \qquad \text{Eq. ( 6-23)}$$

$$u^* = \sqrt{\frac{\tau_w}{\rho}} \qquad \text{Eq. ( 6-24)}$$

Previous equitation (Eq. ( 6-25)) is the definition of the axial intensity; radial intensity is defined as the ratio of $V_{RMS}$ to friction velocity.

$$TI_{Radial} = \frac{V_{RMS}}{u^*} \qquad \text{Eq. ( 6-25)}$$

#### 6.4.8.1 Axial Intensities

Axial intensities measured by PIV technique for flow of water at six Reynolds numbers are reported in Figure 6-22 to Figure 6-27. Note that each plot contains the data for both walls at a fixed Reynolds number.

From the axial intensities it is obvious that the outer wall always show bigger value comparing to the inner wall. Higher level of turbulent intensities around the outer wall has been confirmed in previous studies but it also been stated that higher level of turbulence around the outer wall don't lead to earlier transition to turbulence around this wall.

Turbulent intensities seem to take their peak in a dimensionless distance from the wall less than 30. This is clear for lower Reynolds numbers and as Reynolds numbers

increases this peak vanishes. The explanation is that for lower Reynolds numbers the thickness of the viscous sublayer or at any given $y^+$ is higher in real world dimension because friction velocity is lower.

$$y^+ = \frac{y\rho u^*}{\mu} \qquad \text{Eq. ( 6-26)}$$

The number of measurement points in the region close to the wall in wall coordinate reduces as Reynolds number increases although the actual distance is not changing and that is why the behaviour of the axial intensities looks different. Concluding from axial intensities for lower Reynolds numbers, it is expected that TI takes its peak in wall region and more specifically in buffer layer.

Summary: axial turbulent intensities have shown grater values for the outer wall of the annuli for all the Reynolds numbers studied. These intensities take their peak in the vicinity of the solid walls for usually $y^+ < 30$.

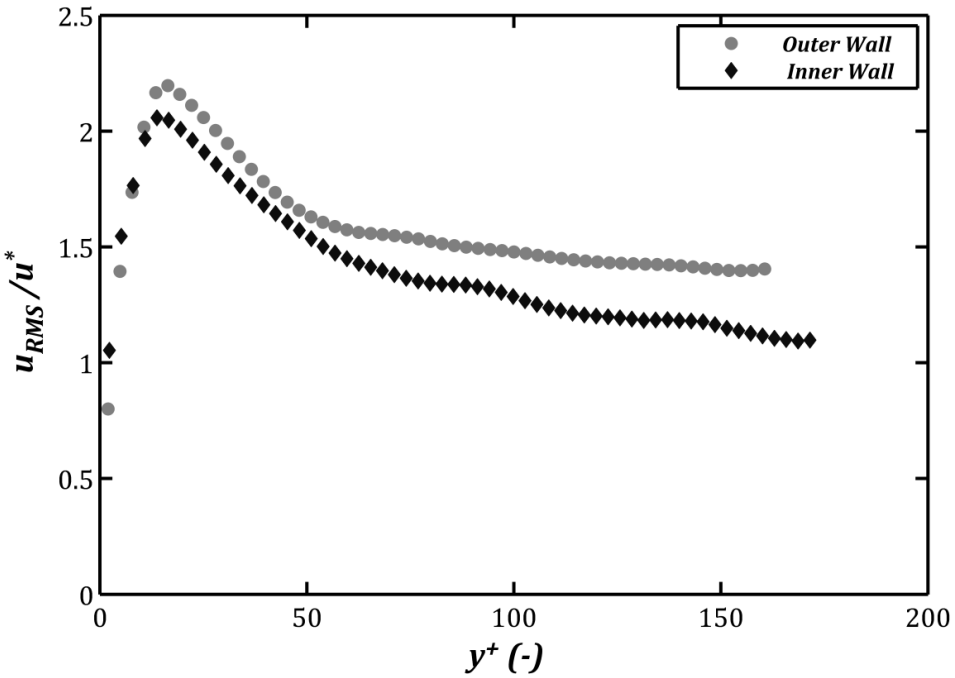


**Figure 6-22 Axial Turbulent Intensities for Flow of Water at $N_{Re} = 17700$ in Wall Coordinate**

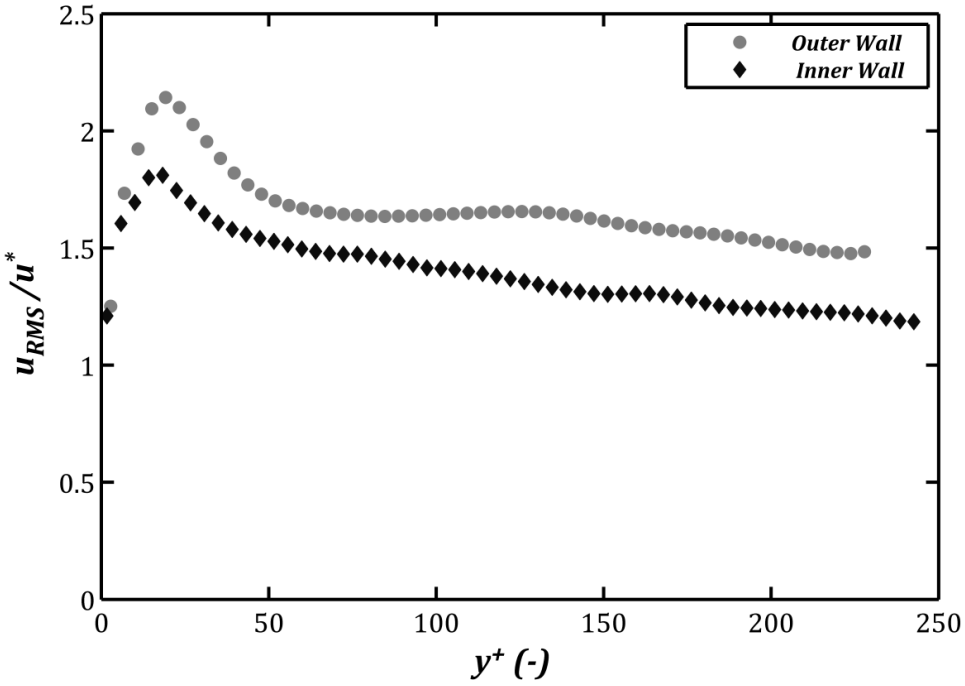


**Figure 6-23 Axial Turbulent Intensities for Flow of Water at $N_{Re} = 26800$ in Wall Coordinate**

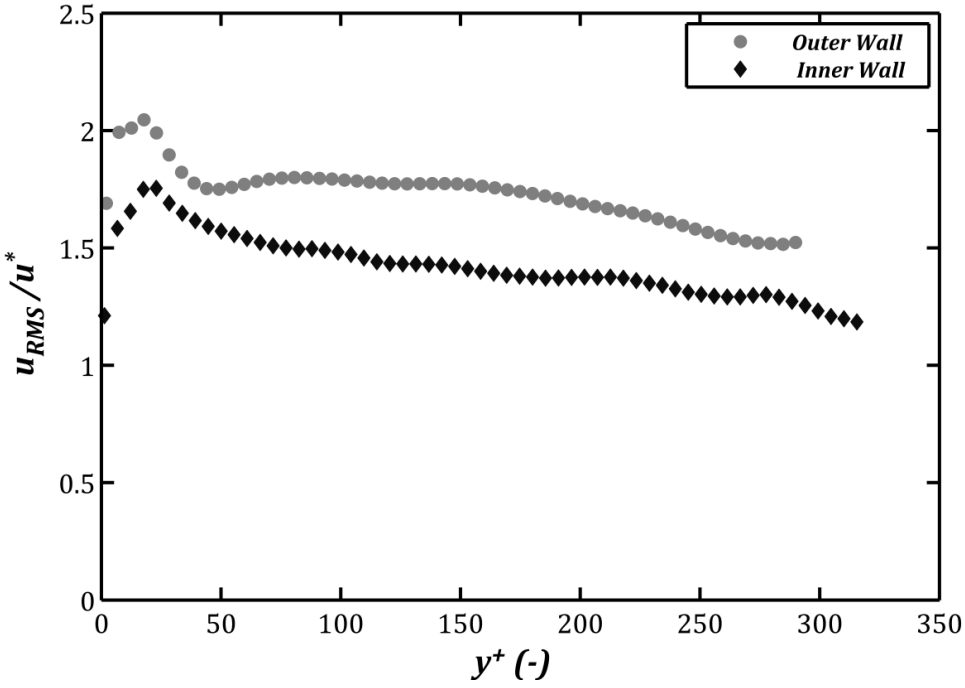


**Figure 6-24 Axial Turbulent Intensities for Flow of Water at $N_{Re} = 38000$ in Wall Coordinate**

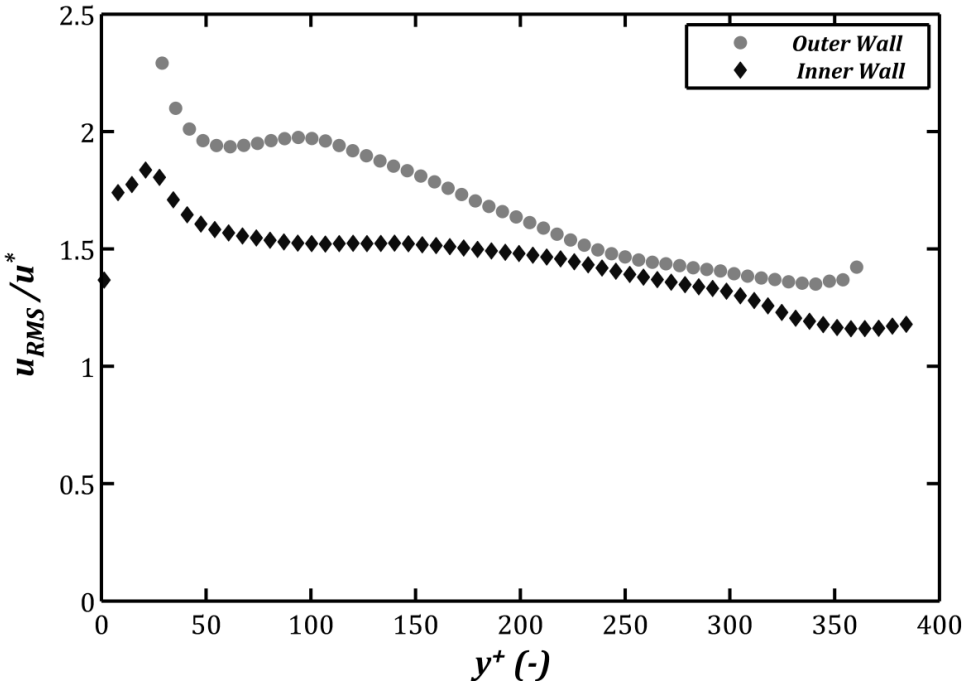


**Figure 6-25 Axial Turbulent Intensities for Flow of Water at $N_{Re} = 46000$ in Wall Coordinate**

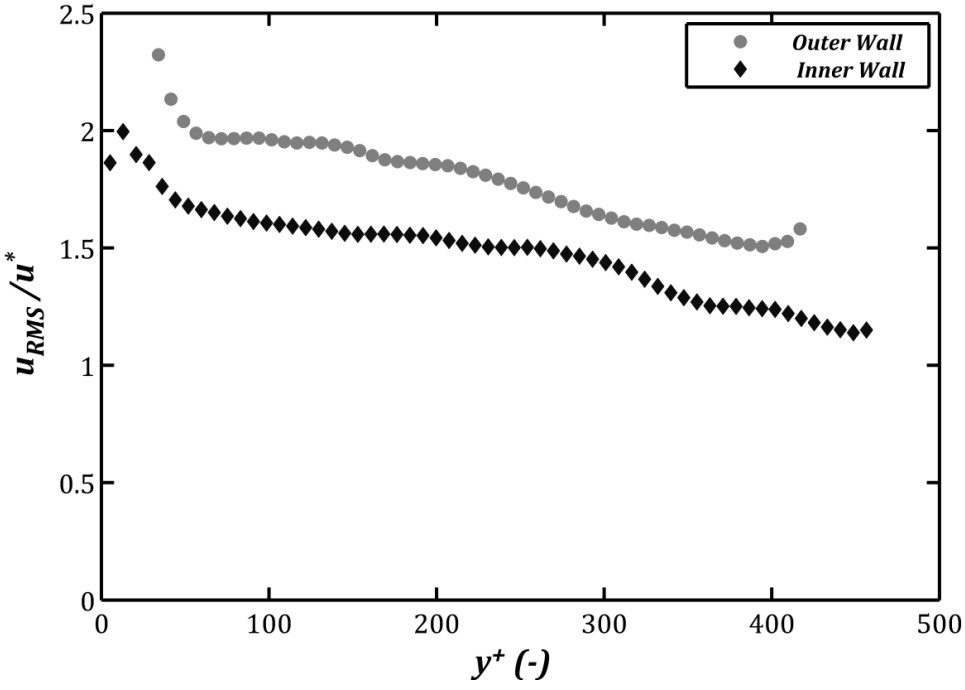


**Figure 6-26 Axial Turbulent Intensities for Flow of Water at $N_{Re} = 54000$ in Wall Coordinate**

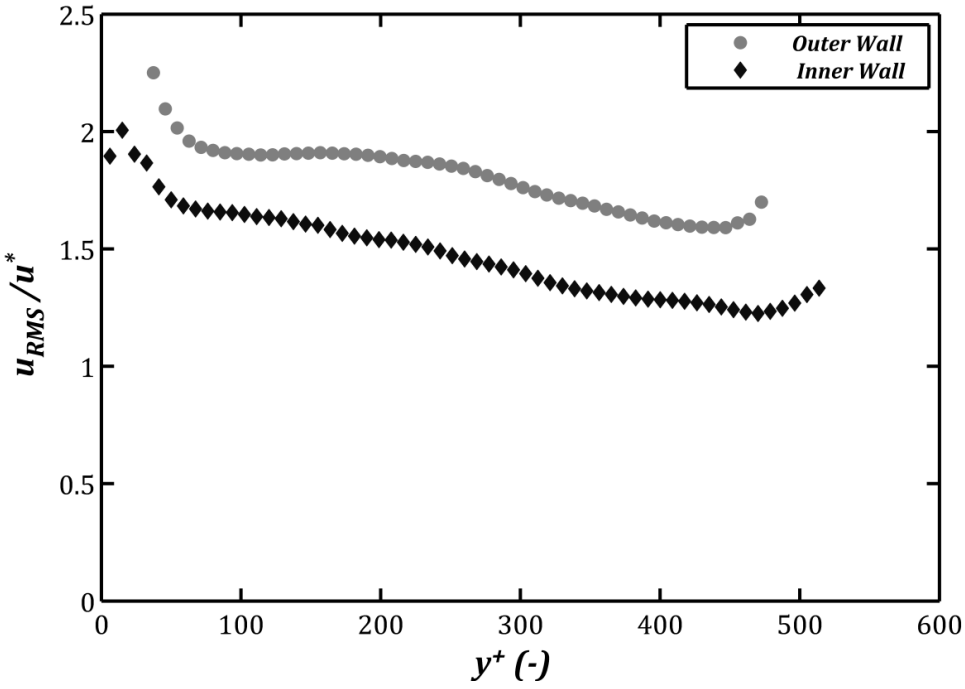


**Figure 6-27 Axial Turbulent Intensities for Flow of Water at $N_{Re} = 68000$ in Wall Coordinate**

#### 6.4.8.2 Radial Intensities

Radial intensities, similar to axial intensities, are reported in wall coordinate in Figure 6-28 to Figure 6-33.

Radial intensities for both inner and outer wall of the annuli are close with outer wall data in some cases a bit higher but not as much to make any conclusion based on that. The trend is different than that of axil component which has a peak and reduces rapidly afterward, radial component of the fluctuation velocity it becomes almost constant at some distance from the wall. It looks like those radial intensities don't show any maximum point but a minimum point very close to the walls.

Using the friction velocity to non-dimensionalizing the intensities seems a sound procedure for compassion as all the radial intensities are showing magnitudes very close to each other at six different Reynolds number.

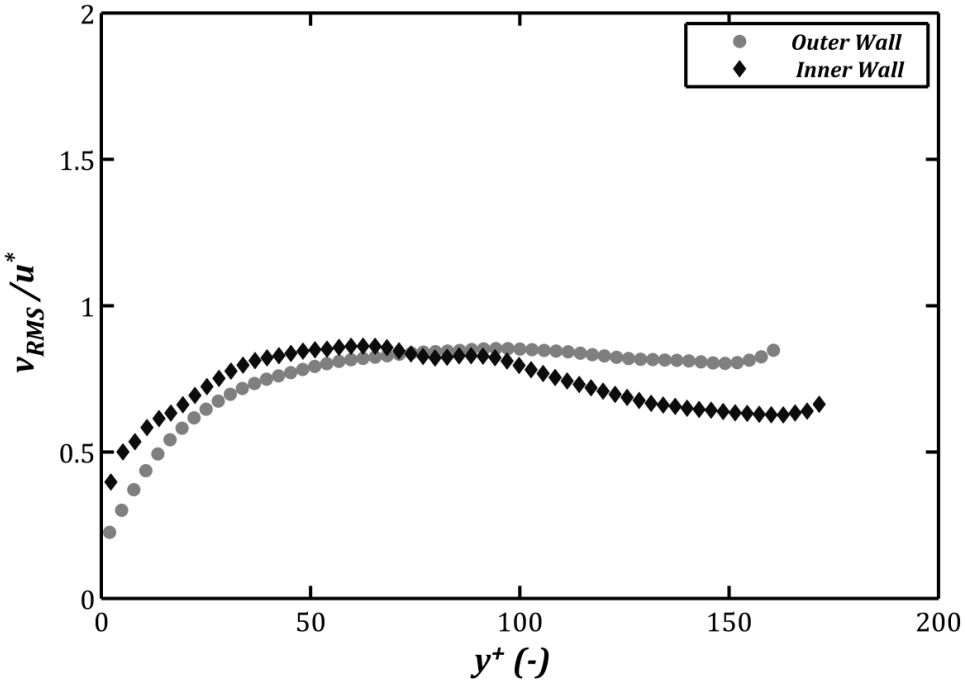


**Figure 6-28 Radial Turbulent Intensities for Flow of Water at $N_{Re} = 17700$ in Wall Coordinate**

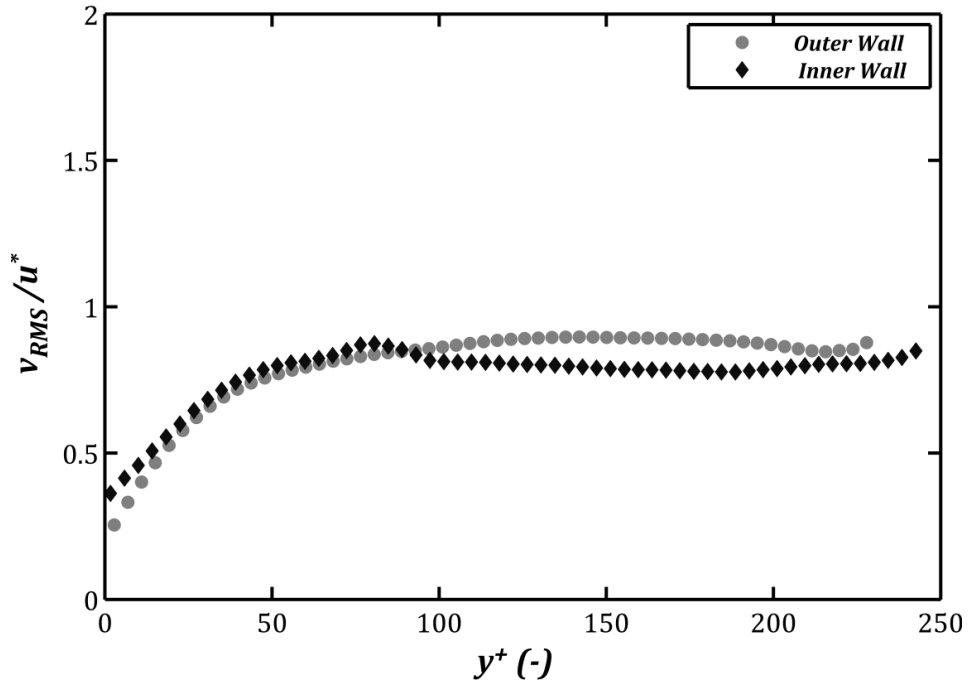


**Figure 6-29 Radial Turbulent Intensities for Flow of Water at $N_{Re} = 26800$ in Wall Coordinate**

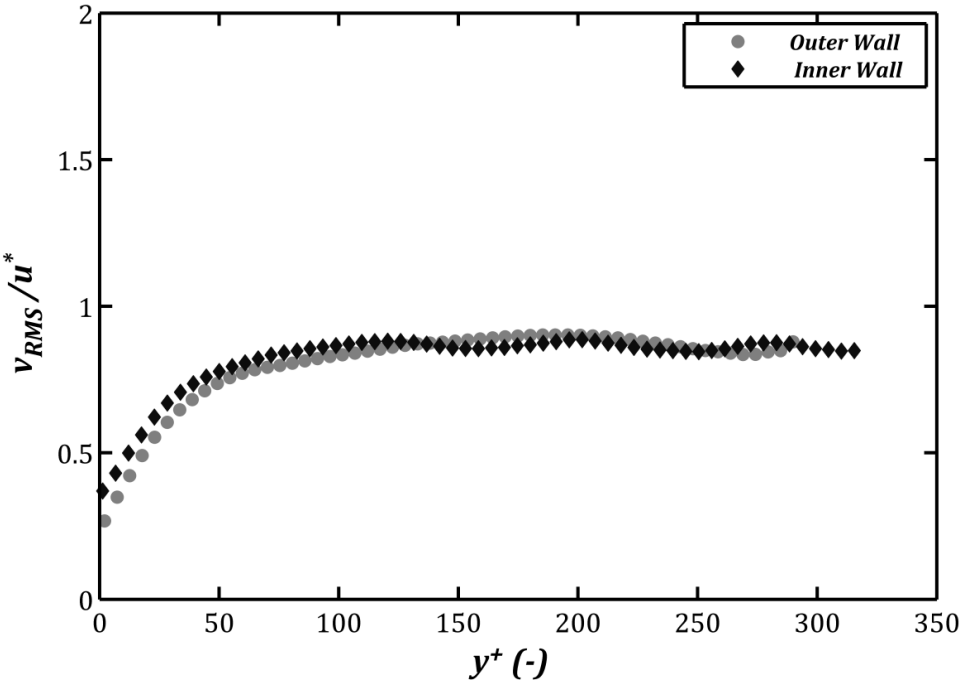


**Figure 6-30 Radial Turbulent Intensities for Flow of Water at $N_{Re} = 38000$ in Wall Coordinate**

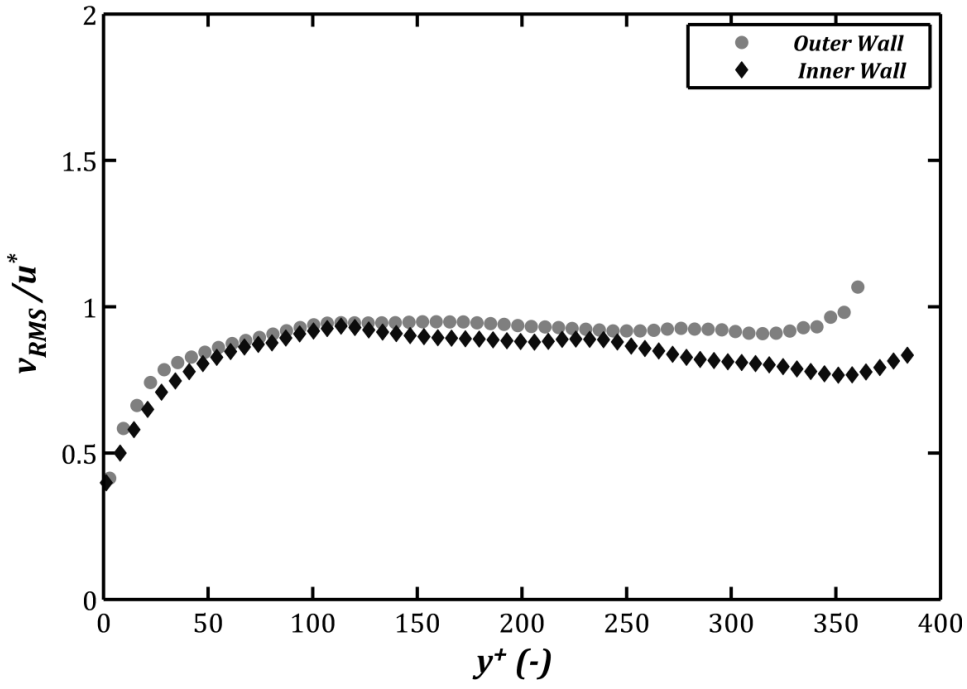


**Figure 6-31 Radial Turbulent Intensities for Flow of Water at $N_{Re} = 46000$ in Wall Coordinate**

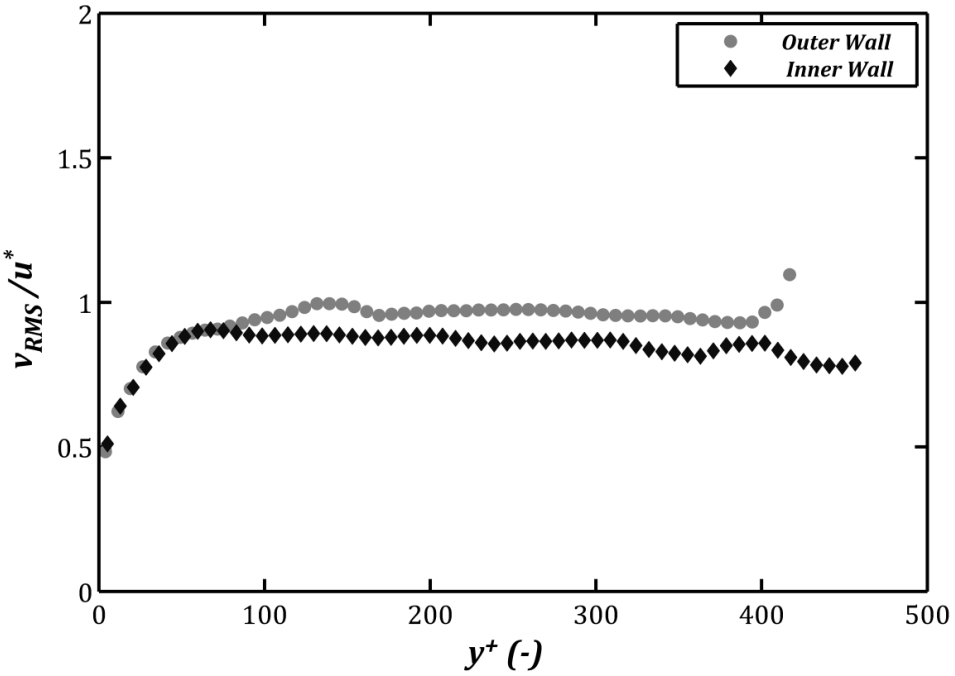


**Figure 6-32 Radial Turbulent Intensities for Flow of Water at $N_{Re} = 54000$ in Wall Coordinate**

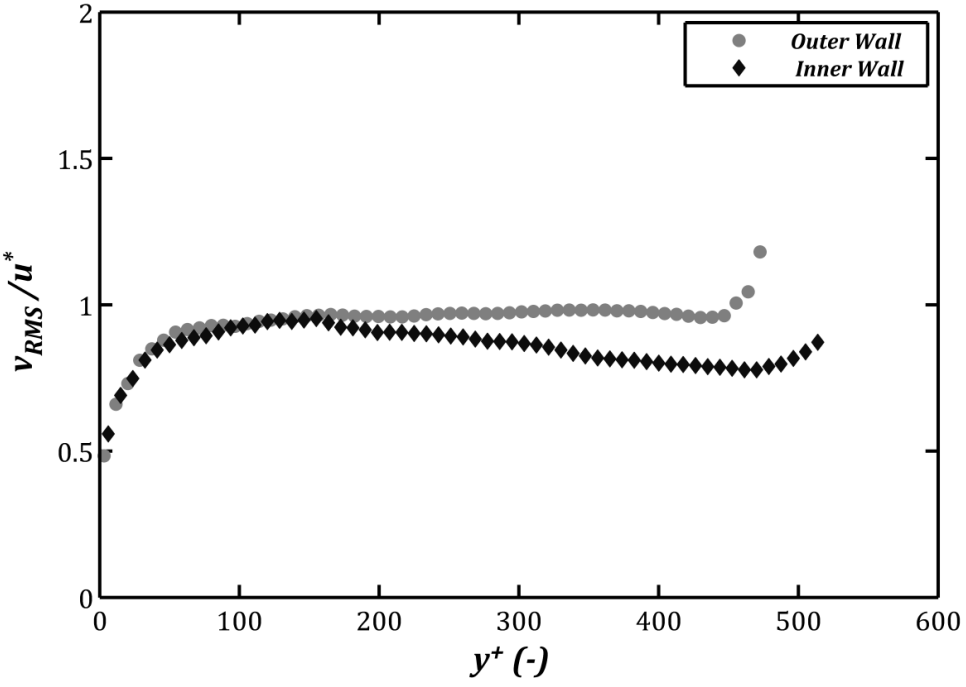


**Figure 6-33 Radial Turbulent Intensities for Flow of Water at $N_{Re} = 68000$ in Wall Coordinate**

Summary: Radial intensities have been found to have a flat profile in the core flow region. Although in some instances radial intensity of the outer wall is higher than inner wall but this is not a repeating behaviour for all the cases and so no conclusion is made about that. Radial intensities have shown a minimum value very close to the walls.

### 6.4.9 Conclusions

Experiments for Newtonian fluids have been done using water. Operational Reynolds numbers ranged from 17700 to 68000. Measurements have been taken for both pressure drops and velocity data.

- ✓ Friction factor for flow of water in the annuli has been found to be in agreement with Jones and Leung correlation in turbulent flow regime and no data has been obtained for the laminar flow
- ✓ Near wall velocity data in law of the wall coordinate were found to follow the universal law of the wall for $y^+ < 10$ and for both walls of the annuli at all Reynolds numbers
- ✓ Velocity data for $y^+ > 10$ in wall coordinates were in agreement with logarithmic law consistent with flow through pipes for all the Reynolds numbers and both inner and outer wall
- ✓ Strong asymmetry has been observed in velocity profiles in whole annular gap
- ✓ The radius of maximum velocity was found to be independent of Reynolds number
- ✓ Radius of maximum velocity has been found to be closer to the inner wall of the annuli
- ✓ Reynolds stress profiles have shown zero values close to the solid surfaces
- ✓ Reynolds stress profiles were found to be asymmetry despite the fact that Reynolds stress tensor is symmetric
- ✓ Reynolds stress profiles showed a maximum very close to walls of the annuli and tend to zero in the core flow
- ✓ Viscous stress profiles have shown zero or very small magnitudes in the core regions of the flow
- ✓ Viscous stress increased sharply as any of the walls of the annuli approached

- ✓ Viscous stress tends to the actual wall shear stress at walls of the annuli for lower Reynolds numbers tested but doesn't converge to this value at higher Reynolds numbers
- ✓ Zero shear stress radiuses were found to be closer to inner wall of the annuli
- ✓ Zero shear stress radiuses are independent of Reynolds number change
- ✓ Zero shear stress radius were found to be smaller than radius of maximum velocity meaning that zero shear occurs closer to the inner wall of the annuli
- ✓ Axial turbulent intensities in wall coordinate have shown higher values for the outer wall of the annuli
- ✓ Axial turbulent intensities were found to reach a maximum very close to the walls and in wall coordinate at $y^+ \sim 20$ which means TI takes its peak in the buffer layer
- ✓ Radial intensities have also been measured and reported and were found to be in the same order for both walls of the annuli (outer wall data were higher a bit but the difference is not as much as it was in axial intensities and no general conclusion could be made about that)
- ✓ Radial intensities have shown a different behaviour than axial intensities, no peak point for the radial intensities have been observed
- ✓ Radial intensities were found to be almost constant in the core regions of a turbulent flow of water

## 6.5 Non-Newtonian Fluid Flow through Annuli[9]

### 6.5.1 Friction Factor & Pressure Drop Data

Refereeing to the discussion given on friction factor in previous section, most of the definitions are similar to those of Newtonian fluids with the biggest difference being in viscosity. For a non-Newtonian fluid viscosity is a function of shear rate and because of that there is no unique definition of Reynolds number for non-Newtonian systems. Dodge et al. has redefined the Reynolds number for power law type of fluids based on flow behaviour and consistency indexes; this definition has not been found the best of all available correlations and is not used in this study. Another approach which has been adopted by many investigators is to define the Reynolds number based on viscosity of the fluid at the wall of the annuli.

$$N_{Re} = \frac{\rho U D_H}{\mu_w} \qquad \text{Eq. ( 6-27)}$$

$$\mu_w = k{\gamma_w}^{n-1} \qquad \text{Eq. ( 6-28)}$$

Shear rate at the wall could be calculated simply from the rheology model using wall shear stress which comes from pressure drop data

$$\gamma_w = \left(\left(\frac{1}{k}\right)\tau_w\right)^{\frac{1}{n}} \qquad \text{Eq. ( 6-29)}$$

Friction factor- Reynolds number for flow of two aqueous solutions of polymer has been measured and is reported in Figure 6-34. The data in the laminar flow regime has been compared with the theoretical solution for power law types of fluids and satisfactory agreement has been achieved.

$$f.N_{Re} = 23.9\left(\frac{2n+1}{3n}\right) \qquad \text{Eq. ( 6-30)}$$

This definition of theoretical prediction is coming from Fredrickson and Bird analysis which has been given in this form by Escudier [11].

[9] A version of this chapter has been presented

Bizhani M., Rodriguez-Corredor F. E, Kuru E., 2013, "An Experimental Study of Turbulent Non-Newtonian Fluid Flow in Concentric Annuli Using particle Image Velocimetry Technique", ASME 2013 International Mechanical Engineering Congress & Exposition (IMECE), November 13-21, 2013, San Diego, California, USA

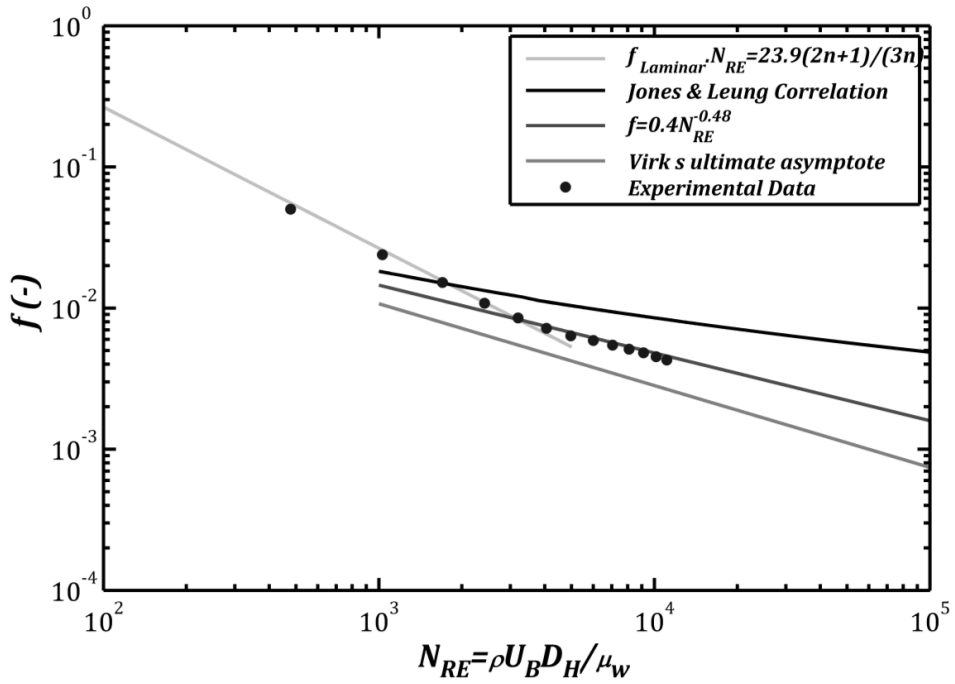


**Figure 6-34 Friction Factor Data for Flow of 0.175% Polymer Aqueous**

Friction factors in Figure 6-34 are in term of weighted average of the wall shear stress on the two walls.

$$\tau_A = \frac{1}{4}(D_o - D_i)\frac{dP}{dx} \qquad \text{Eq. ( 6-31)}$$

$$f = \frac{2\tau_A}{\rho {U_B}^2} \qquad \text{Eq. ( 6-32)}$$

From the experimental data, in the laminar flow regime an exceptionally good agreement is achieved with the theoretical prediction of a power law type of fluid presented in Eq. ( 6-30). In the turbulent flow regime the data are showing significantly lower value comparing with predictions of Jones and Leung correlation; this correlation was found to be valid for flow of water in previous section. The reduction of the friction factors in the turbulent flow is related to drag reduction phenomenon and is out of interest of this research.

Turbulent flow friction factors also have been compared with Virk's ultimate asymptote[24] which is for the condition of maximum drag reduction. The experimental

data were found to be higher than the predictions of this correlation which implies that this results are not for the condition of maximum drag reduction as Virk's original propose is for this condition only.

Turbulent flow friction factors for flow of polymer aqueous were found to be best represented by the following correlations.

$$f = 0.4{N_{re}}^{-0.48} \qquad \text{Eq. ( 6-33)}$$

This correlation has been found to be valid for both concentrations of the polymer studies in this thesis.

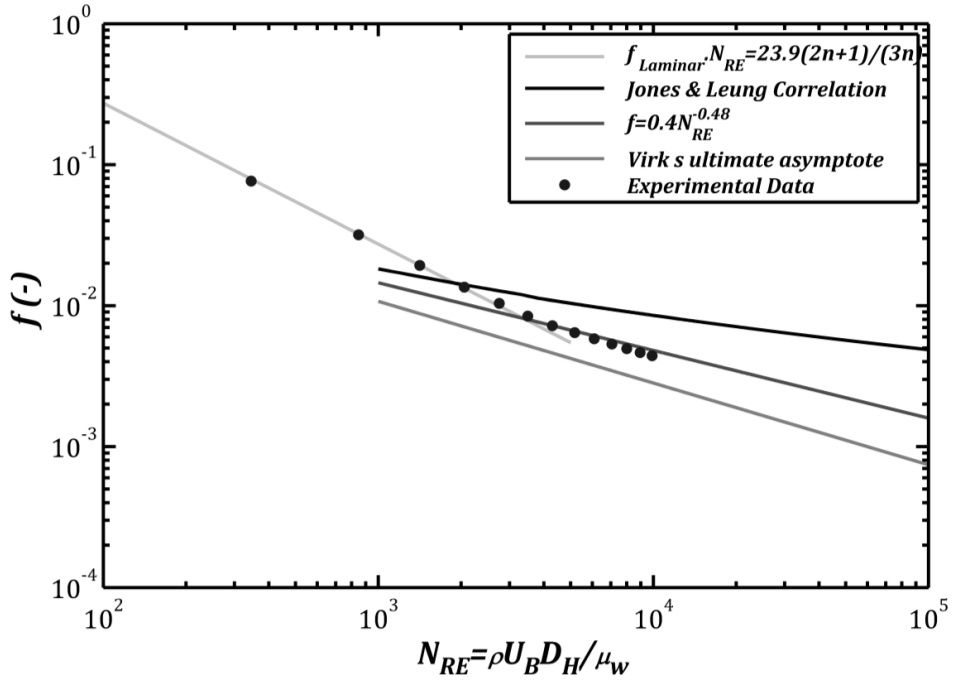


**Figure 6-35 Friction Factor Data for Flow of 0.2% Polymer Aqueous**

Summary of the results: friction factor of the polymer solutions at two concentrations have been measured and were found to follow the theoretical predictions of a power law type fluid in the laminar regime. In the turbulent flow the data felt well below the curve for Newtonian fluids predicted by Jones and Leung correlation which is an indication of drag reduction. The data in turbulent regime also were higher than that of Virk's

correlation for condition of maximum drag and were best represented by an empirical correlation.

### 6.5.2 Flow regime Assessment

Transition from laminar flow to turbulence in annuli for non-Newtonian fluids has been one of the main questions which have not been addressed properly in the literature. Although its known that for shear thinning fluids transition to turbulence occurs at higher Reynolds numbers than Newtonian fluids but this is rather a general conclusion and finding the critical Reynolds number have to done for each fluid based on data obtained for that experiment.

In this study, as the title of the thesis implies, the aim of the study has been investigation of turbulent flow through annuli. Also another goal has been studying effect of high viscous fluids on cutting transport in the annuli in turbulent flow. Based on the objectives of the project two concentrations of polymer aqueous was selected through analysis on small samples; 0.175 and 0.2 percent solutions. These two concentrations have been selected for further analysis.

According to friction factor data (Figure 6-34and Figure 6-35 ) in the range of operational pump flow rate all the three flow regimes (laminar, transitional and turbulent) are encountered and decision must be taken about the operational flow rates for performing PIV experiments which ensures a fully developed turbulent flow. Another consideration on selection of the proper flow rates is that these flow rates must be similar to those at which flow of Newtonian fluid (Water) has been studied in order to facilitate comparison at the same bulk flow rate.

Critical Reynolds numbers at which friction factor data start deviating from laminar curve has been taken as the onset of transition to turbulence, this Reynolds numbers ensure that the flow is no longer laminar. Table 6-6 contains the information on critical Reynolds numbers achieved for two polymer solutions.

**Table 6-6 Critical Reynolds Numbers for 0.175% and 0.2% Polymer Solutions**

| Concentration | Critical Reynolds Number |
|---|---|
| 0.175% | 3200 |
| 0.2% | 3400 |

The reported critical Reynolds numbers are the start point of deviation of friction factor data from laminar flow values. Bigger Reynolds numbers would ensure that flow is not laminar but doesn't guarantee a turbulent. In order to make sure that flow is in turbulent flow the last three velocities from the end have been chosen for further experiments. Table 6-7 is a summary of the selected flow rates and their corresponding Reynolds numbers.

**Table 6-7 Operational Conditions for Experiments with Non-Newtonian Fluids**

| | C=0.175% | C=0.2% |
|---|---|---|
| $U_B$ | $N_{RE}$ | $N_{RE}$ |
| 0.827 | 6950 | 5960 |
| 0.999 | 9100 | 7780 |
| 1.164 | 10950 | 9460 |

The lowest Reynolds number for the selected velocities is about 6000 which is almost twice the critical Reynolds number for that concentration.

Another way of proving that a flow is not laminar is by using the definition of turbulent flow instantaneous velocity. The instantaneous velocity in turbulent flow as discussed in chapter 2 is a function of time and space and fluctuates about a mean value while for laminar flow the fluctuations are zero. High level of fluctuation is a characteristic of a turbulent flow and could be used to monitor the transition to turbulence. Figure 6-36 and Figure 6-37 are the instantaneous velocity profiles close to wall for flow of the two polymer fluids at the lowest velocities reported in Table 6-7. High level of fluctuations also confirms that transition to turbulence has already taken place for the three velocities picked up.

Summary: a brief discussion on the flow regimes for flow of the polymer solutions has been given. Critical Reynolds number for transition from laminar flow was founded and reported. Three velocities for further examination in PIV experiments have been pick up and flow regime at these velocities was proven to be turbulent.

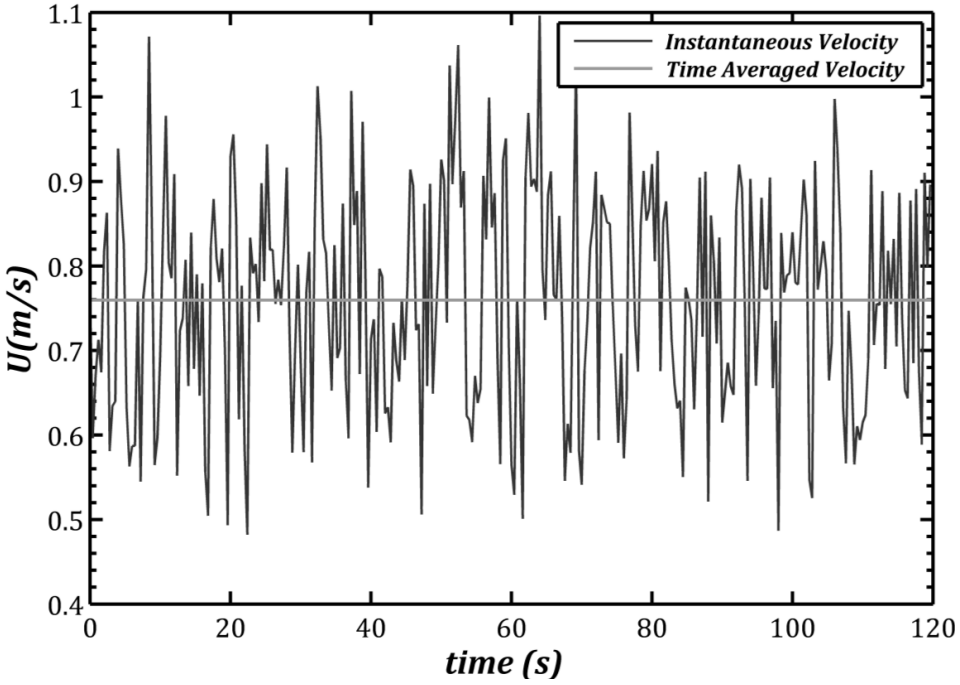


**Figure 6-36 Instantaneous Velocity Profile at ξ=0.9 for Flow of 0.175% Polymer Solution**

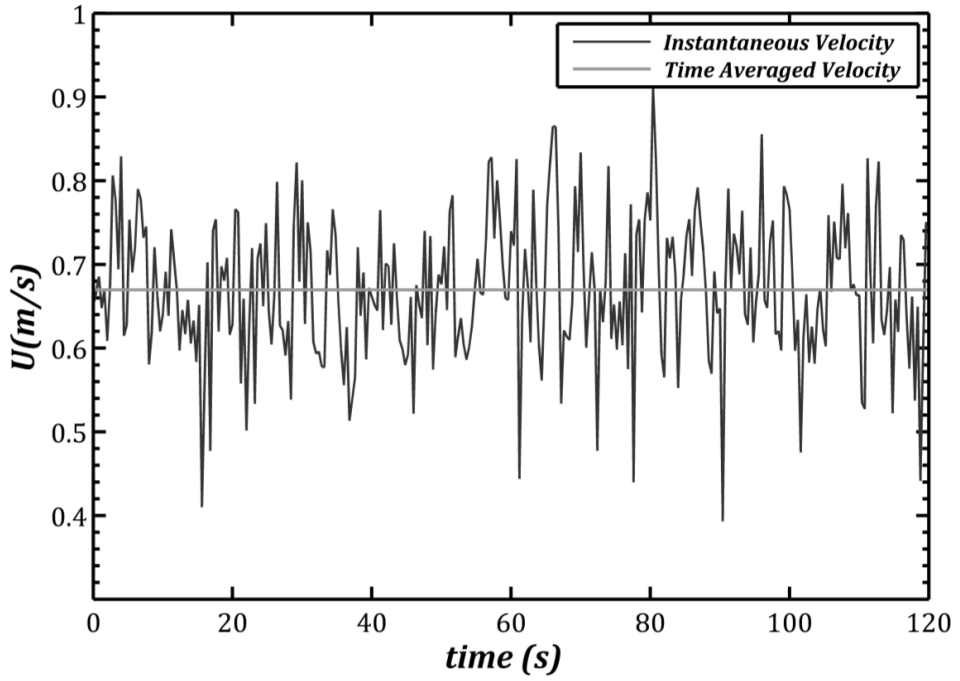


**Figure 6-37 Instantaneous Velocity Profile at ξ=0.9 for Flow of 0.2% Polymer Solution**

### 6.5.3 Wall region: Velocity Data

Velocity data has been obtained using PIV technique for two concentrations of polymer solutions and at three bulk velocities. These data close to the wall has been transformed into dimensionless form and are plotted in Figure 6-38 to Figure 6-43. Before discussing these plots the procedures for transforming u and y data into dimensionless form for non-Newtonian fluids must be given as this is different from Newtonian case.

$$y^+ = \frac{y\rho u^*}{\mu_w} \qquad \text{Eq. ( 6-34)}$$

$$u^+ = \frac{u}{u^*} \qquad \text{Eq. ( 6-35)}$$

Although $u^+$ and $u^*$ definitions are the same as before, but for dimensionless distance viscosity has been replaced with viscosity at the wall. In previous section it has been explained from pressure drop data one can obtain wall shear stress (Note that radius of zero shear stress has been found and reported in following sections).

$$\tau_i = -\left(\frac{dp}{dl}\right)\left(\frac{{R_0}^2 - {R_1}^2}{2R_1}\right) \qquad \text{Eq. ( 6-36)}$$

$$\tau_o = -\left(\frac{dp}{dl}\right)\left(\frac{{R_2}^2 - {R_0}^2}{2R_2}\right) \qquad \text{Eq. ( 6-37)}$$

Once wall shear stresses are obtained, the rheology model is used to calculate the shear rate at the wall and ultimately viscosity at the wall is obtained.

Calculating the viscosity at the wall could also be done by using the velocity data; shear rate is the derivate of velocity with respect to distance (This is true because at the wall Reynolds stresses are zero). Shear rate profile which is called strain rate in DAVIS software could be calculated; value of this at the wall represents shear rate at the wall. Once the viscosity at the wall is calculated, y data could be transformed into its dimensionless form using Eq. Eq. ( 6-34).

For $y^+ < 10$ the velocity data have been found to follow the universal law of the wall. The agreement between the experimental data and theoretical prediction is

acceptable and that does apply for all the cases studied including inner wall and outer wall of the annuli and both concentrations of the polymer.

$$u^+ = y^+ \qquad \text{Eq. ( 6-38)}$$

Further away from the viscous sublayer the velocity data are showing a shift comparing to logarithmic law consistent with Newtonian fluids (Eq. ( 6-36)) which has been validated in previous section with water. The deviation of velocity data in this region of the flow is a clear indication of drag reduction which was observed in the behaviour of the friction factor as well.

$$u^+ = 2.5\, ln(y^+) + 5.5 \qquad \text{Eq. ( 6-39)}$$

The velocity data in the logarithmic zone has been compared with Virk's ultimate asymptote[24] and a satisfactory agreement was achieved for all the experiments. The velocity data tend toward this correlation and fall somewhere between this curve and Newtonian fluids flow correlation.

$$u^+ = 11.7\, ln(y^+) - 17 \qquad \text{Eq. ( 6-40)}$$

Another conclusion based on the evidence given in velocity profiles is that velocity data for the inner wall are showing slightly higher values than outer wall of the annuli. That is expected because it's already known that shear stress profiles are not symmetric in annuli and hence wall shear stress is not the same on both walls of the annuli. Higher wall shear stress on the inner wall causes a higher shear rate and lower viscosity which in turn cause this difference in the velocity profiles.

Summary: velocity data in law of the wall coordinates was found to be in good agreement with universal law of the wall for $y^+ < 10$ with an upward shift in data comparing to logarithmic law consistent with Newtonian fluids further away from the wall. Virk's asymptote of maximum velocity was found to be able to predict the velocity data in annuli despite the fact that it has been derived for pipe flow.

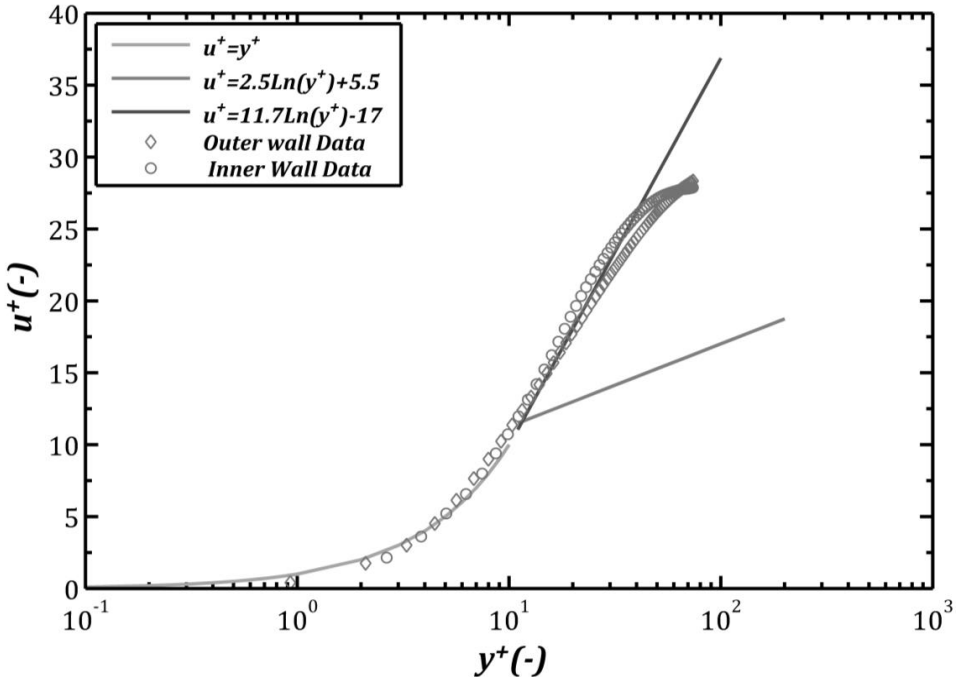


**Figure 6-38 Near Wall Velocity Profile in Wall Coordinate for Flow of 0.175% Polymer Aqueous at an Effective $N_{Re} = 6950$**

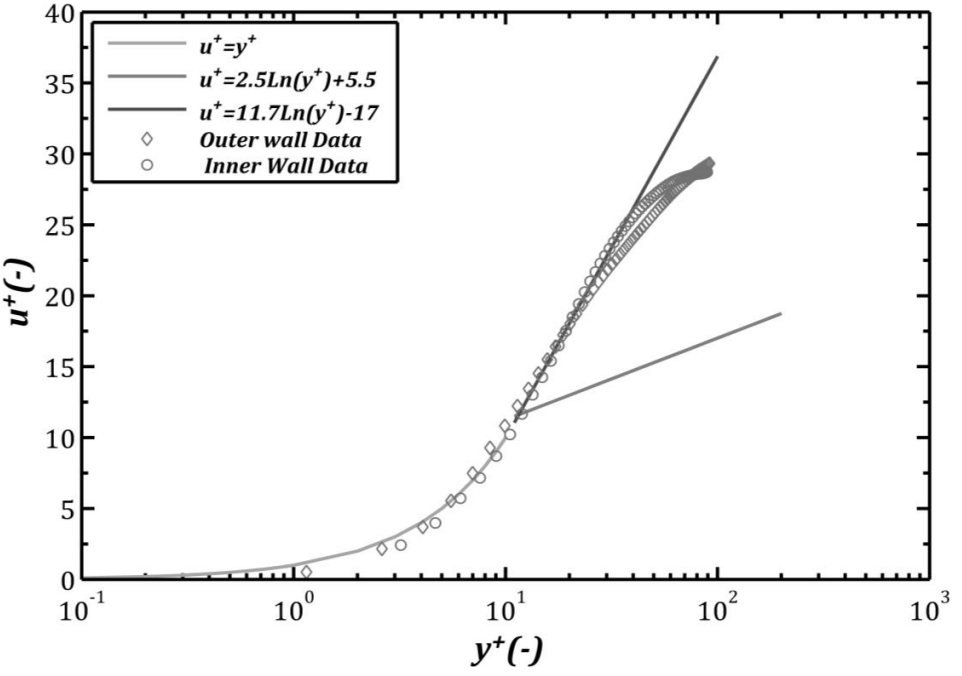


**Figure 6-39 Near Wall Velocity Profile in Wall Coordinate for Flow of 0.175% Polymer Aqueous at an Effective $N_{Re} = 9100$**

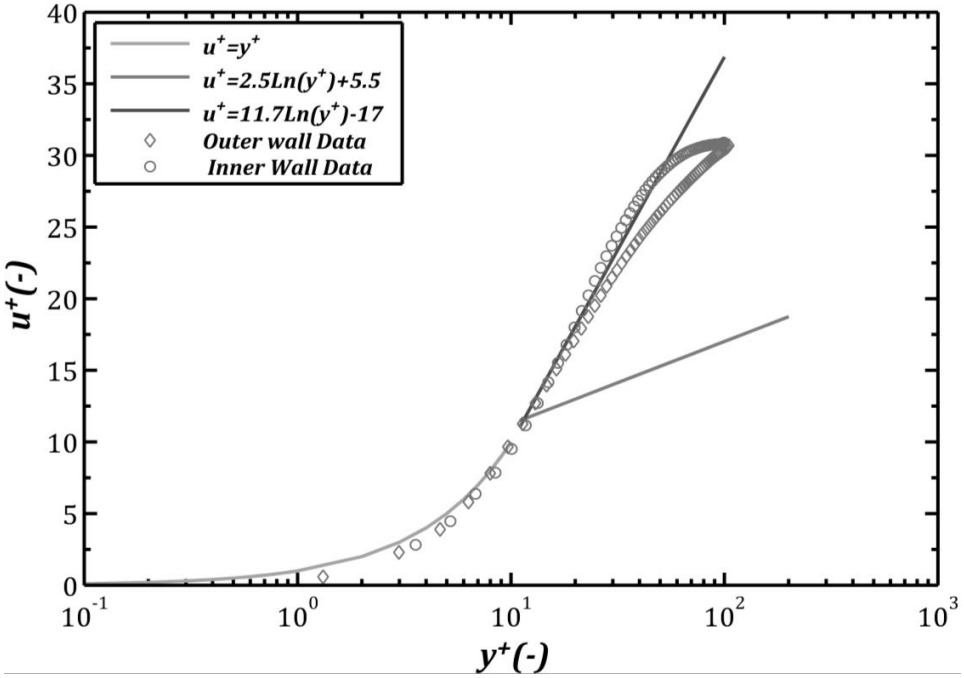


**Figure 6-40 Near Wall Velocity Profile in Wall Coordinate for Flow of 0.175% Polymer Aqueous at an Effective $N_{Re} = 10950$**

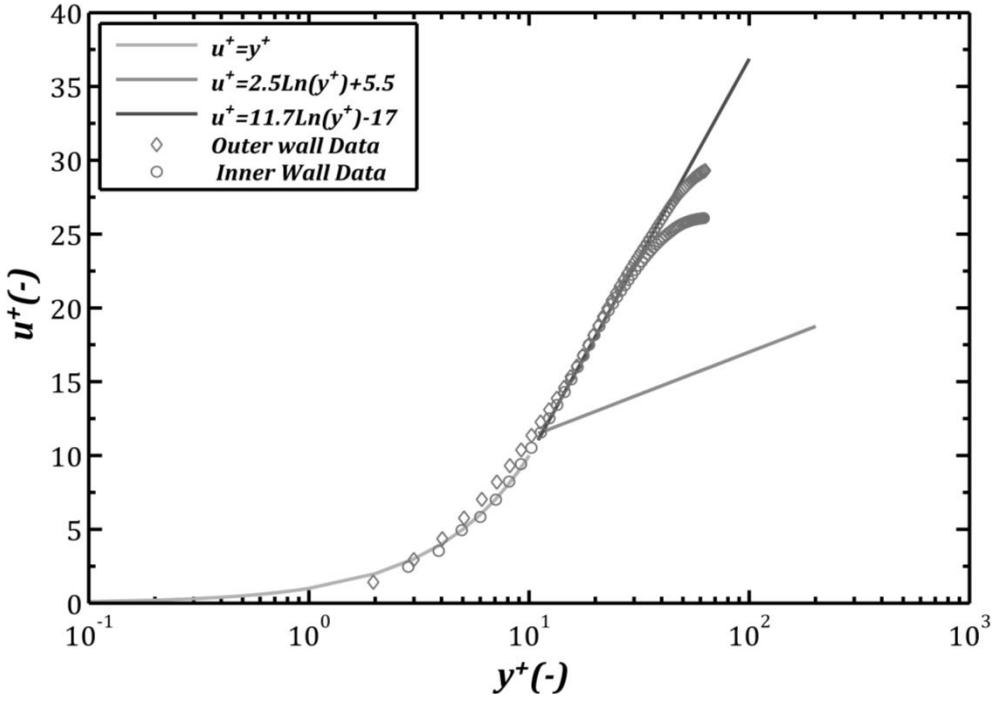


**Figure 6-41 Near Wall Velocity Profile in Wall Coordinate for Flow of 0.2% Polymer Aqueous at an Effective $N_{Re} = 5960$**

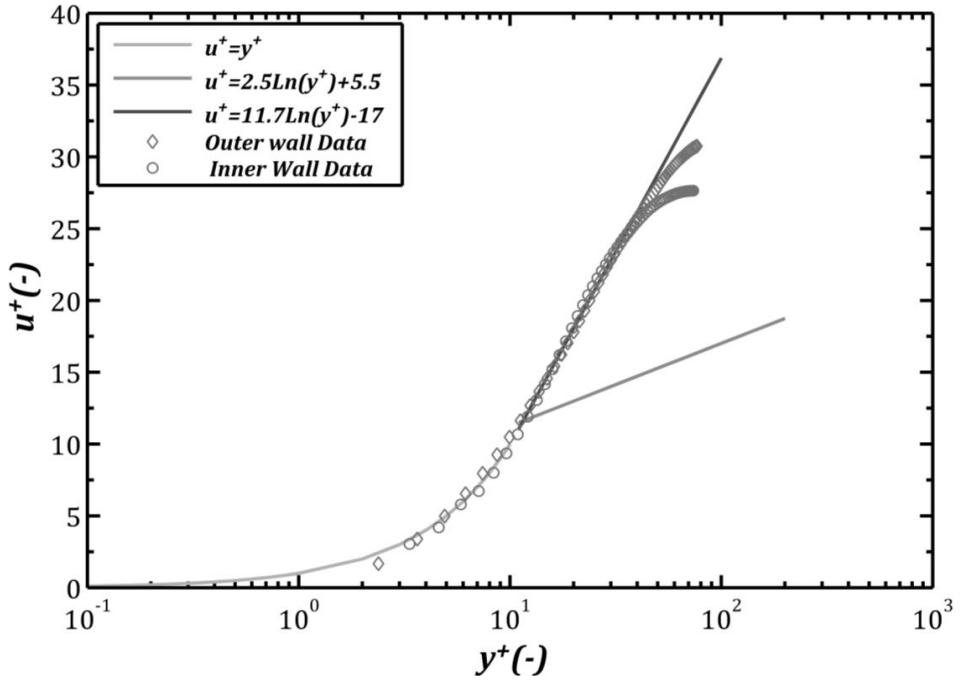


**Figure 6-42 Near Wall Velocity Profile in Wall Coordinate for Flow of 0.2% Polymer Aqueous at an Effective $N_{Re} = 7780$**

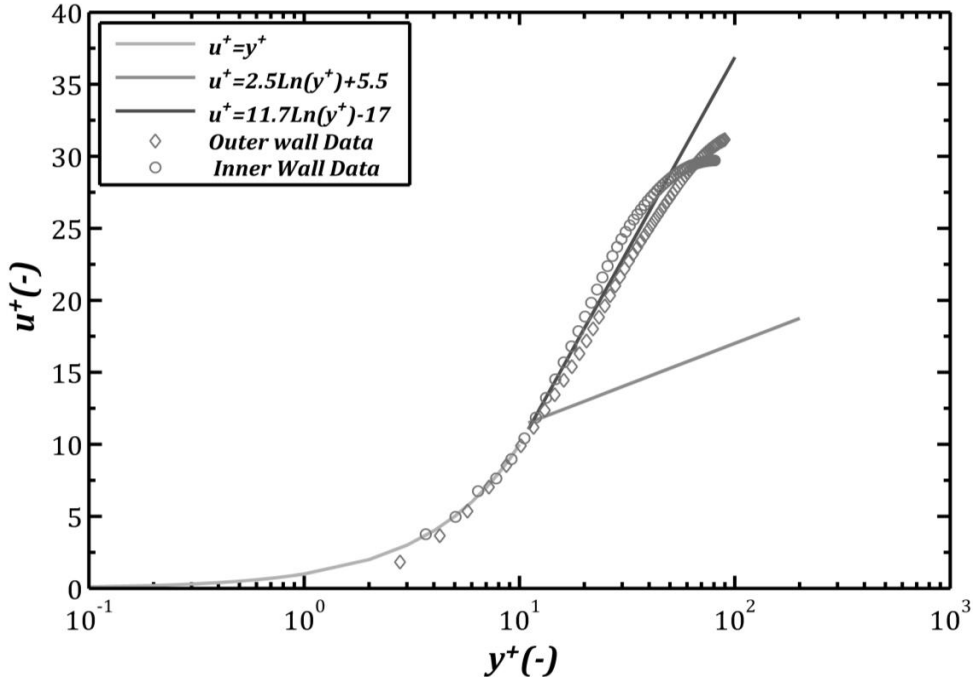


**Figure 6-43 Near Wall Velocity Profile in Wall Coordinate for Flow of 0.2% Polymer Aqueous at an Effective $N_{Re} = 9460$**

### 6.5.4 Velocity Profiles in Whole Annular Gap and Radius of Maximum Velocity

Analogues to Newtonian fluid case, velocity data in whole annular gap from outer wall to inner wall of the annuli have been measured. These data has been further analysed to obtain radius of maximum velocity in annuli. Figure 6-44 to Figure 6-46 are the measured velocity data with PIV for two concentrations of the polymer.

The velocity profiles are very similar for the two fluids because velocity data has been normalized with maximum velocity. It's obvious from velocity profiles that maximum velocity is closer to the inner wall of the annuli.

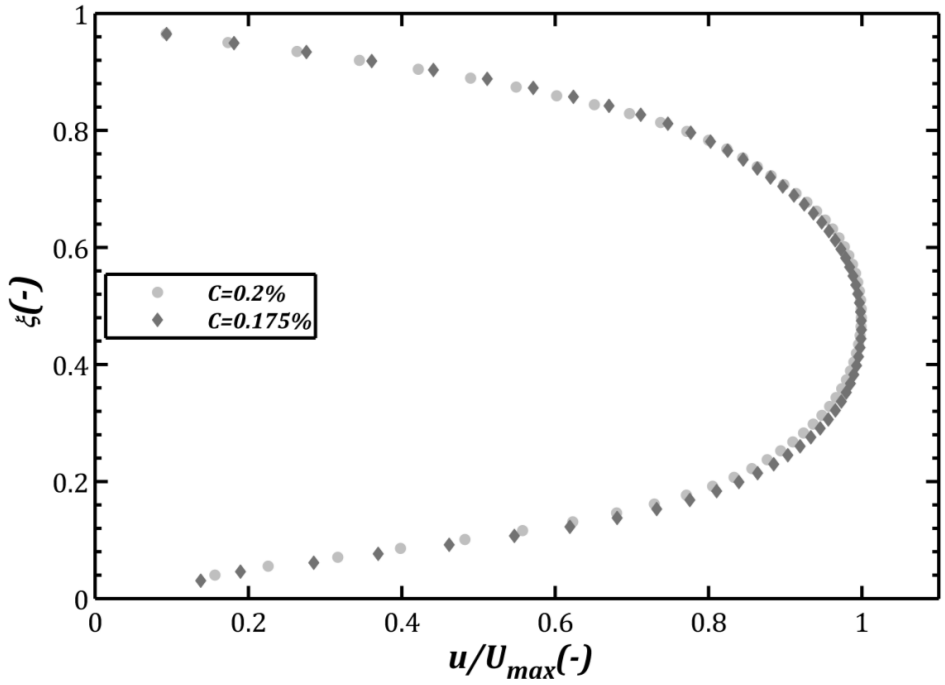


**Figure 6-44 Velocity Data in Whole Annular Gap for Flow of Two Polymer Solutions at $U_B = 0.827\ m/s$**

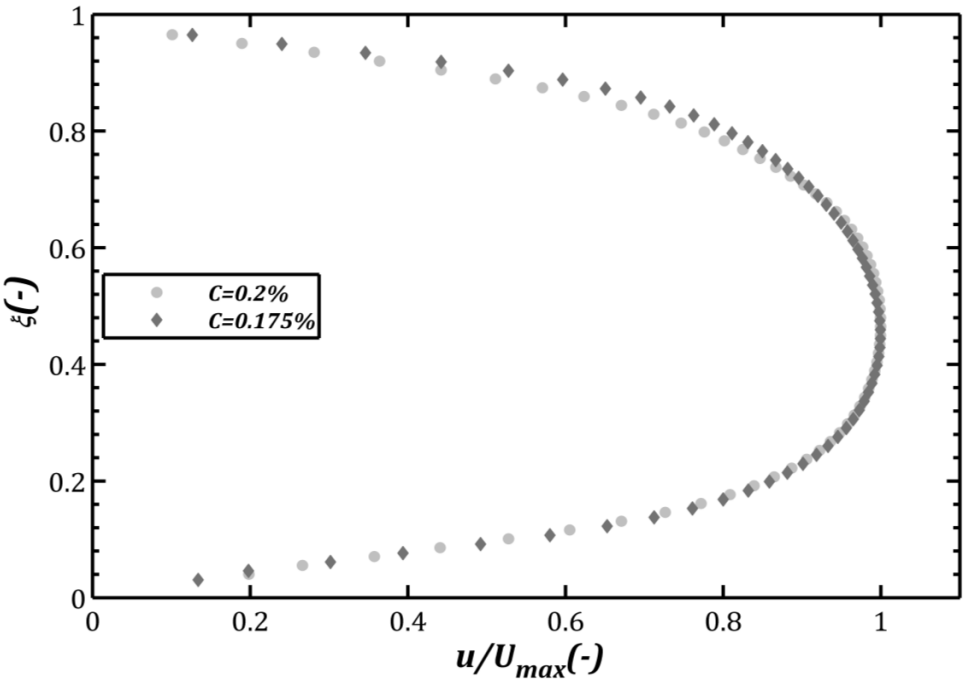


**Figure 6-45 Velocity Data in Whole Annular Gap for Flow of Two Polymer Solutions at $U_B = 0.999\ m/s$**

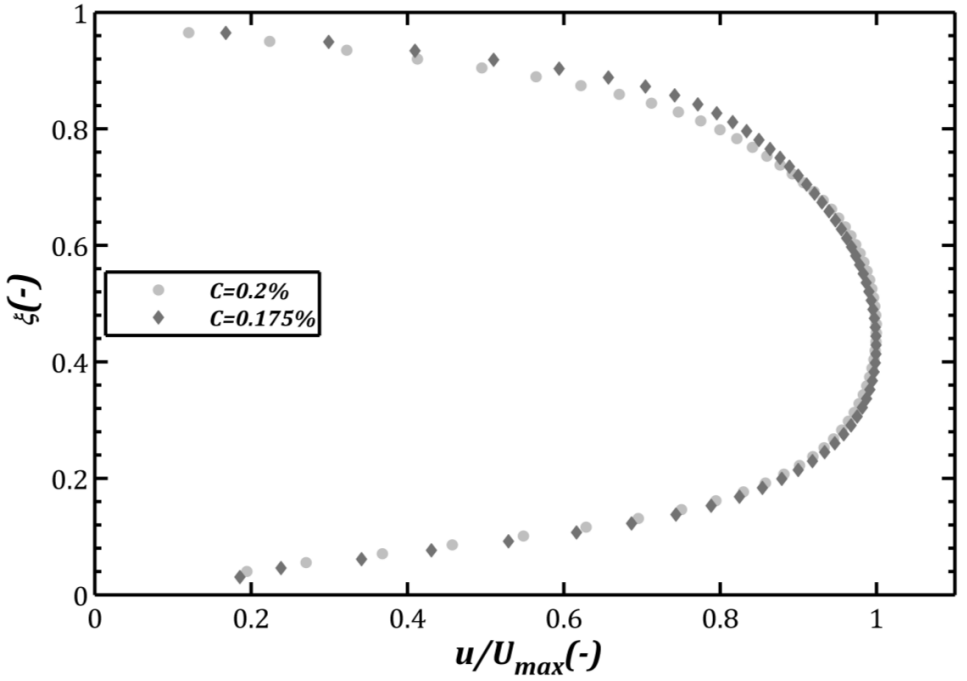


**Figure 6-46 Velocity Data in Whole Annular Gap for Flow of Two Polymer Solutions at $U_B = 1.164\ m/s$**

Radius of maximum velocity has been calculated using MATLAB; these radiuses are summarized in Table 6-8 to Table 6-10

**Table 6-8 Radius of Maximum Velocity for Flow of 0.175% and 0.2% Flowing at $U_B = 0.827\ m/s$**

$U_B$=0.827

| | C=0.175% | C=0.2% |
|---|---|---|
| $R_{max}$(mm) | 31.69 | 32.03 |
| $\xi_{max}$(-) | 0.4453 | 0.4573 |

**Table 6-9 Radius of Maximum Velocity for Flow of 0.175% and 0.2% Flowing at $U_B = 0.999\ m/s$**

$U_B$=0.999

| | C=0.175% | C=0.2% |
|---|---|---|
| $R_{max}$(mm) | 31.25 | 31.6 |
| $\xi_{max}$(-) | 0.43 | 0.4421 |

**Table 6-10 Radius of Maximum Velocity for Flow of 0.175% and 0.2% Flowing at $U_B = 1.164\ m/s$**

$U_B$=1.164

| | C=0.175% | C=0.2% |
|---|---|---|
| $R_{max}$(mm) | 30.81 | 30.73 |
| $\xi_{max}$(-) | 0.4147 | 0.4118 |

Radius of maximum velocity has been found to be a function of Reynolds number for the range of Reynolds numbers studied. The dependency is in such a way that by increasing Reynolds number this radius moves toward the inner wall of the annuli and get a smaller value and that trend is consistent for all the cases. Figure 6-47 is a graphical representation of the dependency of radius of maximum velocity on Reynolds number, also Figure 6-48 is the same plot but in dimensionless format.

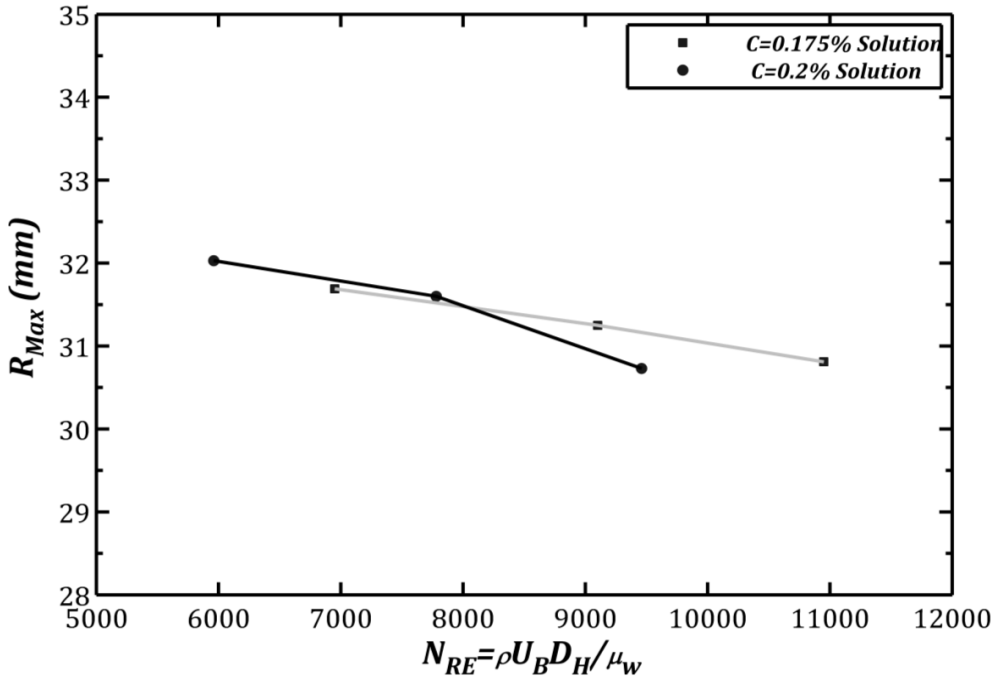


**Figure 6-47 Radius of Maximum Velocity versus Reynolds Number for Flow of Two Polymer Solution**

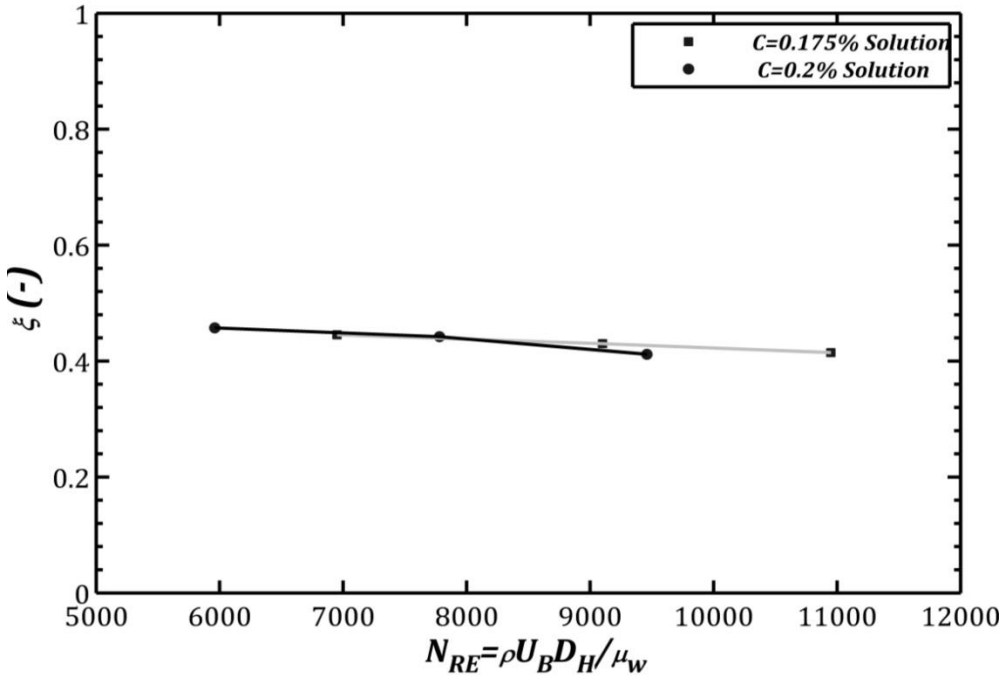


**Figure 6-48 Dimensionless Radial Location of Maximum Velocity versus Reynolds Number for Flow of Two Polymer Solution**

Summary: velocity profiles in whole annular gap has been measured and reported. Radius of maximum velocity was obtained and reported and it has been found that this radius is a function of Reynolds number. As Reynolds number increases radius of maximum velocity moves toward the inner wall.

### 6.5.5 Shear Stresses

#### 6.5.5.1 Viscous Stresses

Viscous stress arises from the action of viscosity and is defined as Eq. ( 6-41).

$$\tau_v = \mu_a \frac{\partial u}{\partial y} \qquad \text{Eq. ( 6-41)}$$

In Eq. ( 6-41) the viscosity is apparent viscosity of the non-Newtonian fluids and is a function of the velocity gradient itself.

$$\mu_a = k\left(\frac{\partial u}{\partial y}\right)^{n-1} \qquad \text{Eq. ( 6-42)}$$

Combining these two equations results in an equation describing viscous stress term for flow of a non-Newtonian power law fluid,

$$\tau_v = k(\frac{\partial u}{\partial y})^{n-1}\left(\frac{\partial u}{\partial y}\right) = k(\frac{\partial u}{\partial y})^{n} \qquad \text{Eq. ( 6-43)}$$

Note that Eq. ( 6-43) reduces to Eq. ( 6-41) if n=1 which is the case of Newtonian fluid.

Viscous stresses has been calculated by using the velocity profiles in the whole annular gap presented in previous sections and rheology models which has been discussed in chapter 4; just to remind these models are presented in Eq. ( 6-44) and Eq. ( 6-45).

$$C = 0.175\%\,; \quad \tau = 0.0315\gamma^{0.7527} \qquad \text{Eq. ( 6-44)}$$

$$C = 0.2\%\,; \quad \tau = 0.047\gamma^{0.7003} \qquad \text{Eq. ( 6-45)}$$

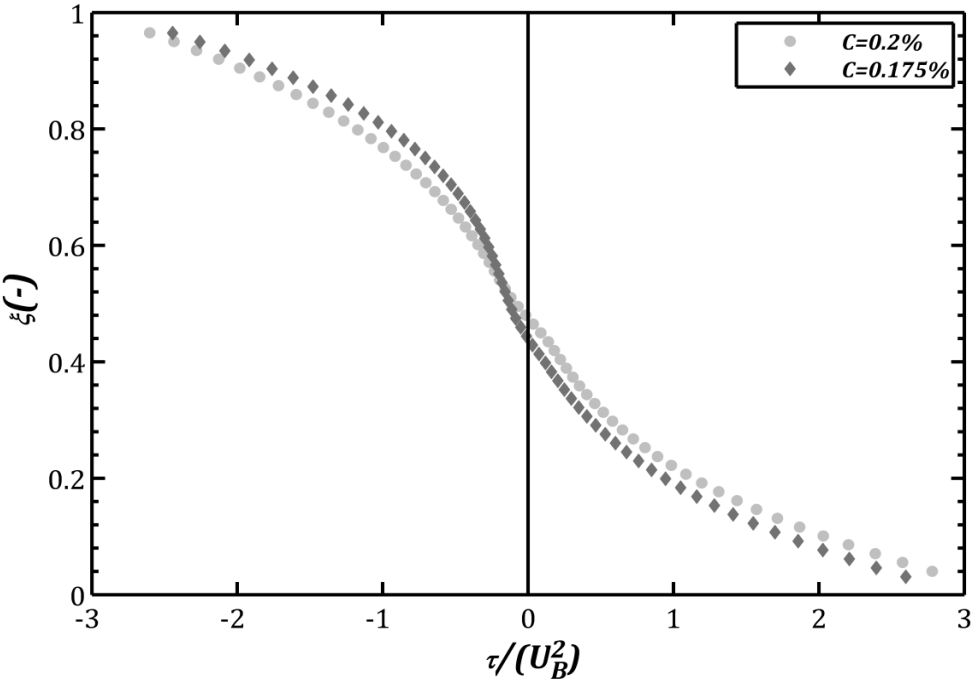


**Figure 6-49 Viscous Stress Profiles for Flow of 0.175% and 0.2% Polymer Solutions at $U_B = 0.827\ m/s$**

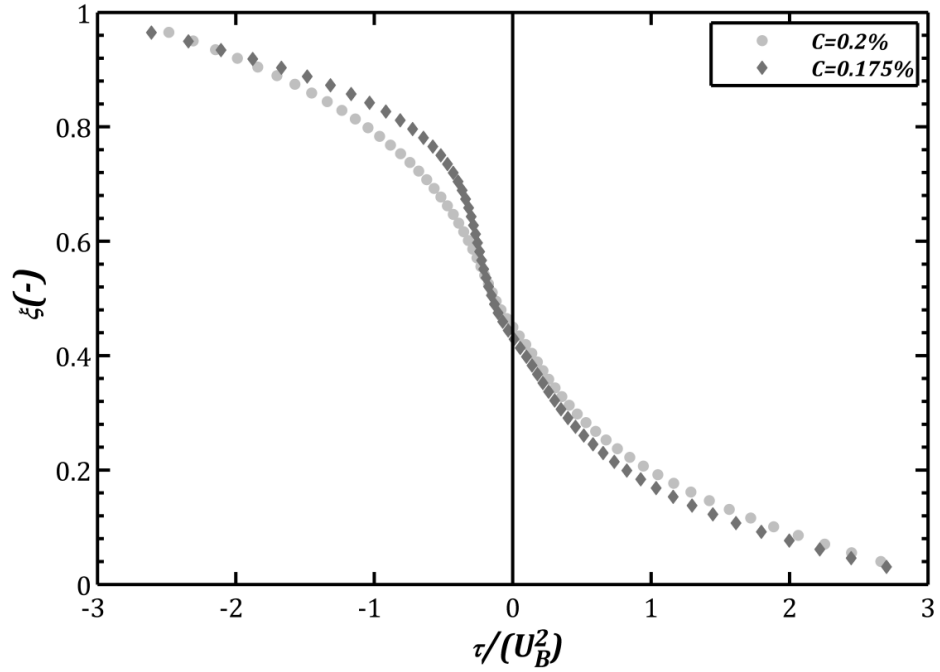


**Figure 6-50 Viscous Stress Profiles for Flow of 0.175% and 0.2% Polymer Solutions at $U_B = 0.999$**

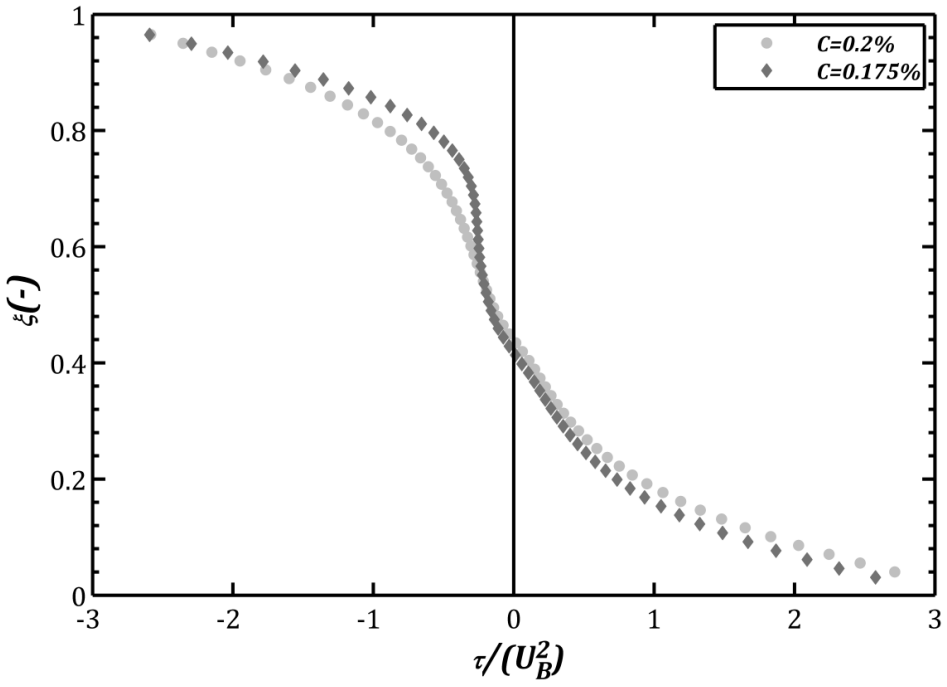


**Figure 6-51 Viscous Stress Profiles for Flow of 0.175% and 0.2% Polymer Solutions at $U_B = 1.164$**

Viscous stresses for both polymer concentrations studied show their highest value close to the walls ($\xi = 0 \; or \; 1$). That is expected from fluid mechanics as the boundary conditions needs to be satisfied (velocity is forced to go to zero at solid surfaces). Big velocity gradient close to the walls is arises due to no slip boundary which causes the high viscous stress.

It is known from fluid mechanics that Reynolds stresses are negligible in the viscous sublayer (although this layer is turbulent but yet comparing to viscous stresses, Reynolds stresses are zero) and also it is known that highest shear stress in the flow exist at the walls (wall shear stress). This means that viscous stress at the walls must show a value equal to wall shear stress required by pressure drop data. Looking at the viscous stress profiles one can conclude that at the walls the highest shear stresses are those which has been obtained from pressure drop data. This would validate the accuracy of the measurements.

Summary: viscous stress profiles for flow of polymer solutions has been found and reported. These profiles showed that viscous stresses are high close to solid surfaces and

go down as one move away from the walls. Viscous stresses at the walls equals the wall shear stresses caused by pressure drops which means Reynolds stresses are zero at the wall and also confirms the accuracy of the measurements.

#### 6.5.5.2 Reynolds Stresses

Reynolds stresses are caused by fluctuations in the velocity and are defined as the time average of the product of fluctuation velocities.

$$\tau_{Re} = -\rho\overline{u'v'} \qquad \text{Eq. ( 6-46)}$$

Figure 6-52 to Figure 6-54 are Reynolds stress data which has been measured for flow of two polymeric liquids in the annuli. Note that stress data has been normalized with the square of bulk velocity.

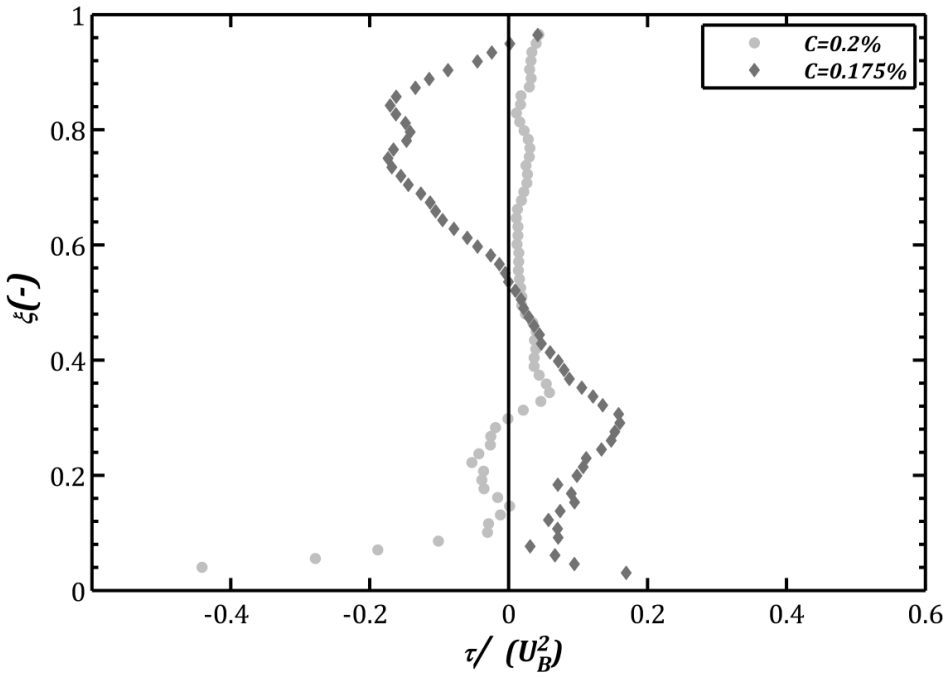


**Figure 6-52 Reynolds Stress Profiles for Flow of 0.175% and 0.2% Polymer Solutions at $U_B = 0.827\ m/s$**

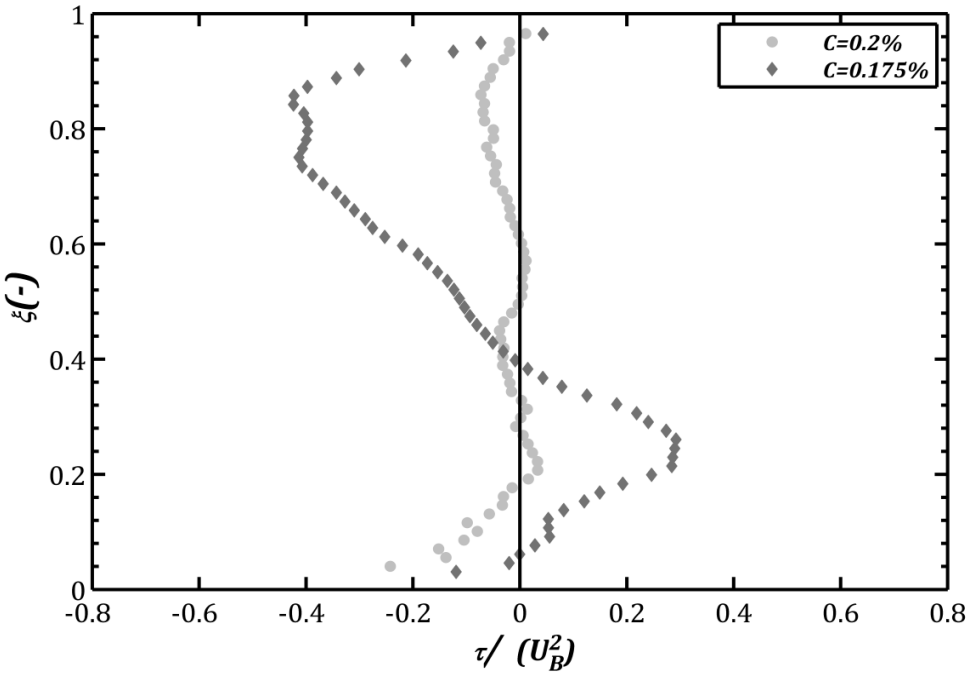


**Figure 6-53 Reynolds Stress Profiles for Flow of 0.175% and 0.2% Polymer Solutions at $U_B = 0.999\ m/s$**

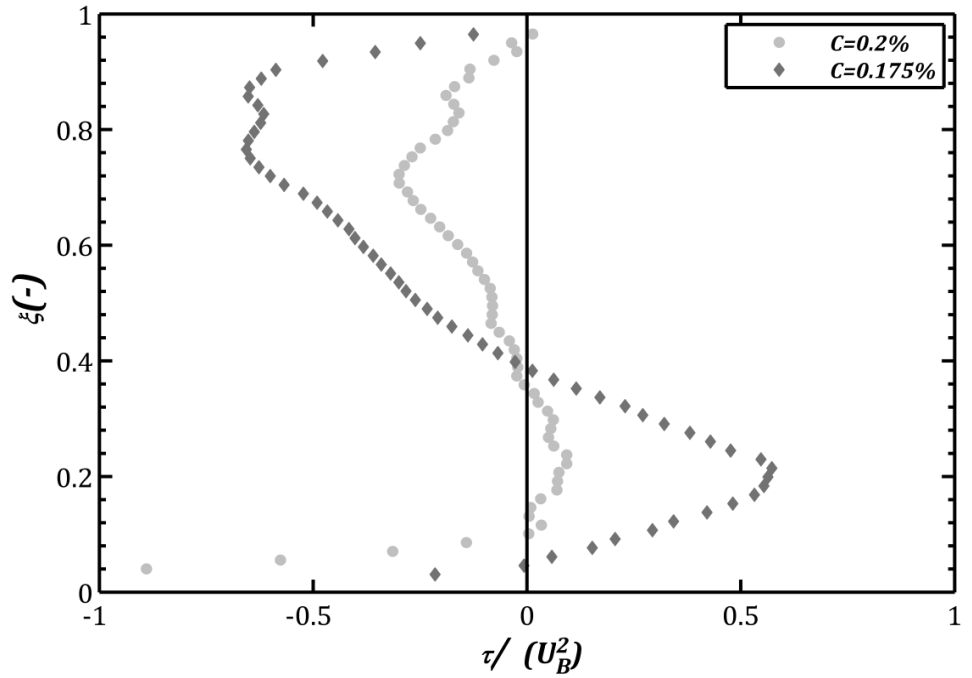


**Figure 6-54 Reynolds Stress Profiles for Flow of 0.175% and 0.2% Polymer Solutions at $U_B = 1.164\ m/s$**

From Reynolds stresses data, the Reynolds stress for flow of 0.175% solution is always higher than 0.2% solution. In fact Reynolds stress for the higher concentration is so close to zero. That is the effect of Reynolds number or the level of turbulence in the flow. Recall the definition of Reynolds number which is the ratio of inertial forces to viscous forces; according to this definition the higher the Reynolds number the higher would be the inertial forces which ultimately mean higher level of turbulence. Reynolds stress is the contribution of turbulence to the shear stress tensor, i.e. if the flow is laminar this component would be zero and as Reynolds number gradually increases the magnitude of Reynolds stresses would increase as well.

Another conclusion based on Reynolds stress profiles is that this component of total stress is tending toward zero as walls are approached; this has been explained in the viscous stresses distribution to be expected to happen. In fact total stress at the wall should show a value required by pressure drops, when viscous stress is equal to wall shear stress that mean Reynolds stresses must be negligible in this zone.

Moving away from the walls, Reynolds stress increases rapidly and reaches a maximum. This maximum is not in the center of the annuli but rather it is close to the walls; it is believed that Reynolds stress takes its maximum in the buffer layer which is next to viscous sublayer.

Summary: Reynolds stress profiles have been obtained and reported. Reynolds stresses are showing zero value close to solid walls and increase as moving away from the walls. This component of the total stress is always higher for the lower concentration of the polymer fluid tested which indicates the effect of higher Reynolds number or the lower viscosity of this fluid comparing to the highest concentration tested.

#### 6.5.5.3 Total Stress

According to Navier-Stockes equation solved in chapter 2, total stress of a turbulent flow is the summation of viscous stress and Reynolds stress.

$$\tau = \tau_v + \tau_{Re} \qquad \text{Eq. ( 6-47)}$$

Figure 6-55 to Figure 6-57 are the total stresses distribution for flow of polymer aqueous in the annuli.

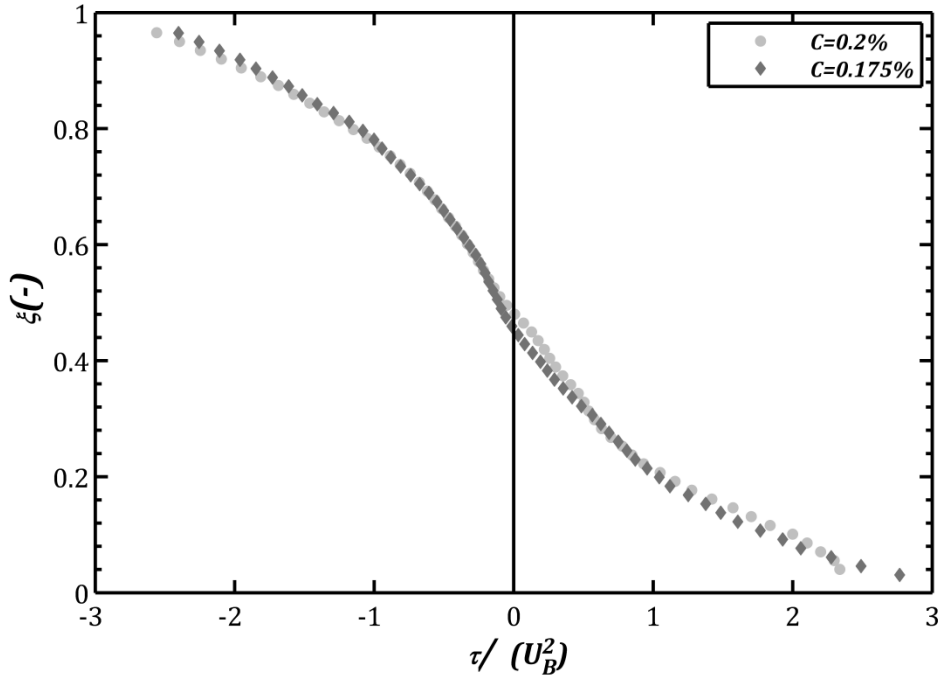


**Figure 6-55 Total Stress Profiles for Flow of 0.175% and 0.2% Polymer Solutions at $U_B = 0.827\ m/s$**

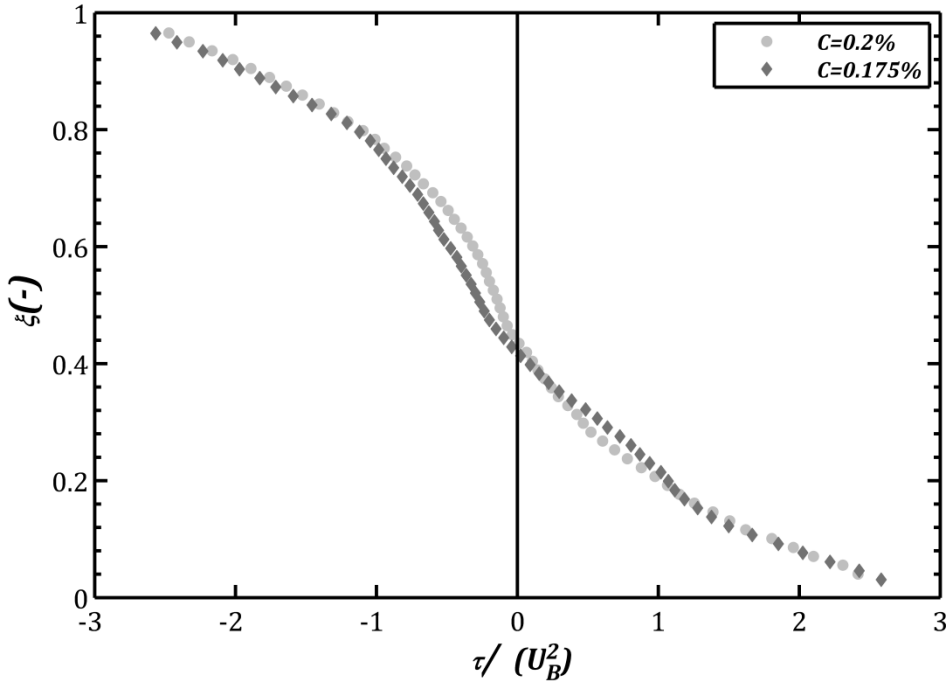


**Figure 6-56 Total Stress Profiles for Flow of 0.175% and 0.2% Polymer Solutions at $U_B = 0.999\ m/s$**

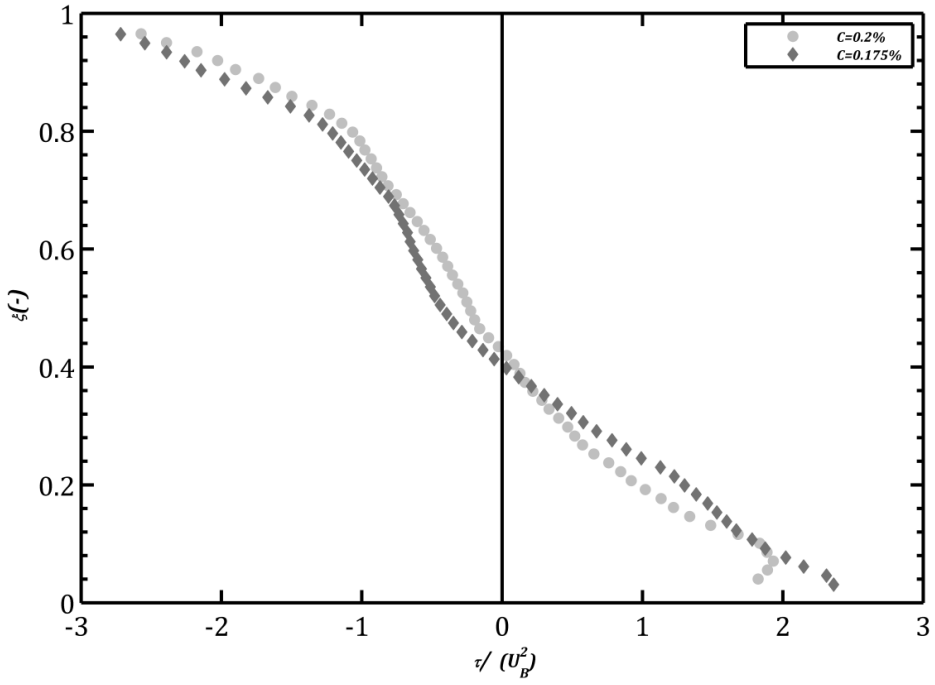


**Figure 6-57 Total Stress Profiles for Flow of 0.175% and 0.2% Polymer Solutions at $U_B = 1.164\ m/s$**

Total stresses in the annuli are having the same behaviour as the viscous stresses which mean that at the operational Reynolds numbers in this study the flow is in the lower turbulent regime where the viscosity is more effective. Another reason for that lays in the well-known Tom's phenomenon which is drag reduction property of polymeric liquids which have been extensively studied in the past. In fact drag reducing agents reduces the shear stress by reducing the Reynolds stresses and that is why viscous stresses seems dominating the total stresses.

Total stresses have the same value of shear stress at the walls required by pressure drop data. Radiuses of zero shear stress have been obtained by using total stress distributions and are discussed in upcoming section.

### 6.5.6 Radius of Zero Shear Stress

Radius of zero shear stress has been obtained from total stress distribution; these radiuses are reported in Table 6-11 to Table 6-13 in both dimensional and non-dimensional radial location in the annuli.

**Table 6-11 Radius of Zero Shear Stress in the Annuli for Flow of 0.175% and 0.2% Aqueous Solution of Polymer Flowing at $U_B = 0.827\ m/s$**

| | $U_B$=0.827 | |
|---|---|---|
| | C=0.175% | C=0.2% |
| $R_0$(mm) | 31.9675 | 32.7313 |
| $\xi_0$(-) | 0.455 | 0.4818 |

**Table 6-12 Radius of Zero Shear Stress in the Annuli for Flow of 0.175% and 0.2% Aqueous Solution of Polymer Flowing at $U_B = 0.999\ m/s$**

| | $U_B$=0.999 | |
|---|---|---|
| | C=0.175% | C=0.2% |
| $R_0$(mm) | 30.94435 | 31.483 |
| $\xi_0$(-) | 0.4191 | 0.438 |

**Table 6-13 Radius of Zero Shear Stress in the Annuli for Flow of 0.175% and 0.2% Aqueous Solution of Polymer Flowing at $U_B = 1.164\ m/s$**

| | $U_B$=1.164 | |
|---|---|---|
| | C=0.175% | C=0.2% |
| $R_0$(mm) | 30.4969 | 31.18375 |
| $\xi_0$(-) | 0.4034 | 0.4275 |

Radiuses of zero shear stress for three bulk velocities are showing a reducing trend with increasing the velocity; these radiuses are function of Reynolds number. In fact as Reynolds number increases, radius of zero shear stress moves toward the inner wall of the annuli; this behaviour was also observed for the radius of maximum velocity as well.

Another conclusion from radiuses of zero shear stress is that this radius for the lower concentration of the polymer aqueous (0.175%) is always lower than that of the higher concentration solution. Summary: radiuses of zero shear stress were found to be dependent upon Reynolds number for the range of Reynolds numbers studied. The dependency is in such a way that by increasing Reynolds number radius of zero shear stress moves toward the inner wall of the annuli. In addition it was found that this radius is always smaller for the fluid with lower polymer concentration.

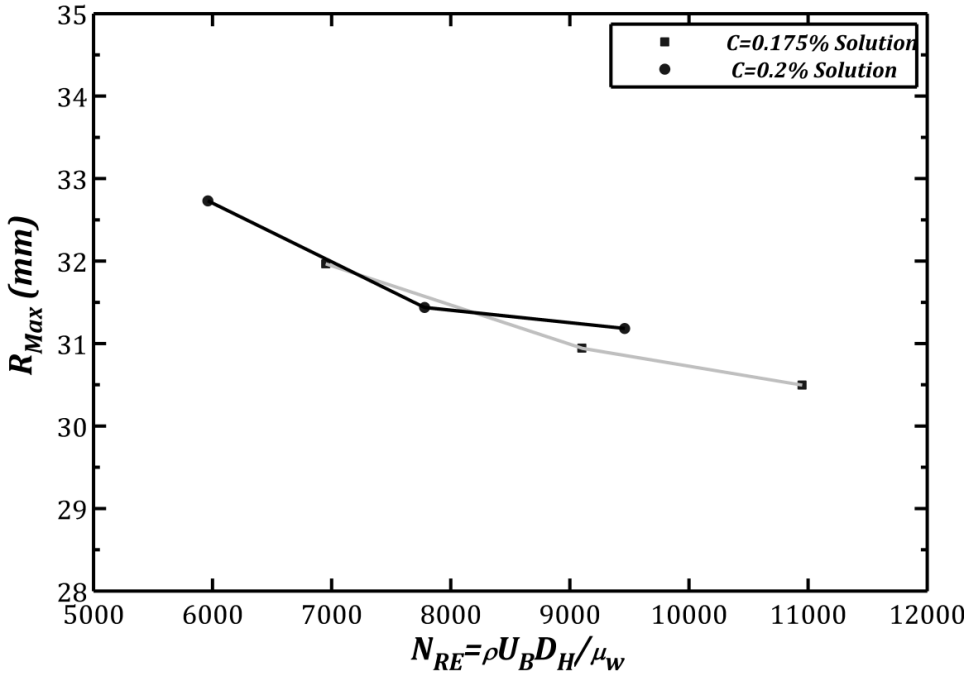


**Figure 6-58 Radius of Zero Shear Stress versus Reynolds Number for Flow of Two Polymer Solution**

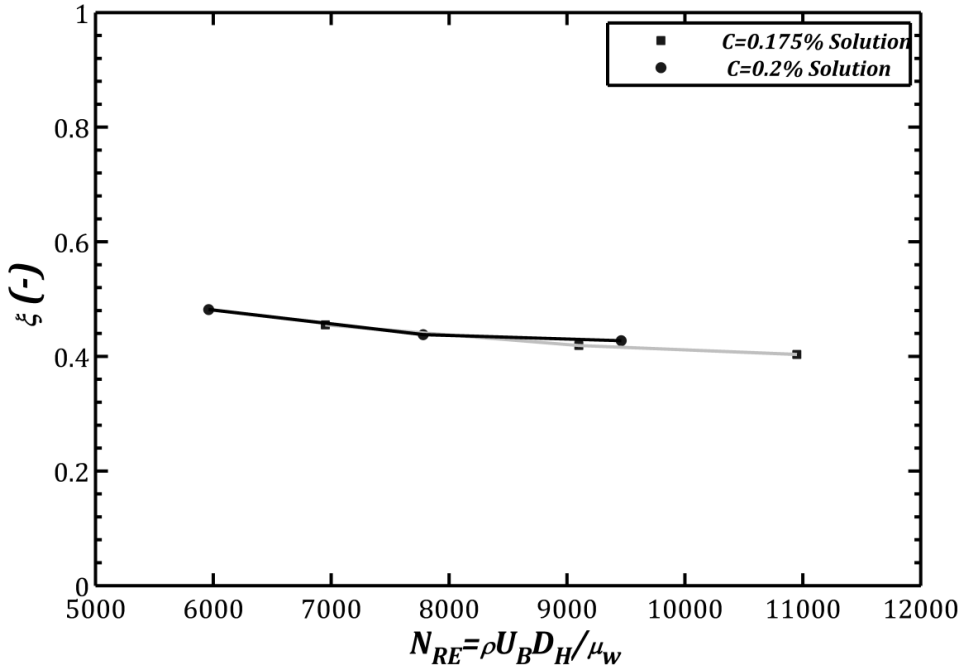


**Figure 6-59 Dimensionless Radial Location of Zero Shear Stress versus Reynolds Number for Flow of Two Polymer Solution**

### 6.5.7 Radius of Maximum Velocity versus Radius of Zero Shear Stress

While it has been discussed in the literature review and background chapter, the radius of maximum velocity and zero shear stress doesn't coincide. This has been confirmed for Newtonian fluids but for non-Newtonian fluids, however, the radius of zero shear stress has not been reported in literature and in most studies with non-Newtonian fluids coincidence of these two radiuses has been assumed.

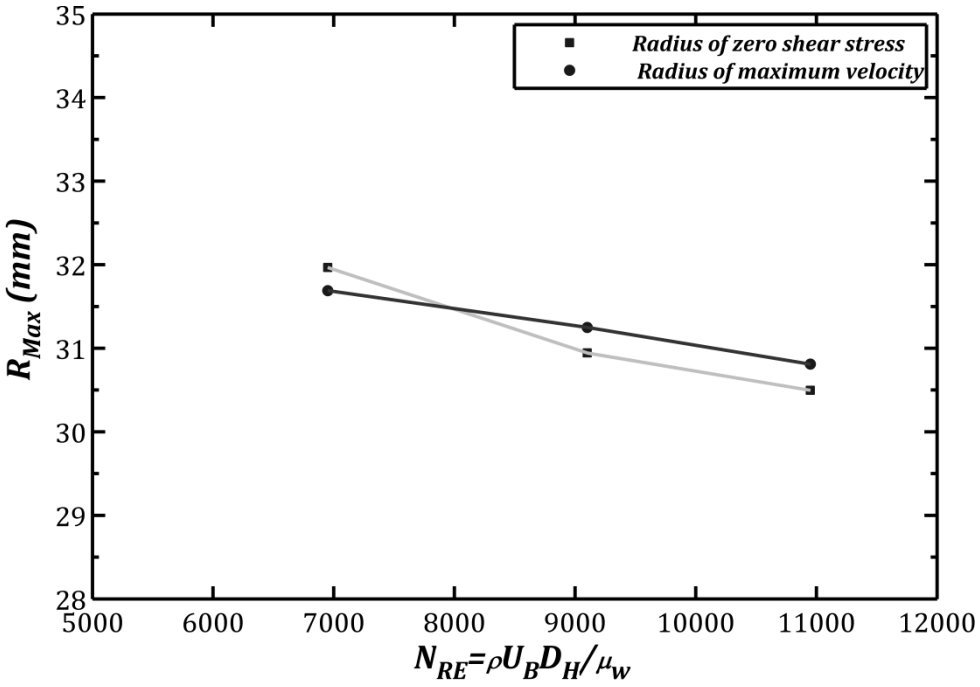


**Figure 6-60 Comparison of Radius of Maximum Velocity and Radius of Zero Shear Stress for Flow of 0.175% Polymer Fluid**

Radius of zero shear stress for the lower concentration of polymer aqueous has been found to be lower than radius of maximum velocity, a finding which has been confirmed for Newtonian fluids. From Figure 6-60 its seems that at the first Reynolds number studied the velocity maximum shows a smaller radii than that of zero shear a behaviour which seems anomalous and repeats for the higher concentration for two Reynolds number. This behaviour seems to be a function of the Reynolds number and cannot be explained so far.

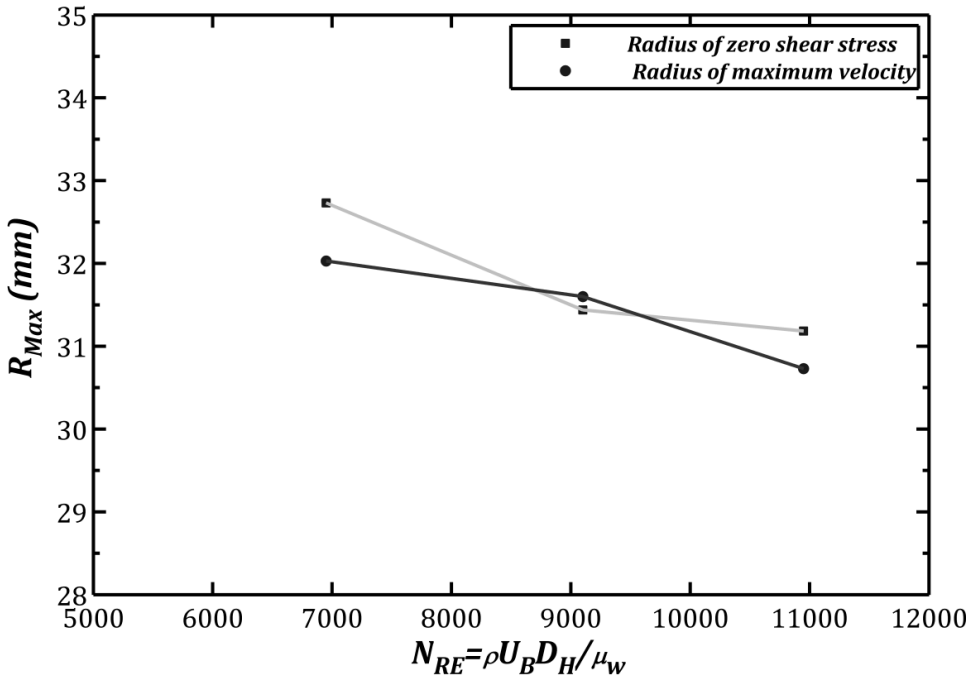


**Figure 6-61 Comparison of Radius of Maximum Velocity and Radius of Zero Shear Stress for Flow of 0.175% Polymer Fluid**

### 6.5.8 Turbulent Intensities

#### 6.5.8.1 Axial Intensities

Axial turbulent intensities in dimensionless form are presented in Figure 6-62 to Figure 6-63; each figure includes the intensity for flow of two polymer aqueous flowing at the same bulk velocity and for both walls of the annuli.

Generally the highest axial intensity could be observed for flow of the 0.175% polymer solution; TI for both walls (inner and outer) of the annuli is higher for the lower concentration polymer. This in fact could be explained by using the definition of the TI itself, more turbulent intensities occur at flows with bigger Reynolds number or higher level of turbulence. High viscosity for 0.2% causes suppression in the axial component of the RMS velocities because at the same flow rate it has much lower Reynolds number or lower turbulence.

From the figures more or less it is obvious that for all the cases TI takes its peak at a $y^+ = 20$; this has been confirmed earlier in experiments with Newtonian fluids as well.

In fact the explanation is that the buffer layer close to the wall is a region where most turbulent activities took place, including vortex actives. As discussed in chapter 2, vortical structures causes fluctuations in turbulent flows, so one would expect to get the highest level of fluctuations where the vortical activities are highest which does occur in the buffer layer.

When comparing the intensities for flow of one polymer solution at both walls, higher level of fluctuation is observed for the outer wall in all the cases. This phenomenon has been observed and reported by many authors. The gap between the intensities for the lower concentration of polymer tested is much bigger than that of higher concentration polymer. The behaviour may be caused by drag reduction property of the polymer solution.

Summary: axial intensities have shown higher values for flow of polymer solution with lower concentration and also it has been observed that turbulent intensities are always higher for outer wall of the annuli. Another finding was that TI has a peak which occurs close to the walls and falls into the buffer layer.

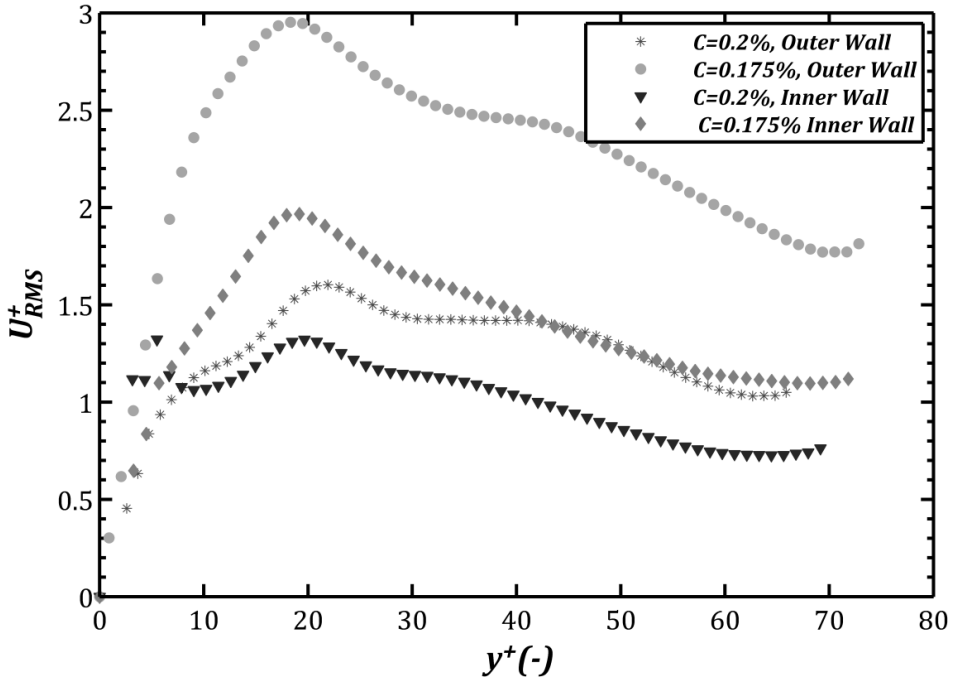


**Figure 6-62 Axial Turbulent Intensities in Wall Coordinate for Flow of 0.175% and 0.2% Polymer Solutions Flowing at $U_B = 0.827\ m/s$**

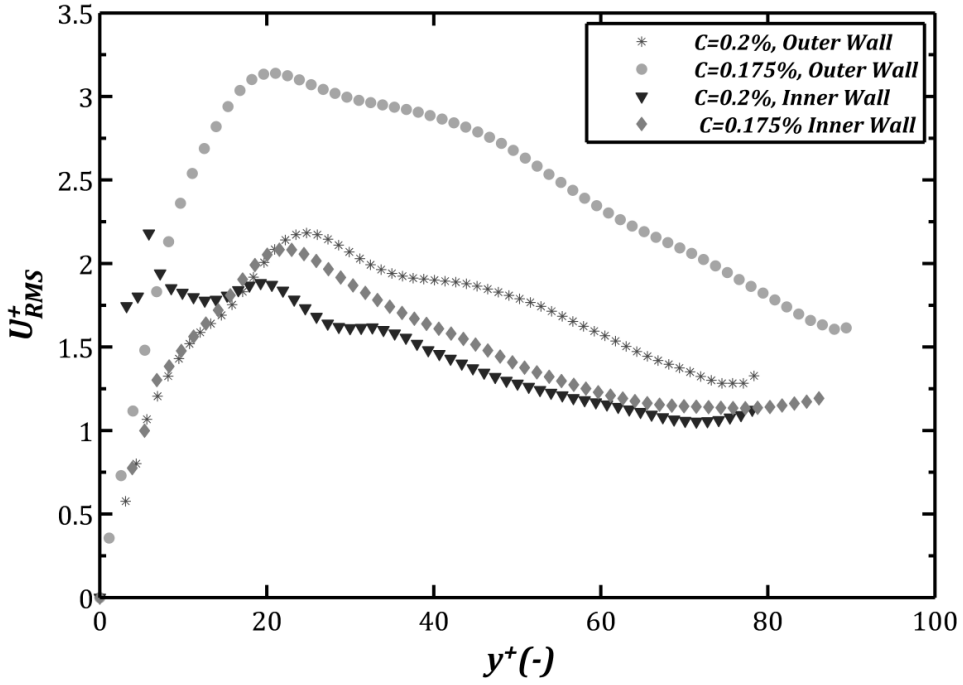


**Figure 6-63 Axial Turbulent Intensities in Wall Coordinate for Flow of 0.175% and 0.2% Polymer Solutions Flowing at $U_B = 0.999\ m/s$**

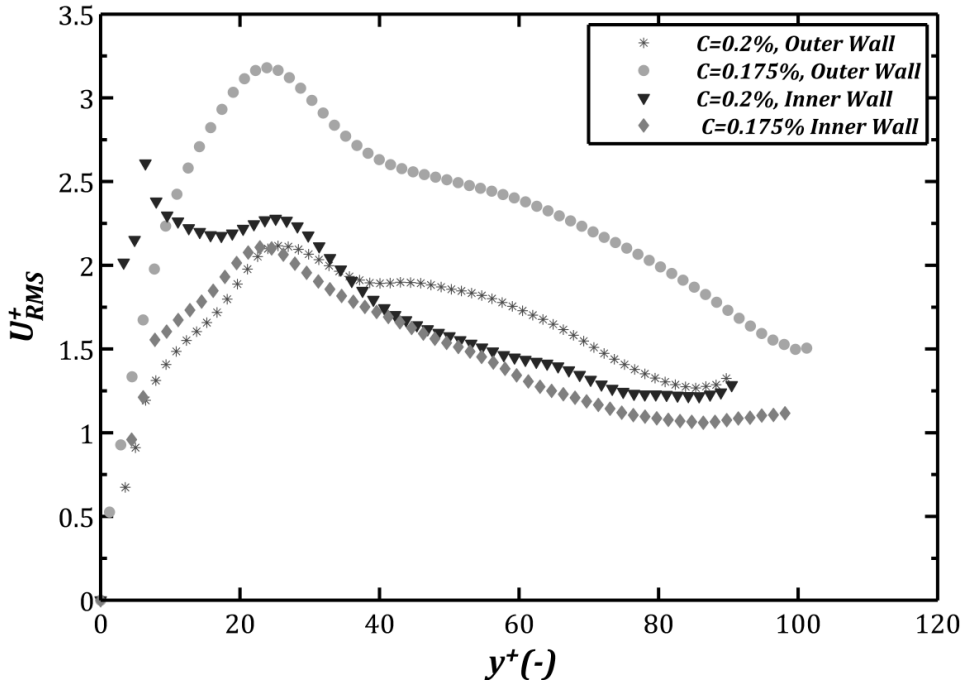


**Figure 6-64 Axial Turbulent Intensities in Wall Coordinate for Flow of 0.175% and 0.2% Polymer Solutions Flowing at $U_B = 1.164\ m/s$**

### 6.5.8.2 Radial Intensities

Similar to axial intensities, radial intensities have also been measured and reported in dimensionless form. The importance of radial intensities is in drag reduction phenomenon which is not of interest in this work.

The most striking feature of radial intensities is that they all are having the same order of magnitude (in dimensionless form) for all the fluids studied. The separation between inner wall and outer wall data, in contrast with axial intensities, are much less but yet one can conclude that outer wall intensities are higher than those of inner wall in general. The radial intensity profiles are showing almost a flat region away from the wall which indicates the level of turbulence in transverse direction of the flow is not changing that much in the core flow.

Regions very close to the wall $y^+ < 10$ is showing an anomalous behaviour which have not been reported in previous works. The intensities are showing almost a peak in this region of the flow and decrease rapidly afterward.

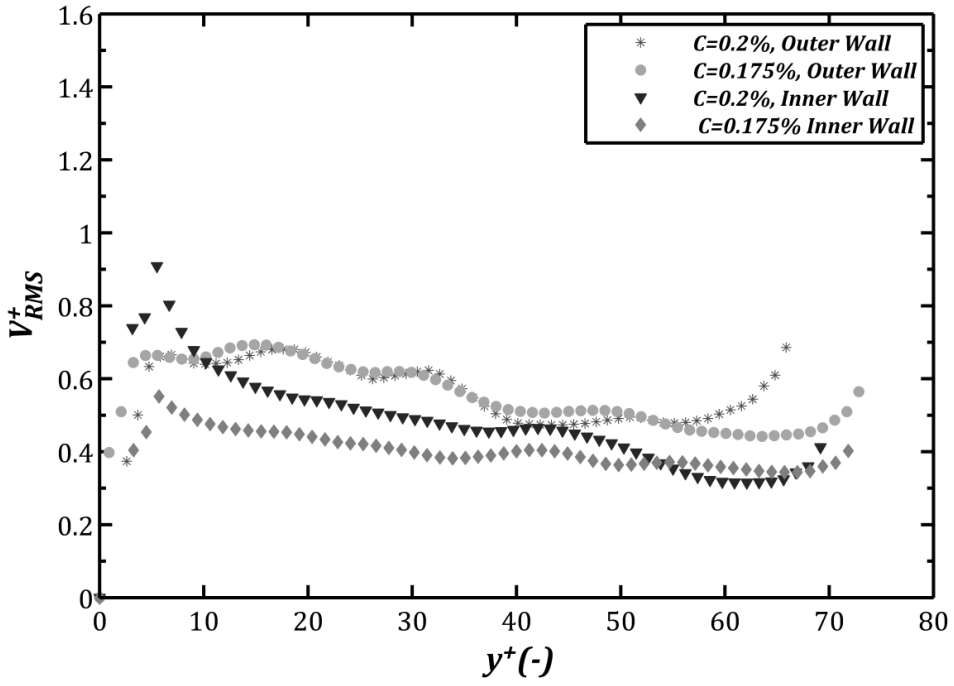


**Figure 6-65 Radial Turbulent Intensities in Wall Coordinate for Flow of 0.175% and 0.2% Polymer Solutions Flowing at $U_B = 0.827\ m/s$**

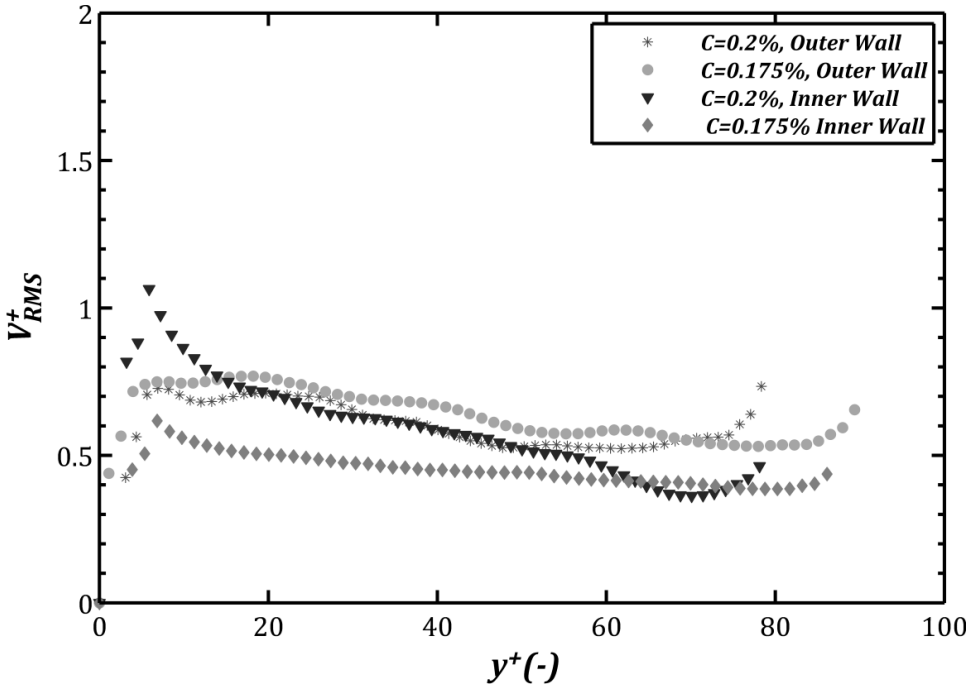


**Figure 6-66 Radial Turbulent Intensities in Wall Coordinate for Flow of 0.175% and 0.2% Polymer Solutions Flowing at $U_B = 0.999\ m/s$**

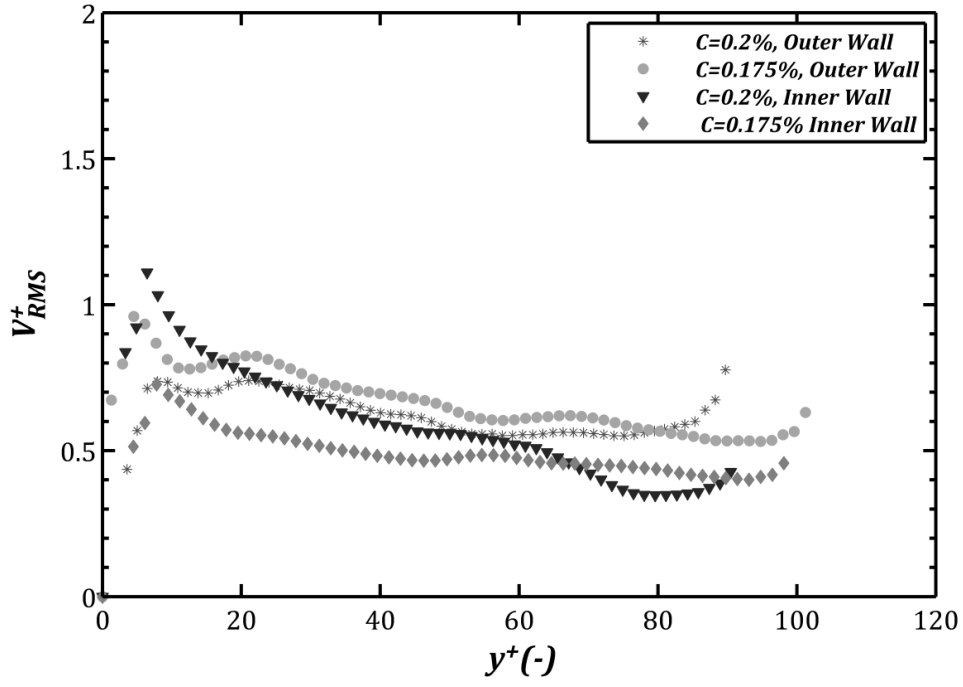


**Figure 6-67 Radial Turbulent Intensities in Wall Coordinate for Flow of 0.175% and 0.2% Polymer Solutions Flowing at $U_B = 1.164\ m/s$**

Summary: radial component of the RMS of fluctuation velocities which have been reported in dimensionless are showing slightly higher values for outer wall of the annuli behaviour observed for axial intensities as well. Radial intensity seems to have a peak in regions very close to the walls but decreases rapidly afterward to a value almost constant for the rest of dimensionless distance.

### 6.5.9 Conclusions

Two concentrations (0.175% and 0.2%) of a polymer aqueous have been tested. Operational conditions were chosen in such a way that assured a turbulent flow. PIV has been used to study the turbulent related aspects of the flow in concentric annuli. Pressure drops has been taken for friction factor analysis and further analysis of PIV data.

- ✓ Both polymer solutions were found to follow a power law relation in the range of shear rates encountered during experiments
- ✓ Friction factors for both fluids studied were found to be in good agreement with theoretical prediction of a power law type fluid in the laminar flow regime
- ✓ Friction factor data in the turbulent regime felt well below the Jones and Leung correlation which is valid for flow of Newtonian fluids
- ✓ Friction factor data in turbulent flow were also higher than those predicted by Virk's ultimate asymptote which is valid for the condition of maximum drag reduction
- ✓ Turbulent friction factors were found to be best represented by $f = 0.4{N_{re}}^{-0.48}$ for both fluids
- ✓ Velocity data for $y^+ < 10$ were found to follow the universal law of the wall for all the experiments with non-Newtonian fluids
- ✓ For $y^+ > 10$ major deviation from the logarithmic law consistent with flow of Newtonian fluids has been observed with an upward shift in velocity data for polymeric liquids
- ✓ Velocity data in the logarithmic region of the flow were found to be in good agreement with Virk's asymptote in wall coordinate
- ✓ Radiuses of maximum velocity have been found to be a function of Reynolds number for the range of Reynolds numbers studied

- ✓ Radiuses of maximum velocity decreased as Reynolds numbers were increased for both fluids
- ✓ Radiuses of maximum velocity were found to be closer to the inner wall of the annuli for all cases
- ✓ For two Reynolds numbers studied radius of maximum velocity was closer to the inner wall for 0.175% solution comparing to 0.2% polymer solution
- ✓ Viscous stresses were found to be higher close to the walls and decrease further away from the walls
- ✓ Viscous stresses were higher for 0.2% solution because of higher viscosity of that fluid
- ✓ Viscous stresses have converged to wall shear stress calculated from pressure drops at the walls of the annuli
- ✓ Reynolds stresses for the 0.2% solution were too close to zero
- ✓ Reynolds stresses are always higher for flow of 0.175% because of lower viscosity of this fluid
- ✓ Total stress data has been reported and were found to be dominated by viscous stress term for the range of Reynolds number studied
- ✓ Radiuses of zero shear stress for flow of 0.175% and 0.2% polymer solutions have shown higher values for 0.2% solution
- ✓ Radius of zero shear stress has been found to be depending on Reynolds number
- ✓ Dependency of radius of zero shear stress on Reynolds number has been found to be a decreasing trend of this radius with increasing the Reynolds number
- ✓ The radius of zero shear stress was found closer to the inner wall of the annuli
- ✓ Radius of maximum velocity and zero shear stress were compared and it was found that in general radius of zero shear stress is smaller than radius of maximum velocity
- ✓ Axial turbulent intensities in wall coordinate have shown much higher values for the outer wall of the annuli comparing to inner wall data
- ✓ Axial turbulent intensities were higher for flow of 0.175% comparing to 0.2% solution

- ✓ Axial turbulent intensities reached a maximum at $y^+ = 20$ for all the cases considered
- ✓ Radial intensities were found to be flat over a wide range of the flow
- ✓ Close to the wall in wall coordinate ( $y^+ < 10$) an anomalous behaviour has been observed for radial intensities

## 6.6 Newtonian Fluids versus Non-Newtonian Fluids

In this section the results which have been already discussed in previous sections will be presented in such a form that allows comparison between Newtonian fluids and non-Newtonian fluids. The similarities and differences will be highlighted.

### 6.6.1 Friction Factor

The first observed difference in flow of Newtonian fluids and non-Newtonian fluids has been the pressure drops. Although the experiments were conducted at the same bulk velocity or flow rate different pressure drops has been recorded. The Reynolds numbers for each fluid at the same bulk velocity is different depending upon their viscosity.

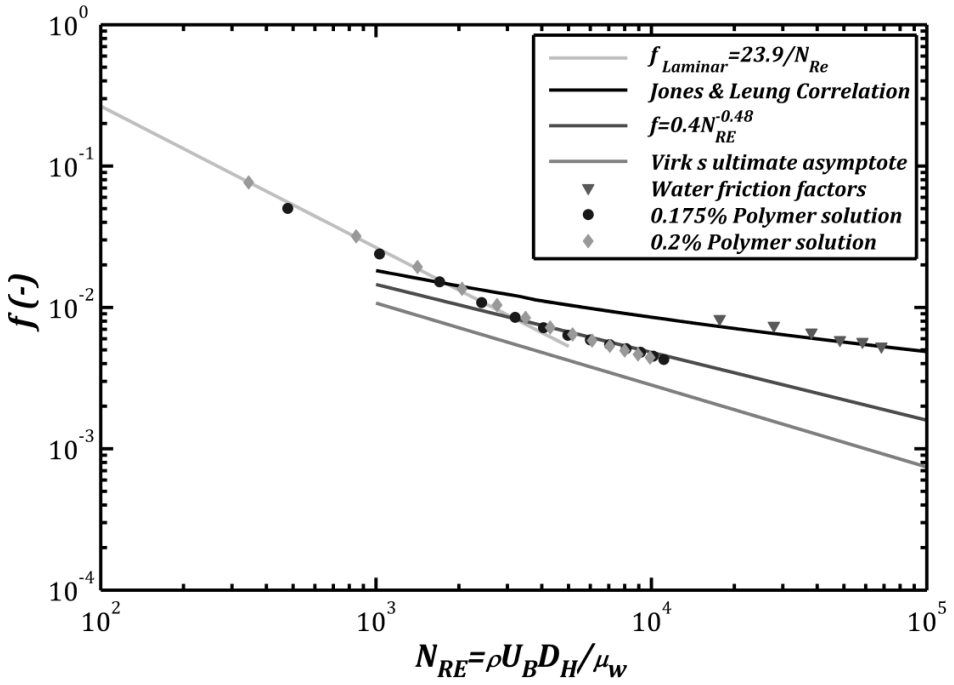


**Figure 6-68 : Friction Factor Data for All the Fluids Studied**

In Figure 6-68 polymers data seems to be pretty much similar but friction factors resulted for flow of water is completely different than those of polymers. Due to operational limitations no data point in laminar flow regime could be obtained for flow of water and so no conclusion could be made about this flow regime.

For turbulent flow the data clearly showing a reduction in friction factors for polymer solutions comparing to water which may be related to drag reduction phenomenon.

### 6.6.2 Near Wall Velocity Data

Another difference in flow of water and polymer has been observed in the velocity profiles close to the walls. In this region although all the fluids studied tend toward the law of the wall in the immediate vicinity of the walls, major deviations occurs further away in the logarithmic zone. Polymer velocity data in this zone best correlates with Virk's ultimate asymptote while velocity data for water follows the correlation valid for pipe flow.

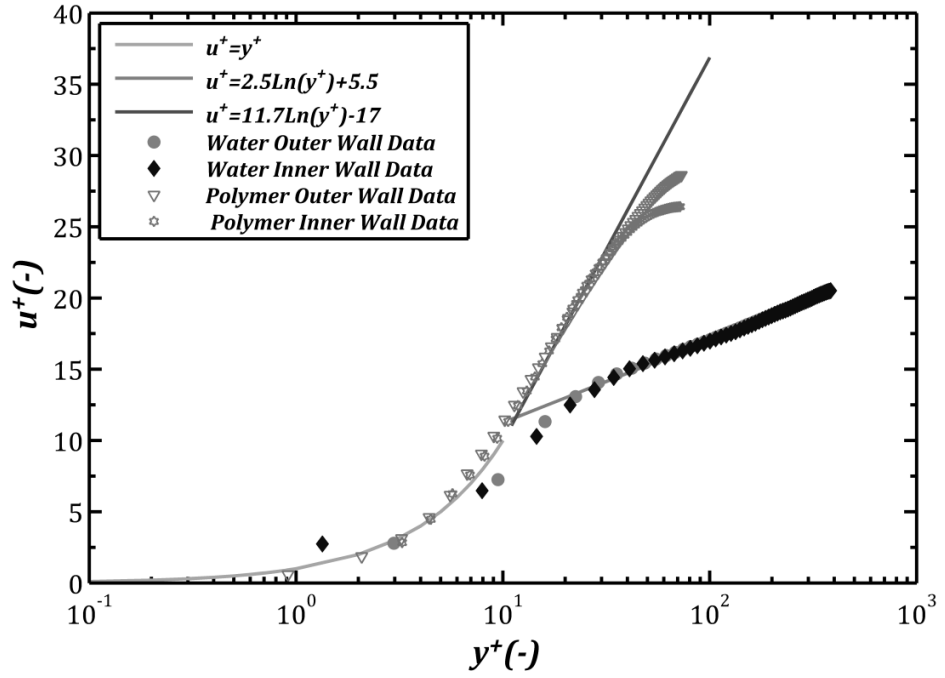


**Figure 6-69 Comparison of Near Wall Velocity Profiles for Flow of Newtonian and Non-Newtonian Fluids in Wall Coordinate**

The difference in velocity profiles is apparently related to friction factors in turbulent flow at which a reduction has been reported for flow of polymer.

**Table 6-14 Conversion of wall units to real world unit ($y^+ = 10$) for outer wall data**

| $U_B(\frac{m}{s})$ | Water (µm) | C=0.175% (µm) | C=0.2% (µm) |
|---|---|---|---|
| **0.827** | 205 | 4830 | 5200 |
| **0.999** | 178 | 3890 | 4369 |
| **1.164** | 156 | 3521 | 3810 |

### 6.6.3 Velocity Profiles in Whole Annular Gap and Radius of Maximum Velocity

Although dimensionless variables are of greater interests in fluid mechanics because they are better for comparison purposes but in this section velocity data will be presented in dimensional form in order to be able to separate the data for different fluids flowing at the same bulk velocity.

From velocity profiles in Figure 6-70 to Figure 6-72 it is obvious that polymer velocity profiles are much more parabolic than those of water. This in fact is the effect of Reynolds number and strength of the turbulence. As it is well-known that velocity profile gets flatter as Reynolds number increases, the Reynolds number for flow of water at the same bulk velocity as polymer solutions is much higher and that is the reason why it is showing a flatter profile in the core region of the flow with sharper gradient close to the walls.

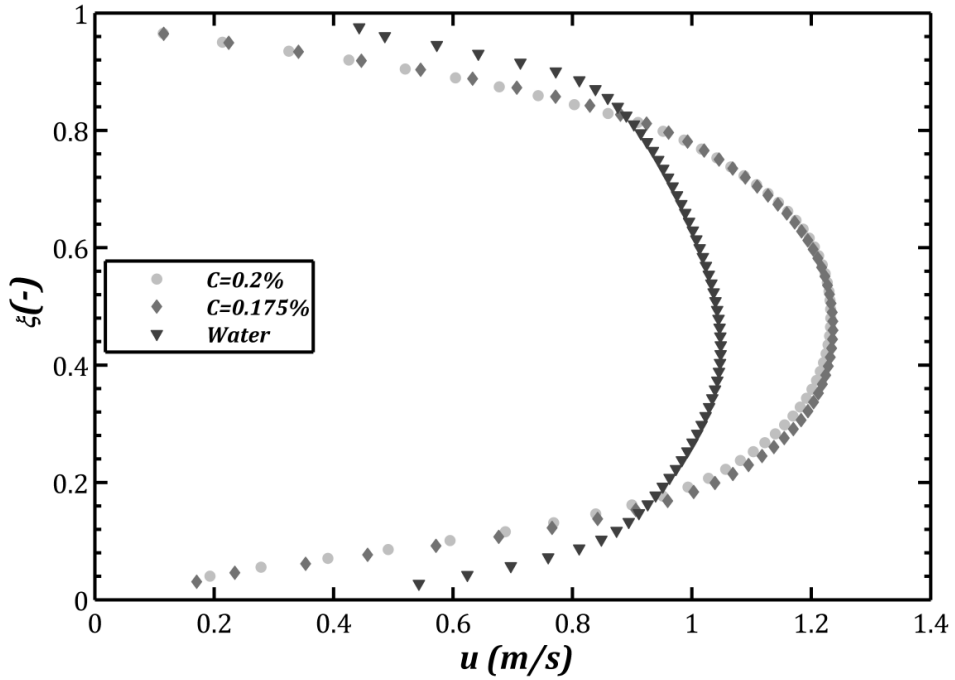


**Figure 6-70 Velocity Profiles in Whole Annular Gap for Flow of Water and Polymeric Liquids Flowing at $U_B = 0.827\ m/s$**

Maximum velocity for polymer solutions is higher than water. This can be explained by using the fact that all fluids having the same bulk or average velocity. While water velocity profile is flat in the core region for a large portion of the flow, the velocity data of polymers are not as flat and they increase gradually to a maximum. Gradient of the velocity data are much higher for polymer, this will show its influence in viscous stress term and will be discussed later. While in the center of the annuli velocity data for polymer are showing greater magnitude, in the regions close to the walls water velocity data are higher.

Summary: Velocity data for polymer solutions are showing profiles which are much more parabolic than water. Maximum velocity for polymer flow is higher. Velocity gradient seems to be higher for polymer flow with exception in the regions close to the walls.

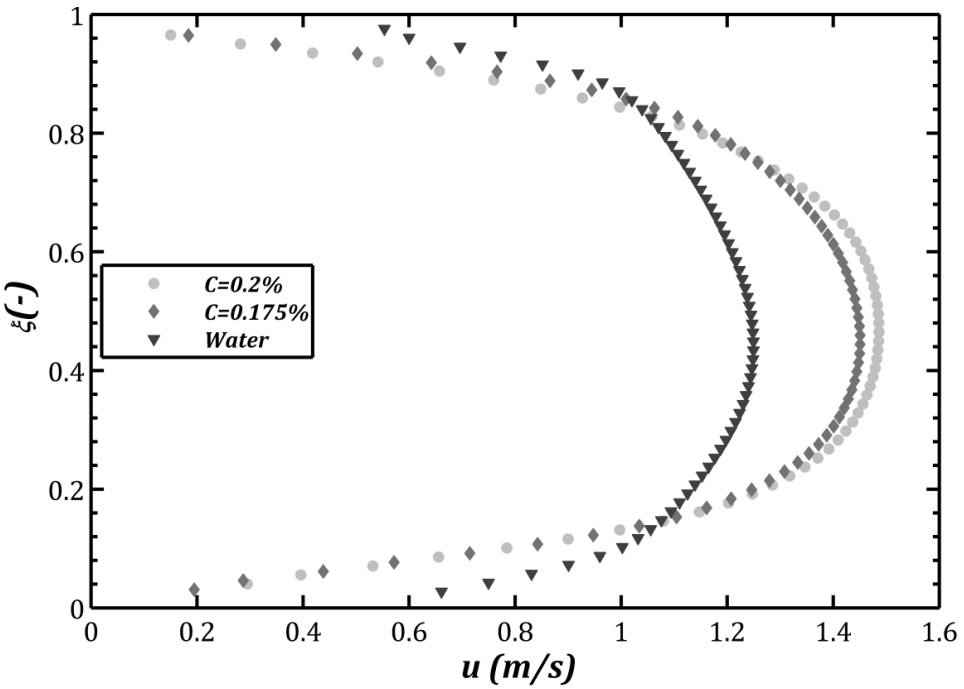


**Figure 6-71 Velocity Profiles in Whole Annular Gap for Flow of Water and Polymeric Liquids Flowing at $U_B = 0.999\ m/s$**

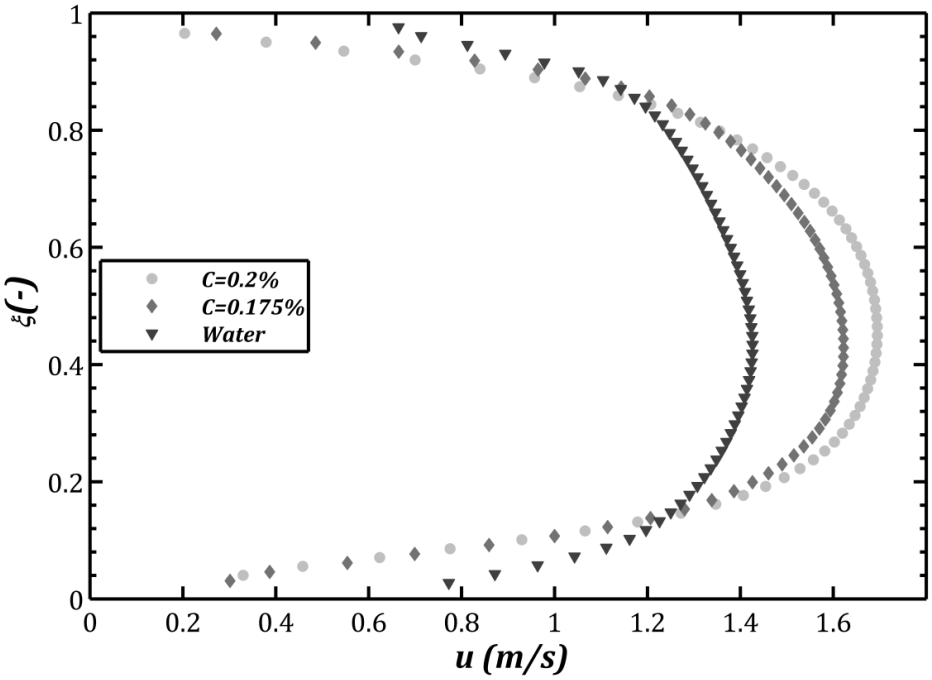


**Figure 6-72 Velocity Profiles in Whole Annular Gap for Flow of Water and Polymeric Liquids Flowing at $U_B = 1.164\ m/s$**

### 6.6.4 Radius of Maximum Velocity

Table 6-15 and Table 6-16 summarizes the radius of maximum velocity obtained for flow of water and polymers with given difference.

**Table 6-15 Radius of Maximum Velocity for Flow of Water and 0.175 % Polymeric Liquids**

| $U_B$(m/s) | Water $R_{max}$(mm) | Polymer $R_{max}$(mm) | Difference (%) |
|---|---|---|---|
| 0.827 | 31.213 | 31.69 | -1.52821 |
| 0.999 | 31.1642 | 31.25 | -0.27532 |
| 1.164 | 31.213 | 30.81 | 1.291129 |

Radius of maximum velocity is always higher for polymer aqueous flowing at the lowest velocity than that of water; that is the case for both concentrations. For the highest bulk velocity this is completely different because radius of maximum velocity is always smaller for polymer solutions comparing with radius of maximum velocity of water.

**Table 6-16 Radius of Maximum Velocity for Flow of Water and 0.2% Polymeric Liquids**

| $U_B$(m/s) | Water $R_{max}$(mm) | Polymer $R_{max}$(mm) | Difference (%) |
|---|---|---|---|
| 0.827 | 31.213 | 32.03 | -2.6175 |
| 0.999 | 31.1642 | 31.6 | -1.3984 |
| 1.164 | 31.213 | 30.73 | 1.547432 |

The difference in radius of maximum velocity of polymeric fluids and water is some number between -2% to +2%.6. Another difference is that while radius of maximum velocity for flow of water has been proved to be independent of Reynolds number, for flow of polymer, however, this radius changes with Reynolds number.

Summary: Radius of maximum velocity has been compared for flow of water and two polymer solutions and it is been found that for flow at lowest bulk velocity, this radius is always higher for polymer solutions. For flow at highest bulk velocity this radius is always smaller for polymers. Also the difference between polymers data and water reported to be in the range from -2% up to 2.6%.

### 6.6.5 Shear Stresses

#### 6.6.5.1 Viscous Stress

Figure 6-73 to Figure 6-75 are the viscous stresses for three fluids studied in this research. It has been discussed earlier in velocity profiles that higher velocity gradient is observed for flow of polymer solutions and that is one reason for the big difference in viscous stress profiles. Another reason which amplifies the difference in viscous stresses and makes the gap between water and polymer data is the viscosity of the fluids; the viscosity of the 0.2% is higher than 0.175% and that is also higher than water so it is expected to have higher viscous stress where the viscosity is higher.

Although viscous stress data for flow of water is expected to be lower than that of polymer in the core region of the flow, but for very close to the wall (within viscous sublayer) it is expected that water data shows higher values consistent with pressure drop data. The reason for this behaviour has been given in previous sections and is related to issues with measurements with water at this distance.

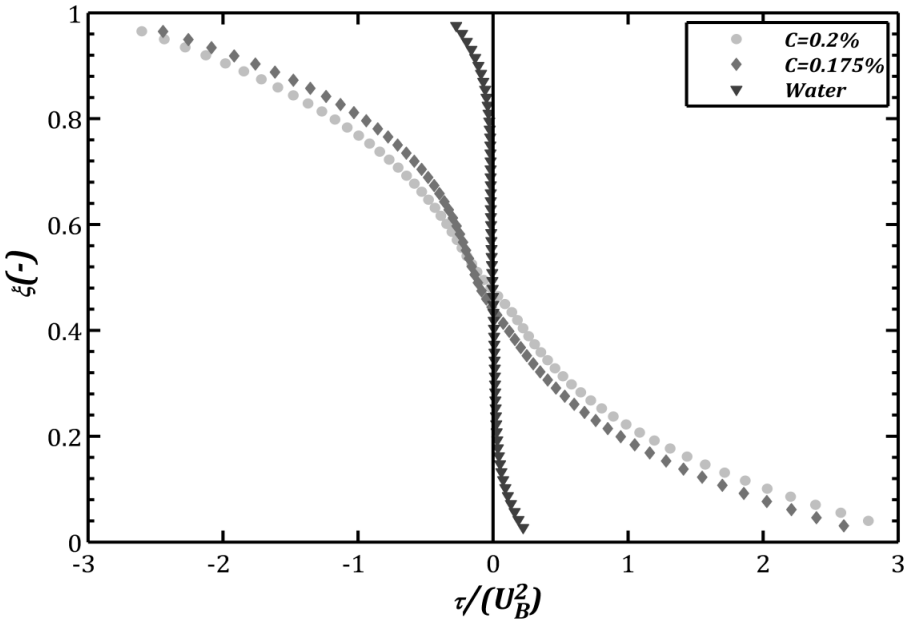


**Figure 6-73 Viscous Stress Profiles for Flow of Water and the Two Polymer Solutions at $U_B = 0.827\ m/s$**

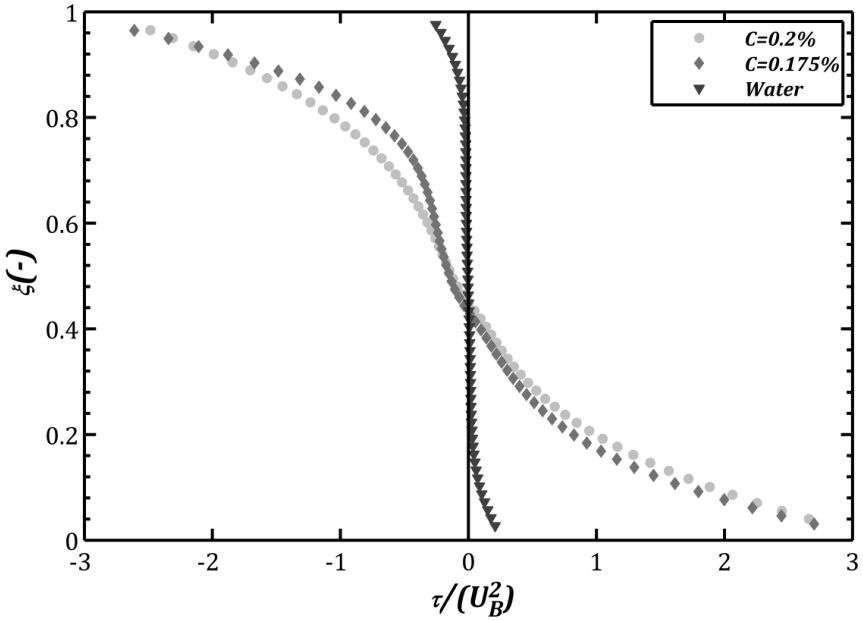


**Figure 6-74 Viscous Stress Profiles for Flow of Water and the Two Polymer Solutions at $U_B = 0.999\ m/s$**

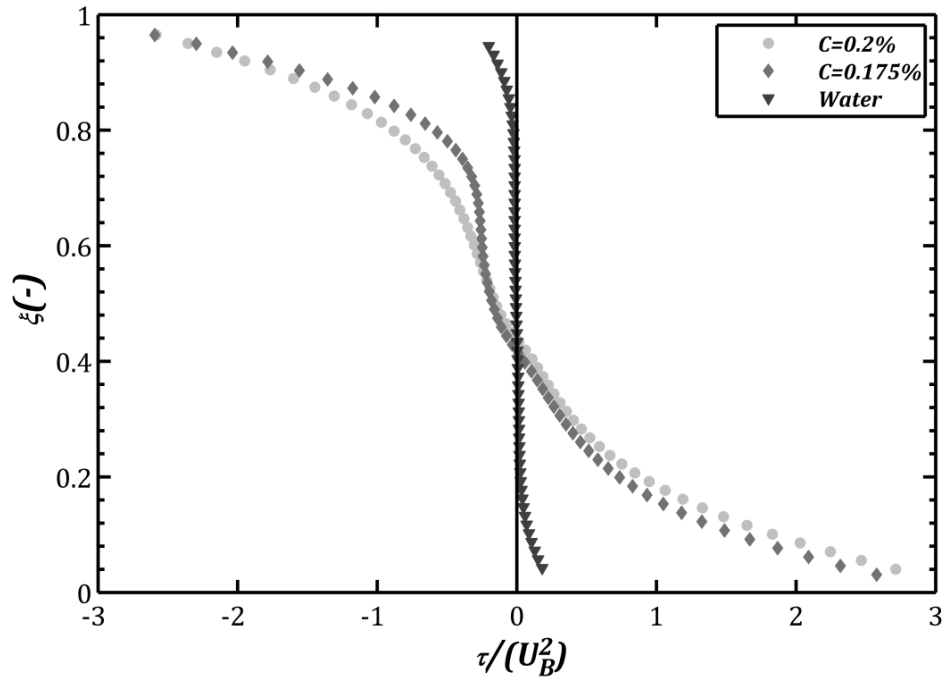


**Figure 6-75 Viscous Stress Profiles for Flow of Water and the Two Polymer Solutions at $U_B = 1.164\ m/s$**

Summary: viscous stress profiles were found to be much higher for polymer solution for the whole range of Reynolds numbers studied.

#### 6.6.5.2 Reynolds Stresses

Reynolds stresses are the contribution of turbulence to the total stress and is expected to be lower for lower Reynolds numbers. Another thing which have been observed and reported in many studies is that drag reduction property of polymeric liquids causes a reduction in Reynolds stresses.

A consistent trend is observed when comparing the Reynolds stresses for polymer fluids with two different concentrations with water; Reynolds stress for flow of the fluid with more polymer concentration (0.2%) is always lower than that of the fluid with lower polymer concentration (0.175%). Also observed is that the total Reynolds stress for polymer fluids is always lower than that of water. Reynolds stresses are in direct relationship with Reynolds number; the higher Reynolds number the higher would be Reynolds stresses. As mentioned and explained earlier all the experiments has been done on constant bulk velocity base in order to facilitate comparison between the fluids, based on that, Reynolds number is always higher for water then 0.175% solution and at last 0.2

% polymer solution depending upon their viscosity. Reynolds stresses also following the same trend as Reynolds number which is an indication of turbulence intensity and the effect of effective Reynolds number on Reynolds stresses.

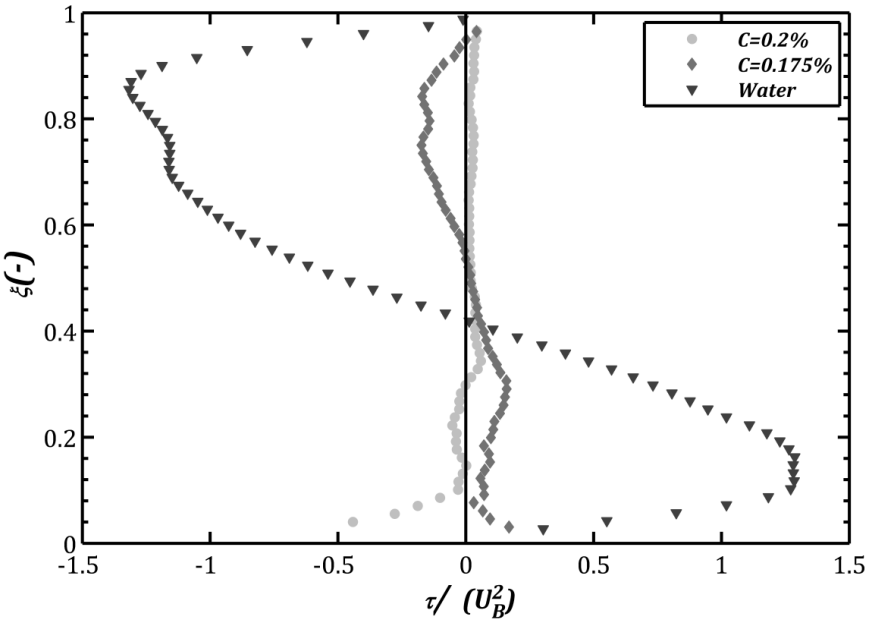


**Figure 6-76 Reynolds Stress Profiles for Flow of Water and the Two Polymer Solutions at $U_B = 0.827\ m/s$**

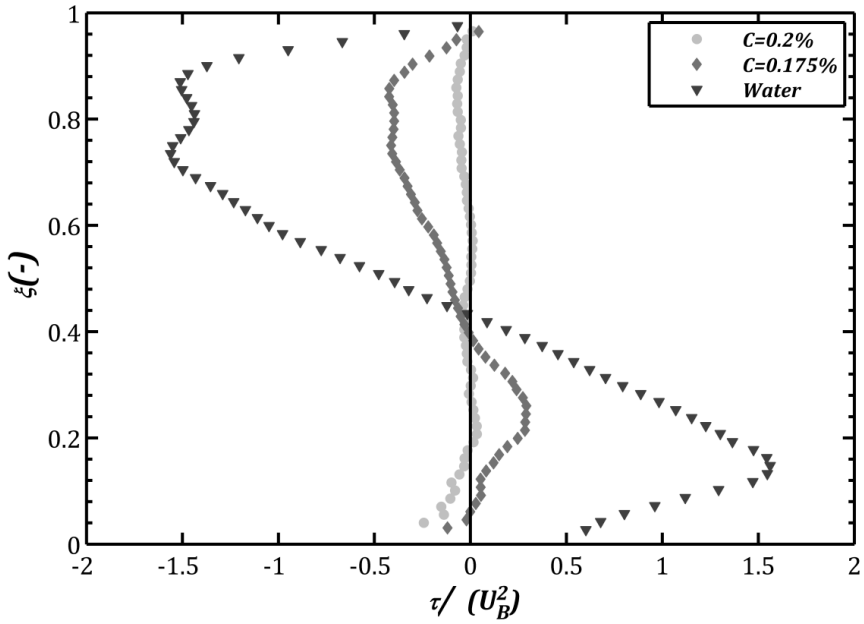


**Figure 6-77 Reynolds Stress Profiles for Flow of Water and the Two Polymer Solutions at $U_B = 0.999\ m/s$**

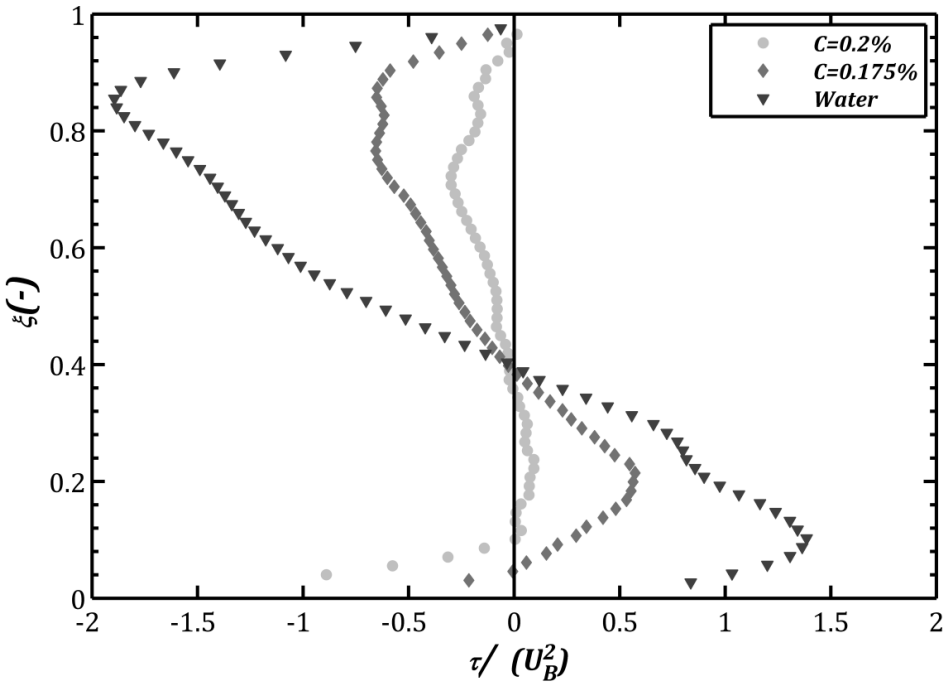


**Figure 6-78 Reynolds Stress Profiles for Flow of Water and the Two Polymer Solutions at $U_B = 1.164\ m/s$**

### 6.6.6 Radius of Zero Shear Stress

Similar to maximum velocity radius, radiuses of zero shear stress has been compared for polymer solutions and water as reported in Table 6-17 and Table 6-18

**Table 6-17 Radius of Zero Shear Stress for Flow of Water and 0.175% Polymer Solution**

| $U_B$(m/s) | Water $R_0$(mm) | Polymer $R_0$(mm) | Difference (%) |
|---|---|---|---|
| 0.827 | 30.2 | 31.9675 | -5.85265 |
| 0.999 | 31.1 | 30.94435 | 0.500482 |
| 1.164 | 30.8 | 30.4969 | 0.984091 |

**Table 6-18 Radius of Zero Shear Stress for Flow of Water and 0.2% Polymer Solution**

| $U_B$(m/s) | Water $R_0$(mm) | Polymer $R_0$(mm) | Difference (%) |
|---|---|---|---|
| 0.827 | 30.2 | 32.7313 | -8.38179 |
| 0.999 | 31.1 | 31.483 | -1.23151 |
| 1.164 | 30.8 | 31.18375 | -1.24594 |

The biggest difference in position of zero shear stress of polymer and water is observed for higher polymer concentration at lowest velocity where radius of zero shear stress for flow of polymer is 8.4% closer to the outer wall of the annuli comparing to water. As bulk velocity increases while radius of zero shear stress for water doesn't change significantly and it could be said that it is independent of Reynolds number, for polymer flow, however, this radius reduces with Reynolds number. The radius of zero shear stress progressively reduces for polymer solutions and as it is reported in Table 6-17 for 0.175% solution this radius while is bigger for polymer comparing to water at lowest velocity, it becomes smaller for higher velocities.

Summary: radius of zero shear stress for flow of polymer solutions and water has been compared and it has been found that this radius for polymer fluids lies in -8% to 0.1% of radius of zero shear stress for flow of water which is constant for the range of Reynolds numbers examined.

### 6.6.7 Turbulent Intensities

#### 6.6.7.1 Axial Intensities

In this section axial turbulent intensities will be compared. In order to highlight the near wall effects the data are presented in wall coordinates. It's been explained in previous sections while the actual distance from the wall is similar for all the fluids studied but depending upon pressure drops and viscosity in wall coordinate these distances are different.

Beside the difference for axial intensities for inner and outer wall of the annuli which has been explained earlier, it is observed that axial intensity around the outer wall for flow of 0.175% polymer solution is slightly higher than water while for the inner wall it is slightly lower.

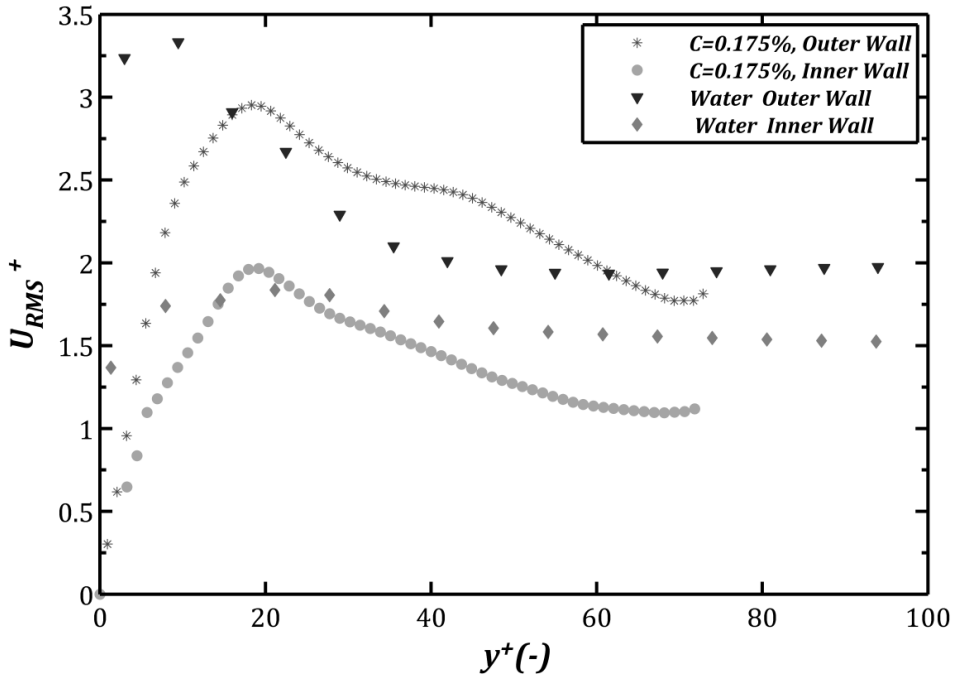


**Figure 6-79 Axial Turbulent Intensities in Wall Coordinate for Flow of Water and 0.175% Polymer Solution Flowing at $U_B = 0.827\ m/s$**

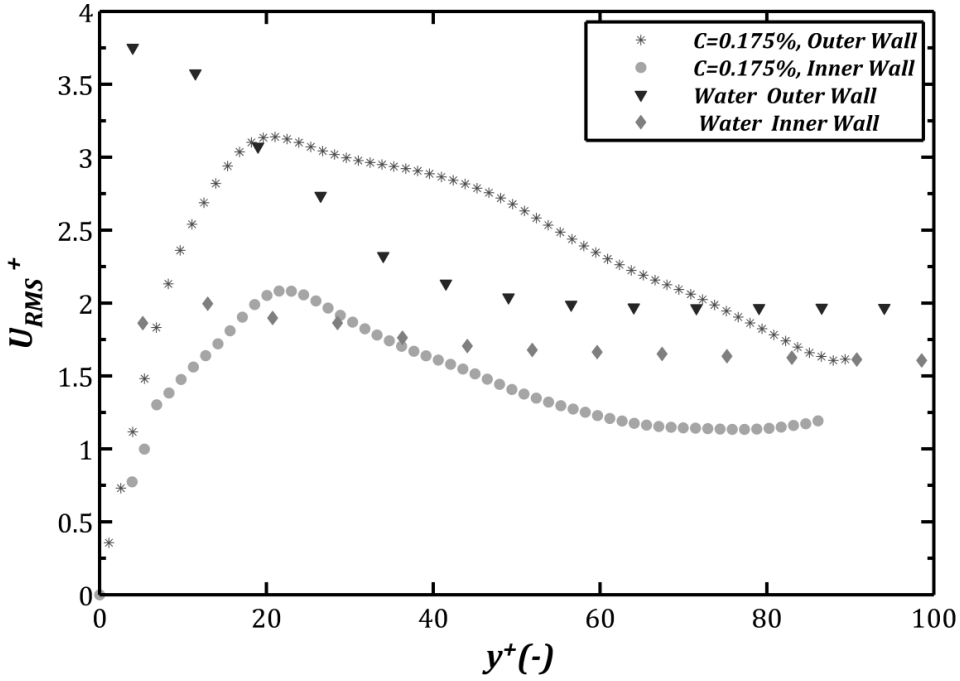


**Figure 6-80 Axial Turbulent Intensities in Wall Coordinate for Flow of Water and 0.175% Polymer Solution Flowing at $U_B = 0.999\ m/s$**

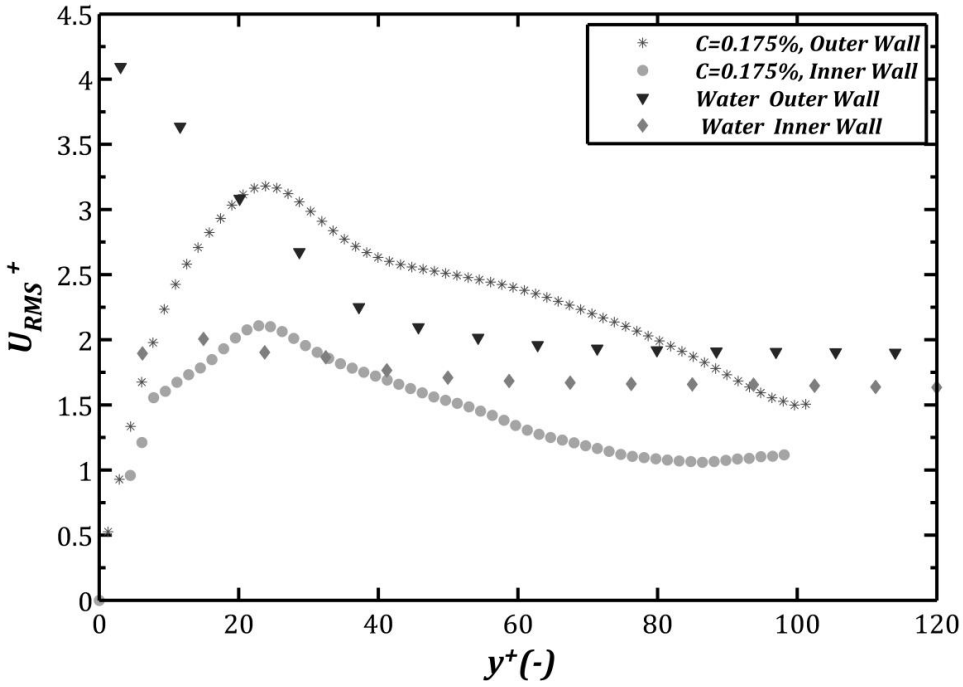


**Figure 6-81 Axial Turbulent Intensities in Wall Coordinate for Flow of Water and 0.175% Polymer Solution Flowing at $U_B = 1.164\ m/s$**

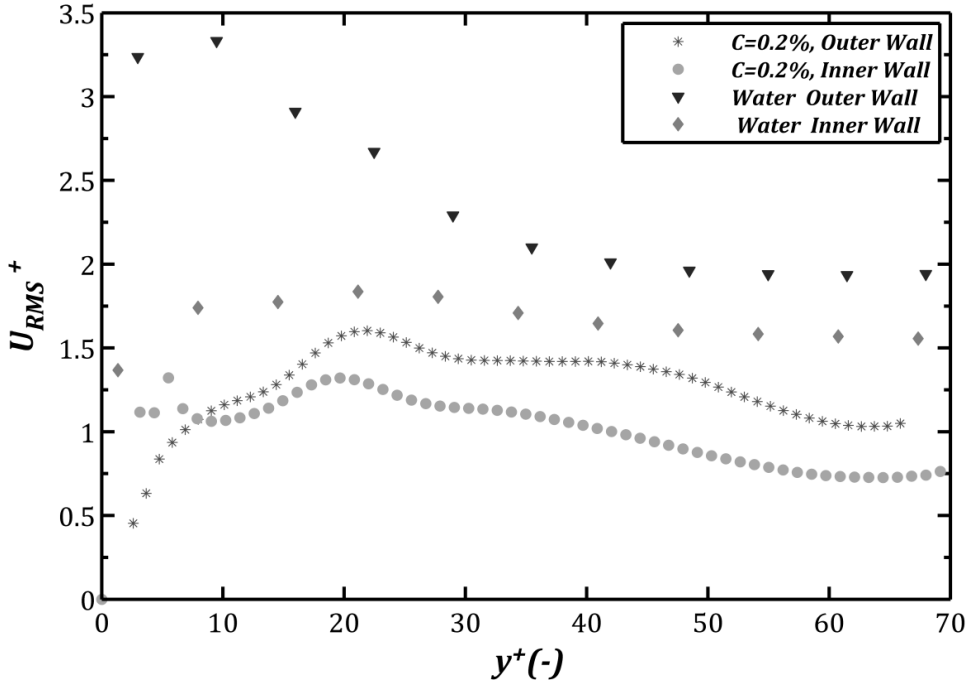


**Figure 6-82 Axial Turbulent Intensities in Wall Coordinate for Flow of Water and 0.2% Polymer Solution Flowing at $U_B = 0.827\ m/s$**

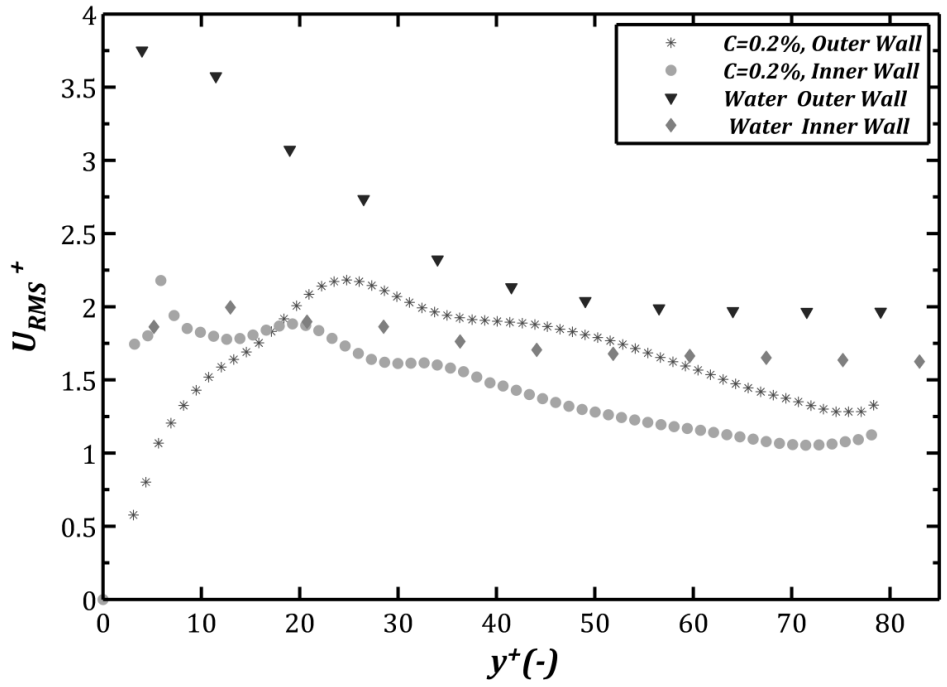


**Figure 6-83 Axial Turbulent Intensities in Wall Coordinate for Flow of Water and 0.2% Polymer Solution Flowing at $U_B = 0.999\ m/s$**

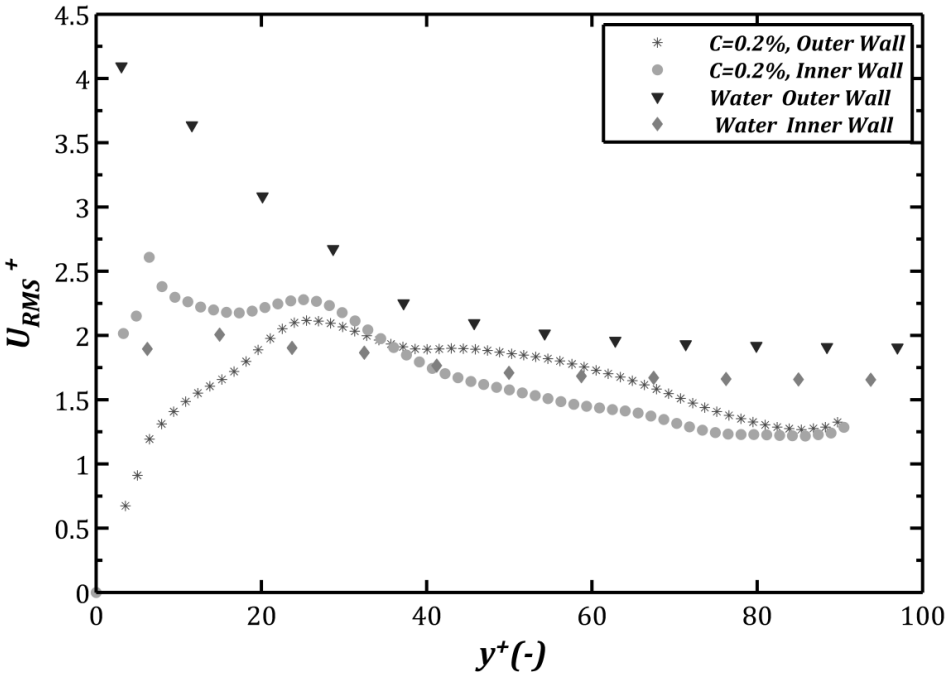


**Figure 6-84 Axial Turbulent Intensities in Wall Coordinate for Flow of Water and 0.2% Polymer Solution Flowing at $U_B = 1.164\ m/s$**

0.2% polymer solution has exhibited a completely different behaviour comparing to 0.175% solution. While the lower concentration showed slightly higher TI values comparing to water data, the 0.2% solution shows smaller TI for all three bulk velocities and for both inner and outer wall.

Summary: turbulent intensities in the axial direction were found to be slightly higher for flow of 0.175% polymer solution than that of water while for the higher concentration (0.2%) this was the other way around. The reason for the suppression of axial intensities for 0.2% aqueous is the high viscosity of this fluid and low effective Reynolds number caused by the high viscosity.

#### 6.6.7.2 Radial Intensities

Radial intensities are of great interest in explaining drag reduction phenomenon, according to previous studies when a drag reducing agent is used the radial component of fluctuation velocities would be suppressed greatly. This in fact could be used to explain the reduction in Reynolds stresses caused by polymeric liquids comparing to Newtonian fluids as well.

For all the fluids studied in this work, it has been found that using polymer additive greatly reduces the radial intensities; that applies for all the experiments. Although polymer intensities are lower than water but in the immediate vicinity of the walls the story is different and polymers intensities are showing higher values, this behaviour of radial intensity is not reported in literature.

Summary: Radial intensities were found to be much lower for polymer solutions comparing to water intensities in the core region of the flow. For $y^+ < 10$, however, polymer's data have shown greater values than water.

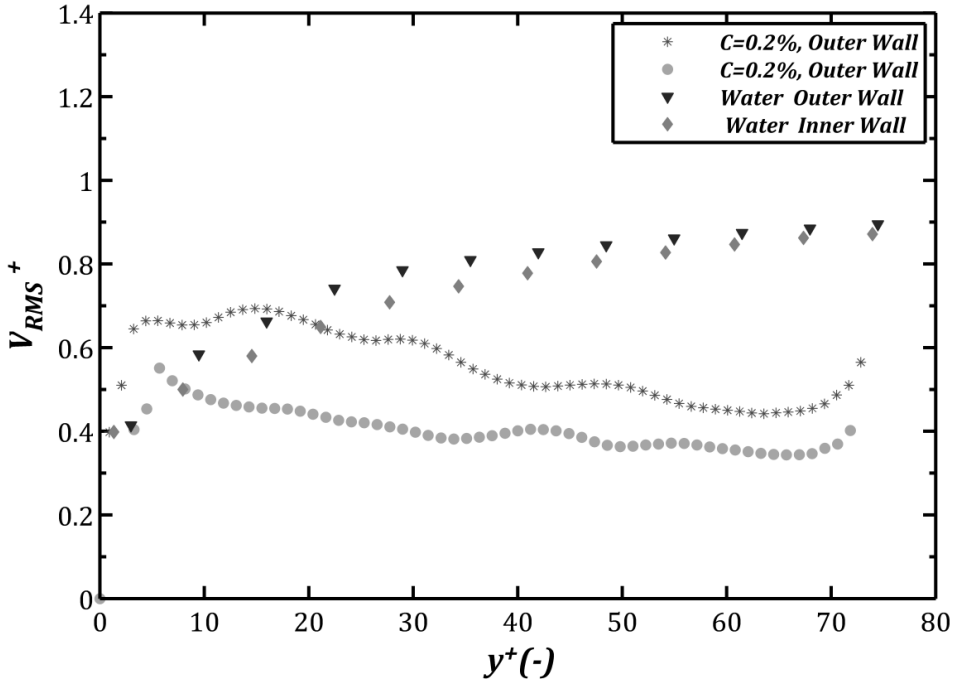


**Figure 6-85 Radial Turbulent Intensities in Wall Coordinate for Flow of Water and 0.175% Polymer Solution Flowing at $U_B = 0.827\ m/s$**

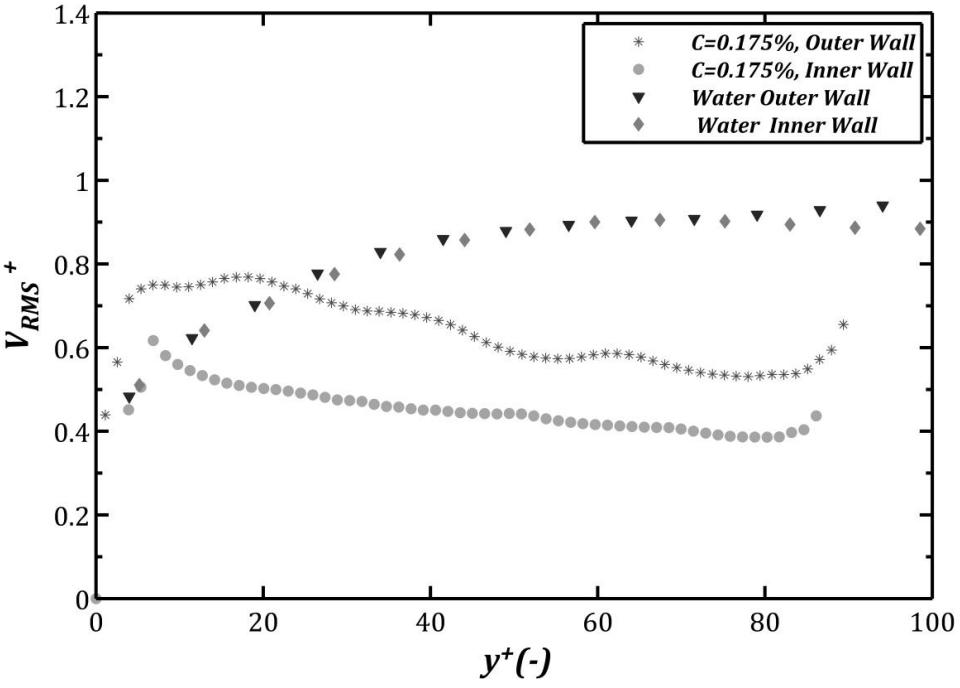


**Figure 6-86 Radial Turbulent Intensities in Wall Coordinate for Flow of Water and 0.175% Polymer Solution Flowing at $U_B = 0.999\ m/s$**

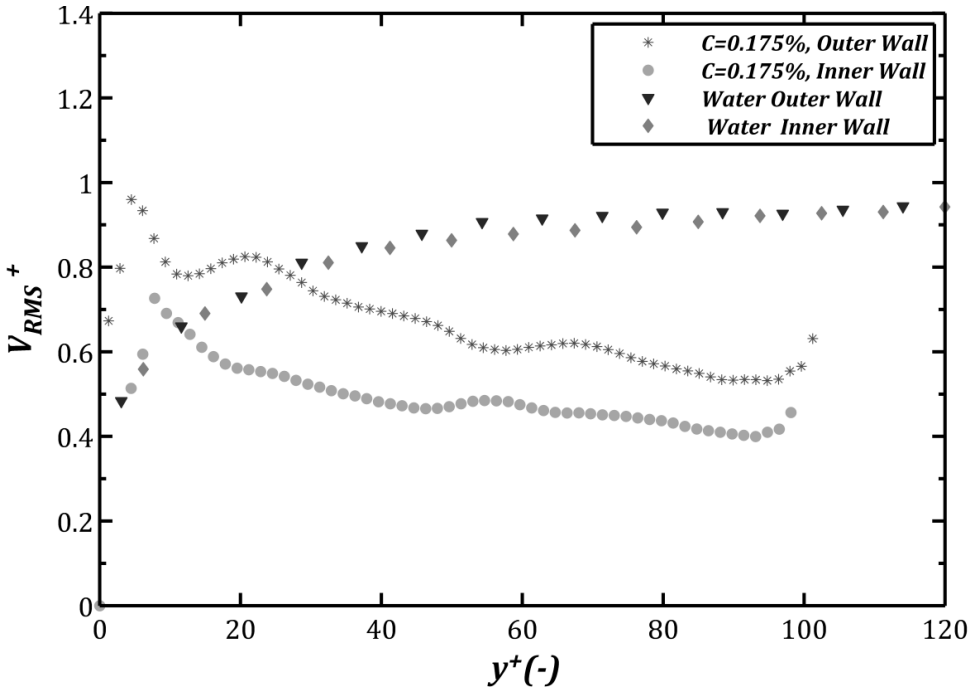


**Figure 6-87 Radial Turbulent Intensities in Wall Coordinate for Flow of Water and 0.175% Polymer Solution Flowing at $U_B = 1.164\ m/s$**

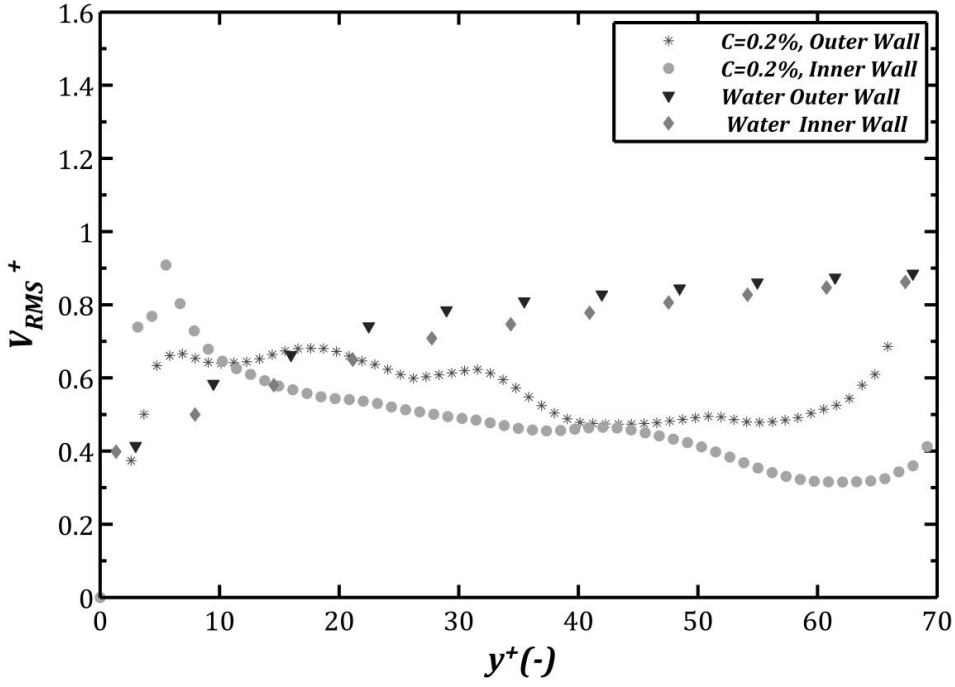


**Figure 6-88 Radial Turbulent Intensities in Wall Coordinate for Flow of Water and 0.2% Polymer Solution Flowing at $U_B = 0.827\ m/s$**

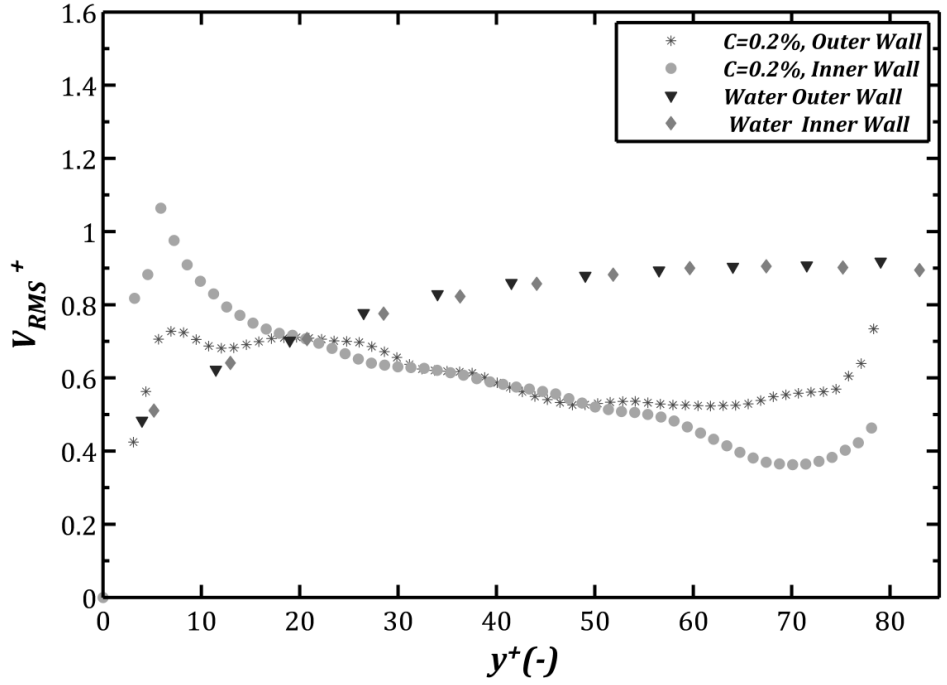


**Figure 6-89 Radial Turbulent Intensities in Wall Coordinate for Flow of Water and 0.2% Polymer Solution Flowing at $U_B = 0.999\ m/s$**

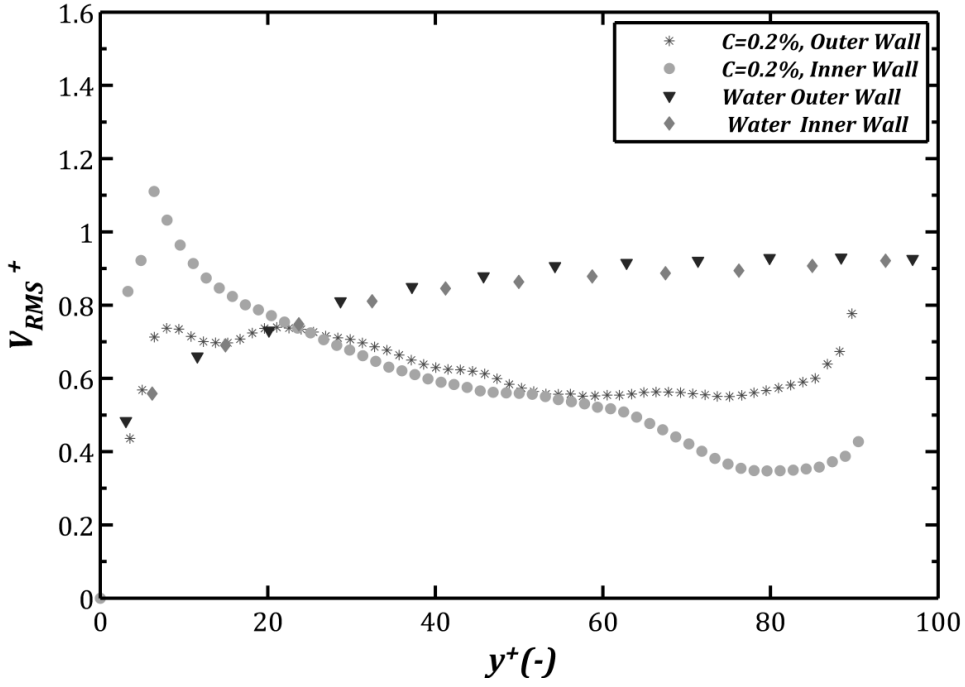


**Figure 6-90 Radial Turbulent Intensities in Wall Coordinate for Flow of Water and 0.2% Polymer Solution Flowing at $U_B = 1.164\ m/s$**

### 6.6.8 Conclusions

- ✓ Friction factors for flow of polymer solutions were found be much lower than water data in turbulent flow regime
- ✓ Velocity data although were the same in the immediate vicinity of the walls, but further away from the wall an upward shift in velocity data of polymer solutions have been observed
- ✓ Velocity profiles in the whole annular gap were compared for the three fluids and it is been confirmed that velocity profiles for polymer aqueous are more parabolic than water
- ✓ Maximum velocity were higher for polymer solution comparing to water
- ✓ Radius of maximum velocity for flow of polymer solutions were found to be some -2.6% to 1.5% different than that of water
- ✓ Although at lowest bulk velocity tested radius of maximum velocity was always bigger for polymer solutions, for the highest bulk velocity this radius was always smaller than that of water
- ✓ Viscous stresses were found to be much higher for flow of polymer fluids which reflected effect of high viscosity of this fluids
- ✓ Reynolds stresses were found to be much lower for polymeric liquids studied comparing to Reynolds stress data of water which reflects the effect of effective Reynolds number at which experiments were done; this also may be related to drag reduction phenomenon as well
- ✓ Radius of zero shear stress for polymer solutions were found to lie in -8% to 0.1% of water data
- ✓ Axial turbulent intensities have shown slightly higher values for 0.175% polymer solution than intensities of water
- ✓ Axial turbulent intensities have shown lower values for 0.2% polymer solution than intensities of water
- ✓ Radial intensities in all the cases considered were found to be greatly suppressed for polymer solutions in the core flow region comparing to water data in wall coordinate
- ✓ Close to the wall, radial intensities of polymer solution have shown higher values but this is just for a very small distance and very close to the walls

## 6.7 Reference


[1]. Kundu P. K., Cohen I. M., 2010, "Fluid Mechanics", Elsevier, Oxford, 4th edition

[2]. Pope S. B., 2002, "Turbulent Flows", Cambridge University Press

[3]. Pinho F. T., Whitelaw J. H., 1990, "Flow of Non-Newtonian Fluids in Pipe", Journal of Non-Newtonian Fluid Mechanics, Vol. 34, pp. 129-144

[4]. Escudier M. P., Oliveira P. J., Pinho F. T., Smith S., 2002, "Fully Developed Laminar Flow of Non-Newtonian Liquids through Annuli: Comparison of Numerical Calculations with Experiments", Experiments in Fluids, Vol. 33, pp. 101-111

[5]. Rothfus R. R., Monard C. C., Senecal V. E., 1950, "Velocity Distribution and Fluid Friction in Smooth Concentric Annuli", Industrial and Engineering Chemistry, Vol. 42, No.12, pp. 2511- 2520

[6]. Brighton J. A., Jones J. B., 1964, "Fully Developed Turbulent Flow in Annuli", Journal of Basic Engineering, 86, 835-842

[7]. Walker J. E., Rothfus R. R., 1959, "Transitional Velocity Patterns in a Smooth Concentric Annulus", A.I.Ch.E Journal, Vol. 5, No. 1, 51-54

[8]. Lawn C. J., Elliot C. J., 1972, "Fully Developed Turbulent Flow through Concentric Annuli", Journal of Mechanical Engineering Science, Vol. 14, No.3, pp. 195-204

[9]. Rehme K., 1974, "Turbulent flow in smooth concentric annuli with small radius ratios", Journal of Fluid Mechanics", Vol. 64, part 2, pp. 263-287

[10]. Nouri J. M., Umur H., Whitelaw J. H., 1993, "Flow of Newtonian and Non-Newtonian Fluids in Concentric and Eccentric Annuli", Journal of Fluid Mechanics, Vol. 253, pp. 617-641

[11]. Escudier M. P., Gouldson I. W., Jones D. M., 1995, "Flow of Shear-Thinning Fluids in Concentric Annulus", Experiments in Fluids, Vol. 18, pp. 225-238

[12]. Rothfus R. R, Sartory W. K., Kermode R. I., 1966, "Flow in Concentric Annuli at High Reynolds Numbers", A.I.Ch.E. Journal, Vol. 2, No. 6, pp. 1086-1091

[13]. Roberts A., 1966, "A Comment on the Turbulent Flow Velocity profile in a Concentric Annulus", J. Hear MOSS Transfer, Vol. 10, pp. 709-712

[14]. Quarmby A.,1967, "An Experimental Study of Turbulent Flow through Concentric Annuli", Journal of Mechanical Science, Vol. 9, pp. 205-221

[15]. Clump C. W., Kwasnoski D., 1968, “Turbulent Flow in Concentric Annuli”, A.I.Ch.E. Journal, Vol. 14, No. 1, pp. 164-168

[16]. Hanks R. W., Bonner W. F., 1971, “Transitional Flow Phenomena in Concentric Annuli”, Industrial & Engineering Chemistry Fundamentals, Vol. 10, No.1, pp. 105-113

[17]. Lee Y., Park S. D., 1971, “Developing Turbulent Flow in Concentric Annuli: An Analytical and Experimental Study”, Wärme- und Stoffiibertragung, Vol. 4, pp. 156-166

[18]. Rehme K., 1975, “Turbulence measurements in smooth concentric annuli with small radius ratios”, Journal of Fluid Mechanics, Vol. 72, part 1, pp. 198-206

[19]. Jones O. C., Leung J.C.M., 1981, “An Improvement in the Calculation of Turbulent Friction in Smooth Concentric Annuli1”, Journal of Fluid Engineering, Vol. 103, pp. 615-623

[20]. Ahn S. W., Kim K. C., 1999, “Characteristics of Turbulent Flow in the Annuli with Smooth and Rough Surfaces”, KSME International Journal, Vol. 13, No. 2, pp. 183-190

[21]. Dou H. S., Khoo B. C., Tsai H. M., 2010, “Determining the Critical Condition for Flow Transition in a Full-Developed Annulus Flow”, Journal of petroleum Science and Engineering”, Vol. 71

[22]. Fredrickson A. G., Bird R. B., 1958, “Non-Newtonian Flow in Annuli”, Industrial and Engineering Chemistry, Vol. 50, No. 3, pp. 347-352

[23]. Dodge D. W., Metzner A. B., 1959, “Turbulent Flow of Non-Newtonian Systems”, A.I.Ch.E. Journal, Vol. 5, No. 2, pp. 189-204

[24]. Virk P. S., Mickley H. S., Smith K. A., 1970, “The Ultimate Asymptote and Mean Flow Structure in Toms' Phenomenon”, Journal of Applied Mechanics, 1970, pp. 488-493

[25]. Bird R. B., 1976 “Useful Non-Newtonian Models”, Annual Review. Fluid Mechanics, Vol. 8, pp. 13-34

[26]. Zakin J. L., Ni C. C., Hansen R. J., 1977, “Laser Doppler Velocimetry Stduies of Early Turbulence”, The Physics of Fluids, Vol. 20, No. 10, pp. 85-88

[27]. Hanks R. W., Larsen K. M., 1979, “The Flow of Power-Law Non-Newtonian Fluids in Concentric Annuli”, Industrial and Engineering Chemistry, Vol. 18, No. 1, pp. 33-35

[28]. Bird R. B., Armstrong R. C., Hassager O., 1987, "Dynamics of polymeric liquids", Wiley-Interscience, New York, Vol. 1

[29]. Luo Y., Peden J. M., 1990, "Flow of Non-Newtonian Fluids through Eccentric Annuli", SPE Production Engineering, SPE 16692

[30]. Japper-Jaafar A., Escudier M. P., Poole R. J., 2010, "Laminar, Transitional and Turbulent Annular Flow of Drag-Reducing Polymer Solutions", Journal of Fluid Mechanics, Vol. 165, pp-1357-1372

[31]. Colebrook, C. R., 1939, "Turbulent Flow in Pipes with Particular Reference to the Transition Region between the Smooth and Rough Pipe Laws", J. Inst. Civ. Eng. (London), Vol. 11, pp. 133-156.

# Chapter 7:

# Results and Discussion (Cutting Transport in Horizontal Annuli)

In this chapter results of cuttings transport experiments, which have been conducted to find critical conditions required for removal of particles from the surface of bed deposits are presented. Two different particle size ranges have been tested along with water and three non-Newtonian fluids prepared by using three different polymer concentrations. Critical velocities, pressure drops and wall shear stresses associated with different modes of particle transport (i.e., rolling, saltation and dune like transport, full suspension) have been measured and reported for all fluids.

The results are categorized and presented separately for each particle size range. Cuttings transport efficiency of each fluid is discussed for each particle size range. Effect of viscosity on the threshold of particle motion is investigated and discussed. A model for predicting critical wall shear stress for rolling type motion of fine particles using power law type fluids has been developed and the predictions of this model are compared with the measured data.

## 7.1 Introduction

The use of directional and horizontal drilling technique has dramatically increased over the past decades but hole cleaning still remained a challenge especially when an extended reach well with a long horizontal or inclined section is to be drilled. The problem seems to be addressed adequately for vertical drilling, however, in directional wells, poor hole cleaning often results in costly non-Productive time (NPT) situations. Pipe sticking have been found to contribute up to 70% of the unscheduled events[28]. It has been reported that one third of all pipe sticking cases resulted from poor well cleaning[29]. It was reported that the cost of NPT due to pipe sticking could be anywhere between 100 to 500 million US dollars per year [30]. Efficient well cleaning strategies and hydraulics program need to be developed to reduce costs associated with hole cleaning and facilitate drilling longer horizontal and extended reach wells.

There are many parameters, which affect the cutting transport efficiency. According to Bilgesu[11], factors controlling the cuttings transport could be categorized under three main groups; fluid characteristics, cuttings related factors and operational variables. Numerous experimental and simulation works have been conducted to study the effect of each of these parameters[11] -[25]. Many theoretical and semi-theoretical models have been developed and proposed.

Fluid properties, which may affect the cutting transport are fluid density and rheology and also flow rate of the fluid[11]. Effect of density in all the studies have been reported to be positive ([5] and [4]) because it generally increases the buoyancy effect. However, there is also a negative effect associated with heavy fluids by reducing the drilling rate, which increases the drilling costs due to longer drilling time[4].

Effect of rheology has been extensively studied but there is no general agreement on how the rheology of the fluid would influence cuttings transport efficiency. Some studies suggest that medium viscosity drilling fluid is superior to low and high viscosity fluids in inclined wellbores[21]. Due to suppression of turbulence, high viscosity drilling fluid has been found to have a detrimental effect on cutting transport in high angle wells[2]. The same study has reported that turbulence is favorable in horizontal annulus, however, transport capacity mainly depends upon fluid density and not rheology[2]. Tomren[1] found that the viscosity effect is a function of flow regime. In laminar flow regime, higher viscosity fluids always perform better. In turbulent flow, both low and high viscosity fluids are the same with a small advantage of high viscosity fluid over the low viscosity fluid. Kelessidis et al., [18] study have shown that rheology in fact has a minimal effect on cutting transport while another study suggested maintain correct rheology is of great importance[16]. Nguyen et.al[4] study has led to the conclusion that increasing the viscosity will enhance the cutting transport. On the contrary, Azar et al.,[4] have reported that increase in viscosity causes a decrease in hole cleaning ability. Results of a three layer bed model proposed by Cho et al.,[23] suggested that an increase in the flow behaviour index would result in a thicker stationary bed. More recently, Duan[6] stated that small cuttings are easier to transport with PAC solution over water, which means a positive effect of higher viscosity for transporting finer particles.

Effect of mud flow rate on cuttings transport has been reported to be always positive. However, there is an upper limit of flow rate, which is dictated by capacity of rig hydraulics and borehole wall erosion [4]. Based on the positive effect of flow rate, using larger drill pipes have been recommended by some investigators[5]. Turbulent flow regime has been found to work better for cuttings transport in directional drilling[2]. Payne et al.,[16] have recommended that transitional flow regime should be avoided because it has a negative effect on cutting transport.

Physical properties of solids which affect the cutting transport ability and are the size, shape and density of the solids [11]. Most of these parameters are not controllable. Size and shape of the cuttings depend on the type of the bit and the formation. Most of the studies investigating the cuttings size effect reported that small cuttings are more difficult to transport ([21][6][2]). Duan et al., [6] have shown that when water is used, smaller cuttings are more difficult to remove. However, when a solution of PAC is used, small cuttings are easier to transport than large cuttings.

Third group of parameters are related to operational conditions such as inclination angle, inner pipe rotation speed or eccentricity[11]. Effect of inclination angle has been found to be extremely important [21][1]; for angles of inclination less than 10 degrees, cutting transport remains similar to vertical case [1],[7] but for larger inclination angles dramatic reductions occurs in the cuttings transport efficiency [1]. The main reason for this is the reduction in the vertical component of the fluid velocity, which increases the tendency of cuttings to move downward toward the borehole wall[7]. Formation of bed of cuttings has been observed for angles of inclination beyond 30 degree[1]. At angles between 35 to 55 degrees a back sliding of cuttings bed has been reported[21][1], [2]. Some experimental studies have suggested that critical velocity is a function of inclination angle[18].

Eccentricity of inner pipe has also been found to affect the cutting transport. The effect of eccentricity has been reported to be negative in many studies mainly because eccentric configuration causes the fluid to be driven away from the lower side of the annuli where cuttings tends to go[4],[1],[4].

Inner pipe rotation has been found to have a positive effect on critical velocity and cutting transport capacity. However, the interaction between different parameters such as rheology, cutting size and pipe rotation is rather complicated and makes it difficult to conclude the degree of influence of pipe rotation[4]. Pilehvari et al.,[2] has reported a reduction in critical velocity of solid transport based on Larsen's experiments[21] in presence of drill pipe rotation. Duan et al.,[6] have shown that in transporting small cuttings, key parameters, which control the transport are the pipe rotation and rheology. In fact, pipe rotation has been found to have a profound effect on cutting transport. Lokett[15] by using computer simulation, showed the possibility of an increase in vortical activities due to inner pipe rotation, which may enhance the cuttings transport capacity.

Tomren[1] found a minimal effect of pipe rotation on cuttings transport in concentric arrangement but an improvement in the cutting transport in eccentric annuli with pipe rotation. Thomas[16] reported pipe rotation enhances cutting transport in laminar flow and has a little effect otherwise. Azar[4] argued that rotation of drill string with vibration has a significant impact on hole cleaning. The impact of pipe rotation has been reported to be function of cutting size, rheology, flow rate and also dynamic behaviour of drill string[4].

Available mechanistic models are mostly based on force balance on a multi-layer bed[7], [9], [7][7]. These models have been developed to define the critical velocities required for different type of particles motion. The assumptions used for developing these models are very limiting and also parameters involved in the model such as drag coefficient or lift coefficient are sometimes difficult to calculate, which altogether restrict the practical use of these models.

## 7.2 Experimental Program

The large scale horizontal flow loop was the main experimental facility used for obtaining the results presented in this chapter. A detailed description of the experimental facility, measurement tools and techniques are all discussed in chapter 3.

Rheological analyses of all the fluids used in this study are presented in chapter 5 of this thesis. Information on particles size distribution analysis is also reported in chapter 5.

In this thesis, the term fine particles are referred to particles which have a mean diameter of 349 micron ($d_{50}$ =349 micron) while the term coarse particles are referred to those particles which have a mean diameter of 1.2146 mm ($d_{50}$=1.214).

## 7.3 Cuttings Transport Experiments with Fine Particles

Statistical analysis and particle size distribution of fine particles used in this research are presented earlier in chapter 5. Fine particles were found to be uniform in size with a mean diameter of 349 micron. For the rest of this discussion, 349 micron will be assumed as the representative diameter of these sands. Also these particles are natural sands with a density of 2650 kg/m$^3$.

The primary focus of the experiments in this study has been the investigation of the influence of the fluid rheology, more specifically the viscosity on the cutting transport

ability in annuli. In order to do so, 4 fluids with different rheological behaviour have been tested and critical velocities along with pressure drops have been measured. The term critical velocity is referred to a velocity at which particles sitting on a bed start to move in rolling type motion along the bed at an acceptable rate (for velocities lower than the critical velocity there may be some occasional particle movement but not continuously).

Four fluids have been tested in an attempt to find the critical velocity and more generally critical conditions for particle movement. One of the fluids was water. . Three other fluids were prepared by using polymer concentrations of 0.05%, 0.1% and 0.175%. These fluids are non-Newtonian in nature and theologically can be characterized as power law type. The explicit rheological models describing the characteristics of these fluids are given by Eq. ( 7-1) to Eq. ( 7-3).

C=0.175% Fluid $\begin{cases}\tau = 0.031\gamma^{0.6977} \\ \mu_a = 31\gamma^{-0.3023}\end{cases}$ **Eq. ( 7-1)**

C=0.1% Fluid $\begin{cases}\tau = 0.015\gamma^{0.804} \\ \mu_a = 0.015\gamma^{-0.196}\end{cases}$ **Eq. ( 7-2)**

C=0.05% Fluid $\begin{cases}\tau = 0.0059\gamma^{0.948} \\ \mu_a = 0.0059\gamma^{-0.052}\end{cases}$ **Eq. ( 7-3)**

The procedure for conducting cuttings experiments is in such a way that experiments always start with the lowest possible velocity and increase the velocity stepwise gradually until the critical velocity is achieved. At each velocity, pressure drop is recorded as well. The results of the experiments for all the fluids are reported in Table 7-1to Table 7-4. In these tables along with velocity and pressure drop measurement, terms such as wall shear stress ($\tau_w$), shear velocity (u* ) fluid Reynolds number ($N_{Re}$) ,viscous sublayer

thickness ( $\delta_v$) , particles Reynolds number ($R_{ep}$) and dimensionless wall shear stress or shield's parameter (τ*) are also reported as calculated from the following equations:

$$\tau_w = -\frac{D_H}{4}\frac{dp}{dl} \qquad \textbf{Eq. ( 7-4)}$$

$$u^* = \sqrt{\frac{\tau_w}{\rho}} \qquad \textbf{Eq. ( 7-5)}$$

$$\delta_v = \frac{5\mu_w}{\rho u^*} \qquad \textbf{Eq. ( 7-6)}$$

$$R_{ep} = \frac{u^* \rho \, d_p}{\mu_w} \qquad \textbf{Eq. ( 7-7)}$$

$$\tau^* = \frac{u^{*2}}{Rgd_p} \qquad \textbf{Eq. ( 7-8)}$$

$$R = \frac{\rho_s - \rho}{\rho} \qquad \textbf{Eq. ( 7-9)}$$

**Table 7-1 Experimental Results for Critical Velocity of Particle Movement with Water and Fine Particles**

$d_p = 349\mu m$

| $U_B(m/s)$ | $\Delta P\ (Pa)$ | $\tau_w\ (Pa)$ | $u^*\ (m/s)$ | $N_{Re}$ | $\delta_v(\mu m)$ | $R_{ep}$ | $\tau^*$ | Entrainment | Bed Type |
|---|---|---|---|---|---|---|---|---|---|
| 0.11 | 31 | 0.142 | 0.012 | 6267 | 419 | 4.16 | 0.026 | None | Stationary |
| 0.18 | 35 | 0.164 | 0.013 | 10475 | 390 | 4.47 | 0.03 | None | Stationary |
| 0.24 | 47 | 0.218 | 0.015 | 13489 | 339 | 5.16 | 0.04 | Rolling | |
| 0.26 | 58 | 0.269 | 0.016 | 14969 | 305 | 5.73 | 0.049 | Saltation/Rolling | Dunes |
| 0.28 | 70 | 0.326 | 0.018 | 16145 | 277 | 6.3 | 0.059 | Saltation/Rolling | Dunes |
| 0.33 | 92 | 0.428 | 0.021 | 18550 | 242 | 7.22 | 0.078 | Saltation/Rolling | Dunes |
| 0.37 | 112 | 0.518 | 0.023 | 21011 | 220 | 7.94 | 0.095 | Saltation/Rolling | Dunes |
| 0.41 | 128 | 0.594 | 0.024 | 23398 | 205 | 8.51 | 0.109 | Saltation/Rolling | Dunes |
| 0.45 | 155 | 0.716 | 0.027 | 25793 | 187 | 9.34 | 0.131 | Saltation/ Suspension | Continues Moving Bed |
| 0.5 | 178 | 0.822 | 0.029 | 28255 | 174 | 10.01 | 0.15 | Saltation/ Suspension | Continues Moving Bed |
| 0.54 | 212 | 0.982 | 0.031 | 30697 | 160 | 10.94 | 0.179 | Suspension | No Bed |
| 0.58 | 228 | 1.054 | 0.032 | 33231 | 154 | 11.33 | 0.192 | | |

**Table 7-2 Experimental Results for Critical Velocity of Particle Movement with 0.05% Polymer Solution and Fine Particles**

| | $U_B(m/s)$ | $\Delta P\ (Pa)$ | $\tau_w\ (Pa)$ | $u^*\ (m/s)$ | $N_{Re}$ | $\delta_v(\mu m)$ | $R_{ep}$ | $\tau^*$ | Entrainment | Bed Type |
|---|---|---|---|---|---|---|---|---|---|---|
| $d_p = 349\mu m$ | 0.44 | 93 | 0.142 | 0.021 | 8891 | 682 | 2.56 | 0.078 | None | Stationary |
| | 0.53 | 121 | 0.558 | 0.024 | 11138 | 572 | 3.05 | 0.102 | None | Stationary |
| | 0.58 | 141 | 0.653 | 0.026 | 12582 | 515 | 3.39 | 0.119 | None | Stationary |
| | 0.64 | 163 | 0.754 | 0.027 | 14169 | 468 | 3.72 | 0.138 | None | Stationary |
| | 0.71 | 192 | 0.886 | 0.03 | 16156 | 421 | 4.14 | 0.162 | None | Stationary |
| | 0.77 | 217 | 1.006 | 0.032 | 17950 | 387 | 4.51 | 0.184 | None | Stationary |
| | 0.83 | 240 | 1.111 | 0.033 | 19490 | 362 | 4.82 | 0.203 | Rolling | |
| | 0.88 | 272 | 1.258 | 0.035 | 21212 | 334 | 5.23 | 0.23 | Rolling | |
| | 0.91 | 288 | 1.33 | 0.036 | 22101 | 322 | 5.43 | 0.243 | Saltation/Rolling | Dunes |
| | 0.94 | 317 | 1.466 | 0.038 | 23196 | 302 | 5.79 | 0.268 | Saltation/Rolling | Dunes |
| | 0.99 | 355 | 1.642 | 0.041 | 24920 | 280 | 6.24 | 0.3 | Saltation/Rolling | Dunes |
| | 1.04 | 503 | 2.328 | 0.048 | 27594 | 222 | 7.86 | 0.425 | Saltation/Rolling | Dunes |
| | 1.08 | 494 | 2.284 | 0.048 | 28695 | 225 | 7.76 | 0.417 | Saltation/Rolling | Dunes |

**Table 7-3 Experimental Results for Critical Velocity of Particle Movement with 0.1% Polymer Solution and Fine Particles**

$d_p = 349\mu m$

| $U_B(m/s)$ | $\Delta P\ (Pa)$ | $\tau_w\ (Pa)$ | $u^*\ (m/s)$ | $N_{Re}$ | $\delta_v(\mu m)$ | $R_{ep}$ | $\tau^*$ | Entrainment | Bed Type |
|---|---|---|---|---|---|---|---|---|---|
| 0.38 | 114 | 0.53 | 0.023 | 4503 | 1059 | 1.65 | 0.096 | None | Stationary |
| 0.48 | 155 | 0.716 | 0.027 | 6151 | 837 | 2.09 | 0.131 | None | Stationary |
| 0.58 | 192 | 0.887 | 0.03 | 7774 | 711 | 2.46 | 0.162 | None | Stationary |
| 0.7 | 235 | 1.087 | 0.033 | 9887 | 608 | 2.87 | 0.198 | None | Stationary |
| 0.8 | 279 | 1.291 | 0.036 | 11903 | 533 | 3.28 | 0.236 | None | Stationary |
| 0.91 | 319 | 1.476 | 0.038 | 13966 | 481 | 3.63 | 0.269 | None | Stationary |
| 0.95 | 337 | 1.557 | 0.039 | 14807 | 462 | 3.78 | 0.284 | None | Stationary |
| 0.99 | 364 | 1.685 | 0.041 | 15896 | 434 | 4.02 | 0.308 | None | Stationary |
| 1.05 | 406 | 1.877 | 0.043 | 17271 | 400 | 4.36 | 0.343 | None | Stationary |
| 1.11 | 460 | 2.128 | 0.046 | 18873 | 363 | 4.8 | 0.388 | Rolling | |
| 1.16 | 592 | 2.739 | 0.052 | 21127 | 300 | 5.83 | 0.5 | Saltation/Rolling | Dunes |
| 1.18 | 562 | 2.6 | 0.051 | 21212 | 312 | 5.6 | 0.475 | Saltation/Rolling | Dunes |
| 1.2 | 531 | 2.457 | 0.05 | 20164 | 342 | 5.11 | 0.448 | | |

**Table 7-4 Experimental Results for Critical Velocity of Particle Movement with 0.175% Polymer Solution and Fine Particles**

| | $U_B(m/s)$ | $\Delta P\ (Pa)$ | $\tau_w\ (Pa)$ | $u^*\ (m/s)$ | $N_{Re}$ | $\delta_v(\mu m)$ | $R_{ep}$ | $\tau^*$ | Entrainment | Bed Type |
|---|---|---|---|---|---|---|---|---|---|---|
| $d_p = 349\mu m$ | 0.68 | 431 | 1.99 | 0.045 | 8001 | 546 | 3.19 | 0.364 | None | Stationary |
| | 0.75 | 471 | 2.18 | 0.047 | 9079 | 502 | 3.47 | 0.398 | None | Stationary |
| | 0.81 | 505 | 2.337 | 0.048 | 10143 | 470 | 3.71 | 0.427 | None | Stationary |
| | 0.87 | 536 | 2.482 | 0.05 | 11264 | 444 | 3.93 | 0.453 | None | Stationary |
| | 0.92 | 583 | 2.695 | 0.052 | 12340 | 411 | 4.24 | 0.492 | None | Stationary |
| | 0.98 | 598 | 2.768 | 0.053 | 13281 | 401 | 4.35 | 0.505 | None | Stationary |
| | 1.04 | 629 | 2.911 | 0.054 | 14413 | 382 | 4.56 | 0.531 | None | Stationary |
| | 1.11 | 674 | 3.116 | 0.056 | 15740 | 358 | 4.87 | 0.569 | None | Stationary |
| | 1.16 | 714 | 3.302 | 0.057 | 16930 | 339 | 5.14 | 0.603 | Rolling | |

As a summary of the experiments, the critical conditions for initiation of particle movement in rolling are summarized in Table 7-5.

**Table 7-5 Critical Conditions for Rolling Motion of Fine Particles**

$d_p = 349\mu m$

| Fluid | $U_B(m/s)$ | $\Delta P\ (Pa)$ | $\tau_w\ (Pa)$ | $u^*\ (m/s)$ | $\tau^*$ | $\delta_v(\mu m)$ |
|---|---|---|---|---|---|---|
| Water | 0.24 | 47 | 0.22 | 0.015 | 0.04 | 339 |
| 0.05% | 0.83 | 240 | 1.111 | 0.033 | 0.203 | 362 |
| 0.1% | 1.11 | 460 | 2.128 | 0.046 | 0.388 | 363 |
| 0.175% | 1.16 | 714 | 3.302 | 0.057 | 0.603 | 339 |

Critical velocity at which particles starts to roll along the bed was found to be varying with the change in viscosity of the fluid. The critical velocity was about 0.24 m/s when water was used. Critical velocity of particle rolling increased up to 1.16 m/s when the fluid with highest polymer concentration was used. Critical velocities of particle rolling are also summarized in Figure 7-1. The only difference in these experiments was the viscosity of the fluids. All the other conditions such as particle diameter and initial condition of each experiment remained same in all the experiments. So, for the mean particle diameter used ($d_{50}$=349 micron), increasing fluid viscosity has a negative effect on the critical velocity at which particle rolling starts.

Critical velocity of saltation has a very similar behaviour to that of rolling. Small increase in the velocity of rolling would results in appearance of saltation type movement. In this type on motion, particles go into suspension for a very short distance before they fall into the bed again. The dominating bed form is dunes or separated sands clusters. Effect of viscosity on the velocity of saltation is exactly the same as the effect on critical velocity of rolling. Figure 7-1 also includes the critical velocity of saltation for each fluid as well. For the highest polymer concentration no saltation type movement could be achieved.

Critical velocity of suspension could only be measured for water and so no conclusion can be made about the effect of viscosity on this type of particles entrainment.

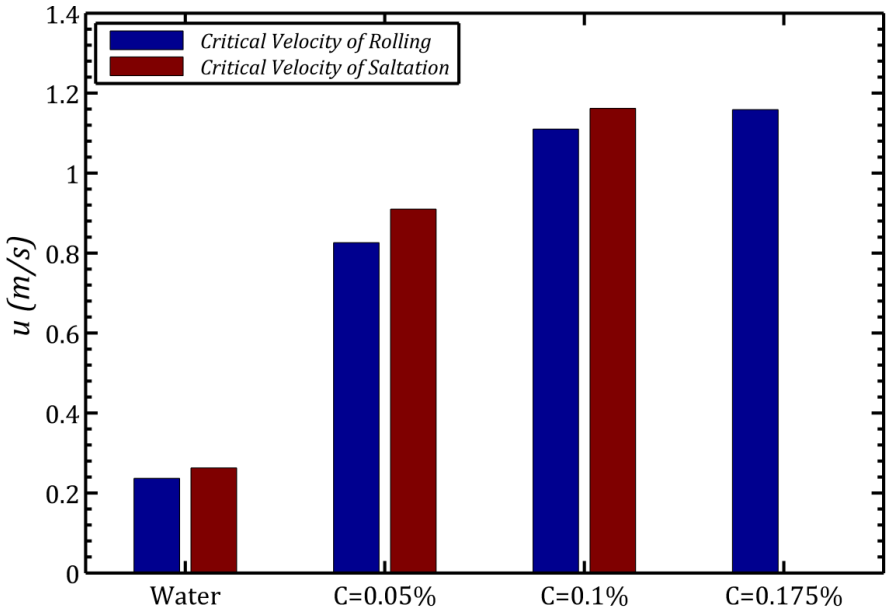


**Figure 7-1 Comparison of Critical Velocity for Initiation of Rolling and Saltation of Four Different Fluids for Fine Particles**

### 7.3.1 Critical Pressure Drops and Wall Shear Stresses at the Onset of Rolling

In this section pressure drop and wall shear stresses values corresponding to critical velocities are compared for the four fluids used in the experiments. Figure 7-2 presents the pressure drop data, which are also reported in Table 7-5.

Pressure drop measured at critical velocities where particles start to move in rolling mode increases significantly as the fluid viscosity increases. As shown in Figure 6.2, the lowest pressure drop was measured as 47 Pa when water was used to carry the solids, and the highest pressure drop was recorded as 714 Pa when fluid with the highest polymer concentration was used to carry the solids, all in rolling mode. Figure 7-2 is showing the negative effect of high viscosity on pressure drops required for particle movement when particles of micron sized are used.

Figure 7-3 presents the critical wall shear stress at which particles rolling was initiated. The critical shear stress required to initiate rolling of particles was the highest when particles were transported with fluid with highest polymer concentration.

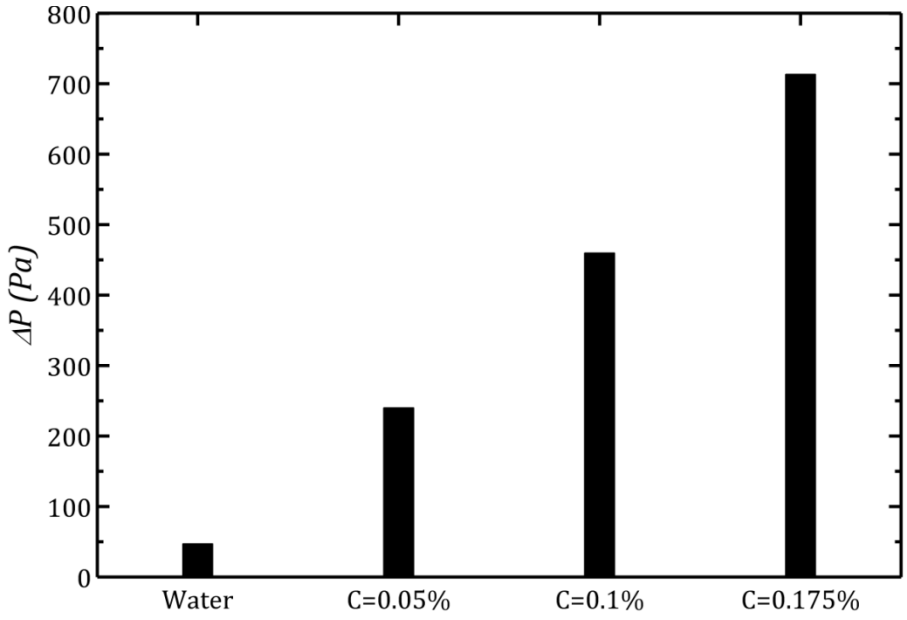


**Figure 7-2 Comparison of Critical Pressure Drops of Four Different Fluids for Fine Particle**

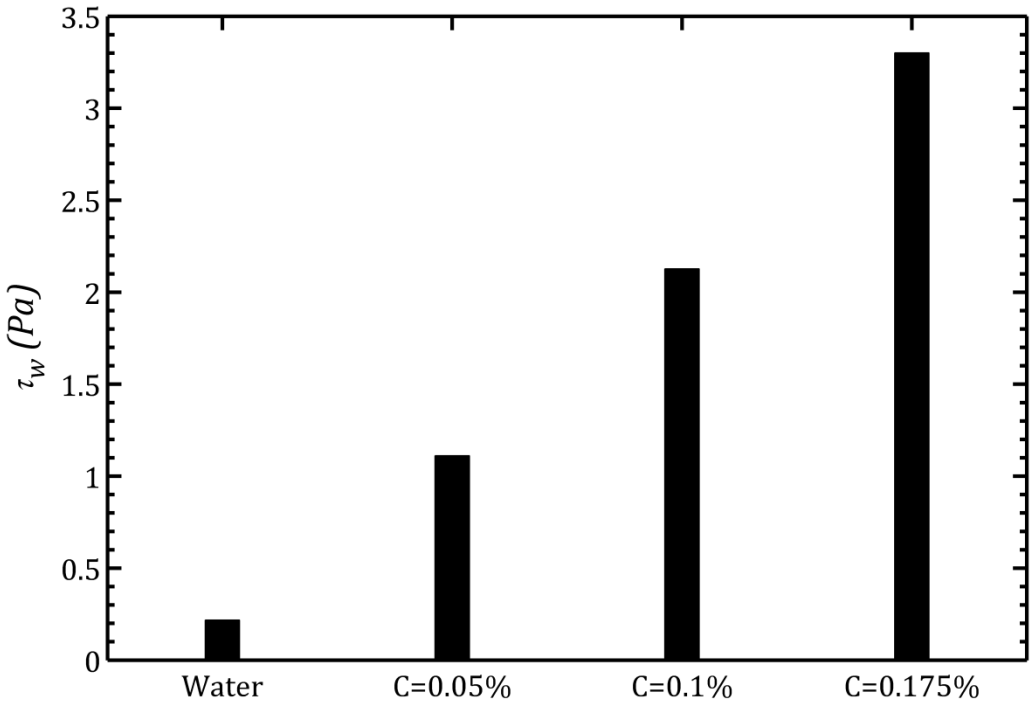


**Figure 7-3 Comparison of Critical Wall Shear Stress of Four Different Fluids for Fine particle**

### 7.3.2 Transport Velocity of Particles vs. Pressure Drop

Results from the preceding section clearly show that transport fine particles using high viscosity fluids require higher velocities and as a result, higher frictional pressure losses are anticipated. Dynamic pressure losses may be a limiting factor for cleaning long horizontal wellbore sections, therefore, the use of low viscosity fluids (or even water) is preferable most of the time. From the economics point of view, however, one of the most critical parameters is the net transport velocity of particles, which determines the time it takes to clean the hole for a given horizontal well length and ultimately, the cost of the hole cleaning job.

In the following section, we want to present and compare the net transport velocity of the fine particles when they are carried by fluids of different viscosities.

### 7.3.3 Viscous Sublayer Thickness Effect

Viscous sublayer was studied with the aid of PIV technique and the results were presented in Chapter 6. It was found that mean velocity profile follows the law of the wall near the wall ( $y^+ \leq 5$). One of the major findings of cuttings transport experiments is that the threshold of particle movement (i.e., critical velocity of particle rolling) is related to the viscous sublayer thickness. The following section presents the results and discussion on how the viscous sublayer thickness relate to critical velocity of particle movement by rolling.

Experimental results presented in Chapter 6 have shown that in the near wall region ( $y^+ \leq 5$ ) Reynolds stresses are zero and viscous stresses are dominating. Velocity gradient is high but magnitude of velocity itself is much lower that the velocity in the core flow of a turbulent flow.

Particles which are at rest on the bed deposits are under the effect of several forces related to dynamic flow conditions. These forces can be categorized into two groups, holding forces and lifting forces. Holding forces are net weight and adhesion force. For the range of particle diameters used in this study ($d_{50}$ = 349 micron), the adhesion forces arising from Van Der Waals effect may be neglected. Adhesion force is dominant for very fine particles with mean diameter usually less than 60 micron. The lifting forces are mainly the drag force and other forces which are related to turbulence (i.e., updraft under a burst).

Before attempting any explanation of forces acting on solid particles within the turbulent boundary layer, the definition of critical conditions for particle movement needs to define properly. It is the condition at which particles in a bed start to move at a high flux rate. There may be some particle movement at conditions well below the critical one but these movements are very rare and occasional.

If the particle diameter is sufficiently small, so that it can be hidden within the viscous sublayer, the only force which may cause this particle to be entrained into the flow is the so called updraft under a burst. This force arises as a result of coherent structures and causes the particles to be directly suspended in a saltation type movement. The frequency of bursts and sweeps and the level of turbulence are important in considering this force. Within the experimental conditions of this study (i.e., particle size range and fluid Reynolds number), no significant movement of particles were observed which could be attributed by this type of lifting forces. There were some instances where occasional particle entrainment was observed, but the flux rate of particle movement was very low and considered negligible.

With the given definition of threshold of particle motion and also considering the particle diameter, it seems that the main force responsible for moving the particles would be the drag force. This force is direct function of the difference between the fluid and particle velocity (i.e. if the particle is stagnant this velocity would be the fluid velocity). Now referring to earlier discussion on velocity in the viscous sublayer, it is expected that if a particle is completely submerged in the viscous sublayer, the drag force on that particle will be very small. On the other hand, if that particle is in the outer region of the flow or even if some part of that particle is exposed to the core flow where the velocity is high, that particle would experience a much higher drag force than the one which is hidden in the sublayer. This high drag force would cause the particle movement.

The definition of the drag force is given by the Eq. ( 7-10) .

$$F_D = \frac{1}{2}\rho v^2 C_D A \qquad \textbf{Eq. ( 7-10)}$$

Because the velocity is very low in the viscous sublayer, the drag force would be negligible for a particle which is completely submerged in this thin fluid layer. Drag force

is effective where the particles are big enough or the viscous sublayer is thin enough which as a result, creates a condition at where larger surface area of particles are exposed ( i.e., larger projection area in drag equation) to the outer region of the flow where the velocity is higher. So in order to increase the drag force on a particle, one should reduce the viscous sublayer thickness until the particle is exposed to the outer region of the flow. Also it is known that drag force on a particle is in the direction of the flow which means this force would rather move the particles in a rolling and sliding type motion rather than lifting them up and entraining them.

Figure 7-5 shows the thickness of the viscous sublayer in relation to particle size. The thickness of the boundary layer is calculated at critical condition of particle movement for the all the fluids used. Note that the viscous sublayer is assumed to be extending up to a dimensionless wall unit of 5.

A two layer bed is assumed in calculation of viscous sublayer thickness; a bottom stationary and uniform layer and a top layer, which is composed of individual particles which are not continuously attached to each other. The sublayer is then assumed to start from the top of the bottom layer of cuttings (Figure 7-4).

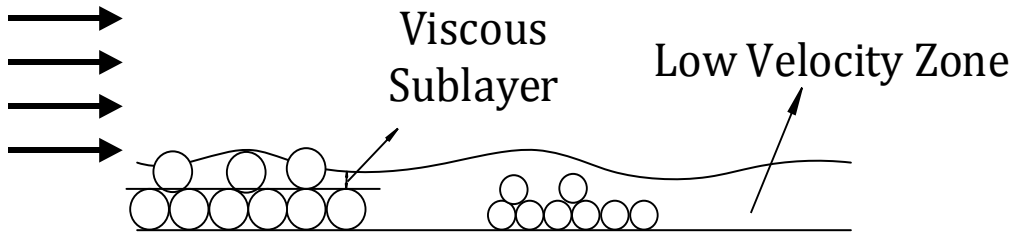


**Figure 7-4 Schematic of Viscous Sublayer and Two Layer Bed Model**

The definition of viscous sublayer thickness is given by the following equation:

$$\delta_v = \frac{5\mu_w}{\rho u^*} \qquad \textbf{Eq. ( 7-11)}$$

Equation 7-11 has been used to calculate the viscous sublayer thickness. In this equation, viscosity at the wall and friction velocity is used.

Figure 7-5 shows the viscous sublayer thickness calculated at the onset of particles motion (i.e., rolling) for water and fluids with 3 different polymer concentrations. Onset

of particles movement for all the four different fluids observed more or less at the similar thicknesses of the viscous sublayer. This in fact is the only parameter, which has the same order of magnitude for all the fluids studied regardless of viscosity.

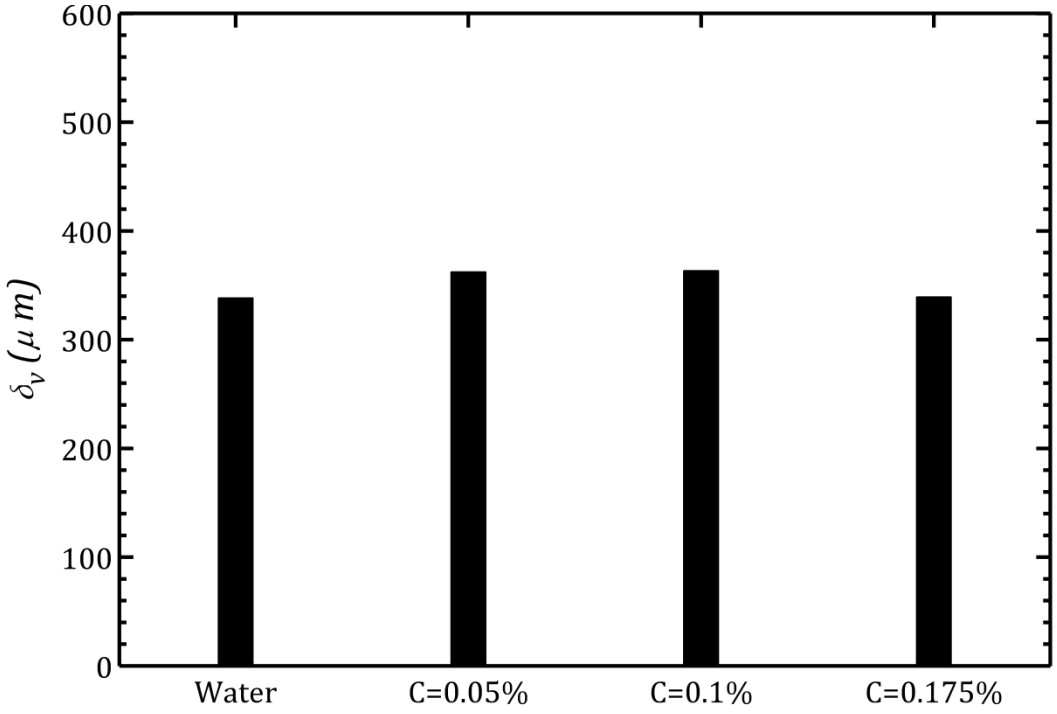


**Figure 7-5 Viscous Sublayer Thickness at the onset of Particle Motion**

Other interesting phenomena shown in Figure 7-5 is that the critical viscous sublayer thickness is very close to the mean diameter of the particles used (349 micron). That means unless the particle diameter is close to the viscous sublayer thickness no significant removal of particles from the bed could be observed. The reason being is the importance and impact of drag force on particles. Unless the particle is big enough to have a significant projection area in the core flow (where the velocity and consequently drag force are high) the chance for removing that particle is low.

Figure 7-6 to Figure 7-9 show the viscous sublayer thickness against bulk velocity for all the fluids studied. These plots also include the critical velocity at which rolling of the particles starts along with the mean diameter of the particles.

One important observation from the results presented in Figure 7-6 to Figure 7-9 is that in all the cases, the observed critical velocities are so close to the intersection of the viscous sublayer thickness and particle diameter. Therefore, it is concluded that the bed

of particles will not start moving unless the thickness of the viscous sublayer is close or smaller than the mean diameter of the particles.

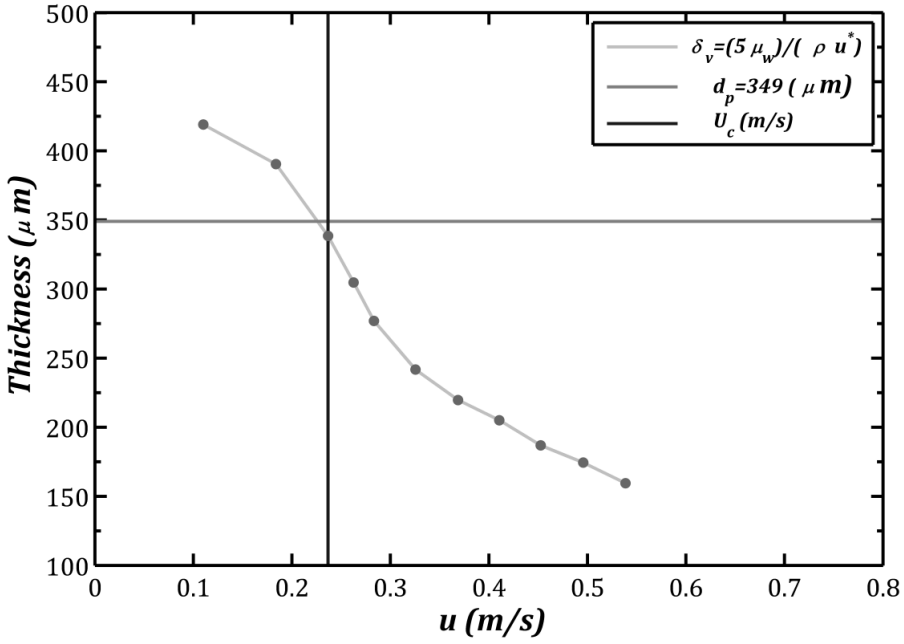


**Figure 7-6 Viscous Syblayer Thickness versus Bulk Velocity and Critical Velocity of Motion for Water and Fine Particles**

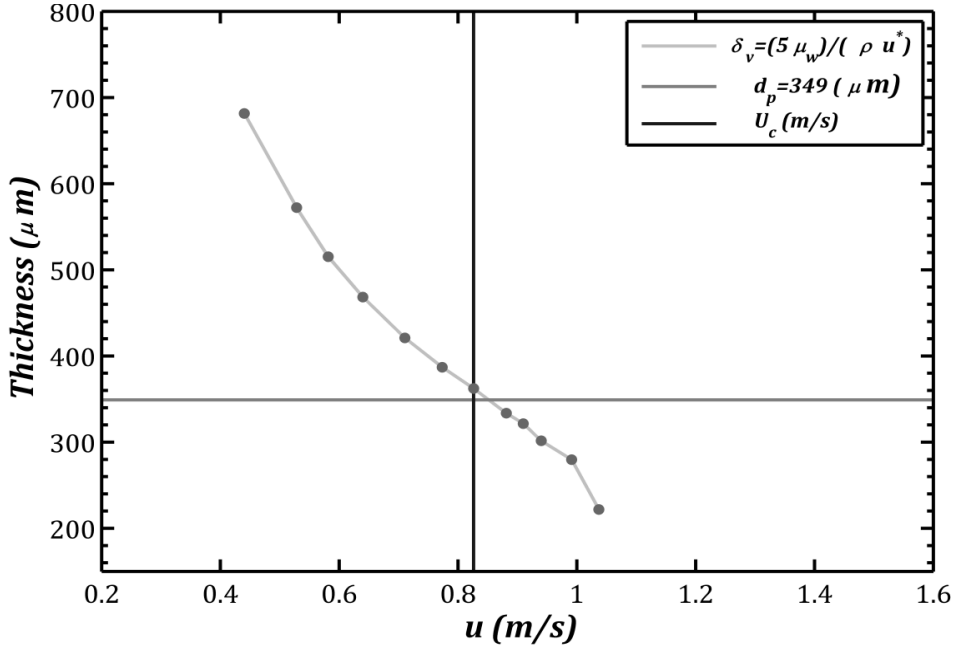


**Figure 7-7 Viscous Syblayer Thickness versus Bulk Velocity and Critical Velocity of Motion for 0.05% Polymer Solution and Fine Particles**

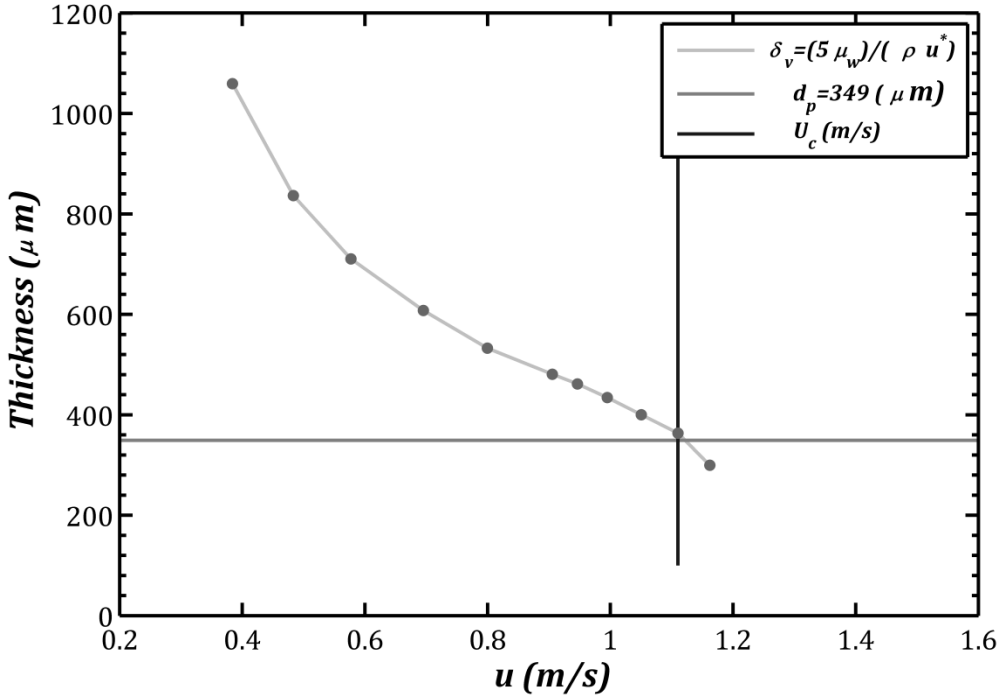


**Figure 7-8 Viscous Syblayer Thickness versus Bulk Velocity and Critical Velocity of Motion for 0.1% Polymer Solution and Fine Particles**

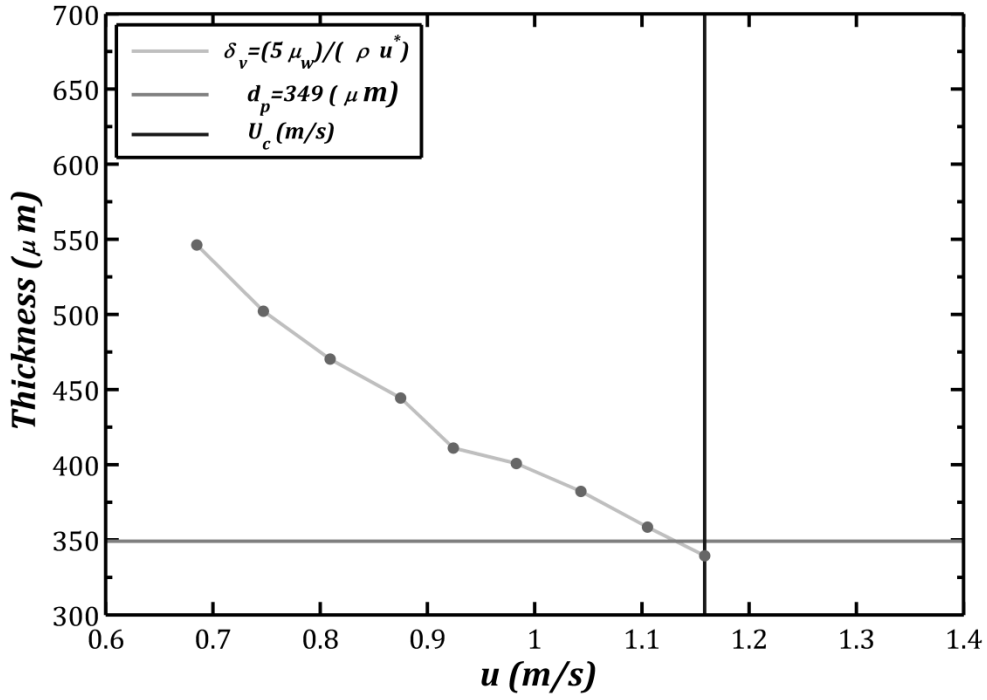


**Figure 7-9 0.175 Viscous Syblayer Thickness versus Bulk Velocity and Critical Velocity of Motion for 0.175% Polymer Solution and Fine Particles**

To explain the effect of viscous sublayer thickness on the initiation of particle movement, the Eq. ( 7-10), which describes the drag force, may be used. The sufficient reason for a particle to start moving along the bed is that lifting forces to overcome or become even with the holding forces. For particle rolling, the momentum of different forces must be equal around the resting point of the particle on top of other particles. Due to small diameter of the particles, the holding forces (which are net weight and friction between particles) are not really big and so small lifting forces may cause the particle movement. Based on the drag force equation, the reference area (i.e., surface area of the particle exposed to core flow) and velocity difference is low in viscous sublayer resulting very low drag force acting on the particle. Therefore, the lifting forces on the particles submerged in the viscous sublayer are negligible because the drag force acting on these particles are negligible. .

As soon as the sublayer thickness becomes less than mean diameter of the particles, the drag force increases rapidly and because the holding forces are not big, the rolling of particles along the bed would start immediately at this point.

In summary; effect of fluid viscosity on the threshold of motion of micron size particles was investigated. Particles used were uniform in size and had a mean diameter of 349 micron. One Newtonian fluid (water) and three polymer solutions (0.05%, 0.1% and 0.175%) were tested. The effect of increasing fluid viscosity was found to be increasing the magnitude of critical velocity of rolling for fine particles. The critical velocity of rolling occurred to be around 0.24 m/s for water. It could be as high as 1.16 m/s for the highest viscosity polymer solution tested. The effect of viscosity on critical pressure drops and wall shear stress were found to be similar to its effect on critical velocity. Viscous sublayer thickness was found to be in direct relationship with the critical velocity of rolling for all the fluids tested. This thickness was found to be very close to the mean diameter of particles at the onset of particle motion, which implies that unless the viscous sublayer is thinner than mean diameter of particles no, significant particle movement could be achieved.

### 7.3.4 A New Criteria for the Initiation of Fine Particles Rolling Movement with Power Law Fluids

The discussion presented in the previous section provided the evidence for the relation between the viscous sublayer thickness and critical velocity of rolling. Following

this discussion, it can be proposed that at the start of rolling, boundary layer thickness should be equal or less than the particle diameter:.

$$\delta_v = d_p \qquad \textbf{Eq. ( 7-12)}$$

Using the definition of viscous sublayer thickness (Eq. ( 7-11)), and initiation criteria for particle movement (Eq. ( 7-12)), the friction velocity at the point of rolling for the fine particles can be defined as follows:

$$u^* = \frac{5\mu_w}{\rho d_p} \qquad \textbf{Eq. ( 7-13)}$$

In the derivation of Eq. (6-13), it was assumed that as soon as the sublayer thickness becomes equal to the diameter of the particle, the particle will start rolling due to drag force. Further simplification of this equation could be obtained by introducing a rheology model.

Rheology model for power law fluids is given as:

$$\tau_w = k{\gamma_w}^n \qquad \textbf{Eq. ( 7-14)}$$

For a power law fluid the viscosity at the wall, ( $\mu_w$), is related to wall shear rate, ($\gamma_w$), as shown by Eq. ( 7-15).

$$\mu_w = k{\gamma_w}^{n-1} \qquad \textbf{Eq. ( 7-15)}$$

The experimental data shown in Chapter-6 confirmed that viscous stresses are dominating in the viscous sublayer (i.e., Reynolds stresses are negligible). Therefore, the equation describing the viscous stress should be adequate to estimate the total stress, which is also to the wall shear stress. The wall shear stress is then introduced into the rheology model (Eq. ( 7-14)) to obtain the corresponding shear rate at that shear stress.

$$\gamma_w = (\frac{1}{k}\tau_w)^{\frac{1}{n}}$$ **Eq. ( 7-16)**

And finally, the Eq. ( 7-17)is obtained, which describes the viscosity at the wall.

$$\mu_w = k^{\frac{1}{n}}\,\tau_w^{\frac{n-1}{n}}$$ **Eq. ( 7-17)**

The definition of shear velocity is given as;

$$u^* = \sqrt{\frac{\tau_w}{\rho}}$$ **Eq. ( 7-18)**

By substitution and simplification, the following form of critical wall shear stress required for the initiation of fine particle movement by rolling with a power law type fluid is obtained.

$$\tau_{wc} = \left[\frac{5k^{\frac{1}{n}}}{\sqrt{\rho}\,d_p}\right]^{\frac{2n}{2-n}}$$ **Eq. ( 7-19)**

Newtonian fluid case: for the limiting case of Newtonian fluids where n=1 and k is the viscosity of the fluid the Eq. ( 7-19)reduces to:

$$\tau_{wc} = \left[\frac{5\mu}{\sqrt{\rho}\,d_p}\right]^2$$ **Eq. ( 7-20)**

### 7.3.5 Comparison of Proposed Model Prediction with Actual Experimental Data

Predictions of the critical wall shear stress required for the initiation fine particle movement with rolling using the proposed model (Eq. ( 7-19)) were compared with the experimentally measured data. Figure 7-10 and Figure 7-11shows the comparison of measured and predicted values of critical wall shear stress and critical pressure drop for the initiation of particle movement with rolling. Table 7-6 presents the summary of this comparison.

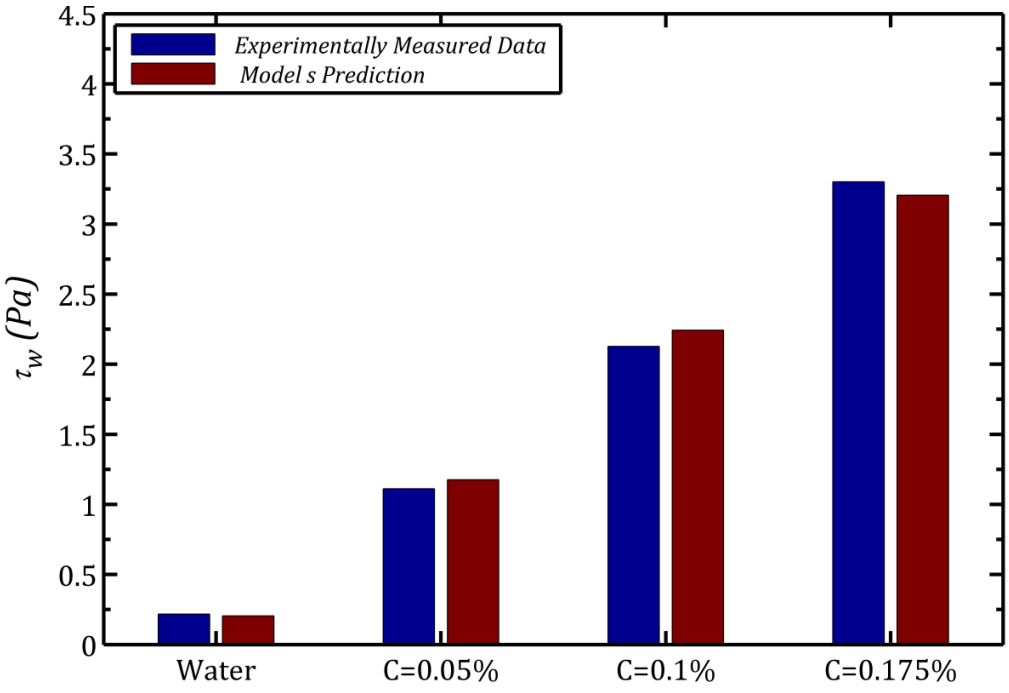


**Figure 7-10 Comparison of Predicted Critical Wall Shear Stress with Actual Experimental Data for Fine Particles**

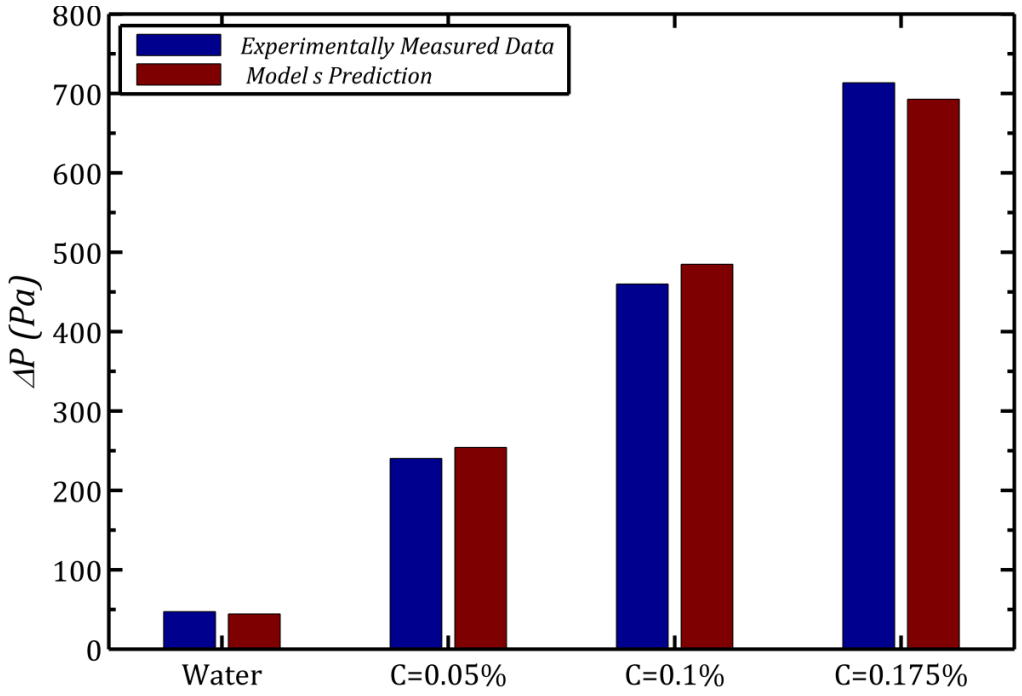


**Figure 7-11 Comparison of Predicted Critical Pressure Drops with Actual Experimental Data for Fine Particles**

**Table 7-6 Comparison of Experimentally Measured Critical Wall Shear Stress with Prediction of the Model**

| Fluid | Measured (Pa) | Model Prediction(Pa) | Error (%) |
|---|---|---|---|
| Water | 0.218 | 0.205 | 5.9 |
| 0.05% | 1.111 | 1.176 | -5.8 |
| 0.1% | 2.127 | 2.243 | -5.4 |
| 0.175% | 3.301 | 3.205 | 2.9 |

A good agreement is observed between the predicted critical wall stress values and the experimentally measured data. The error of prediction is between -5 to +5% which is acceptable and may be related to errors in experimental measurements.

#### 7.3.5.1 Effect of Rheology on the Critical Wall Shear Stress for the Initiation of Particle Movement in Rolling

Using the model presented in the previous section, the critical wall stress for the initiation of particle movement in rolling is calculated and compared for different fluid

viscosity conditions. It is expected that this model is valid within the range of conditions under which it was developed. Range of particle diameter was varying from 150 micron to 800 micron. The lower and upper limit of applicability of this model needs to be validated through experimental results.

Figure 7-12 contains the data which were obtained by using the model, over a range of particle diameter and fluid viscosity, in a linear scale plot. The data indicate that the thinner fluid requires lower critical wall shear stress to initiate particle movement in rolling.

A similar plot but in log-log scale is provided in Figure 7-13. This plot shows the difference between the performances of different fluids in the low diameter range better than the Figure 6-12. plot.

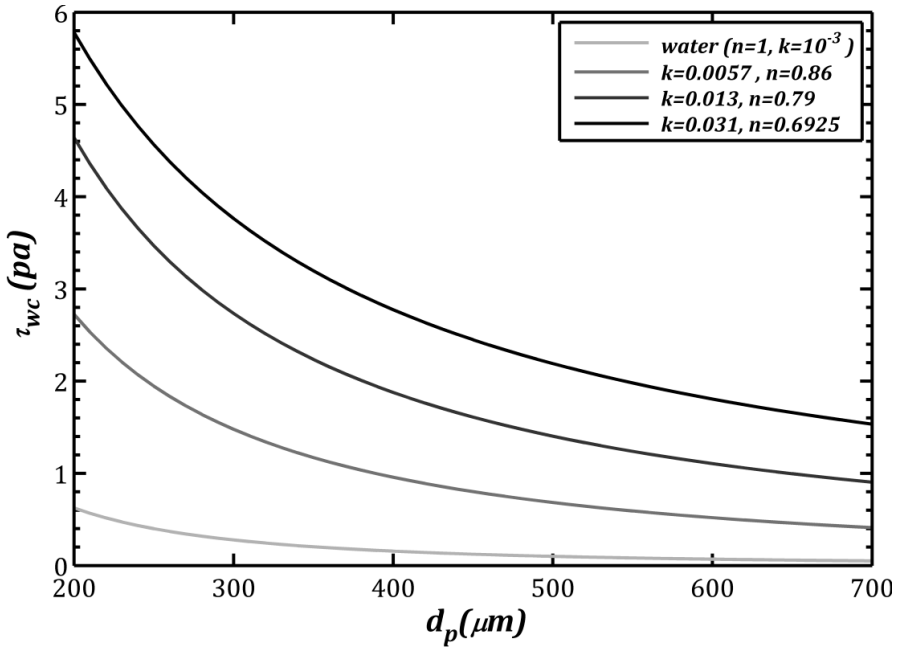


**Figure 7-12 Comparison of Critical Wall Shear Stress for Different Fluids and Particles in Linear Scale Plot**

As shown in Figure 7-13 , in order to roll particles of 100 micron size along the bed, a shear stress more than 10 Pa should be exerted to the bed when a thick fluid is used (0.175%). This was virtually impossible in the operational limits of the horizontal flow loop used in this study. Generally, as the particle diameter increases the critical wall shear

stress required for particle rolling decreases, which means increasing particle diameter has a positive effect on the critical stress.

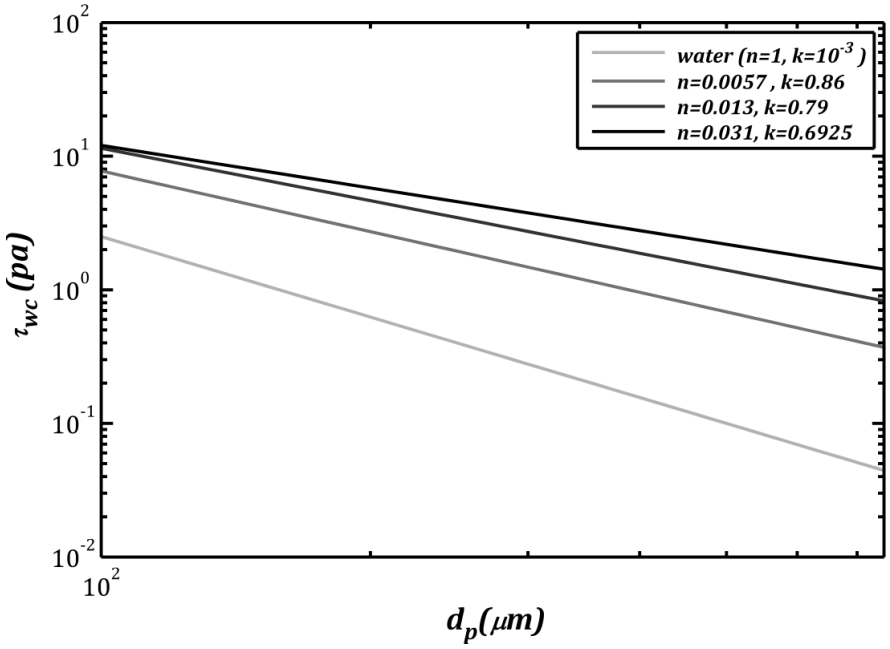


**Figure 7-13 Comparison of Critical Wall Shear Stress for Different Fluids and Particles in Log-Log Scale Plot**

### 7.3.6 Formation of Certain Types of Bed Forms

In the previous section, critical conditions required for initiation of different types of particle motion has been discussed. Generally, at different velocities, different bed morphology has been observed. The existence of different bed types in term of shape and entrainment mode of particles have also been reported in past studies [18]. At velocities lower than that of critical velocity of rolling, continues stationary bed is expected to exist. In this type of beds (Figure 7-14), the cuttings are forming a continuous bed in which particles are static.

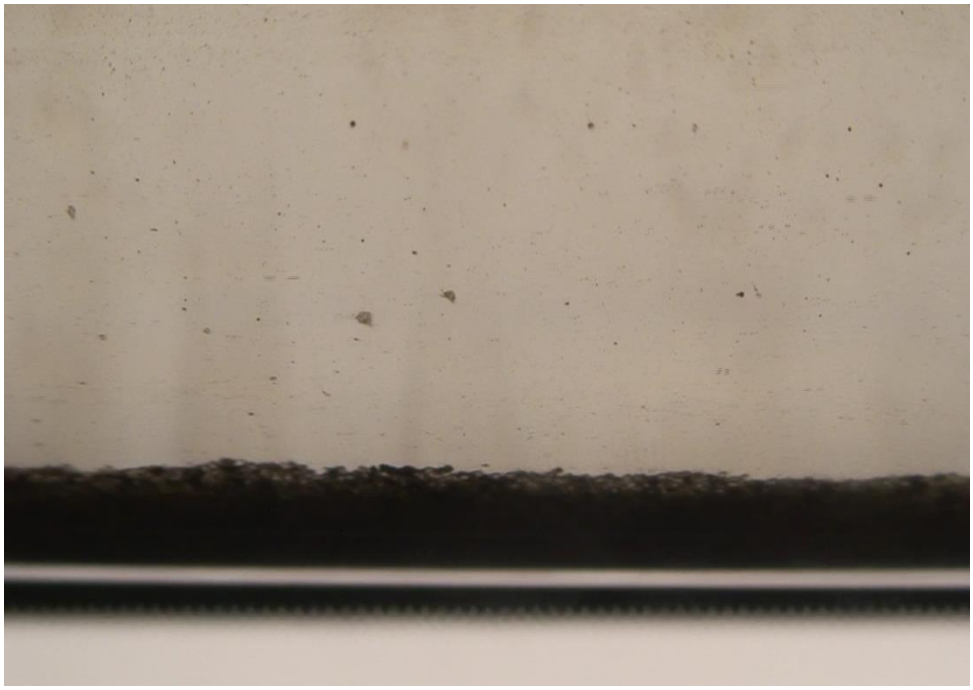

**Figure 7-14 Picture of a Stationary Bed of Particles**

Further increasing the velocity of the fluid, a critical velocity will be encountered at which particles start to roll and in some instances slide along the bed. At this velocity the bed type is still continues but not stationary any longer. Although the shape of the bed is similar to previous domain, but there is an active layer of cuttings which are moving on top of a stationary layer of cuttings. The two layer bed which has been explained previously is expected to exist in this regime. Some investigators have named this regime as continues moving bed.

Dunes or separate moving beds (Figure 7-15) form at higher velocities than that of critical velocity of rolling. Dominating mechanism of particle movement in this regime is a combination of rolling and saltation. From the experimental results reported in Table 7-1 to Table 7-4, it has been observed that dunes are the dominating bed forms for intermediated velocities. In this regime, cuttings tend to form sand clusters and move in the form of separate dunes. Cuttings move in a saltation type movement for a short distance before they fall to the bed again. It has been observed that presence of dunes is associated with big pressure fluctuations, especially with polymeric liquids. Also dunes move at a velocity which has been found to be proportional to the fluid bulk velocity. Calculation and discussion on pressure variation and dunes velocities are given in next sections.

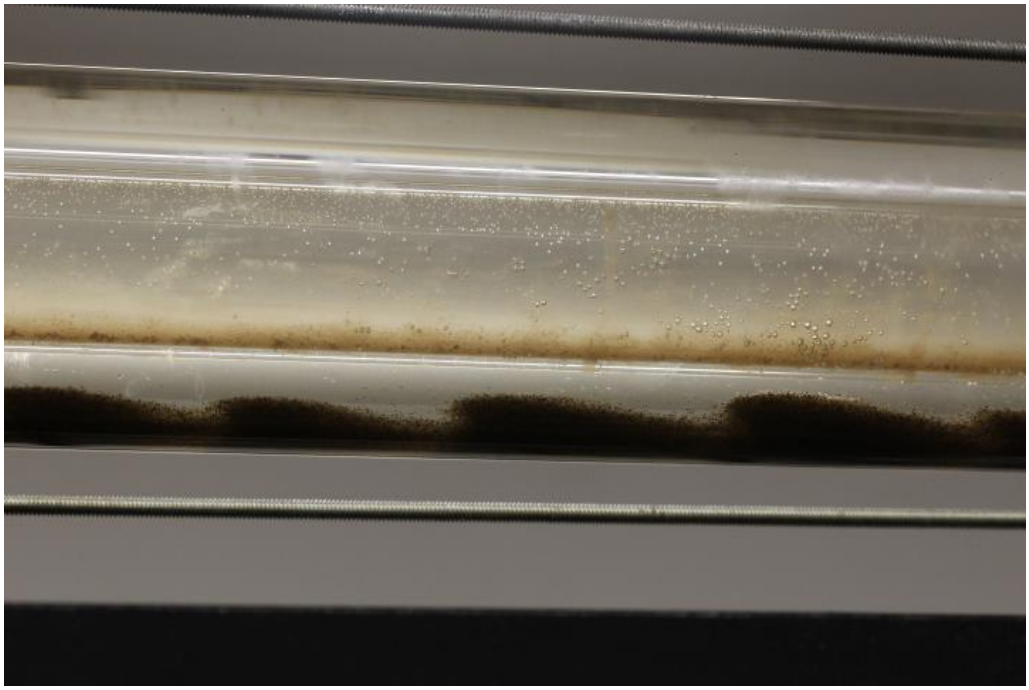

**Figure 7-15 Typical Shape of Dunes for Experiments with Water and Fine Particles**

By increasing the velocity sufficiently, the dunes and sand clusters starts to flatten and form continues bed again. Unlike the continues bed described before, this bed is not stationary and cannot be assumes as a two layer bed. This bed is rather a sliding and moving bed. The whole bed is moving along the pipe wall and there is no stationary layer of cuttings anymore. Suspension and saltation are the main mechanism of cutting transport in this regime. Also the bed slides along the pipe wall. Some investigators named this regime as heterogeneous suspension (Figure 7-16).

At very high velocities, the cuttings start to go into full suspension. In this regime there is no bed any longer which makes it different from the previous regime.

Summary: different bed types occur at different fluid velocities. At low velocities the bed is stationary with no significant movement of the cuttings. At velocities higher than critical velocity of rolling, sand dunes start to form. Main mechanism of particles movement is a combination of saltation and rolling in this domain. One of distinct features of this regime is the fluctuations of pressure drops due to presence of sand clusters. Heterogeneous bed in which particles move in a suspension and saltation type movement is the next regime. In this regime there is a sliding bed which moves along the

wall of the pipe. Full suspension in which no bed appears anymore occurs at highest velocities. In this regime particles move in full suspension.

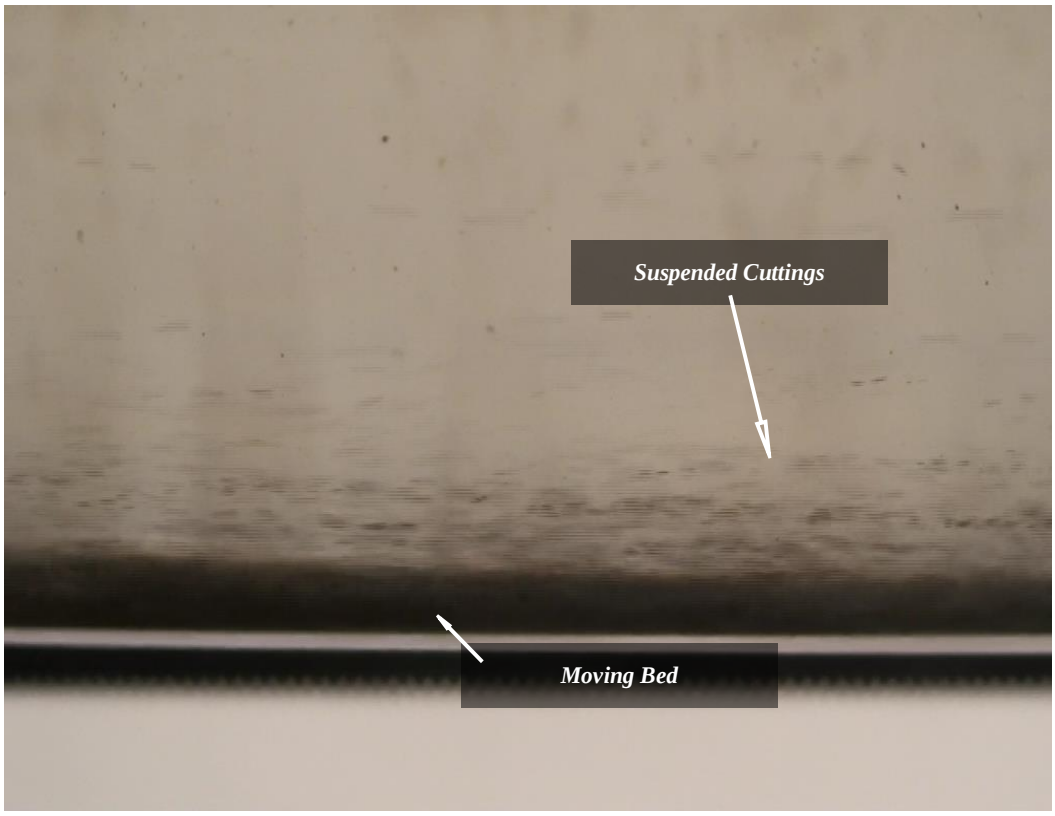


**Figure 7-16 Typical form of Heterogeneous Suspension Regime; Note that there is still a Bed of Particles on the Pipe wall**

### 7.3.7 Detection of Different Regimes

In order to detect different regimes of sediment transport, two alternative ways can be used. First option is to visually observe the bed form and identify the regime. This alternative requires a transparent section of the test facility. Although this may be convenient for laboratory experiments, in real drilling case this is not applicable. Second option which has been proposed by some investigators is to use the pressure drops data [28]. Usually presences of different types of beds are associated with different pressure drops in term of pressure fluctuations and correlation with other parameters. Transition from one regime to another should be detectable from pressure loss data. The dunes domain may be detected by observing big pressure fluctuations. In the stationary bed or continuous bed form, a linear variation of pressure losses with bulk velocity is expected.

It has been explained in chapter 3 that pressure loss in this study has been measured with the aid of a differential pressure transducer and LabView software at a frequency equal to 20Hz. Mean value of the recorded pressure losses for all the fluids studied which have been reported earlier in Table 7-1 to Table 7-4, are plotted versus bulk velocity of the fluids in Figure 7-17 to Figure 7-20. From the data presented in these figures it is obvious that pressure drops for velocities lower than that of critical velocity of rolling always have a linear correlation with bulk velocity of the fluid. Once the critical velocity of rolling is encountered, an increase in the slope of the line which fits the pressure drops is observed. Although after passing the critical velocity, pressure drops still correlates lineally with bulk velocity, but the slope of the line is higher comparing to previous domain. This domain is associated with presence of dunes which have been explained to cause huge pressure fluctuations. These fluctuations cause the data to deviate from a linear correlation. The fluctuations of pressure data are more pronounced in the case of polymeric liquids. The reason being is that the distance between dunes or separated moving bed is higher for polymers which cause bigger fluctuations in pressure data. It is expected that by increasing bulk velocity one should be able to see all the different regimes in pressure drops. The last regime which has been observed in the presented study is homogenous suspension. Although this regime could be observed only for water, but from the pressure drops a change in the slope of the line comparing to dunes domain could be observed.

In general, there are two important conclusions from pressure loss data. One is that there is a change in the slope of the pressure drops versus bulk velocity once transition from one regime to another took place. The other conclusion is that in all the different regimes, pressure drops always show a linear correlation with bulk velocity.

Summary: pressure drops data has been plotted against bulk velocity for detection of transition from one regime to another. A linear correlation has been found to best represent pressure losses in each regime. A sudden increase in the slope of pressure drops has been observed at the onset of the transitions from stationary bed to separated sand dunes. Transition from dunes to suspended load was also observed in pressure drops data.

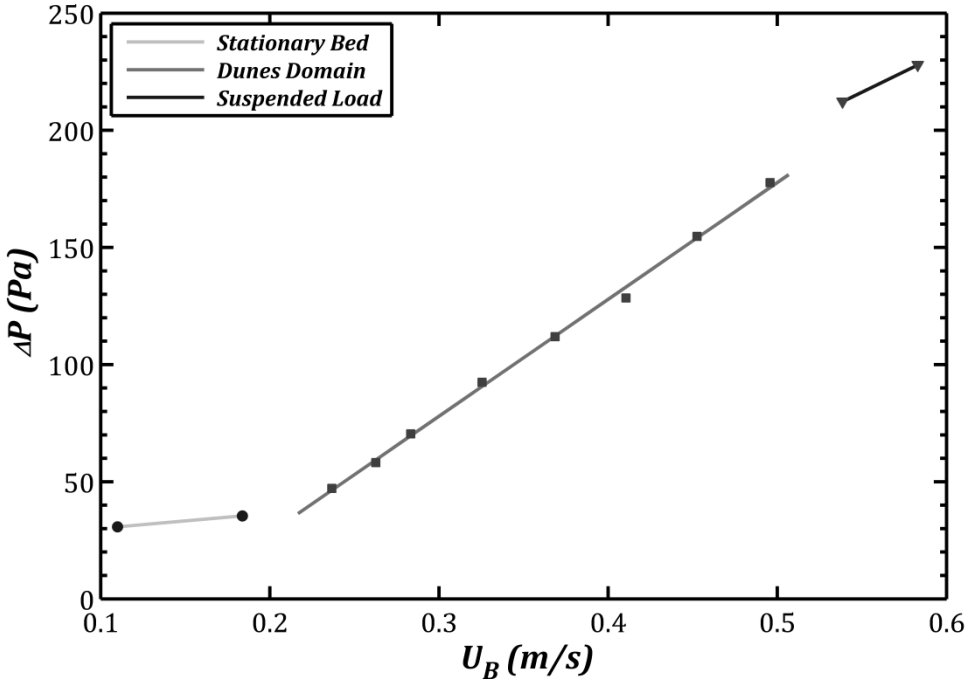


**Figure 7-17 Pressure Drops versus Bulk Velocity for Water and Experiments with Fine Particles**

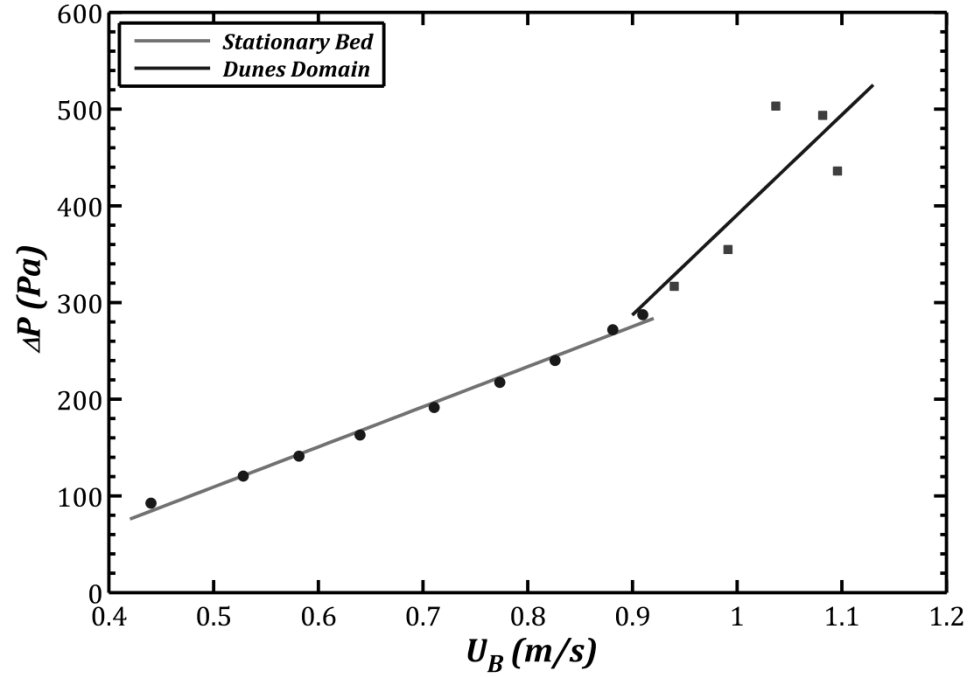


**Figure 7-18 Pressure Drops versus Bulk Velocity for 0.05% Polymer Solution and Experiments with Fine Particles**

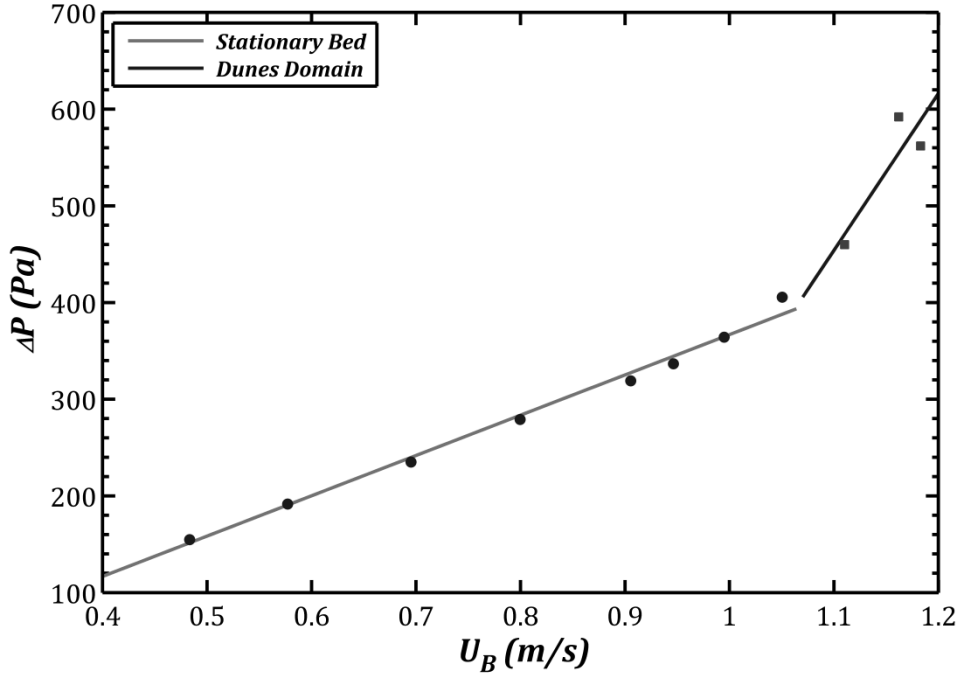


**Figure 7-19 Pressure Drops versus Bulk Velocity for 0.05% Polymer Solution and Experiments with Fine Particles**

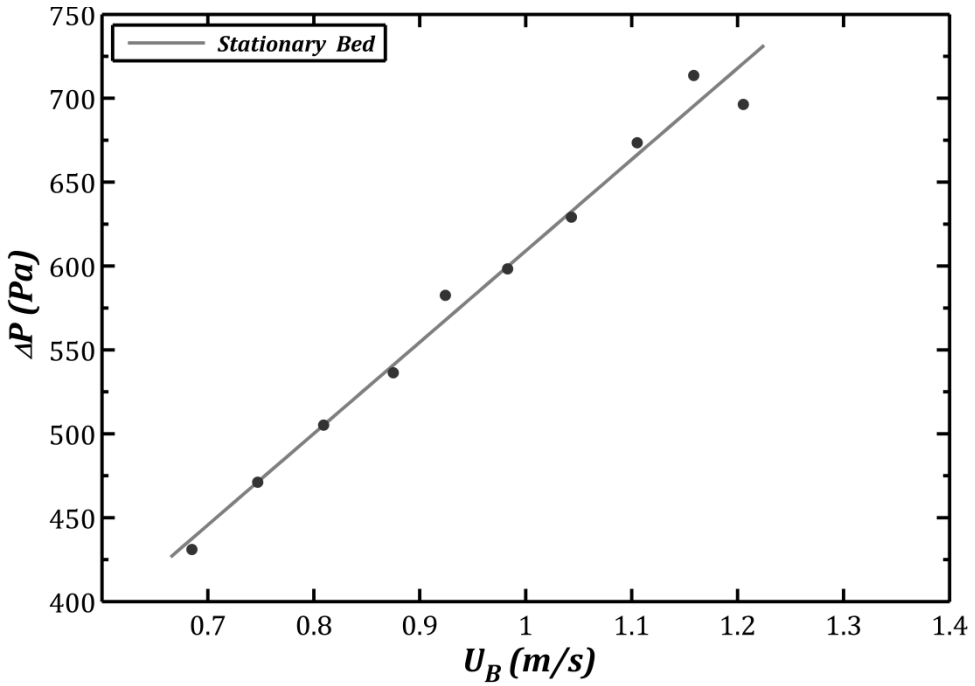


**Figure 7-20 Pressure Drops versus Bulk Velocity for 0.1755% Polymer Solution and Experiments with Fine Particles**

Another feature of pressure drops data is the scattering of pressure data in dunes regime. The scattering of the data is caused by pressure fluctuations induced by presence of separated sand clusters. These fluctuations are bigger for polymer solutions than water. The reason being is the distance between two dunes. This distance increase as the velocity of the fluid increases. Generally for water, the dunes move so close to each other, but for polymer solutions the distance between dunes is big. Figure 7-21 is a typical pressure drop data for dunes domain when experimenting with water. It is obvious that fluctuation of recorded data around the reported mean value is not significant. Figure 7-22, on the other hand, represents a typical pressure variation in dunes domain for polymer solutions. Apparently, the fluctuations around the mean value are so big and any number could be taken for the pressure readings in this figure.

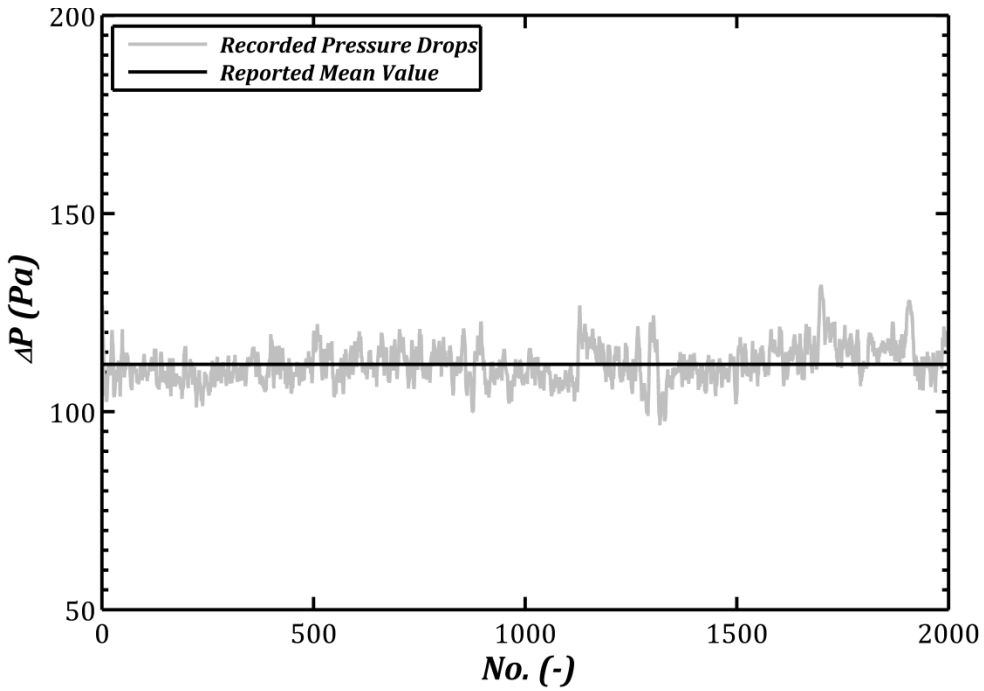


**Figure 7-21 Typical Pressure Drops Variation in Dunes Domain for Water and Fine Particles**

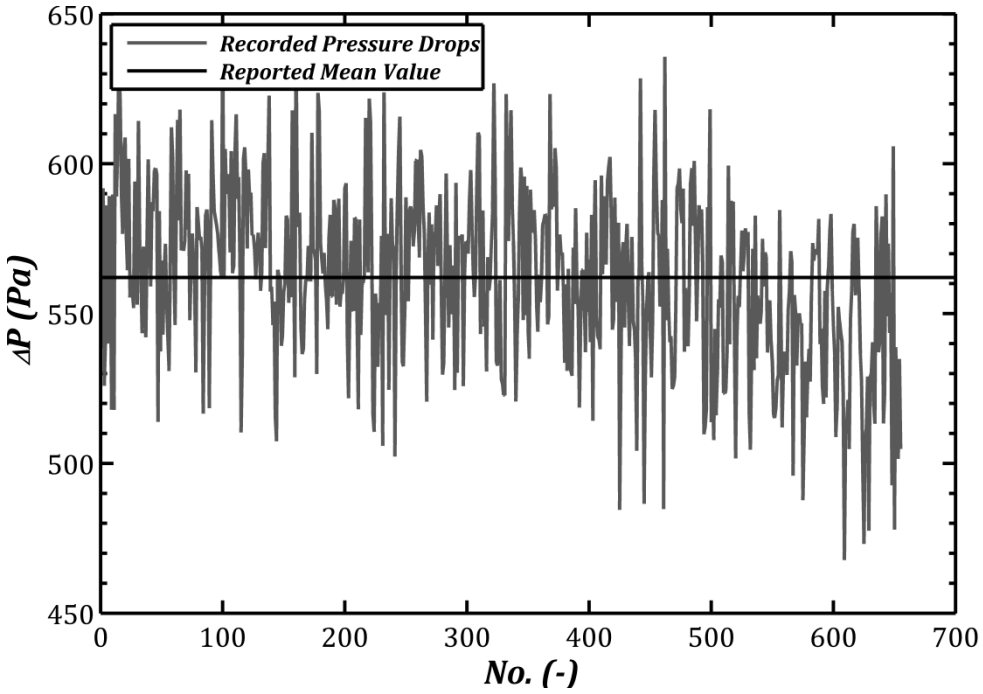


**Figure 7-22 Typical Pressure Drops Variation in Dunes Domain for Polymer Solutions and Fine Particles**

### 7.3.8 Pressure Drops

In previous section it is been shown that pressure drops in different regimes can be represented by a linear correlation. In this section a comparison between pressures drops associated with slurry transport for different fluids is reported. The lines which have been found to fit the pressure drops are used in this section rather than the actual readings.

From the pressure reading (Figure 7-23 to Figure 7-25) no general conclusion could be made about the performance of different fluids in term of pressure loss. That is because critical velocity of rolling and also dunes domains occur and considerably lower velocities for water comparing to polymer solutions. When the performance of polymer solutions are compared with each other, an increase in the pressure drop can be observed with increasing viscosity. In fact, the adverse effect of high viscosity could be seen in these figures. Another conclusion based on Figure 7-25 is that the slope of the pressure drops seems to be similar for all the polymer solutions in the stationary bed regime. For dunes domain, however, no conclusion could be drawn.

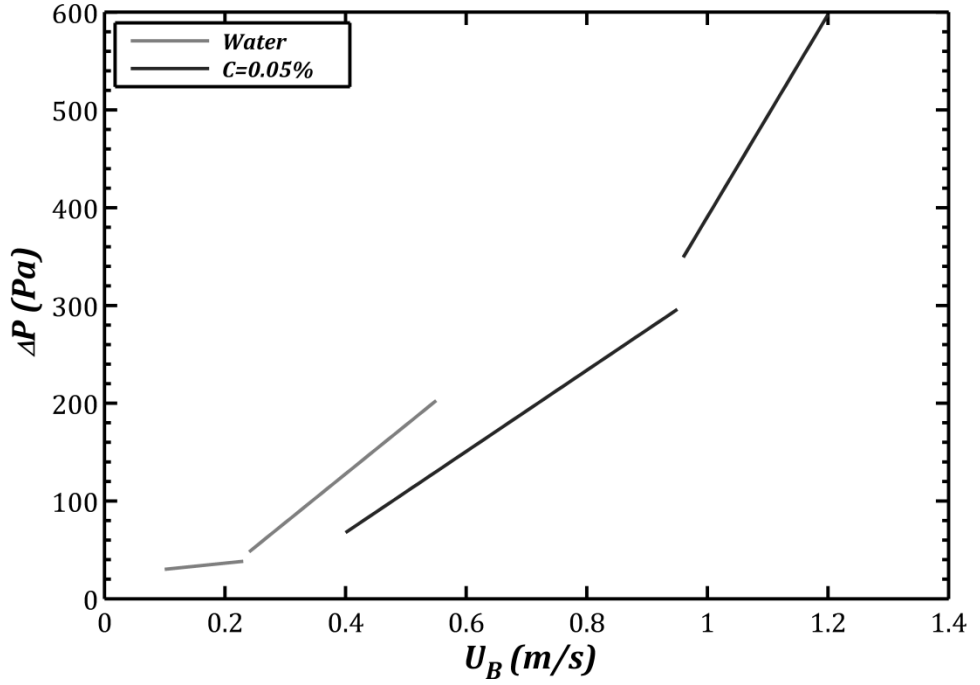


**Figure 7-23 Comparison of Pressure Drops Encountered in Transporting Fine Particles with Water and 0.05% Polymer Solution**

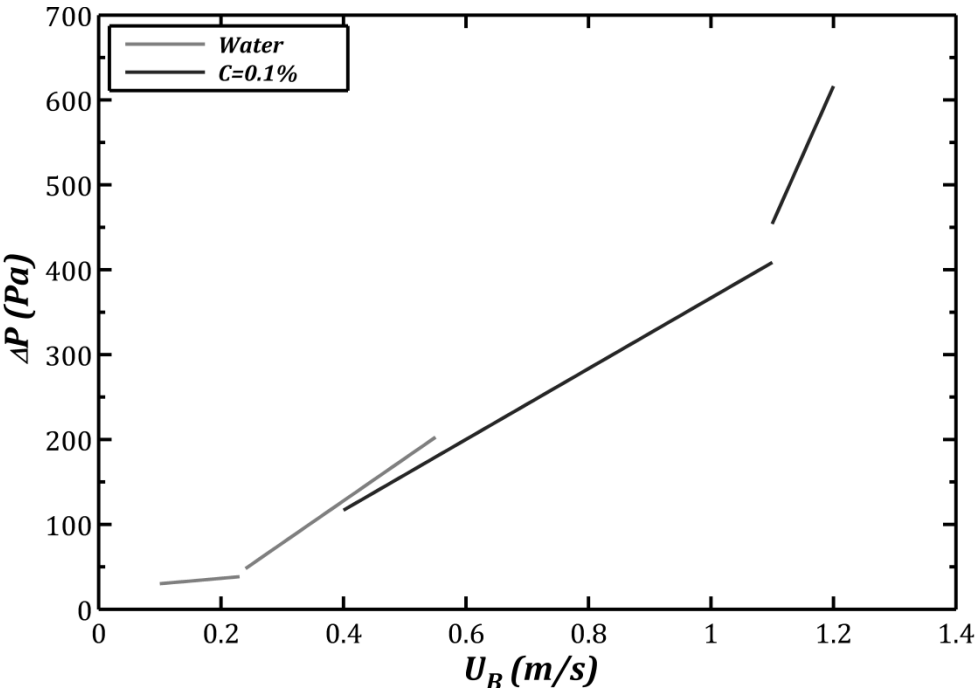


**Figure 7-24 Comparison of Pressure Drops Encountered in Transporting Fine Particles with Water and 0.1% Polymer Solution**

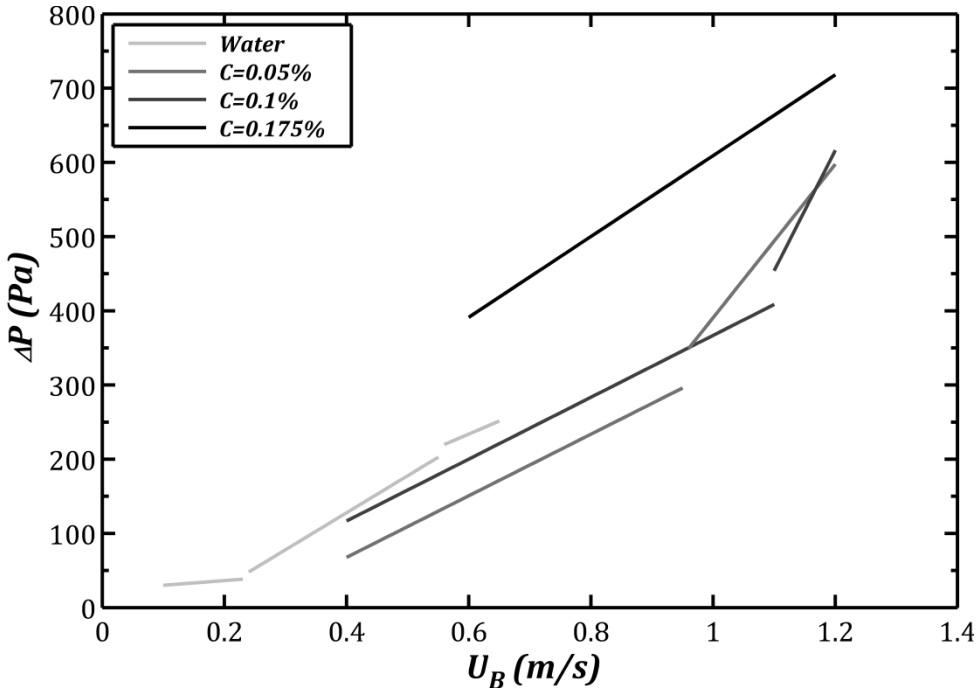


**Figure 7-25 Comparison of Pressure Drops Encountered in Transporting Fine Particles with Water and Polymer Solutions**

### 7.3.9 Dunes Velocity

Dunes or separated bed form at medium range velocities comparing to critical velocity of rolling and suspension. These sand clusters move at relatively low speed comparing to the bulk velocity of the fluid. As the velocity of fluid increases, velocity of the dunes increases accordingly. In this section velocity of moving dunes for different fluids at different bulk velocities are reported. The measurement technique has been explained previously in chapter 3.

Figure 7-26 is the measured dunes velocity for water and fine particles. Dunes velocity is showing a linear correlation with the bulk velocity of the fluid. The magnitude of the dune velocities comparing to bulk velocity of the fluid is almost two orders of magnitude lower. Figure 7-27 and Figure 7-28 are the dunes velocities for two polymer solutions. For the highest polymer solution tested dunes domain couldn't be observed. Based on the fact that dunes velocities correlate linearly with bulk velocity, a linear relation has been assumed for these two fluids as well.

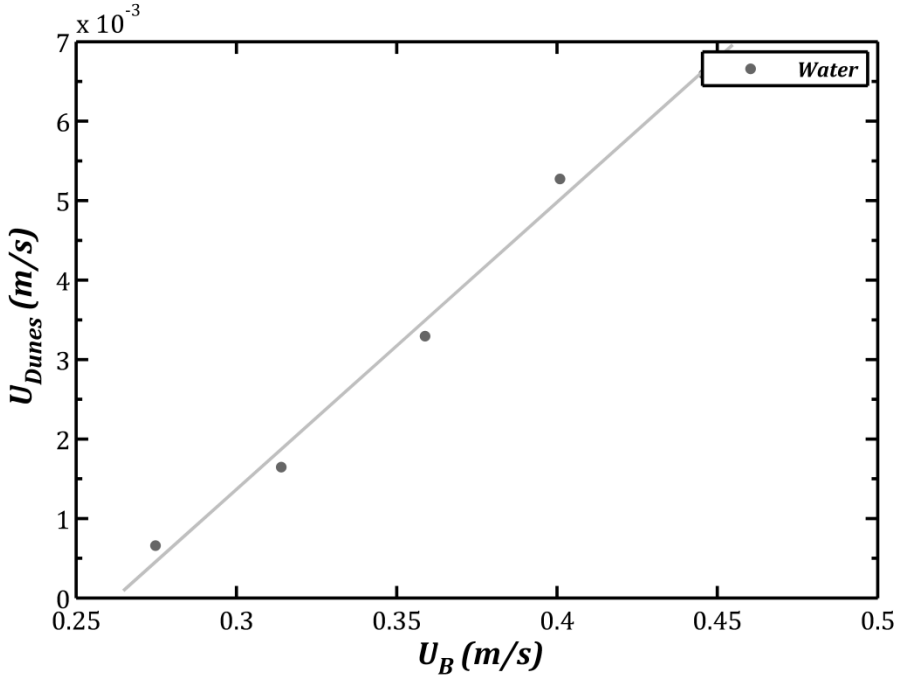


**Figure 7-26 Measured Dunes Velocity for Fine Particles and Water**

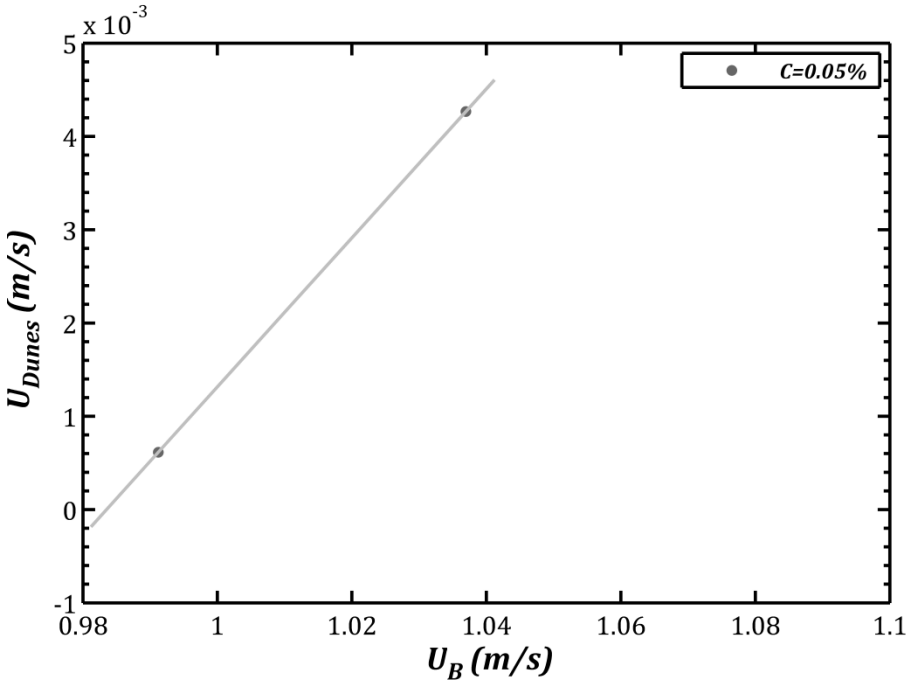


**Figure 7-27 Measured Dunes Velocity for Fine Particles and 0.05% Polymer Solution**

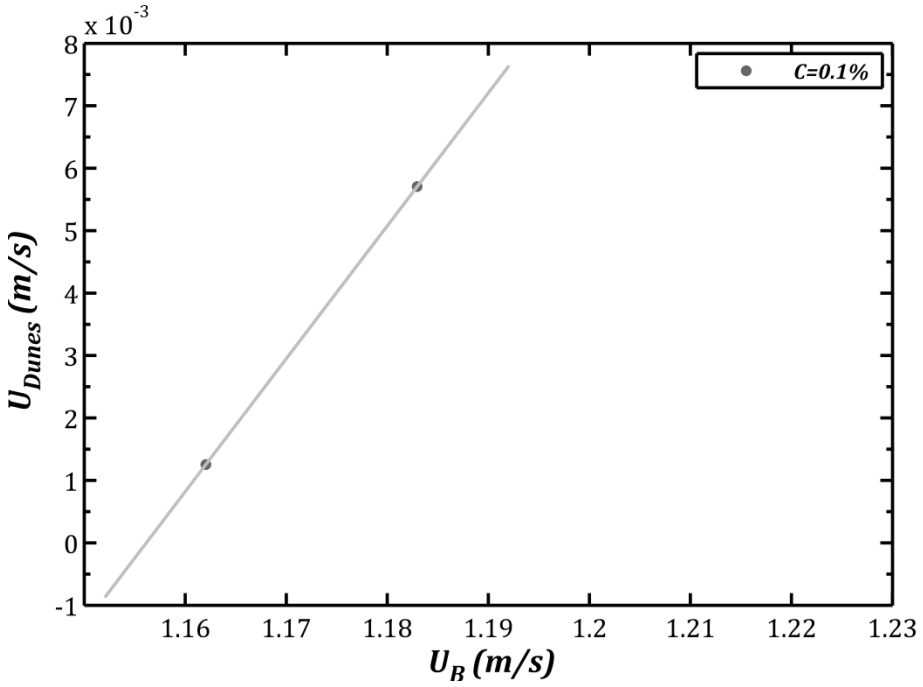


**Figure 7-28 Measured Dunes Velocity for Fine Particles and 0.1% Polymer Solution**

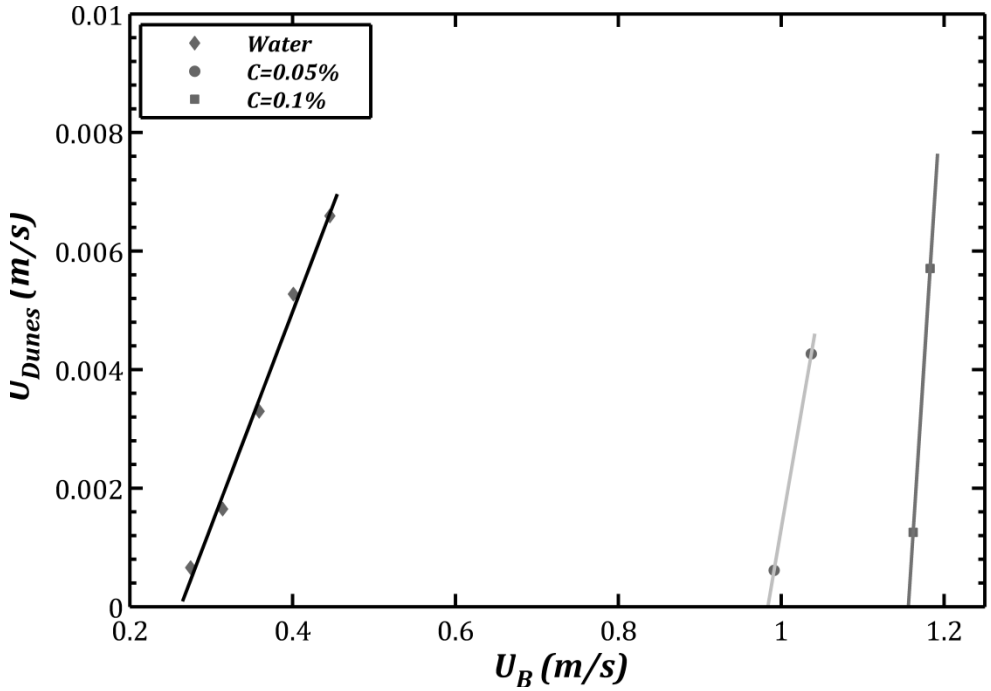


**Figure 7-29 Comparison of Dunes Velocities for Water and Two Polymer Solutions**

Figure 7-29 represents the dunes velocities for all the fluids (water and two polymer solutions). From the data in these figures, it is obvious that for water dunes domain occurs at considerably lower bulk velocities than other fluids. When the lines which represent dunes velocities are compared, it looks that all the fluids are showing lines of more or less same slope but at different locations in the x axes. This clearly can be interpreted as like, all the fluids carry the sand dunes at same dune velocity but at different fluid velocity. In that case water seems to be the promising fluid because it can carry the dunes at the same velocity as polymers but at significantly lower bulk velocity.

Summary: velocity of dunes has been found to be a linear function of the fluid bulk velocity. Dunes velocity in this study was found to be almost two orders of magnitude lower than fluid velocity. Comparison of dunes velocities for different fluids has revealed that these velocities are so close for different fluids but at different velocity of the fluids. Water was found to be the effective fluid in term of dunes velocity and fluid bulk velocity together.

## 7.4 Cuttings Transport Experiments with Coarse Particles

In this section experimental results of critical conditions of particle motion for coarse particles are reported. As shown in Chapter 5, the size distribution of coarse particles used in this study was found to be uniform with a mean diameter of 1.214 mm.

Similar to experiments with fine particles, critical velocity at which rolling of particles over a bed of particles formed in the lower side of a concentric annuli was investigated. Pressure drop was also measured and reported.

Since the effect of fluid viscosity is of great interest in this research, fluids with four different viscosities were studied. Water and fluids with 3 different polymer concentrations were used. In order to facilitate the comparison of performance of different fluids when different particle diameters are used, the concentrations of polymer solutions were similar to experiments with fine particles (0.05%, 0.1% and 0.175%). Rheology measurements and models for these fluids were reported in chapter 5 but as a quick reminder they are reported here as well.

C=0.175% Fluid $\begin{cases} \tau = 0.035\gamma^{0.715} \\ \mu_a = 0.035\gamma^{-0.285} \end{cases}$ **Eq. ( 7-20)**

C=0.1% Fluid $\begin{cases} \tau = 0.0174\gamma^{0.783} \\ \mu_a = 0.0174\gamma^{-0.217} \end{cases}$ **Eq. ( 7-21)**

C=0.05% Fluid $\begin{cases} \tau = 0.0054\gamma^{0.961} \\ \mu_a = 0.0054\gamma^{-0.049} \end{cases}$ **Eq. ( 7-22)**

Experimental procedures were all similar to the ones conducted using with fine particles. Measured velocity and pressure drop along with other calculated parameters are summarized in Table 7-7 to Table 7-10.

**Table 7-7 Experimental Results for Critical Velocity of Particle Movement with Water and Coarse Particles**

$d_{p=1.2142\ mm}$

| $U_B(m/s)$ | $\Delta P\ (Pa)$ | $\tau_w\ (Pa)$ | $u^*\ (m/s)$ | $N_{Re}$ | $R_{ep}$ | $\tau^*$ | Entrainment | Bed Type |
|---|---|---|---|---|---|---|---|---|
| 0.16 | 35 | 0.164 | 0.013 | 9329 | 15.5 | 0.01 | None | Stationary |
| 0.21 | 48 | 0.221 | 0.015 | 11924 | 18 | 0.01 | None | Stationary |
| 0.25 | 62 | 0.286 | 0.017 | 14170 | 20.5 | 0.01 | None | Stationary |
| 0.27 | 69 | 0.319 | 0.018 | 15218 | 21.7 | 0.02 | None | Stationary |
| 0.28 | 76 | 0.351 | 0.019 | 16236 | 22.7 | 0.02 | None | Stationary |
| 0.3 | 84 | 0.388 | 0.02 | 17362 | 23.9 | 0.02 | **Rolling** | |
| 0.33 | 99 | 0.457 | 0.021 | 18858 | 26 | 0.02 | Saltation/Rolling | Dunes |
| 0.4 | 133 | 0.616 | 0.025 | 22534 | 30.1 | 0.03 | Saltation/Rolling | Dunes |
| 0.43 | 132 | 0.61 | 0.025 | 24607 | 30 | 0.03 | Saltation/Rolling | Dunes |

**Table 7-8 Experimental Results for Critical Velocity of Particle Movement with 0.05% Polymer Solution and Coarse Particles**

$d_{p=1.2142\ mm}$

| $U_B(m/s)$ | $\Delta P\ (Pa)$ | $\tau_w\ (Pa)$ | $u^*\ (m/s)$ | $N_{Re}$ | $R_{ep}$ | $\tau^*$ | Entrainment | Bed Type |
|---|---|---|---|---|---|---|---|---|
| 0.35 | 77 | 0.356 | 0.019 | 4330 | 5 | 0.02 | None | Stationary |
| 0.44 | 111 | 0.513 | 0.023 | 5583 | 6.1 | 0.03 | None | Stationary |
| 0.54 | 155 | 0.715 | 0.027 | 6939 | 7.3 | 0.04 | None | Stationary |
| 0.64 | 199 | 0.923 | 0.03 | 8277 | 8.4 | 0.05 | None | Stationary |
| 0.71 | 230 | 1.062 | 0.033 | 9193 | 9 | 0.06 | None | Stationary |
| 0.77 | 255 | 1.182 | 0.034 | 10043 | 9.6 | 0.06 | **Rolling** | |
| 0.84 | 323 | 1.496 | 0.039 | 11115 | 10.9 | 0.08 | Saltation/Rolling | Dunes |
| 0.91 | 475 | 2.198 | 0.047 | 12199 | 13.4 | 0.12 | Saltation/Rolling | Dunes |
| 0.97 | 683 | 3.158 | 0.056 | 13123 | 16.2 | 0.17 | Saltation/Rolling | Dunes |
| 1.02 | 693 | 3.205 | 0.057 | 13825 | 16.4 | 0.17 | Saltation/Rolling | Dunes |
| 1.08 | 652 | 3.016 | 0.055 | 14652 | 15.8 | 0.16 | Saltation/Rolling | Dunes |

**Table 7-9 Experimental Results for Critical Velocity of Particle Movement with 0.1% Polymer Solution and Coarse Particles**

| | $U_B(m/s)$ | $\Delta P\ (Pa)$ | $\tau_w\ (Pa)$ | $u^*\ (m/s)$ | $N_{Re}$ | $R_{ep}$ | $\tau^*$ | Entrainment | Bed Type |
|---|---|---|---|---|---|---|---|---|---|
| $d_{p=1.2142\ mm}$ | 0.38 | 113 | 0.524 | 0.023 | 3162 | 4.1 | 0.03 | None | Stationary |
| | 0.57 | 198 | 0.918 | 0.03 | 5606 | 6.3 | 0.05 | None | Stationary |
| | 0.78 | 307 | 1.421 | 0.038 | 8673 | 8.9 | 0.07 | None | Stationary |
| | 0.85 | 334 | 1.543 | 0.039 | 9619 | 9.5 | 0.08 | None | Stationary |
| | 0.91 | 374 | 1.731 | 0.042 | 10640 | 10.4 | 0.09 | **Rolling** | |
| | 0.97 | 468 | 2.167 | 0.047 | 12118 | 12.4 | 0.11 | Saltation/Rolling | Dunes |
| | 1.03 | 420 | 1.944 | 0.044 | 12413 | 11.4 | 0.1 | Saltation/Rolling | Dunes |
| | 1.08 | 644 | 2.98 | 0.055 | 14767 | 15.8 | 0.16 | Saltation/Rolling | Dunes |
| | 1.14 | 1081 | 5 | 0.071 | 17966 | 23.7 | 0.26 | Saltation/Rolling | Dunes |
| | 1.22 | 1000 | 4.628 | 0.068 | 18709 | 22.3 | 0.24 | Saltation/Rolling | Dunes |

**Table 7-10 Experimental Results for Critical Velocity of Particle Movement with 0.175% Polymer Solution and Coarse Particles**

| | $U_B(m/s)$ | $\Delta P\ (Pa)$ | $\tau_w\ (Pa)$ | $u^*\ (m/s)$ | $N_{Re}$ | $R_{ep}$ | $\tau^*$ | **Entrainment** | **Bed Type** |
|---|---|---|---|---|---|---|---|---|---|
| $d_{p=1.2142\ mm}$ | 0.52 | 275 | 1.271 | 0.036 | 3523 | 5.2 | 0.07 | None | Stationary |
| | 0.61 | 335 | 1.55 | 0.039 | 4490 | 6.2 | 0.08 | None | Stationary |
| | 0.72 | 402 | 1.86 | 0.043 | 5676 | 7.3 | 0.1 | None | Stationary |
| | 0.77 | 430 | 1.991 | 0.045 | 6305 | 7.8 | 0.1 | None | Stationary |
| | 0.83 | 459 | 2.124 | 0.046 | 6906 | 8.2 | 0.11 | None | Stationary |
| | 0.93 | 523 | 2.42 | 0.049 | 8216 | 9.2 | 0.13 | None | Stationary |
| | 1 | 586 | 2.71 | 0.052 | 9183 | 10.2 | 0.14 | None | Stationary |
| | 1.07 | 740 | 3.424 | 0.059 | 10828 | 12.6 | 0.18 | **Rolling** | |
| | 1.13 | 893 | 4.131 | 0.064 | 12279 | 14.9 | 0.22 | Saltation/Rolling | Dunes |
| | 1.16 | 1087 | 5.028 | 0.071 | 13705 | 17.8 | 0.26 | Saltation/Rolling | Dunes |

A summary of the critical values measured/calculated at the initiation of particle movement in rolling is given Table 7-11. The results are reported for all four fluids.

**Table 7-11 Critical Conditions for Rolling Type of Motion for Coarse Particles**

$d_p = 1.214\ mm$

| Fluid | $U_B(m/s)$ | $\Delta P\ (Pa)$ | $\tau_w\ (Pa)$ | $u^*\ (m/s)$ | $\tau^*$ |
|---|---|---|---|---|---|
| Water | 0.3 | 84 | 0.39 | 0.02 | 0.049 |
| 0.05% | 0.77 | 255 | 1.18 | 0.034 | 0.062 |
| 0.1% | 0.91 | 374 | 1.73 | 0.042 | 0.091 |
| 0.175% | 1.07 | 740 | 3.42 | 0.059 | 0.18 |

### 7.4.1 Effect of Fluid Viscosity on the Critical Velocity of Rolling and Saltation for Coarse Particle

Effect of viscosity on critical velocity for rolling and saltation of coarse particles is similar to that of fine particles. In general as the viscosity increases, the critical velocity increases as well.

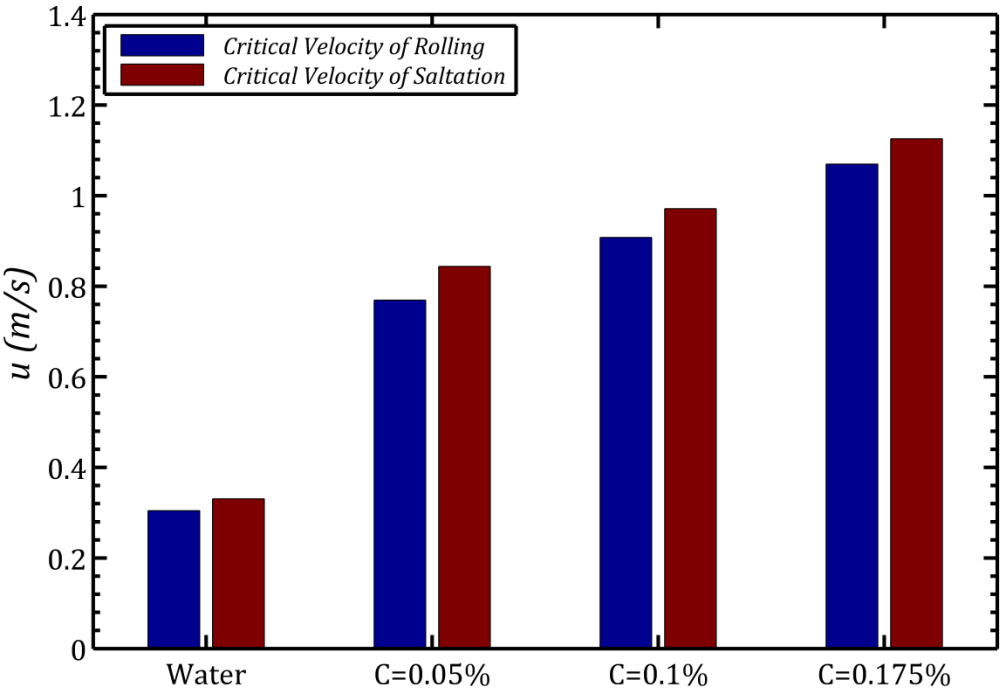


**Figure 7-30 Comparison of Critical Velocity of Coarse Particle Movement in Rolling using Four Different**

Figure 7-30 shows a comparison of critical velocities of rolling for four different fluids. A discussion of effective forces which cause particle movement along the bed or entrainment into the flow was given in the previous section. For large particles, only effective forces are drag and net weight forces. Adhesion and updraft under a burst forces are negligible in this case.

For coarse particles, the holding forces are several times bigger than the finer particles (related to third power of particle diameter ratio) which means in order to move these particles, one should exert a much higher drag force on them comparing to finer particles. This is just a simple force balance. The momentum caused by drag force around the resting point of the particle should overcome the momentum caused by gravity.

Fine particles ($d_{50}$ = 349 micron) could be easily removed as soon as the particle is exposed to the core flow where the drag force is effective. In other words, since the net weight force is not very high, as soon as drag force is exerted on a fine particle, it will start to move. For the coarse particles, however, the net weight force is not low anymore and in order to remove that particle drag force should be increased several times more than what is needed for finer particles. As we may remember that the drag force is negligible in the viscous sublayer and only the part of a particle which is exposed to the core flow experiences a high drag force. Considering the factors involved in drag force (Eq. ( 7-23)), there are several ways to increase the drag force.

$$F_D = \frac{1}{2}\rho v^2 C_D A \qquad \textbf{Eq. ( 7-23)}$$

Assume that a particle is exposed to a flow, in order to increase the drag on that particle one can increase the fluid density or increase the fluid velocity. A more complicated alternative is to increase the drag coefficient. The last option in enhancing the drag force acting on a particle is to increase the projection area of the particle normal to the flow direction (this area is called the reference area).

For the experimental work conducted in this study the fluid density is constant and doesn't have any effect on drag force. Also when testing with a fluid, say water, the drag coefficient is not changeable as this parameter depends on the type of the fluid. The only parameters considered for their effect in our experiments are the velocity difference and

the reference area of the particle exposed to flow, which were somehow related to each other.

For fine particles the reference area is close to zero as long as the particle is hidden in the viscous sublayer; that means regardless of the magnitude of velocity in the core flow, the drag force experienced by the particle would be negligible because the velocity difference around the particle is low. Drag force on the particle would become effective as soon as the particle becomes larger than the sublayer thickness and the larger surface area of the particle (reference area) is exposed to flow large. This explanation is valid for fine particles where the net weight force is negligible.

Coarse particles have diameter of about 1.2 mm. This diameter ensures that these particles are already bigger than the viscous sublayer thickness for the range of velocities and viscosities tested in this study. Based on conclusion on fine particles, coarse particles should move at very low velocities while this is not the case and a new explanation must be adopted. The explanation here goes to the balance between the lifting forces and holding forces. The holding forces for coarse particles are several time bigger than that of acting on fine particles, so in order to move coarse particles from the bed deposits, lifting forces also needs to be several times bigger.

By increasing the velocity of the fluid, the thickness of the viscous sublayer is reduced which in turn increases the reference area of the particle exposed to the core flow. Increasing the velocity causes the drag force on the particles to increase due to increase in velocity difference and increase in reference area of the particle exposed to flow. At one point the drag force exceeds the net weight force (momentum around the rest point) which causes the particle to roll along the bed.

In summary; higher the viscosity of the carrier fluid, higher critical velocity is needed to initiate particle movement in rolling. The differences in critical velocity requirement of different fluids are very much related to the magnitude of the drag force and the viscous sublayer thickness associated with the flow of that particular fluid.

### 7.4.2 Critical Pressure Drops and Wall Shear Stresses at Onset of Rolling

Analogues to critical velocity, critical pressure drops and wall shear stresses necessary for particle movement (coarse particles) have been studied and reported in

Figure 7-31and Figure 7-32. High viscosity has been found to be not favourable in removing the particles in term of pressure drops and wall shear stresses.

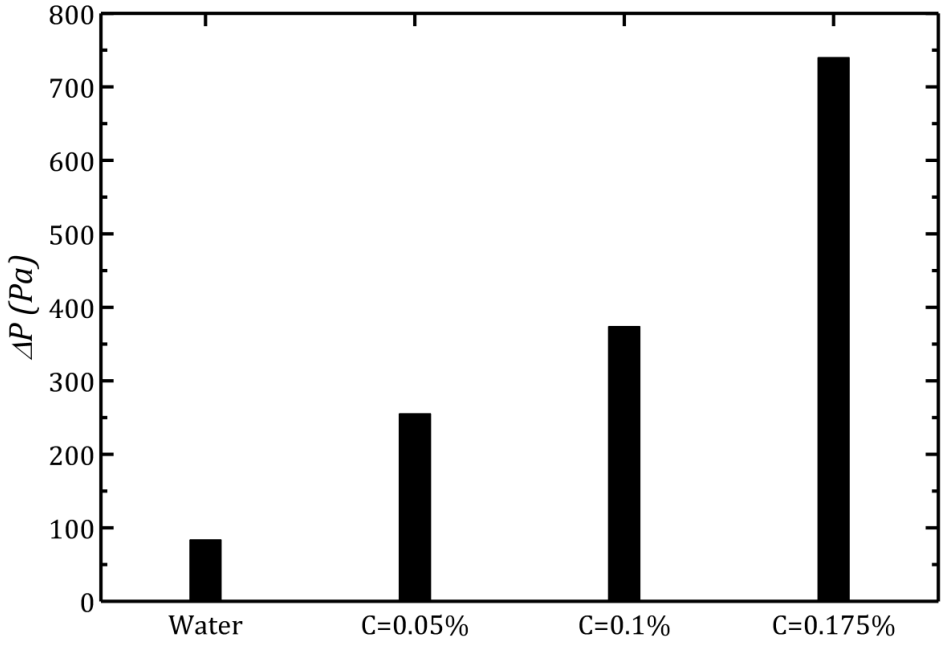


**Figure 7-31 Comparison of Critical Pressure Drops of Four Different Fluids for Coarse particle**

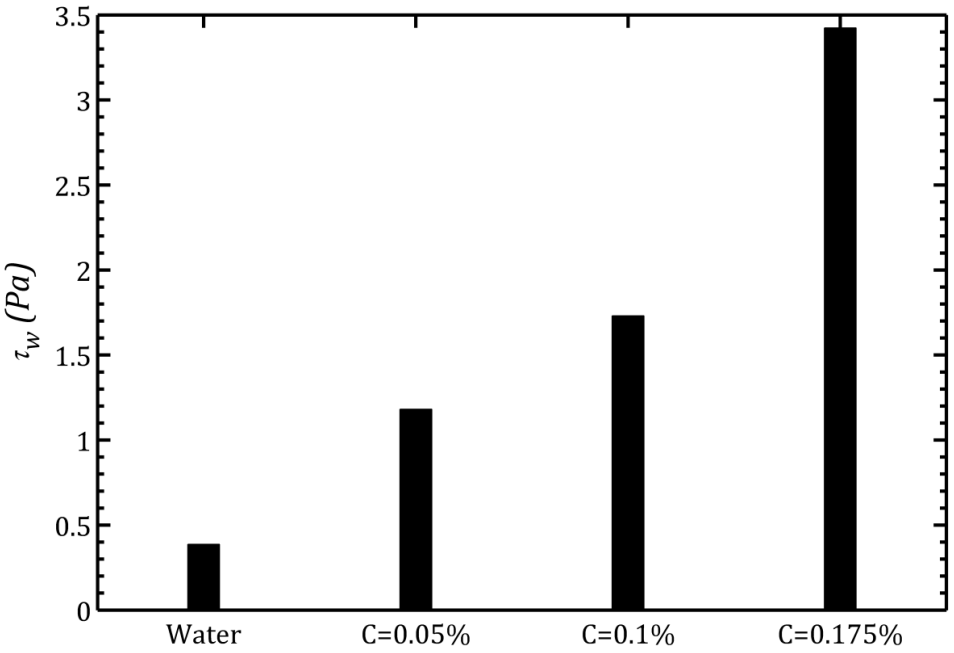


**Figure 7-32 Comparison of Critical Wall Shear Stress of Four Different Fluids for Coarse Particle**

### 7.4.3 Formation of Certain Types of Bed Forms

Similar to experiments with fine particles, different forms of bed have been observed during experiments with coarser particles. Stationary bed and dunes have been the two regime encountered during this phase of the project. The description of these two types of bed type is similar to those discussed in experiments with fine particles.

### 7.4.4 Detection of Different Regimes

From the pressure drops data one should be able to detect transition from one regime to the other. Normally a change in the slope of the pressure drops is observed at the onset of transition from stationary bed to sand dunes.

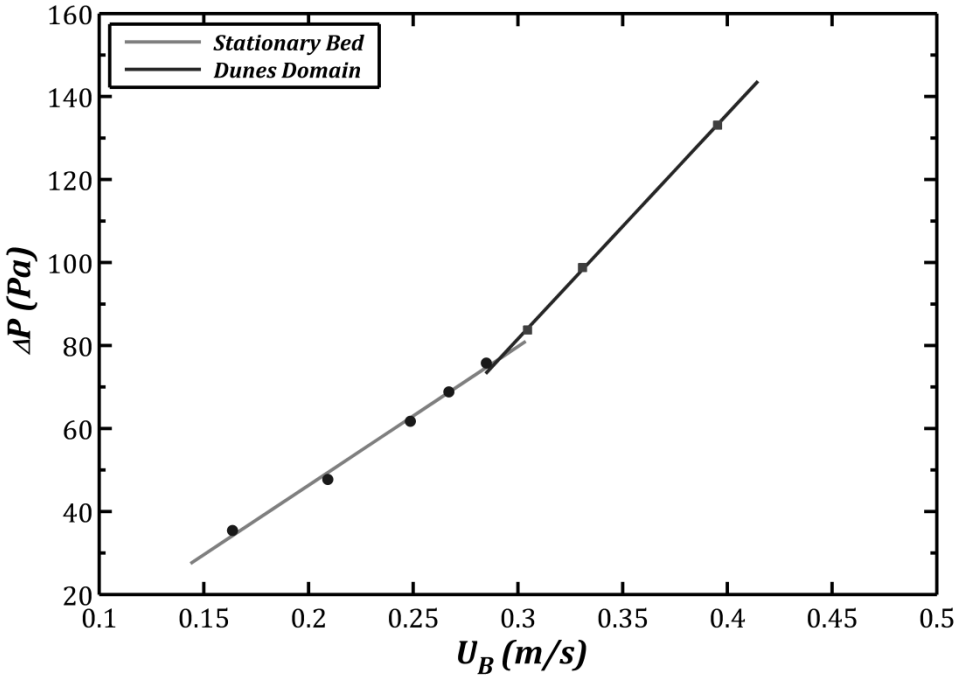


**Figure 7-33 Pressure Drops versus Bulk Velocity for Water and Experiments with Coarse Particles**

As can be seen in Figure 7-33, very similar to fine particles, pressure drops data in each regime best correlates linearly with bulk velocity of the fluids. Transition from stationary bed to dunes is obvious in this figure.

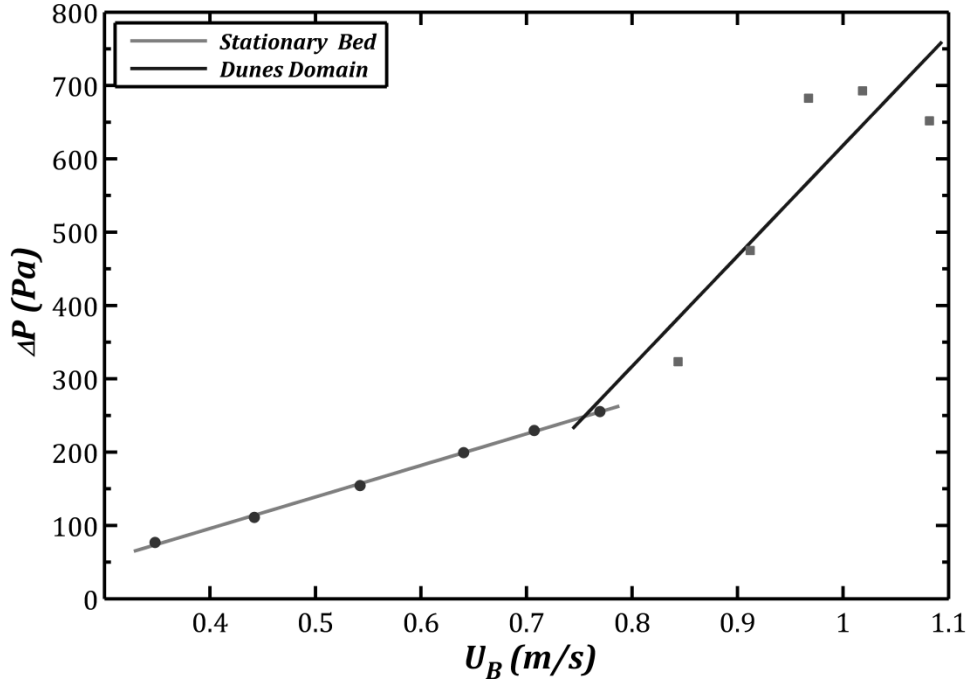


**Figure 7-34 Pressure Drops versus Bulk Velocity for 0.05% Polymer Solution and Experiments with Coarse Particles**

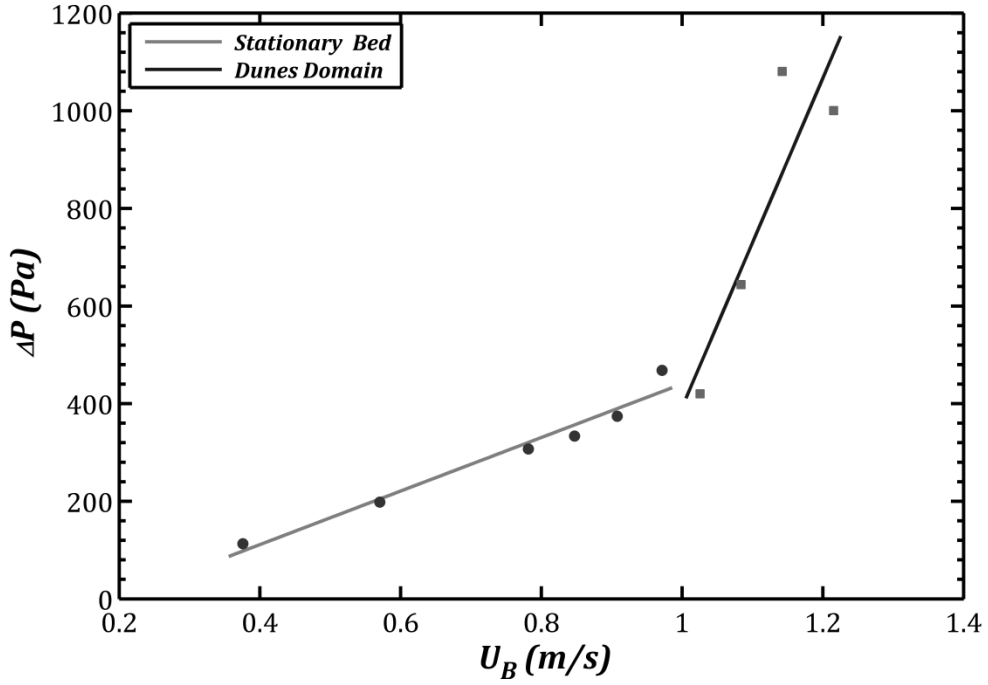


**Figure 7-35 Pressure Drops versus Bulk Velocity for 0.1% Polymer Solution and Experiments with Coarse Particles**

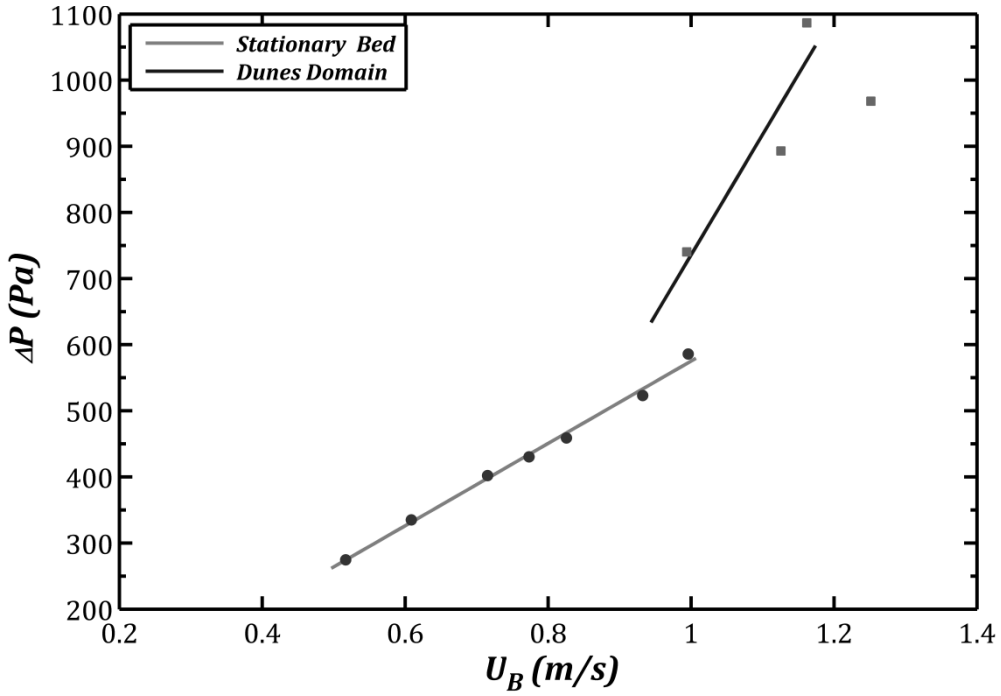


**Figure 7-36 Pressure Drops versus Bulk Velocity for 0.175% Polymer Solution and Experiments with Coarse Particles**

Figure 7-34 to Figure 7-36 are the pressure loss data for three polymer solutions. Pressure drops in the stationary bed are clearly a linear function of the bulk velocity. In the dunes domain, however, the data are more scatter but with the assumptions of linear correlation, there is an increase in the slope of the pressure loss data at the transition velocity.

The deviation of pressure data from a linear regression in dunes domain is caused by fluctuation in pressure drops. These fluctuations have been observed to be a function of the distance between the dunes and also the height of the dunes. The bigger the dunes or the longer the distance between the dunes means greater pressure fluctuations. During experiments with coarse particles it has been observed that the formation of dunes were associated with bigger pressure fluctuations comparing to fine particles. The reason for this phenomenon is because dunes which have formed during experiments with these particles were observed to be much bigger comparing to the dunes in experiments with fine particles. These dunes sometimes grow so big which almost blocks the whole lower annuli. Once these big dunes started to form, huge pressure variation has been recorded.

Figure 7-37 to Figure 7-39 are some typical pressure fluctuations encountered during experiments with coarser particles.

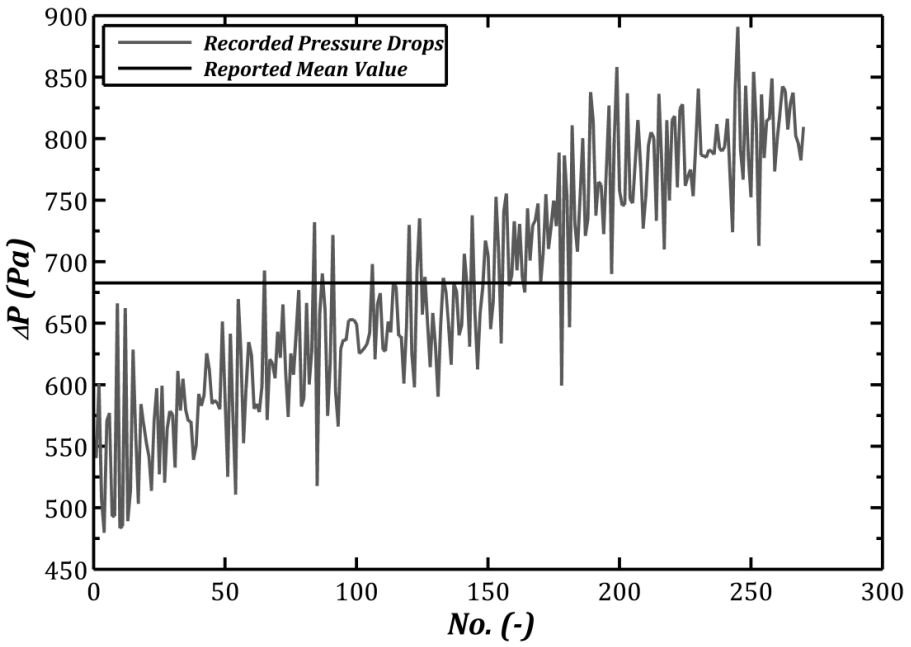


**Figure 7-37 Typical Pressure Drops Fluctuations Associated with Dunes for Coarse Particles and 0.05% Polymer Solution**

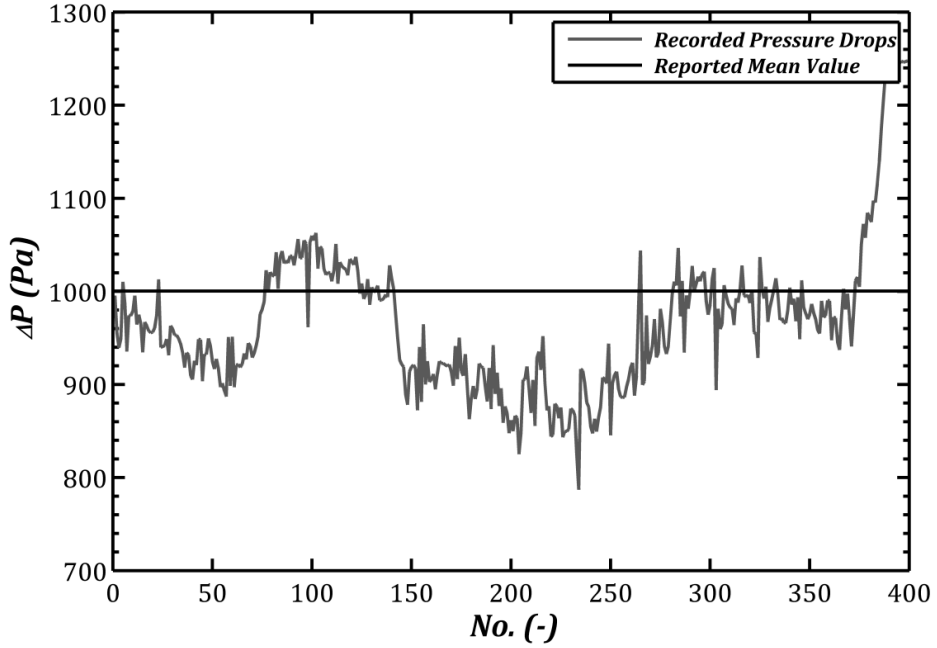


**Figure 7-38 Typical Pressure Drops Fluctuations Associated with Dunes for Coarse Particles and 0.1% Polymer Solution**

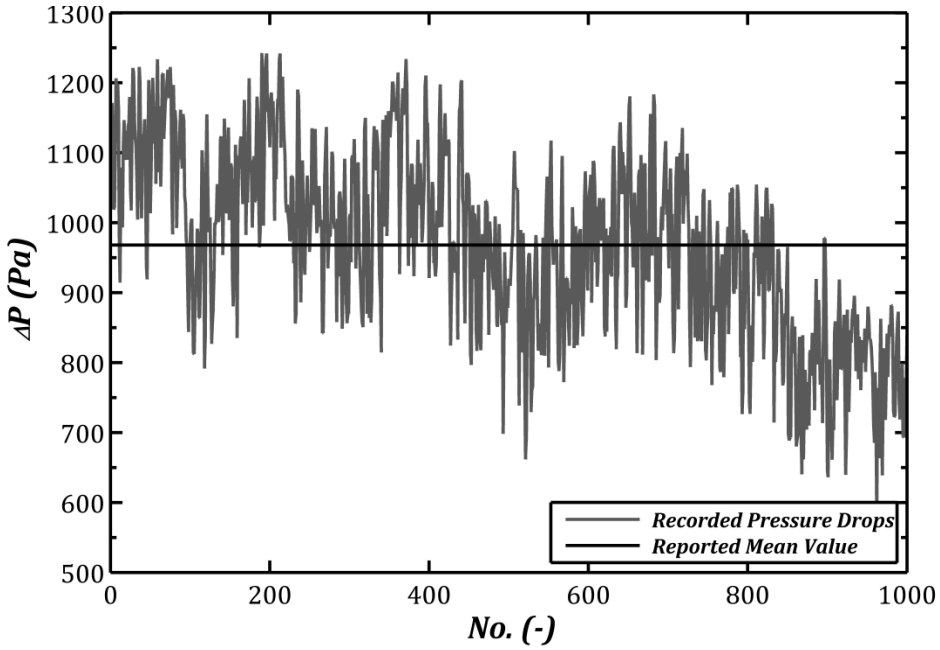


**Figure 7-39 Typical Pressure Drops Fluctuations Associated with Dunes for Coarse Particles and 0.175% Polymer Solution**

### 7.4.5 Pressure Drops

From the pressure drop data reported earlier, a comparison of performance of different polymer solutions with water is reported in Figure 7-40 Figure 7-43. For the same reason given for fine particles case, comparison between water and polymer solutions is not applicable in term of pressure drops. As one can see in these figures, experiments with water ends at relatively low flow rates and so water data is limited to these low velocities. For polymer solutions, on the other hand, pressure data are available for higher velocities. No general conclusions could be mad about the pressure loss data for water and polymer solutions.

Figure 7-43 includes the pressure loss data for all the fluids studied, in this figure, one can conclude that by increasing polymer concentration (or interchangeably fluid viscosity) higher pressure drops are experienced. This is true in the region where a stationary bed is presents and also in dunes domain. The conclusion here is that viscosity has an adverse effect of on the pressure drops in all the different regimes encountered during experiments with coarse particles.

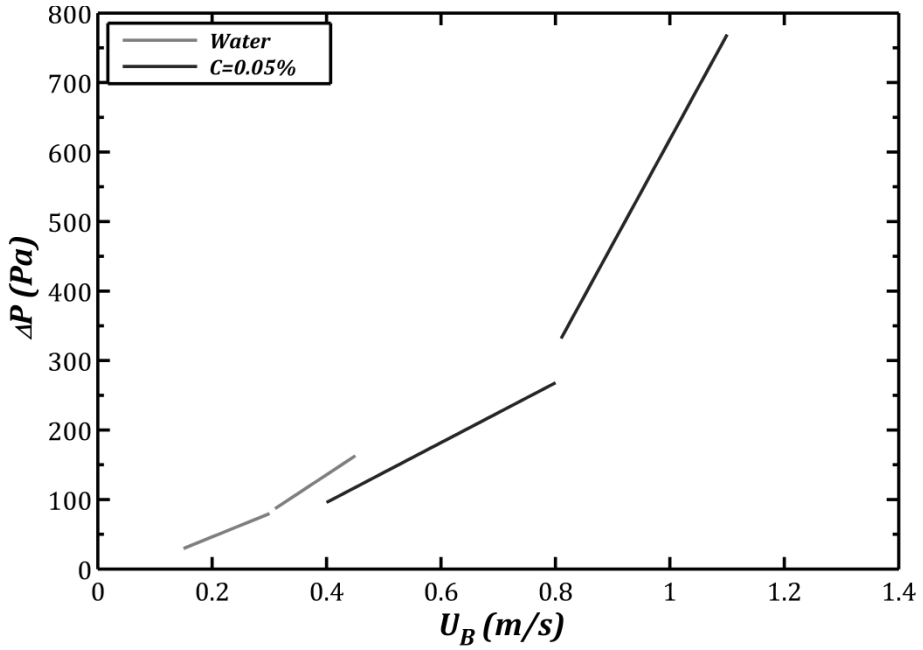


**Figure 7-40 Comparison of Pressure Drops Encountered in Transporting Coarse Particles with Water and 0.05% Polymer Solution**

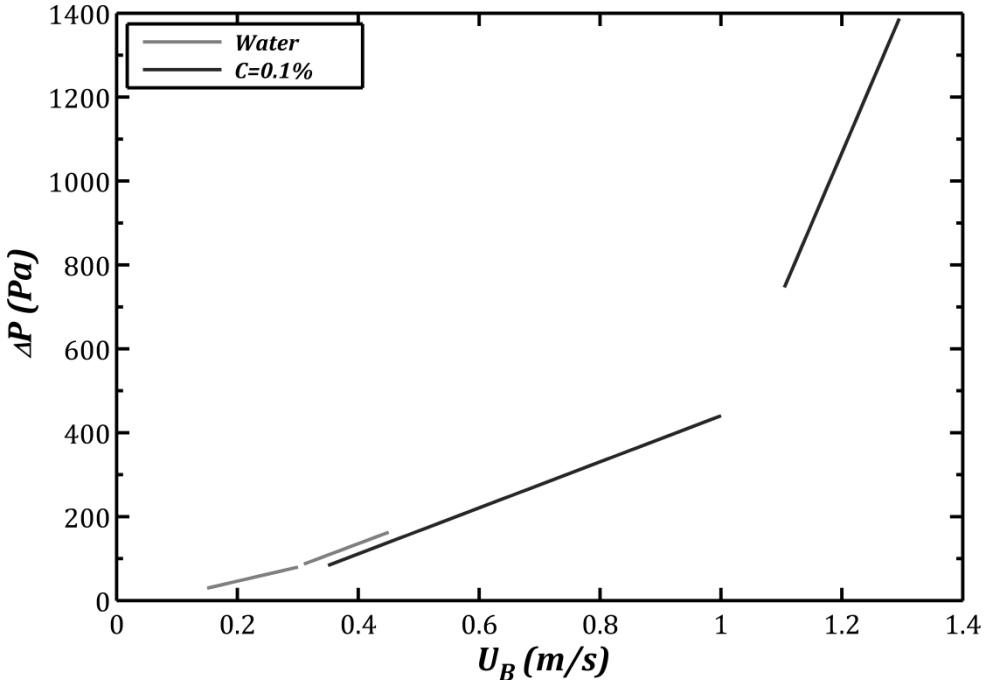


**Figure 7-41 Comparison of Pressure Drops Encountered in Transporting Coarse Particles with Water and 0.1% Polymer Solution**

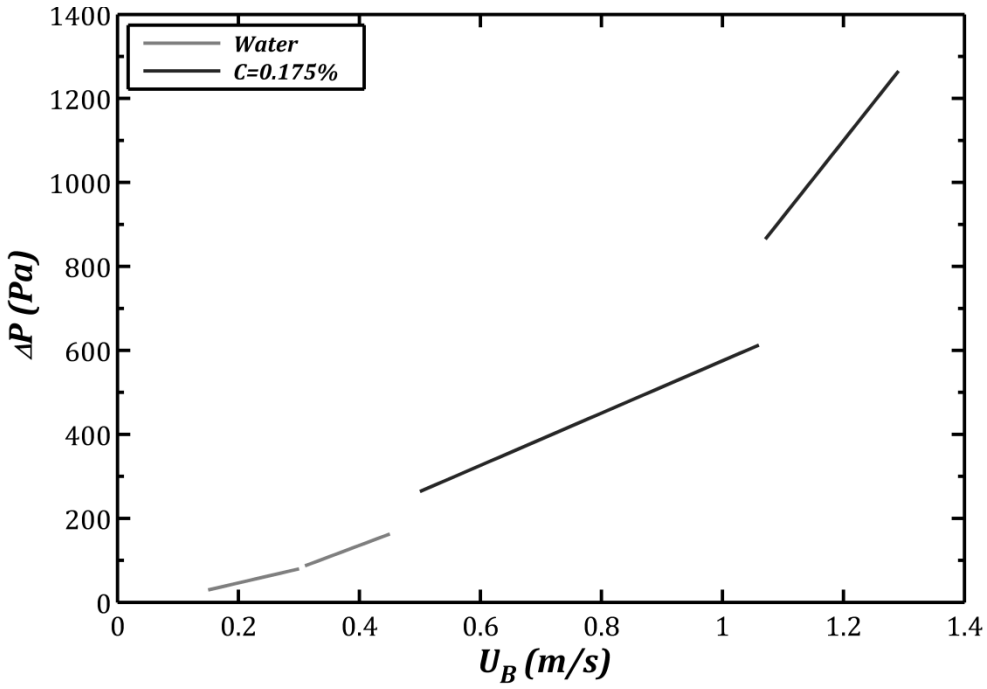


**Figure 7-42 0.175 Comparison of Pressure Drops Encountered in Transporting Coarse Particles with Water and 0.175% Polymer Solution**

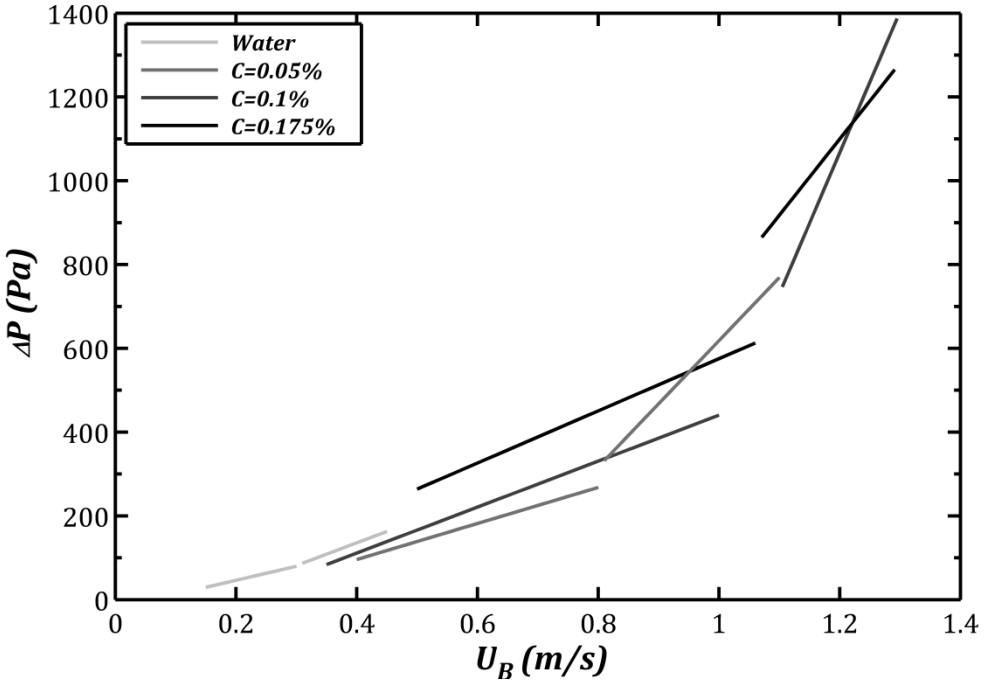


**Figure 7-43 Comparison of Pressure Drops Encountered in Transporting Coarse Particles for all the Fluids**

### 7.4.6 Dunes Velocity

In the previous section with fine particles it has been found that dunes velocities are a linear function of fluid velocity. For coarse particle the same trend was found to be valid for all the fluids tested (Figure 7-44 to Figure 7-47). Dunes velocities are much lower than fluid velocity.

A comparison of performance of different polymer solutions in term of dune velocity is given in Figure 7-48. In this figure it can be concluded that a higher dune velocity can be achieved for lower polymer concentration at lower bulk velocity. The effect of viscosity is apparently negative on both dunes velocities and also the bulk velocity at which dunes occurred.

Comparison of dunes velocities for water and polymer solutions in Figure 7-49 shows that although dunes occur at considerably lower bulk velocity for water but a higher dune velocity can be achieved with polymer solutions. This is especially pronounced for the lowest polymer concentration (0.05%). Dune velocity for this concentration can approximately reach as twice as the velocity of dunes for water.

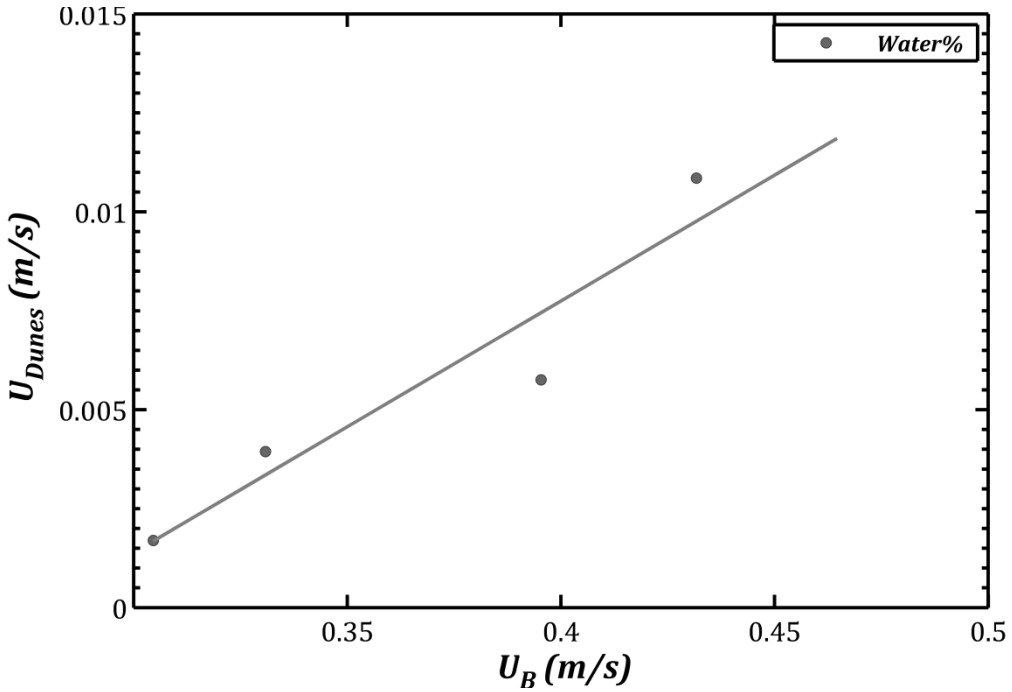


**Figure 7-44 Measured Dunes Velocity for Coarse Particles and Water**

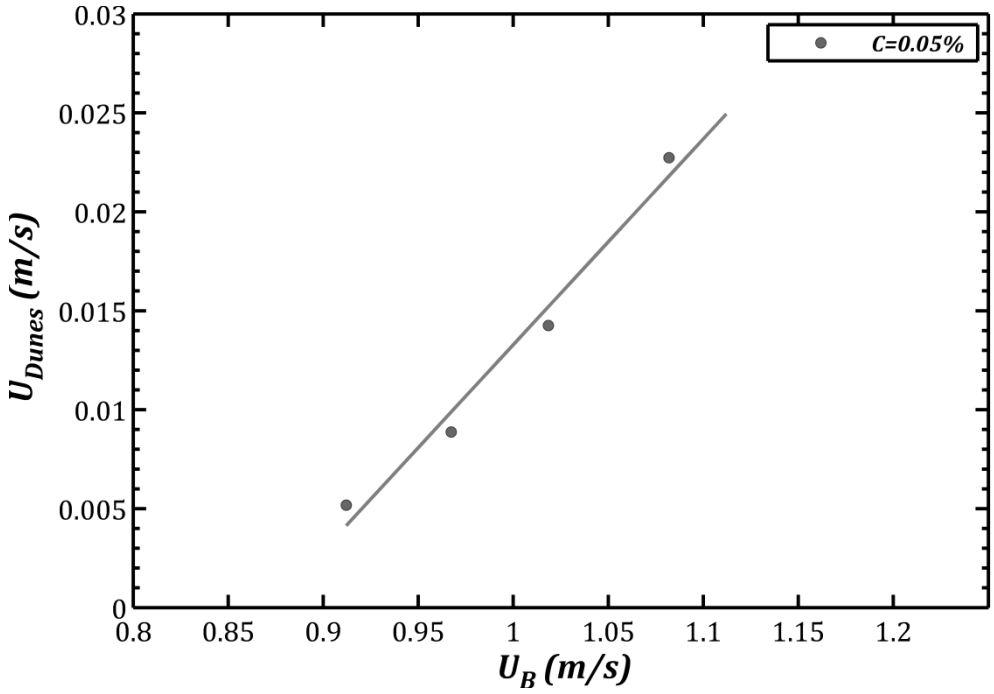


**Figure 7-45 Measured Dunes Velocity for Coarse Particles and 0.05% Polymer Solution**

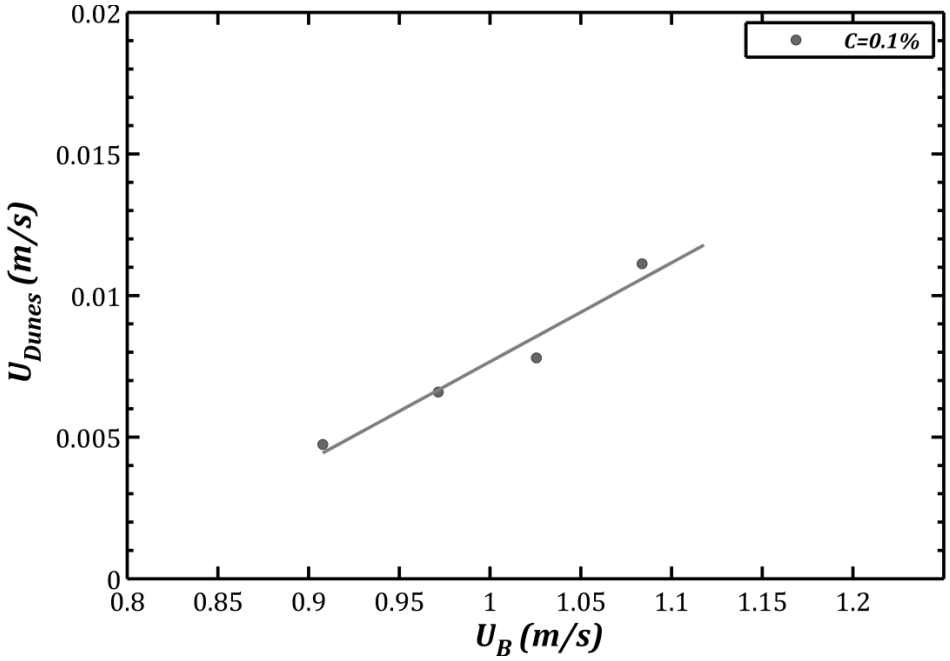


**Figure 7-46 Measured Dunes Velocity for Coarse Particles and 0.1% Polymer Solution**

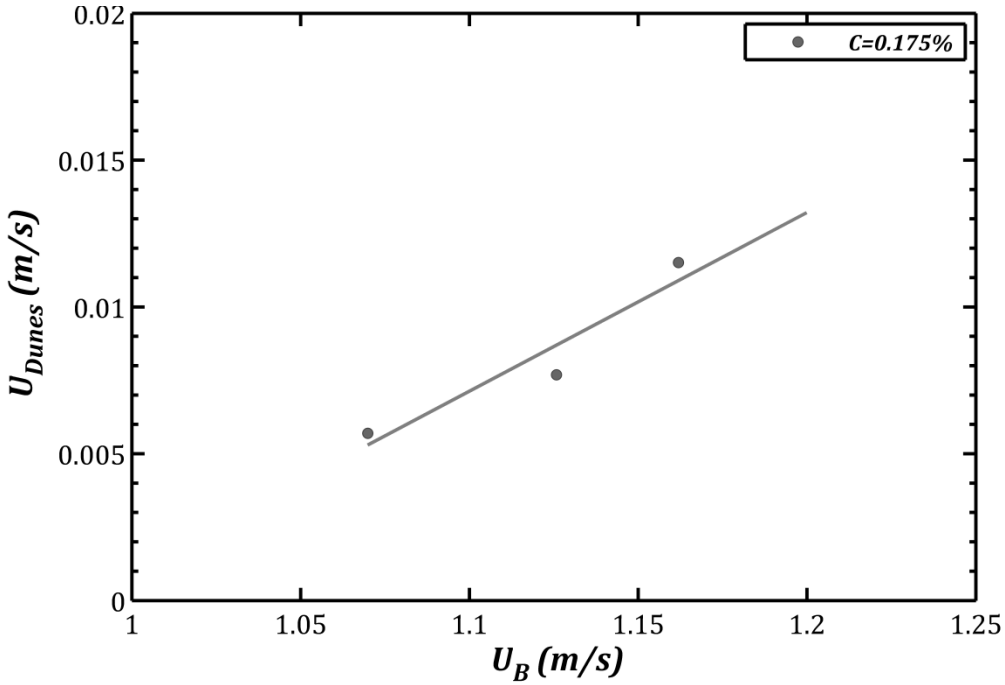


**Figure 7-47 Measured Dunes Velocity for Coarse Particles and 0.175% Polymer Solution**

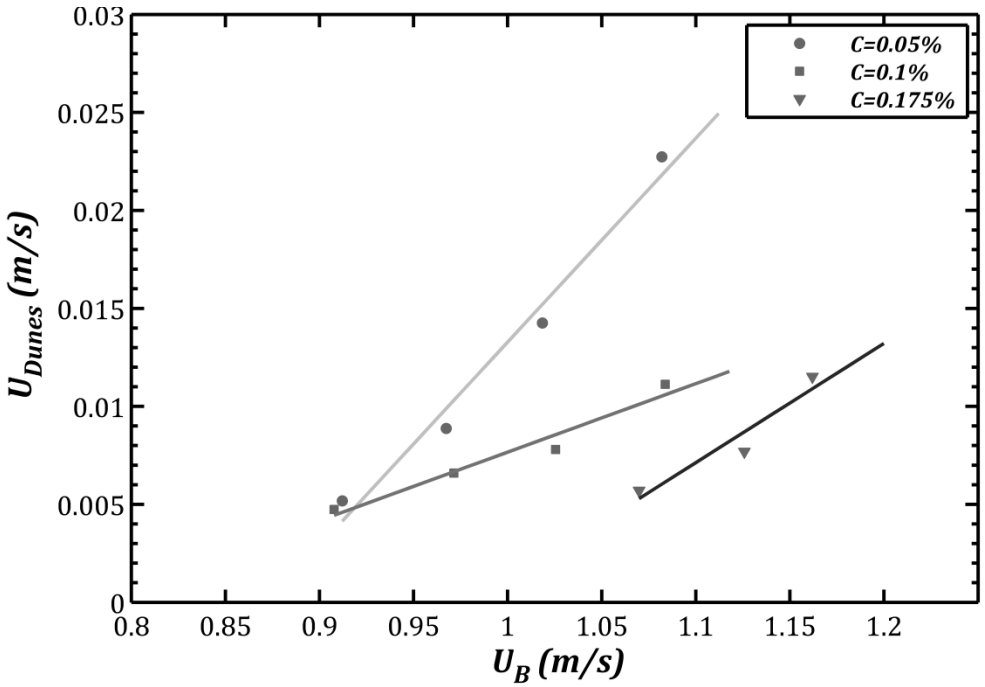


**Figure 7-48 Comparison of Dunes Velocities for Three Polymer Solutions in Experiments with Coarse Particles**

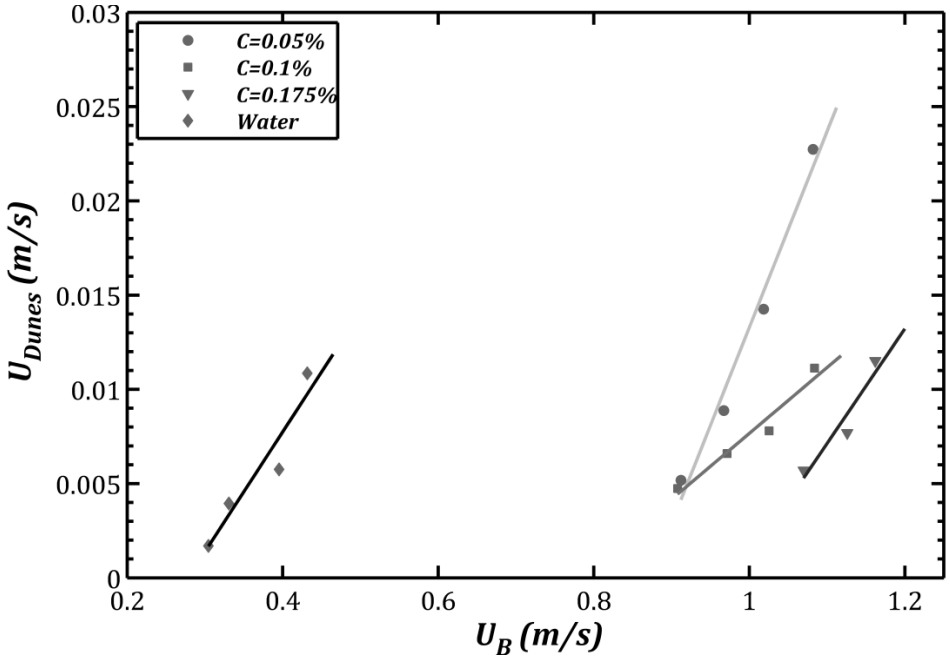


**Figure 7-49 Comparison of Dunes Velocities for Newtonian and non-Newtonian Fluids in Experiments with Coarse Particles**

## 7.5 Fine Particles versus Coarse Particles: Threshold of Particle Movement

In this section a comparison between the performances of different fluids on removing two particle diameters is given. The discussion will be on the critical velocity, pressure drops and wall shear stresses.

### 7.5.1 Critical Velocity of Rolling

Critical velocity of rolling which was reported in previous sections for two particle diameter ranges and four different fluids are plotted in Figure 7-50.

In Figure 7-50 the blue columns are the critical velocity for fine particles and the red ones the critical velocity of coarser particles. For water the critical velocity for coarse particles is slightly higher than that of the ones for fine particles. When using polymer fluids, however, critical rolling velocity of coarse particles is lower than that of required for fine particles for all polymer concentrations.

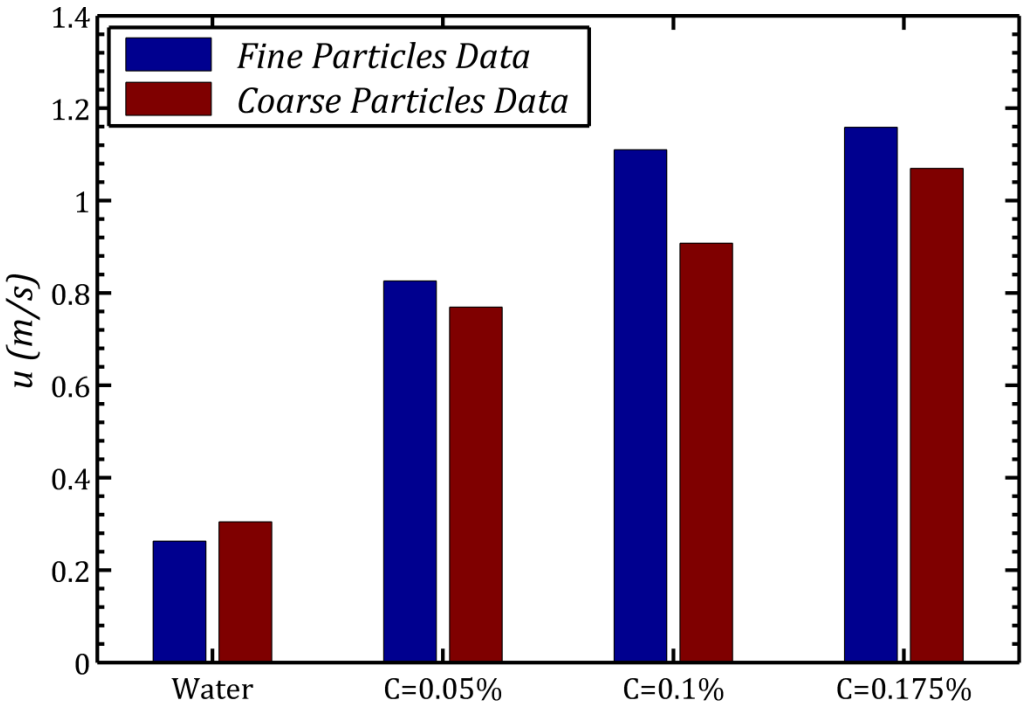


**Figure 7-50 Comparison of Critical Velocity for Two Particle Size Range and Four Different Fluids**

When water is used to remove the fine particles, the important correlating parameter is the thickness of the viscous sublayer as the net weight force of fine particles is negligible. For coarse particles, however, both the reference area (controlled by viscous sublayer thickness) and the net weight force are the controlling parameters because these particles are heavy comparing to previous ones. Due to low viscosity of water, the viscous sublayer is very thin at low velocities and that is the reason why critical velocity of this fluid is much lower than the other fluids tested for fine particles. When the coarse particles are to be removed, the reference area of the particle normal to the core flow is already high at critical velocity for fine particles but it seems that this velocity is not high enough to remove the particle. The reason being is due to low viscosity of water the drag force has to be increased more by increasing the velocity and reference area which ultimately causes an increase in the critical velocity of coarse particles when water is used.

For all the polymeric fluids tested, higher critical velocity is needed to remove fine particles. The reason being is that the high viscosity of the polymer fluids causes the viscous sublayer to be very thick at low velocities and fine particles submerged in the

thick viscous sublayer cannot be removed. Higher velocity is needed to reduce the viscous sublayer thickness and help fine particles to get exposed to the core flow. For the coarser size particles, the viscous sublayer is already thinner than the diameter of the particles and the sufficient condition for particle movement is to increase the drag force by increasing the reference area and velocity.

In summary; effect of particle diameter on the critical velocity of particle rolling was investigated. Critical velocity was found to be higher for larger diameter particles when water is used while for non-Newtonian polymeric solutions, the critical velocity was found to be lower for larger particles. The conclusion is that the high viscosity enhances the critical velocity when larger particles are used.

### 7.5.2 Critical Pressure Drops

Comparison of critical pressure drop for a given fluid and for two particle diameter range is presented in Figure 7-51.

Except for 0.1% polymer solution, for all the fluids studied, the critical pressure drop required to move the larger particles are slightly higher than the pressure drop required for removal of smaller particles. Higher pressure drop observed when removing coarse particles with water, which is in line with the higher critical velocities required for removing coarse particle with water. As for the polymer fluid applications are concerned, however, higher pressure drop measurements were recorded for fluids with 0.05% and 0.175 polymer concentrations. This is in contrast with the critical velocities, which were found to be lower for the bigger particles in polymeric liquids. Pressure drop measurement for fluid with 0.1 % polymer concentration is lower for coarse particles than that of fine particles. This result corresponds well with the lower critical velocity observed for the removal of coarse particles with 0.1% polymer fluid. Based on comparison of critical velocities and pressure drops it is obvious that at a lower velocity (critical velocity of rolling for coarse particles) a somehow equal or larger frictional pressure drop is experienced when coarser particles are used. This may be related to the level of roughness that these particles are introducing to the flow. Generally it is known that higher roughness would results in higher frictional pressure drop at same or even lower velocities. Larger particles increase the roughness comparing to smaller particle and that is why a higher pressure drop occurs at lower velocities with coarser particles.

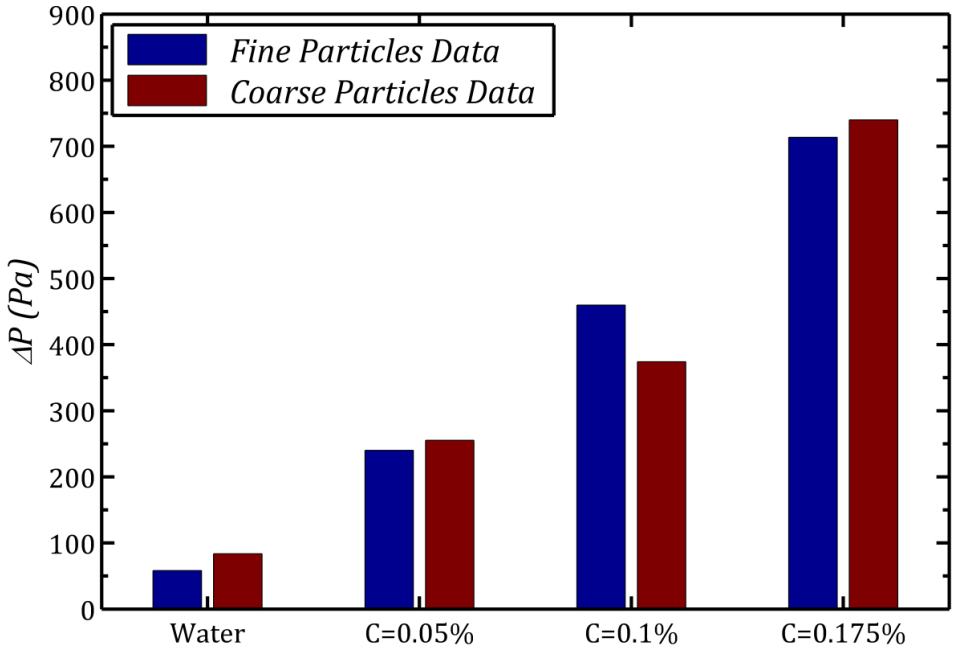


**Figure 7-51 Comparison of Critical Pressure Drops for Two Particles Diamter and Different Fluids**

### 7.5.3 Dunes Velocities

In this section we shall compare the effect of particles diameter on dunes velocities. It is been reported that dunes velocity vary linearly with bulk velocity of the fluid. Figure 7-52 to Figure 7-54 are the comparison of dunes velocities for two different particles diameters. In all the cases it is apparent that an improvement in the velocity of the dunes has happened when larger particles were used. This increase in the dunes velocities is clearer in the case of 0.05% polymer solution where the two lines for two particles diameters are parallel. For the 0.175% polymer solution no dunes data could be obtained for fine particles. Generally, for the reported dunes velocities it is been concluded that particles diameter has a positive effect.

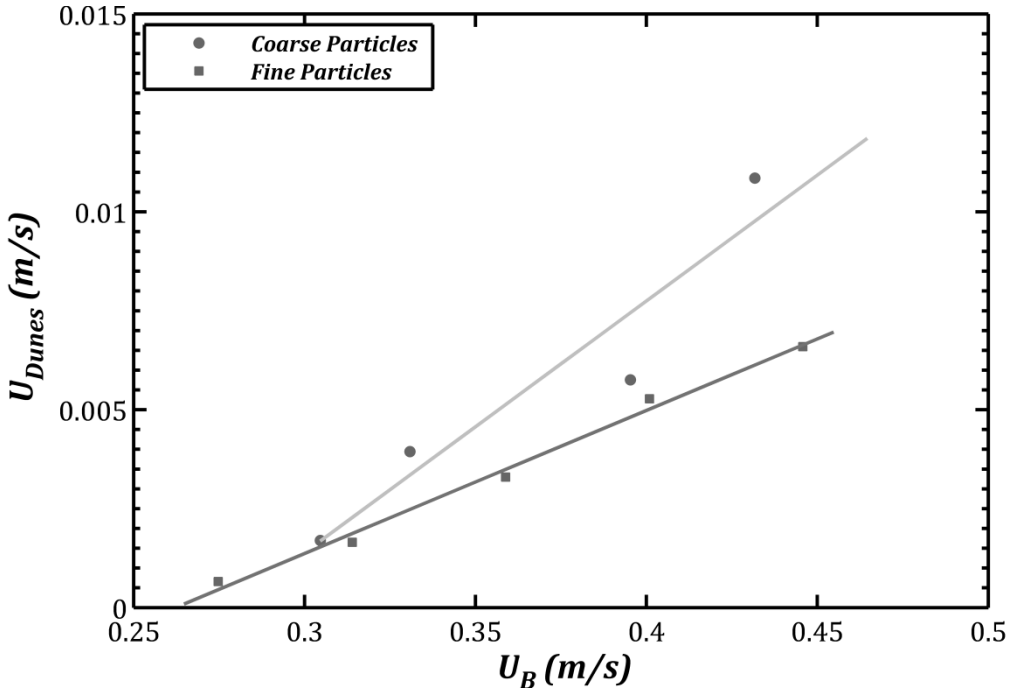


**Figure 7-52 Comparison of Dunes Velocities for Water and Two Particles Diameter**

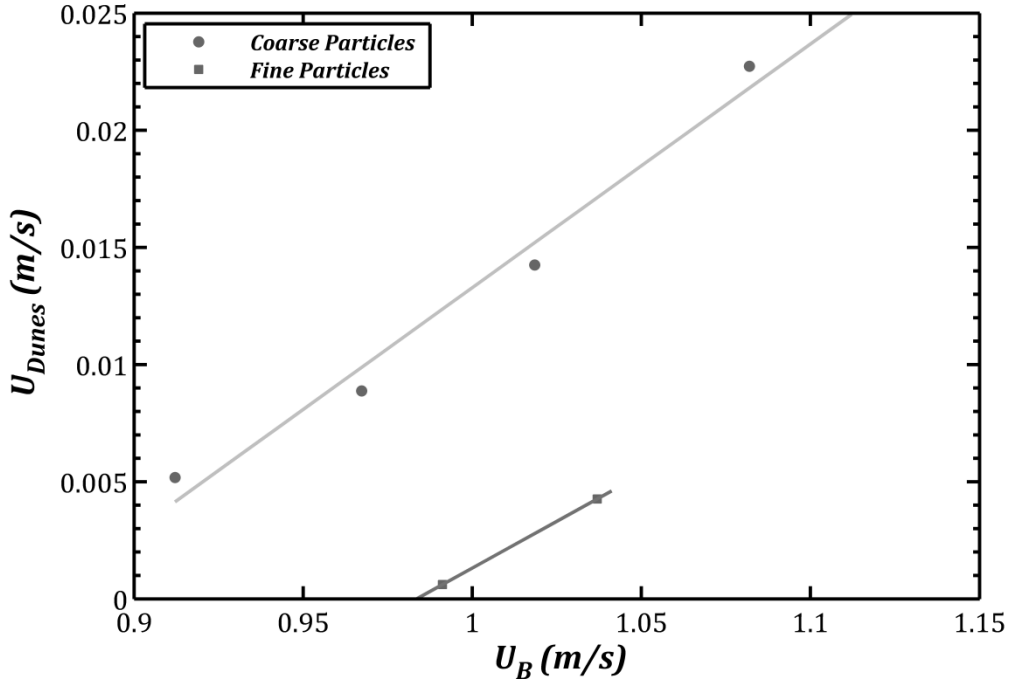


**Figure 7-53 Comparison of Dunes Velocities for 0.05% Polymer Solution and Two Particles Diameter**

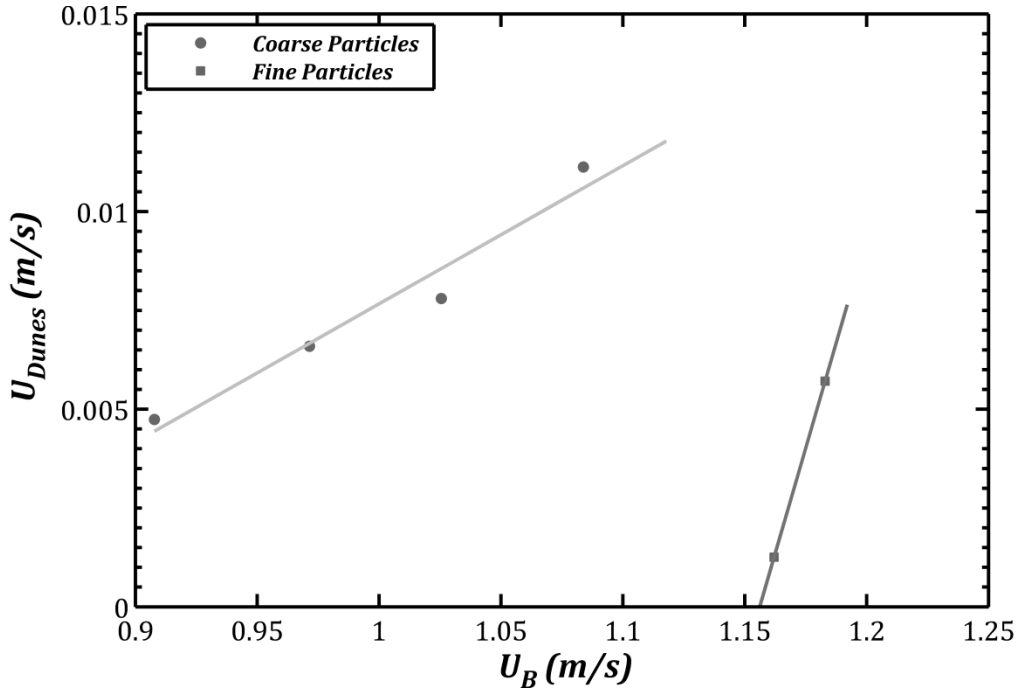


**Figure 7-54 Comparison of Dunes Velocities for 0.1% Polymer Solution and Two Particles Diameter**

## 7.6 Conclusions

Effect of rheology and viscosity on critical conditions of particle movement has been investigated for two different particle diameters (fine particles and coarse particles). Water and three polymer solutions (0.05%, 0.1% and 0.175%) have been tested and the results have been reported in term of critical velocity of rolling and saltation. Formation of certain bed types has been also investigated. Proper conditions for transition from one regime to another have been reported. Velocity of the dunes have been found and reported as well.

- ✓ Two particle diameters of 349 micron and 1.214 mm have been used which were found to be uniform in term of size distribution
- ✓ Critical velocity of saltation were found to be higher than that of rolling
- ✓ High viscosity has been found to have a detrimental effect on critical velocity of rolling and saltation for fine particles
- ✓ While the critical velocity of rolling for fine particles with water was found to be around 0.24 m/s, this velocity continuously increases with increasing

polymer concentration and viscosity of the fluid; a velocity of 1.16 m/s was reported as the critical velocity of rolling for highest polymer concentration

- ✓ Effect of high viscosity on pressure drops at the point of particle movement was found to be similar to its effect on critical velocity; an increasing trend of critical pressure drops has been observed with increasing viscosity
- ✓ For fine particles, the thickness of viscous sublayer has been similar for all the fluids studied at the point of particles movement
- ✓ Thickness of viscous sublayer at the onset of particles motion for fine particles was found to be close to the mean diameter of particles for all the fluids tested
- ✓ Based on the assumption of equity of viscous sublayer thickness and particles mean diameter at the point of rolling for fine particles a model for predicting critical wall shear stress has been proposed which is valid for fine particles; the results of the this model has been compared with actual experimental data and satisfactory agreement was achieved
- ✓ Different bed geometries have been observed at different fluid velocity
- ✓ Stationary bed at lower velocities followed by separated sand dunes for higher velocities and at sufficiently high velocities suspension were found as regime of sediment transport
- ✓ It has been found that a plot of pressure drops against bulk velocity could be used to identify transition from stationary bed to dunes domain and also transition to suspended load
- ✓ Pressure drops in each regime correlated linearly with bulk velocity
- ✓ The slope of pressure drops data were found to be different in each regime
- ✓ Presence of sand dunes has been found to be associated with big fluctuations in pressure drops
- ✓ Dunes velocities were found to be a linear function of the bulk velocity
- ✓ Dunes velocities for fine particles have been found to be affected by viscosity of the fluids in a negative way
- ✓ Effect of viscosity on dunes velocity found to be positive for transporting coarse particles
- ✓ Effect of high viscosity on critical velocity and pressure drops when big particles are used was found to be similar to fine particles

- ✓ Critical velocity was found to be enhanced slightly when larger particles were used in polymer solutions while when water is used as the carrier fluid this velocity increases slightly
- ✓ Critical pressure drops and wall stresses have been found to increase slightly when bigger particles are used despite the fact that critical velocity may be lower when this particles are moving
- ✓ Velocity of the dunes have been compared for two particles diameters and it is been reported that bigger cuttings enhances this velocity

## 7.7 References


[1]. Massie G. W., Castle-Smith J., Lee J. W., Ramsey M.S., 1995, "Amoco's Training Initiative Reduces Wellsite Drilling Problems", Petroleum Engineer International; Vol. 67, No. 3

[2]. Hopkins C. J., Leicksenring R. A., 1995, "Reducing the Risk of Stuck Pipe in the Netherlands", SPE/IADC Drilling Conference, 28 February-2 March 1995, Amsterdam, Netherlands, SPE 29422

[3]. Bradley W. B., Jarman D., Plott R. S., Wood R. D., Schofield T. R., Auflick R. A., Cocking, D., 1991, "A Task Force Approach to Reducing Stuck Pipe Costs", SPE/IADC Drilling Conference, 11-14 March 1991, Amsterdam, Netherlands, SPE 21999

[4]. Bilgesu H. I., Mishra N., Ameri S., 2007, "Understanding the Effects of Drilling Parameters on Hole Cleaning in Horizontal and Deviated Wellbores Using Computational Fluid Dynamics", Presented at the 2007 SPE Eastern Regional Meeting held in Lexington, Kentucky, U.S.A., October 2007, SPE 111208

[5]. Martins A. L. et.al, 1992, " Evaluation of Cutting Transport in Horizontal and Near Horizontal Wells-A Dimensionless Approach", presented at the Second Latin Amencan Petroleum Engineering Conference, II LAPEC, of the Society of Petroleum Engineers held in Caracas, Venezuela, March 1992, SPE 23643

[6]. Azar J. J., Alfredo R., 1997, "Important Issues in Cuttings Transport for Drilling Directional Wells", Presented at the Fifth Latin American and Caribbean Petroleum Engineering Conference and Exhibition held in Rio de Janeiro, Brazil, August 1997, SPE 39020

[7]. Larsen T. I., Pilehavri A. A., Azar J. J., 1997, "Development of a New Cuttings-Transport Model for High-Angle Wellbores Including Horizontal Wells", SPE Drilling and Completion, SPE 25872

[8]. Okrajni S. S., Azar J. J., 1986, "The Effects of Mud Rheology on Annular Hole Cleaning in Directional Wells", Presented at the 1985 SPE Annual Technical Conference and Exhibition held in Las Vegas,, SPE 14178

[9]. Tomren P. H., Iyoho A. W., Azar J. J., 1986, "Experimental Study of Cuttings Transport in Directional Wells", Presented at the 1983 SPE Annual Technical Conference and Exhibition held in San Francisco, SPE 12123

[10]. Kelessidis V. C., Bandelis G. E., 2004 " Flow Patterns and Minimum Suspension Velocity for Efficient Cuttings Transport in Horizontal and Deviated Wells in Coiled-Tubing Drilling", SPE Drilling and Completion, SPE 81746

[11]. Payne M. L., Cocking D. A., Hatch A. J., 1994, " Critical Technologies for Success in Extended Reach Drilling", Presented at SPE 69th Annual Technical Conference and Exhibition held in New Orleans, LA, U. S.A., September 1994, SPE 28293

[12]. Nguyen D., Rahman S. S., 1996, "A Three-Layer Hydraulic Program for Effective Cuttings Transport and Hole Cleaning in Highly Deviated and Horizontal Wells", Presented at IADC/SPE Asia Pacific Drilling Technology Conference, Kuala Lumpur, Malaysia

[13]. Cho H., Shah N., Osisanya S. O., 2000, " A Three-Layer Modeling for Cuttings Transport with Coiled Tubing Horizontal Drilling", Presented at the 2000 SPE Annual Technical Conference and Exhibition held in Dallas, Texas, October 2000 , SPE 63269

[14]. Duan M., Miska S., Yu M., Takach N., Ahmed R., Zettner C., 2008, " Transport of Small Cuttings in Extended-Reach Drilling", SPE Drilling and Completion, SPE 104192

[15]. Pilehvari A. A., Azar J. J., Shirazi S. A., 1999, "State-of-the –Art Cuttings Transport in Horizontal Wellbores" , SPE Drilling and Completion 14 (3), SPE 57716

[16]. Gavignet A. A., Sobey I. J., 1989, "Models Aids Cuttings Transport Prediction", Journal of Petroleum Technology

[17]. Ramadan A., Skalle P., Johansen S. T., 2003, " A Mechanistic Model to Determine the Critical Flow Velocity Required to Initiate the Movement of Spherical Bed Particles in Inclined Channels", Chemical Engineering Science, Vol. 58, pp. 2153-2163

[18]. Ford J. T., Peden J. M., Oyeneyin M. B., Gao E. Zarrough R., 1990, "Experimental Investigation of Drilled Cuttings Transport in Inclined Boreholes", Presented at the 65th Annual Technical Conference and Exhibition of the Society of Petroleum Engineers held in New Orleans, LA, September 1990, SPE 20421

[19]. Lockett T. J., Richardson S. M., Worraker W. J., 1993, " The Importance of Rotation Effects for Efficient Cuttings Removal During Drilling", Presented at SPE/IADC Drilling Conference held in Amsterdam February 1993, SPE/ IADC 25768

[20]. Thomas R. P., Azar J. J., 1982, "Drillpipe Eccentricity Effect on Drilled Cuttings Behavior in Vertical Wellbores", Journal of Petroleu, Technology, Vol. 34, No. 9, pp. 1929-1937

[21]. Yu M., Melcher D., Takach N., Miska S. Z., Ahmed R., 2004, " A New Approach to Improve Cuttings Transport in Horizontal and Inclined Wells", Presented at the SPE Annual Technical Conference and Exhibition held in Houston, U.S.A, September 2004, SPE 90529

[22]. Walker S., Li J., 2000, "The Effects of Particle Size, Fluid Rheology, and Pipe Eccentricity on Cuttings Transport", SPE/ICoTA Coiled Tubing Roundtable, April 2000, Houston, Texas, SPE 60755

[23]. Clark R. K., Bickham K. L., 1994, " A Mechanistic Model for Cuttings Transport", Presented at SPE 69$^{th}$ Annual Technical Conference and Exhibition held in New Orleans, LA, U. S.A., September 1994 , SPE 28306

[24]. Wang Z. M., hao X. N., Guo X. L., Zhai Y. J., Sun L. L., 2011, " A Study on the Thickness of Cutting Bed Monitor and Control in an Extended Reach Well", Petroleum Science and Technology, Vol.29, No.13, pp. 1397-1406

[25]. Sifferman, T.R., Becker, T.E., 1992, "Hole Cleaning in Full-Scale Inclined Wellbores", SPE Drilling Engineering, Vol. 7, No. 2, pp. 115-120

[26]. Li J., Walker S., 1999, "Sensitivity Analysis of Hole Cleaning Parameters in Directional Wells", SPE/ICoTA Coiled Tubing Roundtable, 25-26 May 1999, Houston, Texas, SPE 54498

[27]. Peden J. M., Ford J. T., Oyeneyin M. B., 1990, “Comprehensive Experimental Investigation of Drilled Cuttings Transport in Inclined Wells Including the Effects of Rotation and Eccentricity”, European Petroleum Conference , 21-24 October 1990, The Hague, Netherlands, SPE 20925

[28]. Rabenjafimanantosa H. A., 2007, “Particle Transport and Dynamics in Turbulent Newtonian and Non-Newtonian Fluids”, PHD Dissertation, University of Stavanger, Norway

# Chapter 8:

# Conclusions and Recommendations for Future Works

The most important conclusions derived from the research results reported in this thesis are summarized here. Conclusions are presented in four main sections categorized by using the same titles of the chapters, which covers the related research results.

## 8.1 Newtonian Fluid Flow through Annuli

Experiments were conducted to investigate turbulent flow of Newtonian fluid (Water) in horizontal concentric annulus. Reynolds numbers ranged from 17700 to 68000.

- ✓ Friction factors obtained from experiments with turbulent flow of water in the annuli agree well with the calculated ones from Jones and Leung correlation[46].
- ✓ Near wall axial mean velocity profile follow the universal law of the wall when $y^+ < 10$ . The universal law of the wall applies for both inner and outer pipe wall and for all Reynolds numbers.
- ✓ Axial mean velocity profile follows logarithmic wall law when $y^+ > 10$ (consistent with flow through pipes). Log-law also applies for all the Reynolds numbers and at the inner and outer pipe wall as well. .
- ✓ The axial velocity profile has strong asymmetry in whole annular gap
- ✓ The radial location of maximum velocity does not depend on Reynolds number.
- ✓ The radial location of maximum velocity is closer to the inner pipe wall of the annuli.
- ✓ Reynolds stress profile goes to zero near to the pipe wall and or in the viscous sublayer
- ✓ Reynolds stress profile is asymmetric, while the Reynolds stress tensor is symmetric.
- ✓ Reynolds stress profiles reach a maximum very close to walls of the annuli and tend to be zero in the core flow.
- ✓ Viscous stress profile shows zero or very small value in the core regions of the flow.
- ✓ Viscous stress increases sharply as either of the inner or the outer pipe wall of the annuli is approached.
- ✓ Viscous stress becomes equal to the actual wall shear stress at the inner and outer pipe walls of the annuli for lower Reynolds numbers. However, viscous

stress doesn't converge to wall shear stress value at higher Reynolds numbers.

- ✓ Radial location of zero shear stress is closer to the inner pipe wall.
- ✓ Radial location of zero shear stress is independent of Reynolds number change.
- ✓ Radial location of zero shear stress is closer to the inner pipe wall of the annuli than the radial location of the maximum velocity.
- ✓ Axial turbulent intensities near the outer pipe are higher than that of the ones near the inner pipe wall.
- ✓ Axial turbulent intensities reach a maximum at wall coordinates around $y^+ \sim 20$ , which means turbulent intensities take their peak in the buffer layer.
- ✓ Turbulent intensities in radial direction are in the same order of magnitudes at the both inner and outer pipe walls of the annuli (outer wall data are higher a bit but the difference is not as much as it is in axial intensities and no general conclusion could be made about that).
- ✓ Radial turbulent intensities exhibit different behaviour than axial turbulent intensities such that no peak points exist for the radial intensities. .
- ✓ Radial intensities are almost constant in the core regions of a turbulent water flow.

## 8.2 Non-Newtonian Fluid Flow through Annuli

Aqueous polymer solutions of two different concentrations (0.175% and 0.2%) were used to study turbulent flow of non-Newtonian fluids in the concentric horizontal annuli. Operational conditions were chosen to assure that turbulent flow prevails. PIV was used to study the turbulent flow of polymer fluids in the horizontal concentric annuli. Measured frictional pressure drop was used for determining friction factor and for further analysis of the PIV data.

- ✓ Both polymer solutions showed power law behaviour in the range of shear rates encountered during experiments.
- ✓ Friction factors of both fluids were found to be in good agreement with theoretical prediction of a power law type fluid in the laminar flow regime.
- ✓ Friction factors measured from turbulent flow experiments were much lower than the ones calculated by using the Jones and Leung correlation[46], which is valid for flow of Newtonian fluids.

- ✓ Friction factors of turbulent polymer fluid flow were higher than those predicted by Virk's ultimate asymptote[51], which corresponds to the condition of maximum drag reduction.
- ✓ Turbulent friction factors were found to be best represented by $f = 0.4N_{re}^{-0.48}$ for both fluids.
- ✓ Axial mean velocity profile for $y^+ < 10$ were found to follow the universal law of the wall for all the experiments with non-Newtonian fluids.
- ✓ For $y^+ > 10$ major deviation from the logarithmic law (consistent with flow of Newtonian fluids) was observed with an upward shift in axial mean velocity data for polymer liquids.
- ✓ Velocity data in the logarithmic region of the flow were found to be in good agreement with Virk's asymptote in wall coordinates.
- ✓ Radial location of maximum velocity was found to be a function of Reynolds number for the range of Reynolds numbers studied.
- ✓ Radial location of maximum velocity for both fluids gets closer to the inner pipe wall as Reynolds numbers increases.
- ✓ For the range of Reynolds numbers studied, radial location of maximum velocity was closer to the inner wall for 0.175% solution as compared to 0.2% polymer solution.
- ✓ Viscous stresses are higher close to the pipe walls and decrease further away from the walls.
- ✓ Viscous stresses were higher for 0.2% solution because of higher viscosity of that fluid.
- ✓ Viscous stresses converge to the wall shear stress calculated using measured pressure drop at the walls of the annuli.
- ✓ Reynolds stresses of the 0.2% solution were close to zero.
- ✓ Reynolds stresses were always higher for flow of 0.175% polymer solution because of the lower viscosity of this fluid.
- ✓ Total stress was found to be dominated by viscous stress term for the range of Reynolds number studied.
- ✓ The radial location of zero shear stress was closer to the inner wall of the annuli.
- ✓ Radial location of zero shear stress gets closer to the inner pipe wall as the Reynolds number increases.

- ✓ Radial location of zero shear stress for flow of 0.2% polymer solution was closer to the inner pipe wall than that of 0.175% polymer solution.
- ✓ Radial location of zero shear stress is closer to the inner pipe wall than that of maximum velocity.
- ✓ Axial turbulent intensities near the outer pipe wall of the annuli were much higher than that of near the inner pipe wall.
- ✓ Axial turbulent intensities were higher for flow of 0.175% polymer solution than that 0.2% solution
- ✓ Axial turbulent intensities reached a maximum at wall unit of around $y^+ = 20$ for all the cases considered.
- ✓ Radial turbulent intensities were found to be constant over a wide range of the flow.

## 8.3 Newtonian Fluids versus Non-Newtonian Fluids

- ✓ Friction factors for flow of polymer solutions were much lower than that of water flow in turbulent flow regime.
- ✓ Axial mean velocity profile was the same in the immediate vicinity of the walls. However, further away from the wall, an upward shift in velocity profile of polymer solutions was observed.
- ✓ Velocity profiles in the whole annular gap were compared for the three fluids (i.e., water and two polymer fluids). Velocity profiles of aqueous polymer solutions are more parabolic than that of water.
- ✓ Maximum velocity of polymer solutions was higher than that of water.
- ✓ Radial location of maximum velocity for flow of polymer solutions was found to be some -2.6% to 1.5% different than that of water.
- ✓ At the lowest bulk velocity tested, radius of maximum velocity was always bigger for polymer solutions. However, at the highest bulk velocity, radius of maximum velocity was always smaller than that of water.
- ✓ Viscous stresses were much higher for flow of polymer fluids reflecting the effect of high viscosity of these fluids.
- ✓ Reynolds stresses of polymer fluids were much lower than that of water, which reflects the effect of effective Reynolds number at which experiments were conducted. It may also be related to drag reduction phenomenon as well.

- ✓ Radial location of zero shear stress for polymer solutions was found to lie within -8% to 0.1% of water.
- ✓ Axial turbulent intensities of 0.175% polymer solution were slightly higher than that of water
- ✓ Axial turbulent intensities of 0.2% polymer solution were lower than that of water
- ✓ Turbulent intensities in radial direction were found to be greatly suppressed for polymer solutions in the core flow region as compared to water flow.
- ✓ Turbulent intensities of polymer solution in radial direction have shown higher values for a very small distance and only very close to the walls.

## 8.4 Cutting Transport in Horizontal Annuli

Effects of fluid rheology and viscosity on critical conditions of particle movement were investigated using two different particle diameters, fine particles ($d_{50}$= 349 micron) and coarse particles ($d_{50}$= 1.2mm). Water and three polymer solutions (0.05%, 0.1% and 0.175%) were tested. The results were reported in terms of critical velocity of rolling and saltation. Formation of certain bed types (i.e., flow patterns of solids movement) was also investigated. Critical conditions for transition from one regime to another were reported. Velocity of the dunes movement was measured as well.

- ✓ Two particle diameters of median diameters349 micron and 1.2 mm were used. Particle size distribution (PSD) was uniform in both particle size ranges.
- ✓ Critical velocity to initiate particle movement with saltation was higher than that of to initiate particle movement with rolling.
- ✓ High viscosity was found to have a detrimental effect on critical velocity of rolling and saltation for fine particles (i.e., higher critical velocity is needed to initiate particle movement with the increasing fluid viscosity).
- ✓ The critical velocity of rolling for fine particles with water was found to be around 0.24 m/s. The critical velocity of rolling for fine particles continuously increases with increasing polymer concentration and viscosity of the fluid. The critical velocity of rolling for fine particles was 1.16 m/s when the fluid with the highest polymer concentration (0.175%) was used.

- ✓ Effect of high viscosity on the frictional pressure drop at the point of particle movement was similar to its effect on the critical velocity; an increasing trend of critical pressure drop was observed with increasing viscosity.
- ✓ For fine particles, the thickness of viscous sublayer was similar for all the fluids studied at the point of particles movement.
- ✓ Thickness of viscous sublayer at the onset of particles motion for fine particles was close to the mean diameter of particles for all the fluids tested.
- ✓ Based on the assumption of equity of viscous sublayer thickness and particles mean diameter at the point of rolling for fine particles, a model for predicting critical wall shear stress for fine particles was proposed which is valid; the results of the this model has been compared with actual experimental data and satisfactory agreement was achieved
- ✓ Different bed geometries were observed at different fluid velocity: Stationary bed was observed at lower velocities followed by separated sand dunes as the bulk fluid velocity is increased and finally, at sufficiently high velocities, particles were transported in suspension. .
- ✓ It was found that a plot of frictional pressure drop against bulk velocity could be used to identify transition of flow pattern from stationary bed to dunes mode and also transition from dunes to full suspension flow.
- ✓ Frictional pressure drops in each regime correlated linearly with the bulk fluid velocity.
- ✓ The slope of the lines correlating pressure drop vs. bulk fluid velocity data was found to be different in each flow regime.
- ✓ Presence of sand dunes was found to be associated with large fluctuations in frictional pressure drop measurements.
- ✓ Dunes movement velocities were found to be a linear function of the bulk fluid velocity.
- ✓ Dunes velocities for fine particles were found to be affected adversely by the increasing viscosity of the fluids (i.e., slower dune velocity was observed with increasing fluid viscosity).
- ✓ Effect of viscosity on dunes velocity was found to be positive when transporting coarse particles (i.e., faster dune velocity was observed with increasing fluid viscosity).

- ✓ Effect of high fluid viscosity on critical velocity and frictional pressure drop was similar for both cases of large particle and fine particle transport.
- ✓ Critical velocity was found to be decreasing slightly when larger particles were transported by polymer solutions. When water was used as a carrier fluid, however, critical velocity increased slightly.
- ✓ Critical pressure drop (and the corresponding wall shear stress) was found to increase slightly when large particles were transported despite the fact that critical velocity to initiate movement of large particles was lower.
- ✓ Velocity of the dunes was compared for two particle diameters. It was observed larger particles were transported at the higher velocity than smaller particles.

## 8.5 Recommendations for Future Work

Solid transport in annuli depends on many different parameters, only two were investigated in the present work. It is also known that these parameters interact with each other and the results may differ in presence of other parameters. Generally, with respect to the experimental facility and its limitations, following suggestions seems reasonable for a future work.

- ✓ The current PIV setup could be upgraded to a Stereo PIV for 3-D measurements of flow structures.
- ✓ Investigation of flow in annuli with a different radius ratio by using PIV technique
- ✓ Investigation of flow in through eccentric annuli
- ✓ Considering the investigation of a fluid which exhibits yield stress (this is the common case in real drilling fluids)
- ✓ Investigating solid transport in eccentric annuli and or with a yield power law fluid
- ✓ Investigating transport of cuttings with broad range of size distribution
- ✓ Conducting cutting transport experiments with water and polymer solutions at the same pump HP is so recommended; this is helpful in evaluation of hole cleaning performance of each fluid when the same energy has been given to them. Pressure drops and the time which it takes to clean the well can be measured and compared.